UNIVERSITY OF CALIFORNIA,
IRVINE

Exosomes Secreted by Mesenchymal Stem Cell to Treat Autoimmune Disorders

DISSERTATION

Submitted in partial satisfaction of the requirements for the degree of

DOCTOR OF PHILOSOPHY

In Materials Science & Engineering

By

Mohammadreza Mohammadi

Dissertation Committee:
Professor Jonathan Lakey, Chair
Associate Professor Weian Zhao, Co-Chair
Professor James Earthman
Associate Professor Wendy F. Liu

2020

Pre-published

Chapter 2 © Small 2019 15; 34:1902333 © 2019 M. R. Mohammadi

Chapter 2 © Handbook of Tissue Engineering 2019 1:127-152 © 2019 M. R. Mohammadi

Chapter 2 © ACS Biomaterials Science and Engineering 2020, 6, 5, 2726–2739 © 2020 M. R. Mohammadi

Chapter 3 © ACS Nano 2019, 13, 6, 6670-6688 © 2019 M. R. Mohammadi

Chapter 4 © Advanced Healthcare Materials 2020, e1901874-e1901874 © 2020 M. R. Mohammadi

DEDICATION

To my Parents, Farah and Kavoos, for your unending support and for the infinite levels of sacrifice and selflessness you have displayed in providing for your son.

And to my sister, for her mentorship and love.

LIST OF FIGURES

Page

LIST OF TABLES

Page

ACKNOWLEDGMENTS

I would like to thank **Dr. Jonathan Lakey** for giving me the chance to be his graduate student over the past 4 years. I am extremely thankful for your mentorship, guidance, and friendship over the years and for all the collaborative opportunities that you have provided for me. I genuinely believe you possess a grounded and deep understanding of the importance of translational science and how critical it is for a scientist to understand market and business. I would like to than my co-advisor, **Dr. Weian Zhao**, for his patience and efforts in training me to think scientifically and critically. I believe you know how science should be properly executed in terms of research, mentorship, and lifelong learning. I am also extremely thankful to **Dr. Paul de Vos**, a leader in the biomaterials research, for his advice, support, and friendship. Lastly, I want to express my appreciation to **Dr. Jayakumar Rajadas** who trained me to take initiatives, be persistent, and follow my passion with a hard-work. I was fortunate to spend 2 years in his laboratory at Stanford University, where I got involved in multiple exciting projects. I have had the pleasure of knowing **Dr. Mathew Blurton-Jones** since 2017. He has been also a great mentor and friend, who provided multiple critical research questions and pathways for me to follow. I wish to thank **Dr. Armando Vilatella** and his lab members who helped us with immunological assays and interpretation. Without his help and guidance, we would never have been able to complete the in vitro part of the project. Finally, I would like to appreciate the help and support from my PhD committee members, **Drs. James Earthman**, **Wendy Liu** and **Alon Hochbaum**. They had critical influence on my thought process by valuable questions and guidances.

VITA
Mohammadreza (Reza) Mohammadi

Education

Ph.D. Materials Science & Engineering – *UC Irvine* **Sept 2016 – May 2020**

M.S. Materials Science & Engineering – *Sharif University* **Sept 2010 – Sept 2012**

B.S. Materials Science & Engineering – *Amirkabir University* **Sept 2005 – Sept 2010**

Experience

Ph.D. Candidate **Sep 2016 – May 2020**

Drug discovery, immunoengineering, and biologics development
Stem Cell Research Center, Department of Surgery and Biomedical Engineering
University of California Irvine, Irvine CA

- Invented 3 products, co-authored 14 peer-reviewed publications
- Developed a cell-free approach using stem cell-derived extracellular vesicles to treat multiple sclerosis animal model
  Mentor: Dr. Weian Zhao
- Constructed, for the first time, two therapeutic and immunomodulatory implants (pCM-Alg and AlgXO) for islet xenotransplantation, providing long-term treatment for rodents with Type 1 Diabetes
  Mentors: Dr. Jonathan Lakey and Dr. Weian Zhao
- Lead team and future research strategies to utilize extracellular vesicles as therapies to treat autoimmune diseases, cancer and neurodegenerative disorders.
- Devised a novel immunoregulator and angiogenic implant and bioink (XoInk) using 3D bioprinting
- Mentored 2 graduate, 16 undergraduate, and 3 high-school students to develop professionally and to complete assigned project

Research Scientist **2015 – Sep 2016**

School of Medicine, Stanford University, Palo Alto CA

- Led a U.S. patent and co-authored four publications including two first author publications in peer-reviewed journals
- Co-Developed “Magnosome” technology for guided delivery of stem cells, patented for Stanford University and UCSF
- Formulated a novel physisorbed double-layer coating around Iron Oxide Nanoparticles
- Protein purification using fractionation methods (ultra - centrifugation, ultra / diafiltration, etc.), and chromatographic techniques (affinity, ion exchange, hydrophobic interaction, immobilized metal, and mixed mode chromatography)

Communication

Teaching Assistant –Human Physiology **Sep 2017 – Dec 2018**
–Molecular Pharmacology
Department of Pharmaceutical Sciences, University of California Irvine, Irvine CA

- Presented lectures to the audience of 200+ senior level students
- Hold weekly discussion sessions for the students

Leadership

Project Leader **Sep 2017 – Present**
University of California Irvine, Irvine CA

- Lead team and developed multiple projects in 3 different institutions and strategies to harness extracellular vesicles potentials as therapeutics for autoimmune diseases and regenerative medicine
- Generated novel ideas, secured extramural funding, and led a multi-disciplinary team to fabricate, analyze, and establish AlgXO, Disk-of-Life®, and pCM-Alg® technologies

DECADE PLUS Leadership Coach **Mar 2017-Present**
Department of Education, University of California Irvine, Irvine CA

- Mentored more than 10 First-Gen Chancellor's Scholars
- Led a team of 10 graduate and undergraduate students in group meetings
- Mentoring Excellency Certificate Awarded

Introduction to Project Management Course **Mar 2017 – May 2017**
UCI Extension
University of California Irvine, Irvine CA

- Planning a project from start to finish using Project Management Body of Knowledge guidelines
- Directed project justification, requirements, milestones, budget, and deliverables

Project Leader **Jan 2016 – Sep 2017**
Biomaterials and Advanced Drug Delivery, Stanford University

- Lead team and invented Magnosome and Non-Toxic Iron Oxide Nanoparticles

Technical Skills

Extracellular Vesicles: exosome isolation from *in vitro* cultures and *ex vivo*, uptake assay, nanoparticle tracking analysis, ultracentrifugation and polymer-based precipitation of exosomes, characterization using flow cytometry/western blotting/electron microscopy, exosome quantification, exosomal RNA extraction, bioanalyzer.

Immunology: flow cytometry, experimental autoimmune encephalomyelitis (EAE, MS animal model), NOD and STZ diabetic mouse models, Treg induction and expansion, T cell

proliferation/inhibition assays, T cells differentiation (effector, memory, and regulatory), splenocyte and human PBMCs isolation and characterization, Macrophage modulation assays

Bioengineering and Tissue Engineering: (Bio)-Materials and Nanomaterials synthesis and characterization, Drug Discovery, Engineering immunomodulatory devices through coating and/or controlled release and drug eluting approaches, Targeted Drug and Cell delivery, 3D bioprinting of cells and biomaterials. Red blood cells isolation and nanovesicle formation, In vivo (Live animal IVIS imaging) and in vitro assays for biomaterials biocompatibility, Designed and produced nanofabricated scaffolds, scaffold cell seeding, bioreactor, scaffold biocompatibility & biodegradability tests, Scanning and Transmission Electron Microscopies
Others: AAS, AFM, DLS, DSC, EDX, FTIR, Gel Electrophoresis, ICP (MS and OES), UV/VIS, Fluorescent and Confocal Microscopies, TGA, TURBIDIMETRY, VSM, Western blotting, XPS, XRD, WDX, Viscometer, Tension & Fatigue tests, Casting

Cell Culture: isolation and culture of mesenchymal stem cells derived from humans (Wharton Jelly, Umbilical Cord, Cord Blood, and Bone Marrow), induced pluripotent stem cells (iPSCs) generation and differentiation, perform stem cell differentiation, retinal progenitor cells, neural stem cells, fibroblast, macrophage, PBMCs and Splenocytes isolation characterization and expansion, adipose-derived stem cells isolation and expansion, MTT and XTT assays, Prussian blue, Plate Reader, ROS and NO measurement, chemical and electrochemical transfection

Molecular Biology: nucleic acid extraction, PCR (standard, reverse-transcription, and real time), primer design, bioinformatics, ELISA, MAGPIX Luminex assay, electrophoresis, western blotting, viral vector construction & transduction, bacterial transformation, immunohistochemistry, immunocytochemistry

Cytogenetic: chromosome harvest and slide preparation for karyotyping

Animal Handling: Immunocompetent, Immunocompromised, and genetically modified mice, rat, and rabbit

Biomaterials Fibrosis: Techniques and protocols to quantitatively characterize the immune response against implanted biomaterials

Data Analysis and Scientific Writing: design and interpretation of biological experiments with associated statistical analysis; Python, Matlab, construction of scientific graphs using programs such as Microsoft Word, Excel, PowerPoint, EndNote, FlowJo, GraphPad Prism

Honors & Awards

Engineering Student of the Year	2020
AGS Travel Award	2020
American Society of Anesthesiologists Conference Award	2020
Key personnel in CHOC research grant ($70k)	2019-2020
University of California Chancellor's Club Fellow ($12k)	2019-2020
SoCal Flow Cytometry Scholarship	2019

NEWKIRK Foundation Fellow, UC Irvine ($10k) 2018-2019
Cure-It Category Lemelson-MIT prize-Massachusetts Institute of Technology, USA 2018
DECADE Plus Mentor Fellow, UC Irvine ($7k) 2018-2020
BioADD Annual Award conferred by Dr. Irving Weissman, Stanford University 2017
https://engineering.uci.edu/news/2017/2/grad-student-recognized-collaboration
Graduate Fellowship, University of California Irvine, USA 2016-2019
Awarded funding by Lyme Disease Foundation, Stanford University, USA 2015
Awarded by Persian Nanotechnology Initiative Council for Outstanding Master Thesis 2013
Placed 29th among 7,375 participants in the national university entrance exam for M.S. degree entrance, held in Iran 2010

Publications

1. M. Rezaa Mohammadi, Jennifer Cam Luong, Rui Cao, Ashlyn Elizabeth Wheeler, Samuel Mathew Rodriguez, Hien Lau, Shiri Li, Paul de vos, Weian Zhao, Jonathan RT Lakey, *Controlled Release of Stem Cell Secretome Attenuates Inflammatory Response Against Implanted Biomaterials*, **Adv. Healthcare Mat**., 2020, Accepted.
2. M. Rezaa Mohammadi, Farideh Dehkordi-Vakil, Joni Ricks-Oddie, Robert Mansfield, Himala Kashimiri, Mark Daniels, Weian Zhao, and Jonathan RT Lakey, *Preferences of Type 1 Diabetic Patients on Devices for Islet Transplantation*, **Sci. Rep.**, 2020, Submitted
3. M. Rezaa Mohammadi, Milad Riazifar, Egest J.Pone, Ashish Yeri, Kendall Van Keuren-Jensen, Cecilia Lässer, Jan Lotvall, Weian Zhao, Isolation and characterization of microvesicles from mesenchymal stem cells, **Methods**, 2019
4. JRT Lakey, Samuel Rodriguez, M. Rezaa Mohammadi, Greg G Kojayan, Michael Alexander, Cryopreservation of Pancreatic Islets, **Appl Cell Biol**, 7(2), 2019
5. M. Riazifar*, M. Rezaa Mohammadi*, et al., W. Zhao, Stem Cell-derived Exosomes as Nanotherapeutics for Autoimmune and Neurodegenerative Disorders, **ACS Nano**, 2019. (* Co-first authorship). Featured on: https://physicsworld.com/a/nanoparticles-regulate-harmful-immune-response-in-multiple-sclerosis/ and https://www.eurekalert.org/pub_releases/2019-06/uoc--nts060519.php
6. M. Rezaa Mohammadi, C. Corbo, R. Molinaro, JRT Lakey, *Biohybrid Nanoparticles to Negotiate with Biological Barriers*, **Small**, 2019, 1902333
7. Hien Lau, Nicole Corrales, Michael Alexander, Shiri Li, M. Rezaa Mohammadi, Sandra Smink, Paul de Vos, Jonathan Lakey, *Necrostatin-1 Supplementation Enhances Young Porcine Islet Maturation and In vitro Function*, **Xenotransplantation**, 2019, Accepted.
8. M. Rezaa Mohammadi, Cao, Rui; Rodriguez, Samuel; Tolsma, Danielle; Lakey, Jonathan, *Immunomodulatory Stem Cells to Alleviate the Foreign Body Response Against Implanted Biomaterials*, **Transplantation**, 2019, 103, 9S2 - p S9–S10
9. M. Rezaa Mohammadi, Jennifer Cam Luong, Gahyun Grace Kim, Hien Lau, Jonathan RT Lakey, *Scaffolds Implanted: What Is Next?* **Handbook of Tissue Engineering Scaffolds**, Elsevier (2019)
10. M. Rezaa Mohammadi*, et al., W. Zhao, *Isolation and Characterization of Microvesicles from Mesenchymal Stem Cells*, **Methods**, 2019
11. M. Rezaa Mohammadi**,** Andrey Malkovsky, Preetha Jothimuthu, Kwang-Min Kim, Mansi Parekh, Mohammed Inayathullah, Yan Zhuge, Jayakumar Rajadas, *Double Layer PEG/Dextran Influences Fe ion release and Colloidal Stability of Iron Oxide Nanoparticles*, **Scientific Reports**, 2018, 8 (1), 4286. ***Top 100 SciRep Chemistry papers 2018***
12. A. Dubnika et al., M. Rezaa Mohammadi, *Cytokines as therapeutic agents and targets in heart disease*, **Cytokine and Growth Factor Reviews** 2018, 43, 54-68
13. M. Rezaa Mohammadi, Samuel Rodriguez, Rui Cao, Michael Alexander, JRT Lakey, Immune response to subcutaneous implants of alginate microcapsules, **Materials Today: Proceeding**, 5 (2018) pp. 15580-15585
14. M. Mozafari, M. Rezaa Mohammadi, et al., *Synthesis and characterization of highly interconnected porous poly(ε-caprolactone)-collagen scaffolds: a therapeutic design to facilitate tendon regeneration*, **Materials Technology**, 2018, 33 (1), 29-37
15. M. Jafarkhani, et al, M. Rezaa Mohammadi, M. Mozafari, *Strategies for directing cells into building functional hearts and heart parts*, **Biomaterials Science**, 2018 6(7):1664-1690
16. C. Kopan et al, M. Rezaa Mohammadi, JRT Lakey, *Emerging approaches in immunotherapy, regenerative medicine and bioengineering for type 1 diabetes*, **Frontiers in Immunology**, 2018, 9, 1354
17. M. Karbassi, et al., M. Rezaa Mohammadi, *Microemulsion-based synthesis of a visible-light-responsive Si-doped TiO_2 photocatalyst and its photodegradation efficiency potential*, **Mat Chem and Phy** 220 (2018) 374–382
18. M. Rezaa Mohammadi, Amirali Nojumi, Arita Dubnika, Masoud Mozafari, Mohammed Inayathullah, Jayakumar Rajadas, *Nanomaterials Engineering for Drug Delivery: A Hybridization Approach*, **J Mat Chem B**, 2017, 5, 3995-4018
19. M. Rezaa Mohammadi, Wenchao Sun, M. Inayathullah, J. Rajadas, *Nanoparticles hybridization to engineer biomaterials for drug delivery*, **Nanobiomaterials Science, Development and Evaluation**, Elsevier (2017)

20. M. R. Mohamadi**,** J. Aghazadeh Mohandesi, M. Homayonifar, *Fatigue behavior of polypropylene fiber reinforced concrete under variable amplitude loading,* **J Comp Mater**, 2013, 47 (26), 3331-42

Patent

Jayakumar Rajadas, M. Rezaa Mohammadi, Mohammed Inyathullah, Geoffrey Gurtner, Tejal Desai, *Magnosomes for Targeted delivery of Stem Cells to the skin, Heart, Brain and other Tissues*, **US Patent App. 15/884,736**

PEER REVIEW

RSC Advances, American Journal of Transplantation, BioChimie, Methods.

CONFERENCE TALKS

1. M.Rezaa Mohammadi, et al., JRT Lakey, Microencapsulation for Xentotransplantation, **IXA 2019**, Munich, Germany.
2. M.Rezaa Mohammadi, et al., JRT Lakey, Immunomodulatory biomaterials using stem cells, **SFB 2019**, Washington, USA.
3. A. Abbasi, S. A. Vitorino, M. R. Mohammadi, A. Lucas, C. Indralingam, W. Zhao, E. C. Breen, H. B. Rossiter, **ERS International Congress**, Spain 2019
4. M.Rezaa Mohammadi**,** Andrey V. Malkowsky, Preetha Jothimuthu, Jayakumar Rajadas, *Magnosomes for Targeted Stem Cell Delivery to Ischemic Heart,* **Stanford Drug Discovery Symposium,** Stanford University 2018
5. M.Rezaa Mohammadi**,** Andrey V. Malkowsky, Preetha Jothimuthu, Jayakumar Rajadas, *Double Layer PEG/Dextran Influences Cell Viability, Colloidal Stability, and in vivo Fate of Iron Oxide Nanoparticles,* **Stanford Drug Discovery Symposium,** Stanford University 2017
6. M.R. Mohammadi, C. Nazli, S. Kizilel, '*Water-in-Water Emulsion Based Synthesis of Functional Poly(ethylene glycol) Microgels for Cancer Cell Targeting*', **AIChE Annual Meeting**, Atlanta (U.S.A), 14-22 November 2014, accepted oral presentation

ABSTRACT OF THE DISSERTATION

Exosomes Secreted by Mesenchymal Stem Cell to Treat Autoimmune Disorders

By

Mohammadreza Mohammadi

Doctor of Philosophy in Materials Science & Engineering

University of California, 2020

Professor Jonathan Lakey, Chair

Associate Professor Weian Zhao, Co-Chair

Autoimmune disorders are becoming increasingly prevalent for unknown reasons. Among more than 80 known autoimmune disorders, Type 1 Diabetes (T1D) and Multiple sclerosis (MS) are top prevalent diseases affecting more than 2 million individuals in the United States and at least $40 billion costs per year. Preclinical studies revealed immunomodulatory and immunosuppressive properties of mesenchymal stem cell (MSC) to treat MS and T1D. However, lung entrapment, mal-differentiation, antibody production, phenotype change and potentially tumor formation are current challenges for stem cell therapy. In addition, there is a lack of mechanistic understanding regarding the molecular mechanisms of MSC therapy. Recent evidence suggests that MSCs exert their therapeutic efficacy partly through secreting active biomolecules and vesicles, which are collectively known as secretome. We therefore sought to harness the therapeutic potentials of secretome, study some of its subtypes including exosomes, and understand molecular pathways affected by MSC secretome and exosome.

MS is an inflammatory disease of the central nervous system (CNS) in which autoreactive T cells attack CNS, resulting in demyelination, neuronal injury and death, which account for the neurological disability. Here, using experimental autoimmune encephalomyelitis (EAE) as a MS mouse model, we show that systemic injection of MSC-Exo (30 μg or 150 μg) result in sustained recovery and improved motor function ($p < 0.01$) in a dose dependent manner. *In vivo*, injection of exosomes decreased neuroinflammation, and upregulated the number of CD4+CD25+FoxP3+ regulatory T cells (Tregs) within the spinal cords of EAE mice, and

reduced the infiltration and/or differentiation of Th1 and Th17 cells within the mice spinal cords. Co-culture of exosomes with activated peripheral blood mononuclear cells (PBMCs) cells *in vitro* reduced PBMC proliferation and levels of pro-inflammatory Th1 and Th17 cytokines including IL-6, IL-12p70, IL-17AF, and IL-22 yet increased levels of immunosuppressive enzyme indoleamine 2,3-dioxygenase. This recovery is associated with reduction in neuroinflammation ($p < 0.05$).

We further harnessed the secretome and exosomes to improve the longevity of pancreatic islet xenotransplantation as a treatment for T1D. We first showed that alginate microcapsules loaded with processed conditioned media (pCM-Alg) reduces the infiltration and/or expression of CD68+ macrophages likely through the controlled release of pCM. *In vitro* cultures revealed that alginate could dose-dependently induce macrophages to secrete TNFα, IL-6, IL-1β, and GM-CSF. Addition of pCM to the cultures attenuated the secretion of TNFα ($p = 0.023$) and IL-6 ($p < 0.0001$) by alginate or lipopolysaccharide (LPS) stimulations. Mechanistically, pCM suppressed the NfκB pathway activation of macrophages in response to LPS ($p < 0.0001$) *in vitro* and cathepsin activity ($p = 0.005$) in response to alginate *in vivo*. Using this concept, we fabricated a hybrid alginate microcapsule (AlgXO) that controllably releases exosomes derived from Umbilical Cord Mesenchymal Stem Cells (XOs). Upon release, XOs suppress the local immune-microenvironment and mitigate the FBR against alginate microcapsules, where xenotransplantation of rat islets encapsulated in AlgXO led to > 5 months euglycemia in immunocompetent mouse model of Type 1 Diabetes. AlgXO significantly reduced the immune response in subcutaneous and intraperitoneal sites, while non-inflammatory fibrosis was observed in the subcutaneous space. *In vitro* analyses revealed that XOs suppressed the proliferation of CD3/CD28 activated splenocytes and CD3+ T cells. Comparing suppressive potency of XOs in purified CD3+ T cells versus splenocytes, we found XOs more profoundly suppressed T cells in the splenocytes coculture, where a heterogenous cell population presents. XOs also suppressed CD3/CD28 activated human peripheral blood mononuclear cells (PBMCs) and reduced their inflammatory cytokine secretion including IL-2, IL-6, IL-12p70, IL-22, and TNFα. We further confirmed that XOs mechanism of action is likely through myeloid cells and they suppress both murine and human macrophages partly through interfering with NfκB pathway. We believe that through its local controlled release of XOs, AlgXO is a platform that could alleviate the local immune response to implantable biomaterials.

CHAPTER 1

Introduction

Immunoengineering

Most of the diseases we face are related to the malfunction of the immune system. The immune system is not only defending us against pathogens but is also crucial for tissue repair and regeneration. A malfunctioning immune response can lead to autoimmune disorders and allergies and plays a deterministic role in the pathogenesis and surveillance of cancer. Immune system is capable of dynamically varying its cellular phenotypes and signaling pathways to warrant our hemostasis. Such functional and dynamic immune offers a variety of intervention strategies to tackle immune failure, to modulate immune cell function, and to engineer immune system for tissue regeneration. The concept of "immunoengineering" is to be able to control and regulate the immunocytes function to halt, delay, reduce, or expand the immune response.

Immunoengineering has started to gain much attention in the field of autoimmune diseases and cancer. Years of research on the tumor microenvironment has revealed the importance of immunocytes function in the progression and treatability of tumors. In fact, the density, location, and type of immune cells within tumors predict patient survival. This immune microenvironment—most notably the presence of CD8+CD45RO+ T lymphocytes and Th1 cells—is associated with a good prognosis across at least 20 different cancer types [1]. Most immunotherapies against solid tumors have benefited only a minority of cancer patients, particularly due to immunosuppressive microenvironment around cancer cells. Thus, reactivation of exhausted immunocytes within the tumor microenvironment and facilitating antitumor

immunocytes to surmount the activation energy barrier imposed by the immunosuppressive tumor microenvironment are two immunoengineering approaches under investigation. Delivery of immunostimulatory molecules from nanoparticles and biomaterials can reprogram the immune system to overcome the immunosuppressive microenvironment. Accordingly, immunologists and engineers are collaborating to improve our understanding of which cells and pathways should be modulated to maximize efficacy and what approaches are most appropriate to perturb them as desired.

In **chapter 2**, we will provide in depth background information on the bio- and nano-materials and approach for immune-engineering to treat autoimmune disorders, including MS and T1D. We further discuss the molecular and cellular mechanisms responsible for the foreign body response against transplants, and how immunoengineering approaches could be used. In **chapter 3**, experimental data on MSC exosome isolation, characterization as well as evaluating MSC exosomes efficacy in EAE animal model will be presented. **Chapter 4** introduces a novel implantable microcapsule that holds MSC secretome, where it reduces the foreign body response through a controlled release system**.** In **chapter 5** we used a xenotransplantation of rat islets into diabetic and immunocompetent mice, showing > 5 months normoglycemia. In the **chapter 6**, we have provided a survey study that had asked from ~500 patients with T1D regarding their preferences of transplantation devices. Finally, **chapter 7** is the conclusion of the dissertation.

Impact and Innovation

In this work, we report the possible molecular mechanisms of exosomes in treating inflammatory based diseases. Few works have in detail investigated the MSC secretome mechanism of action on allogeneic and xenogeneic immune cells setting. In addition, this thesis introduces two new formulations of alginate microcapsules that reduce the foreign body response

and remarkably prolong the function of cell (pancreatic islets) transplants in diabetic rodent models.

Expected pitfalls and future work

This work lacks the toxicity studies in vivo. We will need to perform study to measure exosome toxicity in vivo by injecting high concentration of exosomes followed by analyzing tissues from the vital organs (brain, spinal cord, lungs, liver, spleen and kidneys) by H&E staining. Another question remained to be answered is that while the exosomes in the alginate release within a week, with what mechanism transplants continue to function and block the inflammatory response for months. Induction of memory T and B cells as well as more detailed and time-coursed studies on the protein adherence to the microcapsules further may shed light on this question.

Finally, the current paradigm in drug development requires a detailed molecular mechanism of an investigational new drug. One pitfall of the current work is the lack of a single molecule that play a key role in the observed therapeutic mechanism. However, it needs to be mentioned that a complex biologic that has been evolutionary conserved and enhanced in biological systems may have particularly formulated to do multiple functions, rather than interfering with a single entity or pathway. Therefore, it remains doubtful that such therapeutic efficacy is originating from a single RNA, lipid or protein. Indeed, it is more likely that secretome and exosome is a complex package that regulates multiple inflammatory and/or regenerative pathways.

References

1 Goldberg, Michael S. Immunoengineering: How Nanotechnology Can Enhance Cancer Immunotherapy. *Cell* **161**, 201-204, doi:10.1016/j.cell.2015.03.037 (2015).

CHAPTER 2

Bio- and Nano-materials Approach for Immunoengineering

Abstract

The pathology of many diseases strongly linked to the immune system dysregulations. One approach to find therapies for such diseases is an emerging field of immunoengineering, where dysregulated immune system reprograms to reach the healthy state. Interaction of materials (and nanomaterials) with immune system has been matured over the past decade, suggesting the development of possible materials-based approaches to reprogram immune cells. Inspired by communications in biological systems, endowing a "biological identity" to synthetic NPs is one approach to control their biodistribution, and immuno-negotiation profiles. We refer this synthetic-biological combination as biohybrid NPs, which comprise both (i) the engineerable, readily producible, and trackable synthetic NPs as well as (ii) biological moieties with the capability to cross-talk with immunological barriers. Here, we first overview latest understanding on the *in vivo* interactions of NPs, biological barriers they face, and emerging methods for quantitative measurements of NPs' biodistribution. We then introduce some key biomolecules that have been emerged as immunoregulators in the context of cancer and autoimmunity, and their inspirations on biohybrid NPs. Then we introduce biomaterials-based approach for immunoengineering. In doing so, we focus mostly on the responses of innate immune cells (macrophages and dendritic cells), and methods to manipulate their response and polarization. Materials-based approaches in immunoengineering offer many opportunities in

immune-based therapies from serving as a drug reservoir to an immune-educating microenvironment.

Keywords: Bioinspired materials; Biological negotiation; Biological barriers; Protein corona; Personalized Medicine.

Introduction

The ‘magic bullet’ concept introduced by Paul Ehrlich inspired generations of researchers to devise nanomedicine against human diseases. Since then, the challenge has been to design therapeutic agents that selectively attack malignancies in patients while leaving healthy cells untouched. However, lack of comprehensive understanding on immunological barriers [1] and bio-nano interfaces [2] are among critical factors that have impaired the clinical translation of therapeutic NPs. Thus, some recent efforts have attempted to address biological and immunological barriers for NPs. One approach is to design NPs that bypass the sequential immunological barriers by their stepwise responsiveness [3]. Another approach is to mimic the negotiation between biological systems and leveraging them in NPs design [4, 5]. Endowing synthetic NPs with biological identity is one of the emerging angles in designing nanomedicine to effective cross-talk with biological environment [6].

Our every day-evolving perception of communications in molecular biology-scale implies that cell-cell and cell-biomolecules negotiations play deterministic role in body’s homeostasis and pathogenesis. Inspired by these communications, nanomedicine could be designed to effectively imitate, enhance, or interfere with these cross-talks. The combination of engineerable, readily producible, and trackable synthetic NPs with biological negotiators has led the development of biomimetic or biohybrid NPs with implications of enhanced biological properties in terms of negotiation of biological barriers.

In this review, we first discuss current understandings on the general challenges and barriers for targeted delivery of NPs. We also elaborate on challenges regarding the validation of NPs targeting, and emerging techniques to quantitatively study the biodistribution of NPs

ranging from organ to sub-organ distributions. Next, we introduce some examples on biomolecular negotiations that occur during cancer and autoimmunity, and their inspirations on developed biohybrid NPs. Moreover, methods to hybridize biological and synthetic materials as well as fabrication of biohybrid NPs are overviewed. Finally, challenges associated with clinical translation of biohybrid NPs would be introduced. Biohybrid NPs are promising candidates for next generation nanomedicine and personalized medicine.

Challenges and limitations for *in vivo* delivery of NPs

Following by administration of NPs into the body, they experience spontaneous opsonization and absorption of active biomolecules, i.e. lipids, metabolites, sugars, and proteins, leading to the formation of the so called "corona" [7]. Gaining this biological character on their surface makes the NPs recognizable for immune system, in part, through corona-cell communication. Then, clearance pathways, like the mononuclear phagocytic system (MPS), clear the NPs, which mostly end up in the spleen or liver, the two main filtering organs [8]. Once in the blood stream, NPs also interact with other barriers, which sequentially include circulating immune cells, endothelial wall constituting the blood vasculature, extracellular matrix, cell membrane, endo/lysosomal compartments, and efflux pumps [6, 9, 10]. These barriers led current 'active-targeting' or 'stealth-NPs' to be inefficient, where the targeting antibodies or PEGylation strategies do not significantly affect the biodistribution of NPs *in vivo* [11]. In this chapter, some of the notable events following by NPs intravenous administration will be discussed. Specific attention will be paid towards the events that limit the NPs accumulation in the desired target.

Biological barriers

Formation of protein corona

Spontaneous adsorption of proteins onto materials has long been a recognized phenomenon [12]. However, protein adsorption at bio-nanointerface was first acknowledged in 2007 as "protein corona" [7]. Hydrogen bonding, Van der Waals forces, hydrophobic and electrostatic interactions are the main interactions in the formation of this protein mask [2], and covalent bond formation has recently been recognized [13]. The protein corona layer forms within seconds of NPs incorporation with biological fluid, as studied for polystyrene and silica NPs with various sizes and functionalities [14]. Size, shape, surface properties, as well as NPs interaction with endogenous cells are highly regulated by the formed protein mask [2, 15]. This corona then provides a new biological character for the NPs which is different than the initial "native identity", endowing NPs with the negotiation capability with the biological environment. This cross-talk leads NPs to attach to specific receptors on the surface of phagocytes [16, 17]. Formation of protein corona has been shown to influence cell uptake, immune response, biodistribution, and fate of NPs [14, 18-20]. Protein corona could conceal the targeting moieties (such as peptides or antibodies), leading to impairment in NPs targeting capability [11].

The initial protein content is dynamic and reaches equilibrium within few minutes of incubation in plasma [14]. Compositionally, protein corona consists of the inner and the outer layers known as hard and soft coronas, respectively. The most abundant proteins are globular albumins, fibrinogen, fibronectin, complement protein, immunoglobulins and apolipoprotein [2, 13, 21]. High amount of these proteins in blood leads to their rapid collisions with and adsorptions onto NPs surface. From kinetic theory, frequency of collision can be calculated as follows:

$$f_{col} = \frac{RT}{1500\eta} \cdot \frac{(r_{NP} + r_P)^2}{r_{NP} r_P} c_P \propto \exp\left(\frac{\Delta G_{adsorption}}{RT}\right) \qquad \text{Eq. 2.1}$$

Where $\Delta G_{adsorption}$, R, T, η, r_{NP}, r_P, and c_P are Gibbs free energy for a protein adsorption, gas constant, temperature, blood viscosity, radius of NP, radius of protein, and concentration of protein, respectively [22]. $\Delta G_{adsorption}$ is also defined as the difference between activation energy barrier for adsorption (E_{ads}) and potential energy of desorption (E_{des}). The rate of adsorption/desorption of proteins determines whether the collisions lead to successful binding. Proteins exhibit complex interaction with NPs including electrostatic, Van der Waals, and hydrophobic force. The description of electrostatic and Van der Waals force balance between two particles is posited as the Derjaguin Landau-Verwey-Overbeek (DLVO) theory [23, 24]. **Figure 2.1** illustrates the distance-dependent free energy diagram of NPs and protein. In far enough distance between protein and NP, the free energy is zero and no interaction occurs (**Figure 2.1A**). As protein gets closer, free energy drops and approaches the secondary minimum (**Figure 2.1B)**. This regimen implies a weak attraction which is due to the interaction between hydration layers of NP and protein outermost residues. Proteins in this layer are considered as soft corona. Further decrease in the distance leads more pronounced influence of electrostatic repulsions. Moreover, proteins at this proximity lose their conformational flexibility, which reduces the entropy leading to unfavorable positive change in free energy. Passing this adsorption barrier culminates in protein-NP stable immobilization, leading the participation of the protein in hard corona.

Engineering the surface chemistry of NPs basically could alter the E_{ads} and E_{des} as shown in **Figure 2.1C, D**. For instance, PEGylation is known to enhance the circulation half-life of NPs due to formation of a hydration layer, thus limiting the proteins accessibility to the surface of NPs [25]. Recent understandings indicate that PEG causes specific proteins to be formed around PEGylated NPs, leading to reduction of protein absorption [25]. Moreover, the PEG surface

density [26] as well as backfilling [27] are two vital NPs design variants that could be engineered to regulate the protein corona formation [28].

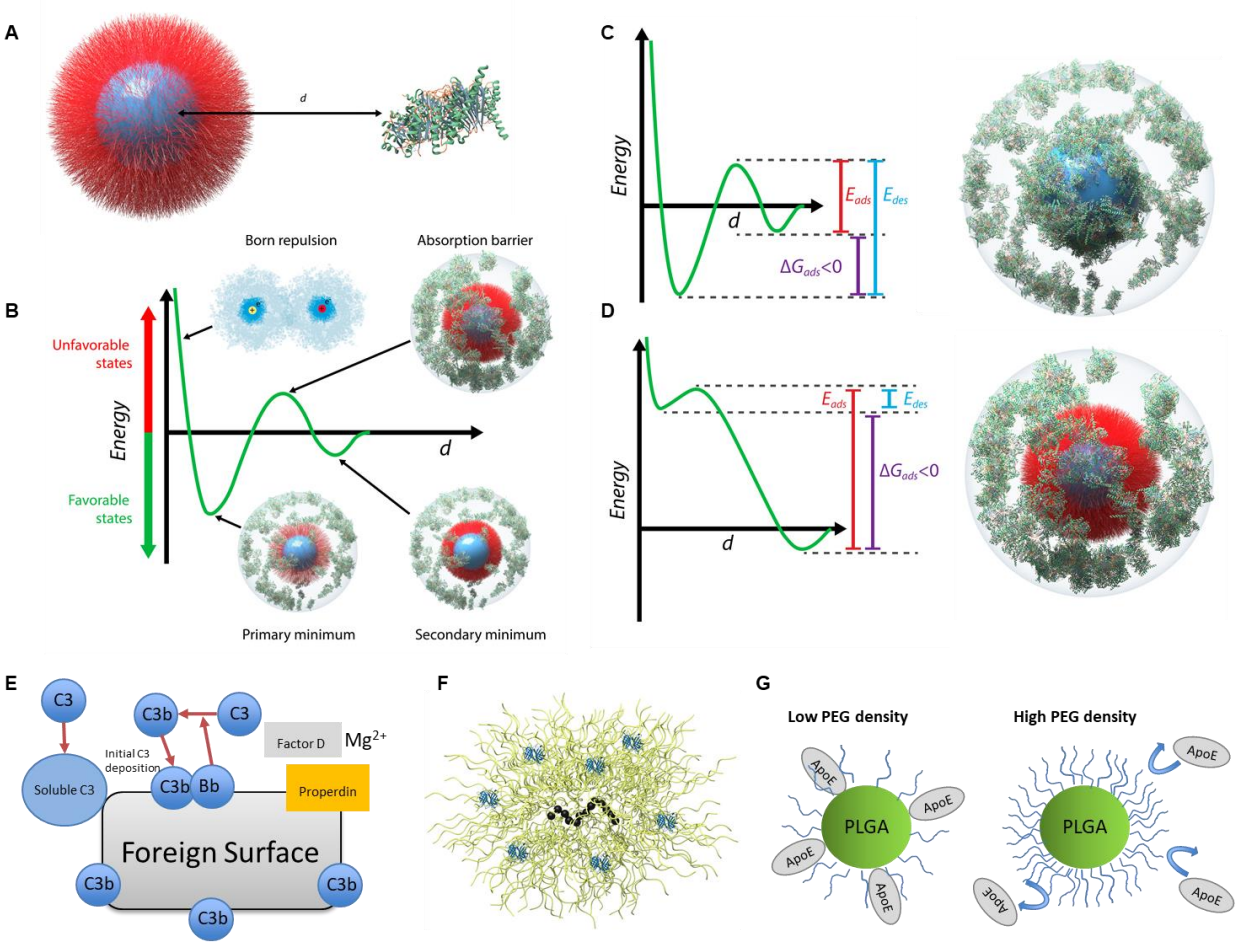

Figure 2.1. Thermodynamics behind protein corona. A) Schematic illustration of the distance "d" between NPs surface and protein nearest residue. **B)** Schematic plot of potential energy curve between a NP and a protein molecule. Negative $\Delta G_{adsorption}$ specifies attractive interactions, whereas the positive one indicates an unstable interaction with a net repulsive force. When the distance is far enough, the free energy is zero and no interaction occurs between protein and NP. As protein gets closer, free energy drops and approaches the secondary minimum. Further decrease in the distance leads proteins to lose conformational flexibility, reducing the entropy. Passing this adsorption barrier culminates in protein-NP stable immobilization, leading the protein to participation in hard corona. **C)** Free energy plot of a particle with a large primary energy well for adsorption and a minor barrier for protein adsorption, leading favorable NP-protein interaction. **D)** Free energy plot of a NP with a minor primary energy well and a high-energy barrier for protein adsorption, culminating in unfavorable NP-protein interaction. **E)** Scheme of complement alternative pathway (AP) activation and amplification on a foreign surface. Initially deposited C3b or C3(H_2O) requires factors B, D, properdin (P) and Mg^{2+} to form AP convertase, which activates additional C3 molecules, leading to amplification of C3b opsonization. **F)** Intercalating complement proteins into the dextran shell coated around iron oxide NPs. C3 complements intercalate into the dextran shell, forming covalent bonds with other proteins in the corona. **G)** In PEGylated PLGA NPs, PEG regulates the apolyproteinE adsorption, which acts as dysopsonic moiety.

In addition to PEGylation, some strategies have focused on endowing biomaterials surface with antifouling properties, including surface coating with poly(ethyl ethylene phosphate) [25]. Highly hydrated group at the biomaterial/body interface is the key to forbid biomaterials fouling. Noteworthy that biofouling initiates from the surface of foreign bodies through different cascades such as alternative pathway (**Figure 2.1E**). To possess anti-fouling properties, materials surface must possess charge neutrality in the scale comparable to proteins size i.e. angstrom-to-nanoscale [29]. Phosphatidylcholine [30], sulfobetaines [31], carboxybetaine [32], cysteine [33] are such functional groups, endowing NPs with a zwitterionic surface chemistry. Noteworthy that polyzwitterions are a class of materials, where alternative cations and anions have conformed a homogenous charge distribution in nanoscale, mimicking the innate charge conformation of proteins.

For the classical NP-polymer/core-shell structures, questions remained to be asked as whether the proteins bind around the shell, or it accommodates within the flexible network of the polymers. In case of dextran coated iron oxide NPs, C3 penetrates within the dextran shell an covalently links with amines and hydroxyls on the foreign surfaces to form ester or amide bonds [13] (**Figure 2.1F**). Interestingly, 90% of the C3 proteins were not bound to the dextran, but rather covalently conjugated with other proteins in both dextran coated iron oxide and PEGylated gold NPs. Similar with these observation, Pelaz et al. reported that if the presence of PEG on NPs surface is below saturation point, both low and high molecular weight proteins diffuse into the PEG shells [34]. Nonetheless, despite proteins can still adsorb onto NP surface, NP uptake by cells is still predominantly reduced. Mechanistic understanding of the protein corona in the PEGylated PLGA NPs have revealed that regardless of PEG density, deposition of complement

is too mild to influence their circulation time [26]. Similar observations have been reported on PEGylated liposomes [35].

Current strategies in targeted delivery are focused on engineering the protein corona to endow NPs with specific organotropic and cell specific targeting capability. For instance, apolipoproteins presence in the protein corona are essential for the targeting of hepatocytes with siRNA-loaded lipoplexes [36], and the amount of apoliproteins could be regulated by PEGylation amount [26] (**Figure 2.1G**). Noteworthy that this is only valid for shorter PEG molecules. For PEGs with higher Mw, proteins could penetrate within the structure even at high densities. This is known to be due to small radius-of-curvature effect [34]. Apoliproteins also alter the cell uptake pathway of liposomes from macropinocytosis to clathrin-dependent endocytosis [21]. One strategy to engineer protein corona is based on the selection of NPs material. For instance, the presence of cholesterol enhanced the binding of opsonins, whereas 1,2-dioleoyl-3-trimethylammonium propane preferentially bound apolipoproteins and vitronectin [37].

Another targeted delivery strategy relies on the selection of NP physical features in terms of size [15], surface charge [38], and surface chemistry [39]. **Figure 2.2** schematizes in broad terms the contribution of those physicochemical parameters on NPs' organ biodistribution. However, it has to be clarified that the biodistribution profile of NPs is not controlled only by their size and surface properties but is the result of an entanglement of different physicochemical parameters of NPs, as Xu and coworkers recently reported [40]. In addition to that, behind the NP-related factors, also the environmental ones have to be taken into account. While *in vitro* parameters like incubation conditions, serum percentage, ionic concentration, protein source have already been widely described [41], much attention has been given recently to the ones

related to the alterations of the plasma proteome. Both in physiologic and pathologic conditions, plasma proteome is very dynamic. In the former case, in healthy patients for instance, protein abundance may change based on age, gender, lifestyle, geographical origin [42]. In the latter case, different diseases are characterized by a different composition of the plasma proteome, hence the term personalized protein corona [43, 44].

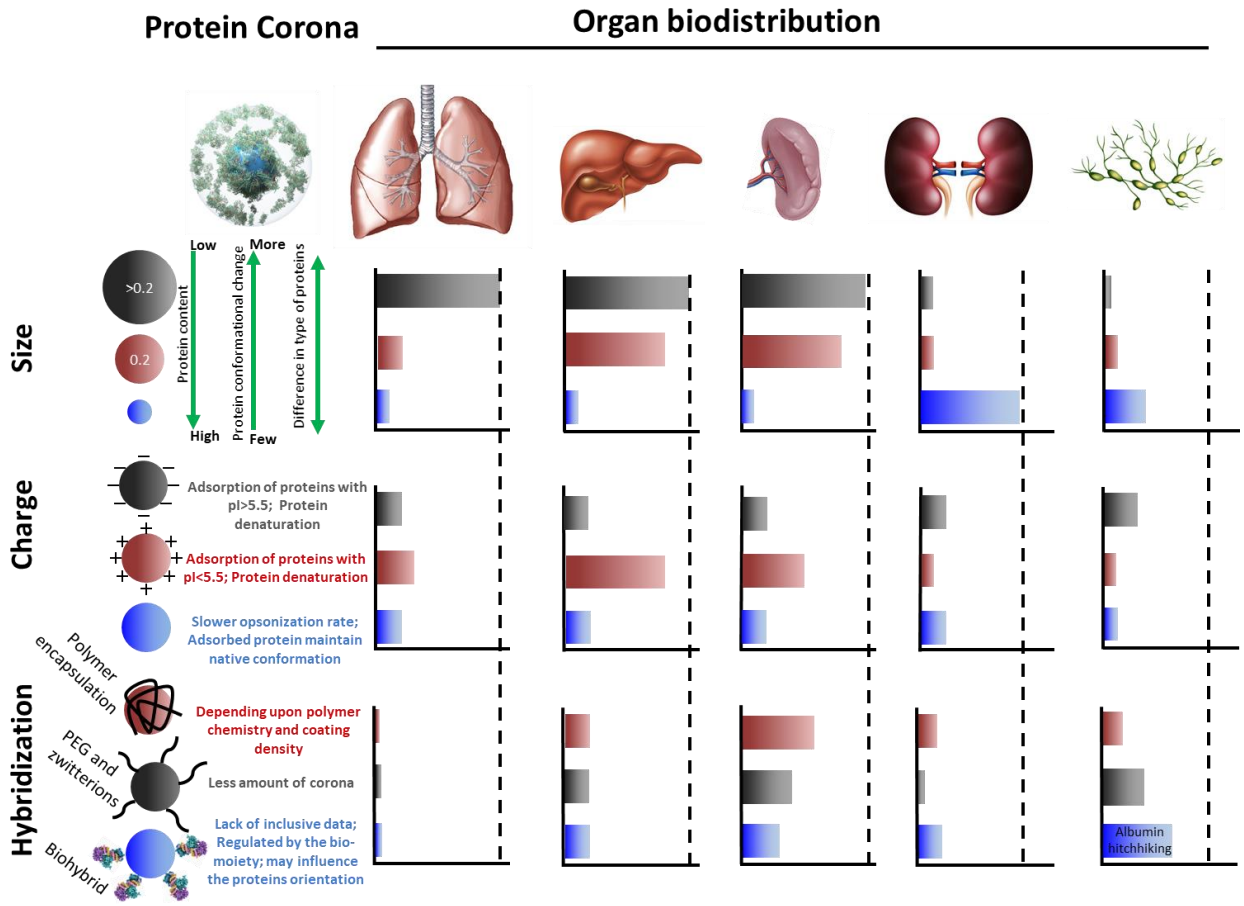

Figure 2.2. Size, surface charge, and surface chemistry are major deterministic aspects to regulate the biodistribution of injected NPs. Primarily, physicochemical properties influence the protein corona. Cationic NPs prefer to adsorb proteins with isoelectric points (pI) below 5.5 such as albumin, while anionic NPs enhance the adsorption of proteins with pI greater than 5.5 such as IgG. Larger NPs entrap into lung capillaries, while NPs with diameters less than 200 nm mostly end up in clearing organs such as kidney and spleen. Ultrasmall NPs (diameters less than 8 nm) extravasate through kidney nephrons. Based on sequential barriers, NPs could then accumulate in kidney or get cleared into urine. Surface charge also impacts the NPs biodistribution mainly through affecting the protein corona.

To summarize, two considerations arise. From one side, there is no direct and univocal relationship between NPs individual physicochemical properties and organ biodistribution. Surely, physicochemical parameters play a major role in the biological fate of NPs, since they also affect protein corona behavior, but they have to be considered in their totality, and not as individual properties. On the other side, individual alterations of the blood proteome, particularly if disease-related, have to be evaluated in the context of a personalized approach since they may affect the biological fate of NPs due to the variability of the protein corona composition, including protein conformation.

Formation of other biomolecule coronas

In addition to proteins, multiple biomolecules are present in the biofluids. While our understanding from protein corona has remarkably matured over the past decade, we lack deterministic understanding of the role of lipid-, glyco-, and other biomolecule- coronas on NPs behavior *in vivo*.

Blood lipids are transported by lipoprotein particles ranging from 8 to several hundreds of nanometers in diameter. At the core of these vehicles, triglycerides and cholesterol esters are surrounded by proteins and phospholipid monolayers. Early discussions on lipid coronas sparked by Hellstrand et al [45], where the surface area and hydrophobicity of NPs was found to influence the cholesterol and triglyceride amount in the lipid corona. More hydrophobic content on a NP leads to more lipid corona. As a matter of fact, to engineer the lipid corona, NP hydrophobicity was modulated by altering the ratio of N-isopropylacrylamide (NIPAM) to N-t-butylacrylamid (BAM) ratio in a NIPAM-BAM copolymer NPs [45]. Similar to this report, hydrophilicity was demonstrated to reduce the amount of lipid corona formation [46].

Over 50% of human proteins are estimated to be glycosylated [47]. This sparks a question as whether the glycans perform a task at bio-nano-interface. Monopoli et al argued that removing the glycans from the preformed protein coronas enhances the cell uptake, culminating in the generation of pro-inflammatory milieu by macrophages [48]. More research on glycan corona also would shed light on NPs corona formation, and their interaction with immune cells.

Mononuclear phagocyte system and NPs clearance

As soon as NPs come in contact with biological media such as blood, specific classes of protein form around them. The formed complex then becomes recognizable by MPS system [14]. The MPS consists of immune and architectural cells, located in 'clearing organs' such as the liver, spleen and bone marrow, with the main task of removing foreign material from the bloodstream. Recently, it has been shown that the protein quantity adsorbed at the surface of NPs determines sub-tissue sequestration of 'hard NPs' by MPS [49]. Quantity and signature of the adsorbed protein is regulated by physicochemical properties of NPs. For instance, cationic NPs are generally more susceptible to MPS clearance than neutral or negatively charged ones [50].

Kidney Kupffer cells are known to be the main cells to clear the injected NPs. In addition to the involvement of protein corona in the NP-Kupffer cell interaction, circulating NPs slow down by a factor of 1000 when they reach the liver. This led to increase the delay in NPs excretion towards central vein, enhancing the probability of interaction between Kupffer cells and NPs. Splenic macrophages are also critical players of MPS system. Splenic macrophages are located within the red pulp of spleen, where the blood flow slows down. However, their involvement in NPs clearance is not as pronounced as Kupffer cells likely due to less accessibility to NPs, and around 20-fold less access to cardiac output in comparison to liver [51].

Renal clearance

Kidney nephrons filter the blood circulation, where NPs could extravasate through the endothelium and secrete into urine. The secretion of NPs into urine is regulated by their size, shape and surface charge. First barrier for renal excretion is the fenestrated endothelium with transcellular holes of 60 to 80 nm, filled with glycocalyx (a >400 nm polysaccharide-rich layer existing on 30–40% of glomerular endothelial cells) [52]. Glycocalyx mechanically restricts the entrance of circulating plasma components to endothelial cell membranes via an interpenetrating structure and a negative charge. Next, the dense matrix of glomerular basement filters are limiting the renal excretion of NPs [53]. Next line of barrier is glomerular basement membrane composed of collagen IV, laminin, and proteoglycans. NPs accumulation in these barriers could be employed for the targeted delivery of nanomedicine to specific cell types in the kidney. Such strategies have been reviewed elsewhere [54].

Filtration slit residing between podocyte extensions with a physiologic pore size of 5 nm. NPs less than 6 nm are small enough to be freely filtered, irrespective of molecular charge [55]. Glomerular filtration of intermediate particles (between 6-8 nm) is dependent on charge interactions between them and the negative charges of the glomerular basement membrane, where positively charged particles are filtered more readily than same sized negatively charged particles. Particles greater than 8 nm do not undergo glomerular filtration. Noteworthy that when introduced into the body, NPs hydrodynamic diameter could be altered as high as 15 nm within seconds of circulation [56]. The dynamic nature of NPs size is regulated by their surface chemistry, where zwitterionic coatings limits the protein adsorption on NPs surface [56].

Physical Barriers

In addition to biological barriers, physical barriers also play pivotal role in the *in vivo* behavior of NPs. Size and shape, for example, have been shown to affect the interaction of NPs with the vascular endothelium. Spherical NPs travel far from blood vessel wall, which significantly reduces their interaction with endothelium. Lack of such interaction impedes both active and passive targeted deliveries. In targeting cancer tumors, one phenomenon that limits the penetration of NPs to the tumor site is the counteracting pressure known as interstitial fluid pressure (IFP). Since tumors possess a leaky vasculature, and the cell growth rate is higher than the normal cell near tumor, a pressure gradient forms. The pressure gradient impedes the absorption of NPs through trans-capillary mechanism [57].

Tight Epithelial and Endothelial Barriers

Blood vessels and lymphatic system within healthy tissues possess a monolayer of endothelial cells that could be continuous, fenestrated, or discontinuous. The continuous endothelium (in arteries, veins, and capillaries of skin, lungs, heart, brain and muscles) safeguards seamless diffusion of small molecules such as O_2 and nutrients but limiting the NPs transport into the tissue. Fenestrated endothelium (in endocrine and exocrine glands, gastrointestinal tract, kidney glomeruli, and a sub-group of renal tubules) also has a continuous basal membrane but comprises 50–60 nm wide transcellular channels. The discontinuous endothelium (in sinusoidal vascular beds of liver, spleen, and bone marrow) is associated with a poorly structured basal membrane with 100–200 nm fenestrations [58]. These variations are partly due to the back and forth communication between endothelial cells, pericytes, and parenchymal cells [59]. It should be noted that the junction permeability between endothelial cells is also regulated by the local inflammation at the target. In case of inflamed tissue, resident and/or recruited macrophages efficiently engulf entered NPs. With this mechanism, iron oxide

nanoparticles have been applied to image the macrophages within the inflamed pancreas in the Non-obese diabetic (NOD) mice and human [60-62]. More detailed discussions on tissue-cell barrier could be found in previous works [58, 63, 64]. Inspired by the negotiation capability of immune cells with inflamed vasculature to extravasate through inflamed endothelium, leuko-like hybrids NPs have been developed to target inflammation [5] and tumor [65].

Extracellular Matrix

Through transmitting a wealth of mechanical and chemical signals, the ECM plays a pivotal role in cells physiology such as migration, adhesion, proliferation, differentiation, and death. The extracellular matrix (ECM) comprises of structural proteins and glycosaminoglycans, including polysaccharides, proteoglycans, and glycoproteins that are tightly interpenetrated. ECM influences the entered NPs in three ways. First, when NPs pass the endothelial barrier and reach the ECM, they collide with matrix fibers and penetrate their 3D structure. Following by this step, NPs diffusion coefficient gets reduced owing to the restricted thermal motion of water molecules adjacent to the fibers (hydrodynamic interactions). Finally, electrostatic interactions with charged components of the ECM introduce an extra impediment for NPs diffusion [66]. For instance, dermatan/chondroitin sulfate or keratan sulfate chains tightly bind to leucine-rich proteoglycans, determining the alignment and spacing of collagen fibers. ECM rigidity is also a disease-specific quantity. The composition of ECM is different than normal tissues. Mechanical rigidity of the ECM in the tumors poses remarkable hindrance for NPs penetration, inducing premature drug release before reaching the tumor cells [67].

Biodistribution, clearance and toxicity of NPs

Due to the biological and physical barriers, only a fraction of administered NPs will end up in the desired target. Through investigating more than 230 published literatures from 2005 to 2015, Wilhelm and colleagues reported that irrespective of the shape of the nanovesicle, the tumor type, and targeting strategy, only a median of 0.7% of the administered dose on NPs will eventually accumulate in the tumor [68]. A follow-up question comes to mind that where the other 99% of the injected NPs end up? **Figure 2.2** schematically illustrates the organ biodistribution of NPs with different physicochemical properties in the major organs, where filtering organs such as kidney and spleen are the main destination for the injected NPs. Inspired by the biomolecules inherent distribution in the body, biohybrid strategies have been proposed to target desired cells/organs such as hepatocytes [36], lymph nodes [69], circulating tumor cells [70], and site of inflammation [5]. It should be noted that the method used to study the organ biodistribution of NPs could dramatically influence the results and specific attention must be paid in quantifying the biodistribution data. Liu et al observed a discrepancy in biodistribution results of NPs labeled with a fluorescent or a radioactive dye [71]. They reported that quantitative data from whole organs was influenced by absorption and scattering properties of the tissue. To overcome such discrepancies, researchers have developed novel analysis modalities such as laser ablation inductively coupled plasma mass spectroscopy (LA-ICP-MS) [72] as well as barcoded NPs [73, 74], and mass cytometry [75] for more accurate biodistribution quantifications (**Figure 2.3**).

The significant off-target accumulation of NPs not only implies their lack of efficiency, but also poses toxicity issues. NPs toxicity, in part, originates from their capability to elevate the oxidative stress mostly adjacent to their surface. Oxidative stress induces toxicity in a dose dependent manner, where low dose upregulates transcription of defense genes through

transcription factor nrf2, medium dose activates inflammation signaling through NFκB pathway, and high levels of oxidative stress activates apoptotic and necrosis pathways [76, 77].

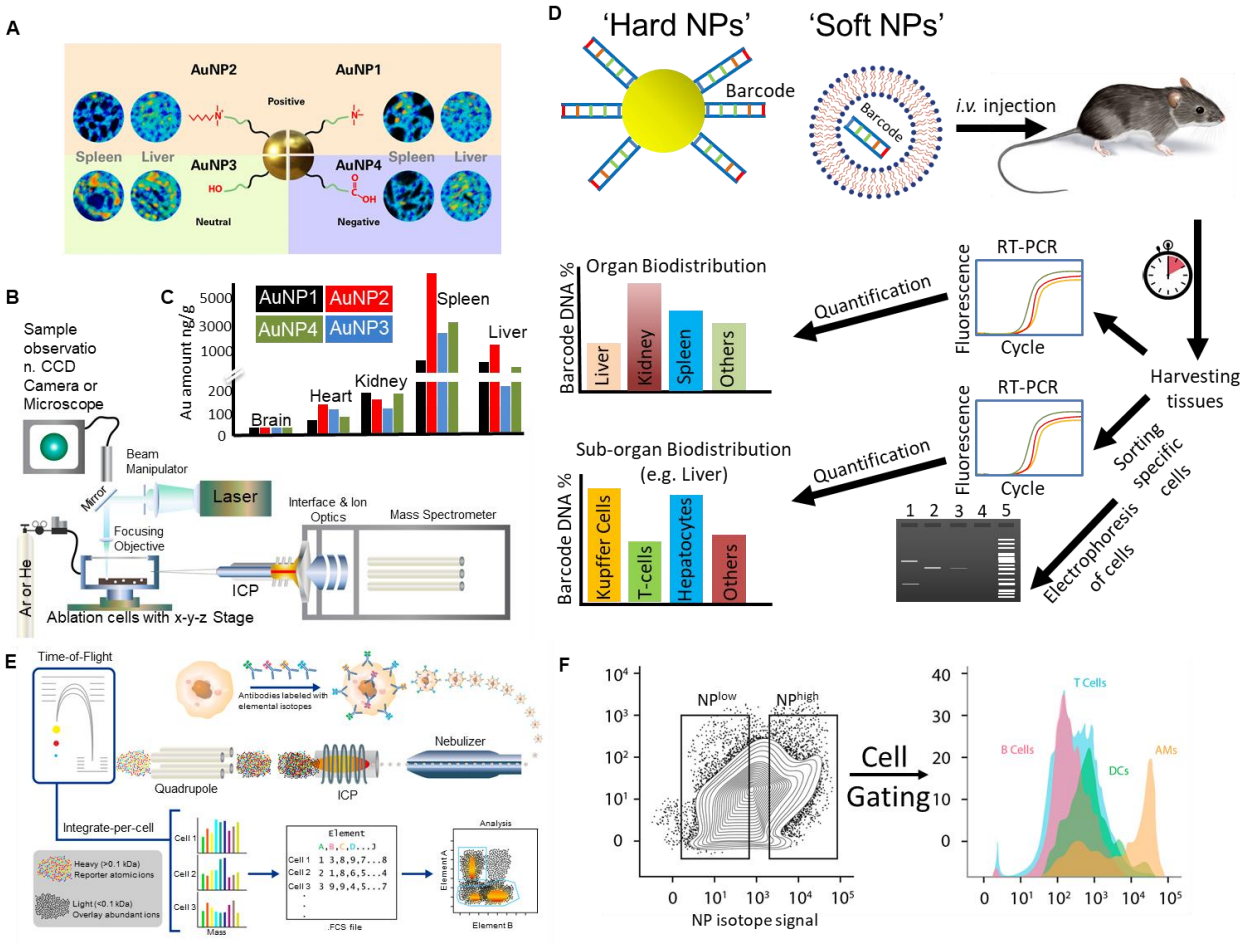

Figure 2.3. Emerging methods for quantification of NPs biodistribution. A) Design and surface chemistry of 4 AuNPs following by sub-organ imaging. **B)** Schematic of Laser ablation inductively coupled plasma mass spectroscopy (LA-ICP-MS) to analyze the organ and sub-organ biodistribution of NPs **C)** Schematic of quantitative analysis of NPs biodistribution using LA-ICP-MS. **D)** Schematic of organ and sub-organ biodistribution analyses using barcoded NPs. Barcodes could be used in both soft and hard NPs platform either through surface conjugation or encapsulation. Following by administration of barcoded NPs, desired tissues would be harvested and analyzed via RT-PCR to detect the barcodes. Fluorescent intensities will be then plotted for each organ to quantify the organ biodistribution. Alternatively, sub-organ biodistribution could be evaluated. Following by harvesting the tissues, each tissue could be sorted, and specific cell lines could go through RT-PCR. Using single cell extraction technologies each specific cell could be also analyzed for barcoded NPs presence using gel electrophoresis, in case the cell contains barcodes amount higher than limit of detection. Lanes of the schematic gel represent (1) Two separate barcodes (2) High expression (or multiple cells) with a barcode, (3) single cell with a barcode, (4) negative control (cell with no barcode NP), (5) DNA ladder. **E, F)** For detection of unlabeled organic NPs, a Mass Cytometry (a technique via merging time-of-flight ICP-MS with flow cytometry) offers detection in single cell level.

So far, the physicochemical properties are recognized to be the determinants of NPs organotropism and sub-organotropism [68, 72, 78, 79]. Using quantitative imaging based on LA-ICP-MS, Elci et al. found that while neutral NPs highly accumulate in white pulp and marginal zones of the spleen, charged ones home into red pulp zones [72] (**Figure** 2.**3A, B, C**). It should be noted that compared to common imaging techniques, such as TEM, confocal microscopy, and AFM, LA-ICP-MS imaging could provide accurate quantitative analyses on NPs biodistributions. This technique also could track NPs without additional physical property requirements, such as fluorescence, for detection.

Another emerging technology in detection of NPs biodistribution is to use a barcode labeling platform [73, 80]. In this approach, specific double-stranded DNA attaches to NPs. NPs distribution then could be quantified by measuring the DNA content in various resolutions including organs, tissues, or cells. **Figure 2.3D** demonstrates schematic of organ and sub-organ biodistribution analyses using barcoded NPs. Following by administration of barcoded NPs, desired tissues would be harvested and analyzed via RT-PCR to detect the barcodes. Fluorescent intensities will be then plotted for each organ to quantify the organ biodistribution. Alternatively, sub-organ biodistribution could be evaluated. Following by harvesting the tissues, each tissue could be sorted, and specific cell lines could go through RT-PCR. Using single cell extraction technologies each specific cell could be also analyzed for barcoded NPs presence using gel electrophoresis, in case the cell contains certain amounts of barcodes that are higher than limit of detection. In **Figure 2.3D**, Lanes of the schematic gel represent (1) Two separate barcodes (2) High expression (or multiple cells) with a barcode, (3) single cell with a barcode, (4) negative control (cell with no barcode NP), (5) DNA ladder.

Mass cytometry is also an alternative approach to quantitatively analyze sub-organ biodistribution of NPs (**Figure 2.3E**). This approach is a combination of time-of-flight ICP-MS with flow cytometry (**Figures 2.3E, F**). In this technique antibodies are tagged with heavy metal ion (rather than fluorochromes in classical flow cytometry). Time-of-flight mass spectrometry would then be analyzed and reported as readout. Considering the limited channels available on classical flow cytometry, mass cytometry allows for the combination of many more antibody detection in a single samples, without significant spillover between channels [18, 75]. Cells are then incubated with desired antibodies against antigens of interest. Nebulized cells then travel into an ICP, where covalent bonds are opened, and ions are liberated. Quadrupole then removes biological elements and enriches the heavy metal reporter ions to be then quantified by time-of-flight mass spectrometry Ion signals are then integrated on an individual cell basis. [81]

Overall, undesired biodistribution seems to be one of the hurdles in clinical translation of NPs. In this context, biodegradable and bioresorbable NPs offer an advantage of short-term accumulation in organs. Apart from synthetic NPs, biological and biohybrid NPs offer a new paradigm in term of efficacy and clearance. 100 billion cells turn over by human body every day mostly through apoptosis. As a result, apoptotic debris accumulate in various organs, creating inflammation. However, a phagocytic process known as programmed cell removal, or 'efferocytosis' has been evolved in human body to rapidly and efficiently clear these cells [82]. This naturally occurring clearance system in human body has inspired researchers to develop safe biohybrid NPs. For instance, red blood cells (RBCs) safely circulate in human body for 120 days after their differentiation. Their elastic and surface-marker properties led them to negotiate with capillaries and MPS. RBCs flow from the peri-follicular areas to the lumen of sinuses in the spleen. Alternatively, they also circulate in the splenic red pulp zones upstream of sinuses

outside conventional vessels without endothelial lining [83]. Biochemical integrity of RBCs is checked every 2 h (~1400 times before their clearance). They also negotiate with phagocytic systems not only in the splenic marginal zones but also with Kupffer cells in the kidney [84]. These properties have led the generation of a class of biohybrid NPs to treat cancer [85], metastasis [86], inflammation, and toxin neutralization [87].

Additional barriers and current biohybrid NPs for Gene Delivery

The presence of endogenous nucleases in vivo degrades the systemic administered bare nucleic acids. The half-life of plasmid DNA has been estimated to be ten minutes following systemic administration in mice [88]. Non-specific interaction between administered bare nucleic acids with cells they interact following their administration, have led the advent of nanocarrier vectors to deliver genomic materials. Moreover, cellular, endosomal and nuclear membranes not only perform as physical barriers for entrance of genomic materials, but also DNA, RNA and proteins cannot efficiently pass through these hydrophobic barriers. Beginning at the site of administration serum nucleases, including 3' exonuclease, initiate the degradation of the injected genomic material. Exonucleases degrade nucleic acids by cleaving the phosphate bonds between nucleotides, thus modification substitutes a sulfur atom for a non-bridging oxygen in the phosphate backbone, which reduces the ability of most nucleases to degrade this bond [89].

There are some gold-standard materials employed for gene delivery with multiple reviews have focused on viral and non-viral gene delivery platforms [90-93]. Zwitterionic lipids, for example, have been demonstrated to form a stable DNA capsule and can be administered with other formulations to enhance gene delivery *in vivo* [94, 95]. Cationic lipids and cationic polymers are other types of materials that could electrostatically immobilize to genomic materials, a phenomenon known as polyelectrolyte complexation. They also aid the

endosomal escape by a mechanism referred to as “proton sponge” or “buffer” [96, 97]. Efficiency of all these systems has been impaired by the unstabilizing influence of the *in vivo* environment. Presence of different biomolecules and high salt concentrations in biological environment reduces electrostatic repulsion between the positively charged complexes, making them susceptible to colloidal instability and aggregation in physiological fluids. Colloidal instability as well as the formation of protein corona in the blood encourages rapid clearance of NPs by MPS and even could cause embolism in lung capillaries [98]. Considering effective communication between emerging biohybrid NPs and *in vivo* immunity, as well as current developments in genomic materials delivery including CRISPR/CAS9, future biohybrid nanoplatforms for gene editing are expected.

During evolution, biological systems have engineered their components to function in a complex biotic environment. For instance, viruses protect their sensitive genetic moiety through encapsulating them in their capsids. Inspired by this, various classes of viral-mimicking biohybrid NPs have been introduced for genome delivery [99, 100]. Understanding the structure of viruses inspired many efforts to engineer protein containers [101] and to synthesize nucleic acid-encapsulating polypeptides [102]. It has recently been shown that protein assemblies could be re-engineered to encapsulate their own genome [103]. This was achieved by introducing additional cationic residues or by genetically fusing RNA binding peptide to the interior of the protein capsule.

Negotiators with biological barriers

The challenge of targeted delivery *in vivo* is a multi-dimensional issue ranging from materials perspective to immune system and organ physiology. From materials perspective, although numerous formulations have been designed for therapeutic NPs, their *in vivo* efficacy is

impaired due to their lack of negotiation capability with body's immunology. Evolution through thousands of years has put complicated immunological barriers to protect our body against foreign invaders, including NPs. The activation or deactivation of immune cells is strictly regulated by negotiation between cells as well as cells with biomolecules. In this context, mimicking these negotiations and leveraging them into nanomedicine design offers a promising strategy for delivery vehicles. In this section, our current understanding from biological negotiators (also known as biologics) in cancer and autoimmunity as well as available biomimetic design to cross-talk with endogenous immune cells will be discussed.

Immune-regulator proteins

The role of proteins in biological negotiations, and the capability of innate immunity members to take up NPs have sparked recent speculations on negotiator peptides encapsulations. Negotiator proteins turn on or off various downstream signaling cascades after binding to their specific ligands.

CD47

CD47 is a glycoprotein and a self-marker expressed in mice, human and other mammals [104]. The crosstalk between the extracellular domain of CD47 and signal regulatory protein-α (SIRP-α; also known as CD172a) expressed on phagocytes is a key regulator in cells phagocytosis. This negotiation leads to phosphorylation of immunoreceptor tyrosine-based inhibition motifs on SIRP-α's cytoplasmic tail and the recruitment of Src homology phosphatase-1 and -2 (SHP-1 and SHP-2 phosphatases). This recruitment is considered to block phagocytosis by inhibiting myosin-IIA accumulation at the phagocytic synapse [105, 106]. When decorated with CD47, polystyrene beads demonstrate less uptake by macrophages [104, 106]. In

comparison with M0 and M2 polarizations, M2 macrophage has recently reported to demonstrate significant reduction in uptake of CD47-coated polystyrene NPs [107].

CD47 also is one of the key regulators in atherosclerosis and cancer. Overexpression of CD47 in the site of atherosclerosis impairs the efferocytosis (programmed cell removal), which leads to atherosclerotic cardiovascular disease [82]. CD47 is also over-expressed on cancer cells, and anti-CD47 mAbs have shown efficacy in xenograft human cancers growing in immunodeficient mice. Leukemia, lymphoma, multiple myeloma as well as solid tumors including breast, colon, prostate, bladder cancers and sarcoma are among the cancer models in studying the efficacy of anti-CD47 mAbs [105, 108-110]. Recently, Gholamin *et al*. engineered a humanized antibody to block the CD47 signaling. They investigated the efficacy of this antibody in patient-derived xenograft models of a variety of pediatric brain tumors, including group 3 medulloblastoma (primary and metastatic), atypical teratoid rhabdoid tumor, primitive neuroectodermal tumor, pediatric glioblastoma, and diffuse intrinsic pontine glioma. The treatment was successful in inhibiting CD47, killing tumor cells by induction of phagocytosis, and extending the animals' survival, all with minimal toxic effects on normal human neural cells both in vitro and in vivo [111]. Owing to negotiation with MPS and longer systemic circulation, CD47-coated biohybrid NPs loaded with chemotherapeutic drugs demonstrated higher degree of intratumoural accumulation and a superior therapeutic benefit compared with that of bare-coated NPs [104]. Theoretically, blocking the CD47 or its ligand SIRP-α on myeloid cells must result is same effect in terms of cancer treatment. To test this hypothesis, Ring et al. developed a humanized anti-SIRP-α antibody and demonstrated that it enhances macrophages and neutrophils activity against tumor cells [112]. Future biohybrid NPs based on CD47/ SIRP-α axis are expected in the context of cancer and atherosclerosis.

On the flip side of cancer, it is shown that blocking CD47 with CD47-Fc fusion protein is an effective strategy in treatment of experimental autoimmune encephalomyelitis (EAE) model, a mouse model of multiple sclerosis [113]. CD47 deficiency inhibits the degradation of iNOS within macrophage proteasomes, elevating the production of nitric oxide. This leads to reduction in migration related chemokine receptors on $CD47^{-/-}$ Th17 cells, which inhibits their infiltration into the central nervous system.

Through negotiations led by CD47, NPs could interact with the body's environment. Owing to the nature of NPs preparation, adjusting the protein density and orientation on the NPs surface is a challenging task. These could severely impede the biological functions associated with CD47 protein [114]. Inspired by the inherently correct orientation of CD47 on the surface of RBCs, top-down approaches could be implemented to fabricate CD47 based biohybrid NPs.

Programmed cell death protein 1

Programmed cell death protein 1 (PD-1; also known as CD274) is an immune checkpoint receptor that is upregulated on activated T cells to induce immune tolerance. Tumor cells often overexpress the ligand for PD-1 (PD-L1), which facilitates their escape from the immune system. Antibodies designed to block the PD-1/PD-L1 communication have demonstrated clinical efficacy in patients with a variety of cancers, including melanoma, colorectal cancer, non-small-cell lung cancer and Hodgkin's lymphoma [115-118]. The main mechanism of PD-1/PD-L1 blockade in cancer therapy is known to be through T cells. However, it was recently demonstrated that tumor associated macrophages in both mice and human express PD-1, where its expression rises over time in mouse models of cancer and with progression of cancer stage in primary human cancers [119]. Targeted delivery of a TLR7/8 agonist to PD-1-expressing T cells was also demonstrated to recruit lymphocytes to non-inflamed tumors

[120]. Inspired by the capability of platelets to home into inflamed areas, anti-PD-L1 decorated platelets were found to accumulate 9-fold higher around the surgical wounds in comparison to monoclonal anti-PD-L1 controls [70]. Recently, it was demonstrated that metastatic melanomas release extracellular vesicles that express PD-L1 on their surface. Interestingly, IFNγ stimulation enhanced the PD-L1expression, suppressing the function of cytotoxic T cells which facilitated the growth of tumor [121].

On other side of cancer, an interesting question comes to mind as whether the expression of PD-1 could be regulated in autoimmunity, since the cross-link of PD-L1/PD-1 inhibits T-cell activation and favors their exhaustion/apoptosis. PLGA NPs loaded with mycophenolic acid immunosuppressant were demonstrated to upregulate the PD-L1 expression on dendritic cells, leading to reduced capability in priming T cells [122]. Nasr et al. demonstrated that hematopoietic stem cells (HSCs) in NOD mice defectively express PD-L1 [123]. Based on the fact that mice deficient in PD-1/PD-L1 expression develop accelerated Type 1 Diabetes (T1D) [124], they further showed that genetically- or pharmacologically-engineered HSCs to express PD-L1 could abrogate autoimmunity and revert hyperglycemia. Another question is whether blocking the immune checkpoints breach the tolerance and enable the pathological T cells to react with self-antigen? In fact, some autoimmune endocrinopathies have been reported in trials involving anti-PDL-1 and anti-CTLA-4 monoclonal antibodies [125, 126], including autoimmune diabetes [127].

Cytotoxic T lymphocyte protein 4

Cytotoxic T lymphocyte protein 4 (CTLA4) is a transmembrane receptor protein which tunes the co-stimulatory signals in T-cell activations. Similar to PD1, expression of CTLA4 is

upregulated upon T cell activation, and ligation of CTLA4 to CD28, its respective protein, downregulates the T cell activation [128].

Many other proteins such as FASL or TGFβ are also capable of negotiating with immune cascades. It has been shown, for example, that microgels presenting FasL enhance the outcome of islet transplantation through upregulation of $CD4^+CD25^+FoxP3^+$ regulatory T cells (Tregs) [129]. TGFβ plays a vital role in multiple cellular communications from development to pathogenesis. TGFβ is a major mediator in immunosuppression, however systemic administration of TGFβR1 inhibitors creates the toxicity owing to interference with other essential pathways in the body [130]. To develop a T cell activation by targeted delivery, SD-208 (TGFβR1 inhibitor) encapsulated in PLGA NPs was demonstrated to restore the function of effector T cells [120]. Moreover, incorporation of TGFβ onto the antigen loaded NPs could enhance the efficacy in lower dosage [131].

Disease-specific peptides

Another strategy is to induce tolerance through hybridizing diseased peptides on the surface of NPs. For instance, myelin-coupled PLGA NPs have shown to reduce the immune cell infiltration (lymphocytes APCs, and microglia) and decrease inflammatory cytokines (IFN-γ and IL17A) production in the central nervous system [132]. Further investigation on the downstream events revealed that their biohybrid NPs downregulates the expression of co-stimulatory molecules such as CD86, CD80, CD40, and PD-L1 on the surface of APCs [133].

NPs could also be designed to selectively suppress disease-causing autoreactive T cells without weakening the whole immune system, which is an emerging technology to treat autoimmunity. In T1D, for example, $CD8^+$ T cells recognize autoantigenic peptides, including epitopes from islet-specific glucose-6-phosphatase catalytic subunit-related protein ($IGRP_{206–}$

$_{214}$) on the major histocompatibility complex (MHC) class I molecules [134]. NPs coated with β-cell-specific peptide pMHC-I could expand cognate memory autoreactive $CD8^+$ T cells that arise from naive T-cell precursors to therapeutic levels. Within the same line, NPs coated with β-cell-specific peptide pMHC-II has been demonstrated to generate and expand antigen-specific regulatory $CD4^+$ T cell type 1 cells, culminating in resolution of induced autoimmunity [135] (**Figure 2.4 A**). EAE relevant immunodominant myelin proteolipid protein $PLP_{139–151}$ epitope coated on NPs (but not NPs coupled with an irrelevant ovalbumin peptide, $OVA_{323–339}$) also have shown induction of central tolerance through reduction in $CD45^+$ leukocytes and $CD4^+$ T cells infiltration to central nervous system [120].

In utero administration of Myelin Oligodendrocyte Glycoprotein (35-55) encapsulated in NPs was demonstrated to eliminate the $CD4^+$ $Tetramer^+$ cells in the spine of EAE mice, demonstrating the induction of central tolerance [136].

Lipids and Glycans

Various lipid particles present in human body, which are composed of apolipoproteins, phospholipids, cholesterol, cholesterol esters, and triglycerides. Lipoproteins are known to be efficient in targeting the hepatocytes *in vivo* [36, 137]. In fact, triglycerides which are the main product of lipogenesis by liver, form a specific package with other lipids and apoliproteins known as very low density lipoproteins (VLDL) [138]. Inspired by this, Dong et al. synthesized 103 lipoamino acid, lipopeptide, and lipopolypeptide derivatives to find the optimum delivery formulation to target the hepatocytes [36]. They utilized high throughput screening method to evaluate their capability to silence hepatic genes in mice, and found that when reacted with 1,2-epoxydodecane, a specific lysine-based dipeptide is the “best-hit” material to target hepatocytes.

They found that ApoliproteinE hybridized onto their lipoprotein NPs not only enhances the cell uptake, but also improves the endosomal escape of siRNA into cytosol.

Lipids participate in the generation of prostaglandins and leukotrienes, which are important inflammation mediators. This topic has been reviewed extensively elsewhere [139]. Lipids that accumulate in cancer associated DCs contain oxidatively truncated electrophilic portions, which covalently interact with major stress-induced peptide chaperone heat shock protein 70. This prevents trafficking of pMHC from the phagosome/lysosome to the cell surface, leading to ineffective cross-talk between DCs and antigen-specific T cells [140].

Glycans decorate surfaces of cells, tissues and viruses. They play multifaceted roles in interactions between the viruses and host organisms that critically govern viral pathogenesis [141].

Mammalian cell membrane- and pathogen-derived negotiators

Biohybrid NPs could be fabricated through taking advantage of biological materials including mammalian cells and pathogens that nature has already designed for specific biological communications. This is not only an exciting approach for successful negotiations between NPs and patients' immune system, but also provides strong foundations for personalized medicine. Fore detailed discussion readers are referred to [6, 99, 100, 142].

Thanks to their immune avoidance and lysosomal escape, viral based NPs have been employed in gene therapy and CRISPR/CAS9 delivery. Safety issues and limited scalability of viral vectors have sparked motivations in developing biohybrid NPs, in which liposomes are incorporated with viral peptides with structure and pH-responsive membrane-destabilizing activity [143].

Similar to disease peptide-NP hybrids discussed earlier in the context of autoimmunity, cancer cell membrane could also be administered into the patients and elicit their own antitumor

immunity. To enhance the antigen presentation, CpG adjuvants incorporated into PLGA NPs followed by cancer cell membrane coating. Combined with immune checkpoint inhibitors, such formulation prevented the tumor occurrence in 86% of mice 150 d following by challenge with the tumor cells [144].

Membranes of RBCs, leukocyte, platelets, mesenchymal stem cells have also been introduced as potential biological moieties to treat cancer, metastasis, inflammation, and biological threads [145].

Innate immunity negotiation

As innate immunity members, APCs are responsible not only as an initial non-specific line of defense, but also to present the antigens derived from self or non-self sources. This capability has made them intriguing targets in autoimmunity [146] and cancer [147]. Here, we review the cross-talk of some innate immunity cells, and possible inspirations for designing biohybrid NPs.

The most abundant leukocyte of innate immunity is macrophage which plays critical roles in innate immunity and inflammation and perform important tasks in development and hemeostasis of both healthy and repairing tissues. Classically, it was believed that diverse developmental origins of macrophages are responsible for the heterogeneity. Current view, however, suggests local niche determines the macrophage function [148]. Zangane et al. demonstrated that dextran coated iron oxide NPs reprogram the tumor associated macrophages to gain inflammatory polarization, where administration of ferumoxytol with tumour xenografts in mice suppressed tumour growth and prohibited metastasis [147]. It should be noted that

proinflammatory macrophages release hydrogen peroxides, provoking iron to release hydroxyl radical via Fenton reaction [77, 149].

Physicochemical characteristics of NPs could be employed to reprogram macrophages. For instance, Polystyrene NPs with surface carboxyl-(PS-COOH) and amino-(PS-NH_2) groups could strongly skew the M2 macrophage polarization without affecting M1 markers [150]. Incorporation of signaling proteins such as CD200 with NPs also could influence the macrophages polarization [151].

Negotiations in cell level are mainly regulated through surface proteins. Therefore, incorporation of cell-surface molecules could endow NPs with negotiation capability via biological environment. Intercellular adhesion molecule-1 is over-expressed transmembrane glycoprotein in tumor vasculature, which is involved in leukocyte adhesion through β2 integrin molecules [152]. With the same rational, incorporation of macrophage-1 antigen on the surface of porous silicon NPs has led them to accumulate in the tumor site [65].

Adaptive immunity negotiation

Through recognizing or failure in recognition of various epitopes, adaptive immunity plays a critical role in autoimmunity or cancer. Biohybrid NPs to reprogram T cells towards regulatory [135] or effector phenotype [96] are emerging approaches to fight against autoimmunity and cancer. For instance, systemic administration of NPs coated with T1D-relevant pMHC class I complexes could blunt the progression of T1D by expanding subsets of $CD8^+$ T cells with regulatory potential but not conventional memory-like phenotype [153]. With the same rationale, NPs coated with pMHCII complexes relevant to the autoimmune disease have shown to expand the antigen-specific regulatory CD4+ T-cells [135]. The topic has been

reviewed extensively [1, 154-158]. We aim to elaborate on the physicochemical aspects of NPs towards successful negotiation with T cells as well as the proposed mechanisms in NPs reprogramming T cells in cancer and autoimmunity.

One critical aspect on designing NPs for T cell stimulation is the density of antigens, which generally designed on NPs surface. For instance, it was demonstrated that peptide MHC complex presentation on the surface of iron oxide NPs has a valency threshold between 9-11 for agonist activity [159].

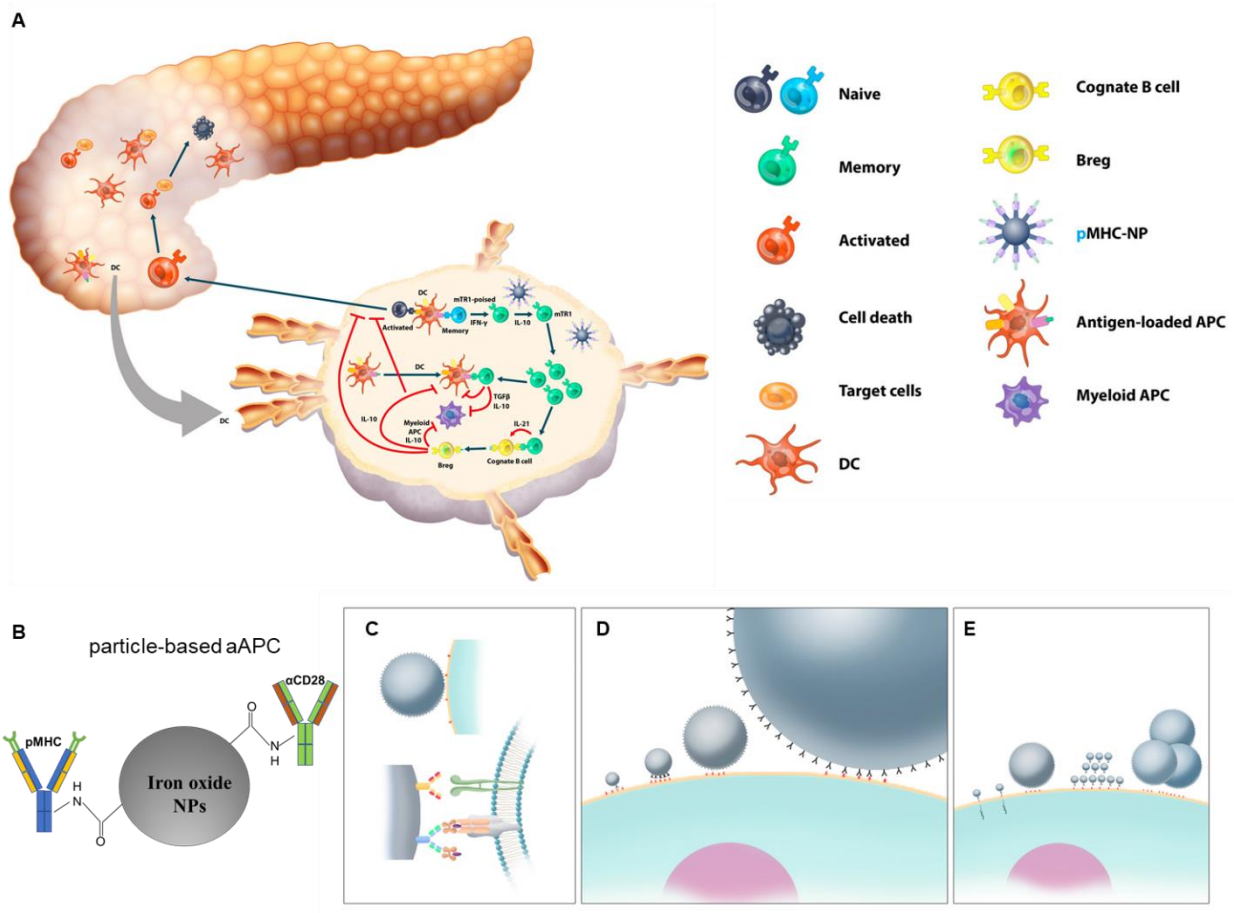

Figure 2.4. Schematic showing interaction between particle-based aAPC and cognate antigen-specific T cell. A) pMHCII-coated NPs (pMHC–NP, lacking costimulatory molecules) promote the differentiation of disease-primed (antigen-experienced) IFNγ-producing $CD4^+$ T_H1-cells into memory T_R1-like $CD4^+$ T cells followed by systemic expansion. This differentiation process (but not the subsequent expansion) requires both IFNγ and IL-10, whereas IL-27 is dispensable. The pMHC–NP-expanded (mono-specific) autoreactive T_R1-like $CD4^+$ T cells then suppress other autoreactive T-cell responses by secreting IL-21, IL-10 and TGF-β, which act on local APCs (B cells, $CD11c^+$ and $CD11b^+$ cells) that have captured the cognate autoantigen

and thus present cognate pMHCII complexes to the expanded T_R1-like cells. This interaction inhibits the proinflammatory function of the targeted APCs and blocks their ability to present other pMHC class I and class II complexes to non-pMHC–NP-cognate autoreactive T-cell specificities (note that the local APCs uptake both cognate and non-cognate autoantigens shed into the milieu simultaneously). Suppression of antigen-presentation requires IL-10 and TGF-β but not IFNγ or IL-21. Furthermore, cognate interactions between the pMHC–NP-expanded T_R1 $CD4^+$ T cells and autoreactive B cells specific for the cognate autoantigen (able to display the cognate pMHCII complex on the surface) promotes their differentiation into B_{reg} cells in an IL-21-dependent manner, which contribute to promote local immunosuppression, likely by secreting IL-10. Suppression of antigen presentation selectively targets APCs displaying the cognate pMHC, but as local APCs that capture the cognate autoantigen also capture other autoantigens simultaneously, the autoregulatory $CD4^+$ T cells expanded by pMHC–NPs blunt the presentation of other autoantigenic pMHC complexes to a broad range of autoreactive T cells. This suppression is disease-specific and self-limiting. Stimulation is mediated through two signals **(B). C)** Signal 1 is antigen-specific and is between peptide loaded MHC-Ig (pMHC) and cognate TCR. Signal 2 is a costimulatory signal mediated between the binding of anti-CD28 and CD28 ligand on the T cell. **D)** Schematic depicting relative sizes and ligand densities of aAPCs to a T cell. Scale bar = 500 nm. **E)** Schematic depicting hypothesis that saturating the T cell with 50 nm aAPCs is needed for the same nano-island cluster-based activation as lower concentration larger 300 nm particles (600 nm aAPCs are depicted).

Similar results have been reported, where the peptide-MHC density of approximately 112 ± 28 molecules/μm^2 was identified as a threshold for T cell activation [160]. However, if the size of NPs is below a certain threshold, even saturating doses of ligand would not initiate a T cell response. Hickey et al. studied the effect of NPs size and antigen density on the Treg stimulation [161] (**Figure 2.4**). Their designed biohybrid NP served as an artificial antigen presenting cell (aAPCs) through dual-signal stimulation of CD28 and pMHC (**Figure 2.4B, C**). They also demonstrated that saturating the T cell with multiple 50 nm aAPCs is needed for T cell constructive stimulation. Interestingly, larger NPs (300 and 600 nm) could initiate the stimulation at lower concentrations (**Figure 2.4D, E**). However, providing the sequential biological barriers that NPs face during their *in vivo* lifetime, NPs size are generally accepted to have diameters less than 200 nm.

Methods to hybridize biological and synthetic materials

Biohybridization of synthetic and biological materials could be done via bio-orthogonal chemistries [162], bio-interfering chemistries [163], extrusion based techniques[164], and microfluidics [165].

As opposed to bio-interfering chemistries that employs side chains of the canonical and proteogenic amino acids (**Figure 2.5A, B**), bio-orthogonal chemical reactions are defined as reactions that do not interfere with biological processes (**Fig. 5 C, D, F**). The motivation for bio-orthogonal chemistries stem from generally unknown consequences of manipulating the endogenous surface biomolecules on cells. In bio-orthogonal chemistries the cross-linking between NPs and biological moieties (such as proteins on cell surface) occurs on exogenous sites introduced on the cells by manipulations.

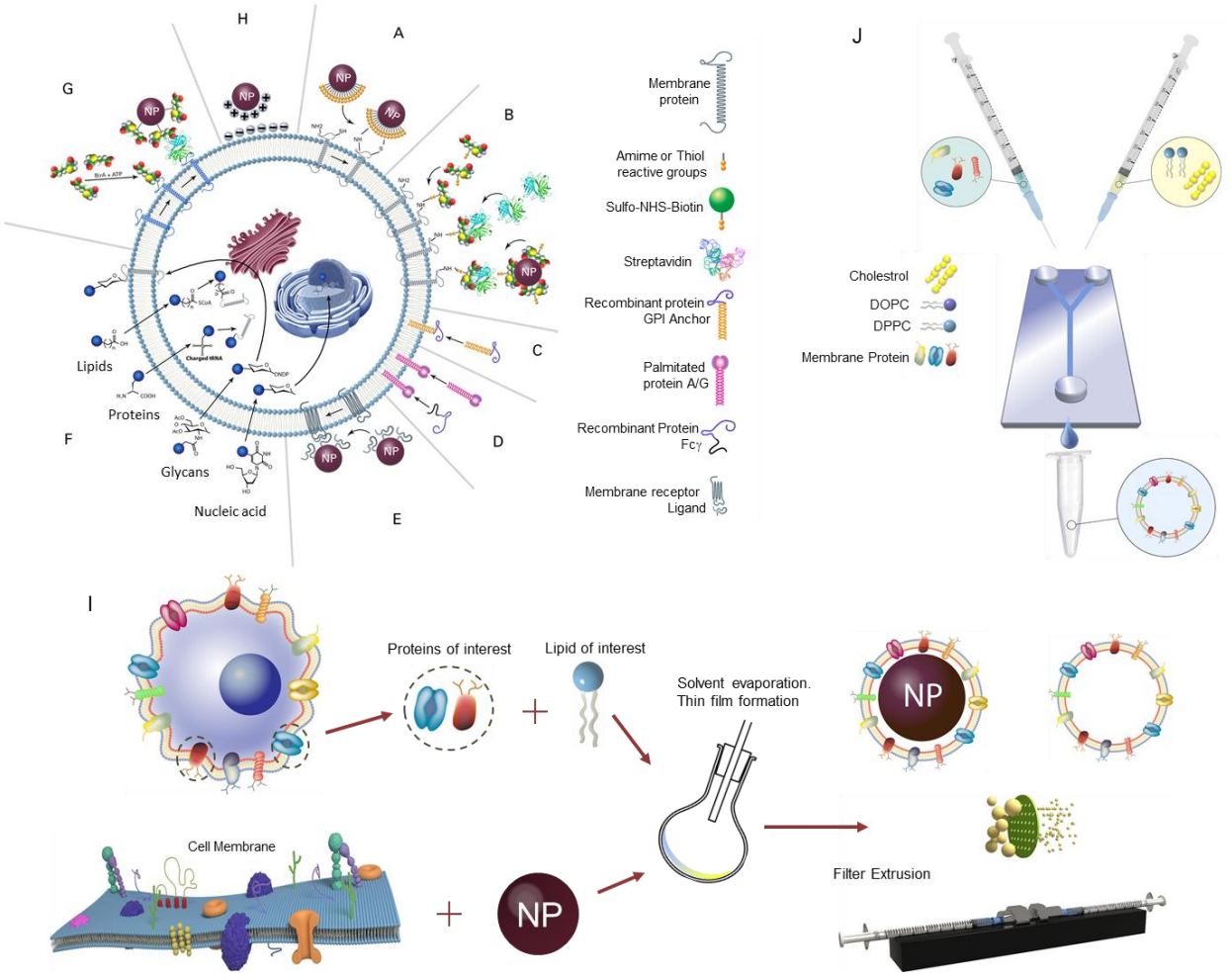

Figure 2.5. Schematics of some bioengineering approaches to fabricate biohybrid NPs with mammalian cells. A) Direct conjugation of functionalized NPs to covalently bond to endogenous amine ($-NH_2$) or thiol ($-SH$) groups of cell membrane proteins. Bio-orthogonal chemistries provide a non-interfering p. *Bioorthogonal reactions of aldehydes/ketones.* Aldehydes and ketones can condense with aminooxy or hydrazide compounds to form oxime or hydrazone linkages. *Bioorthogonal cycloadditions of azides and alkynes to form triazoles.* Cu-I activates terminal alkynes to go through cycloaddition with azides

under physiological conditions. In addition, cyclo-octynes react with azides through a strain-promoted cyclo-addition. **B)** Covalent conjugation of biotin anchors to membrane proteins by reacting *N*-Hydroxysuccinimide (NHS)-activated biotin with primary amine groups on membrane proteins, followed by streptavidin-biotin attachment of NPs. **C)** Exogenous insertion of recombinant glycoinositol phospholipids (GPI)-anchored proteins into the exterior membrane leaflet **D)** Insertion of exogenous palmitate-conjugated protein A (or G) onto the cell membrane to immobilize antibodies or recombinant Fcγ-fusion proteins. **E)** Anchoring ligand-functionalized NPs to membrane receptors naturally present on the cell surface. **F)** Metabolic labeling of surface glycans, proteins, lipids, and nucleic acids through hitch hiking the biosynthesis of unnatural moieties containing favorable functional groups (generally bio-orthogonal groups), which serve as reactive sites for subsequent conjugation of NPs and is absent in human genome. **G)** Targeting NPs to specific surface proteins genetically fused to BirA (biotinylation enzyme acceptor peptide). **H)** Nonspecific electrostatic adsorption of cationic NPs to the negatively charged cell membrane, generally originate from sialic acid. **I)** Whole cell membrane, or signature proteins could be hybridized with NPs using extrusion. **J)** Microfluidics offers a robust tool for NPs synthesis in a reproducible fashion. Biohybrid NPs could be manufactured using this technique.

While the topic has been extensively reviewed elsewhere [162, 166], we are providing some examples here. For instance, in metabolic labeling, metabolites are pre-engineered to possess desired functionalities. Upon hitch-hiking the biosynthesis, the engineered metabolite would be expressed on the cell, offering a possibility for specific cell labeling (**Figure 2.5F**) [167, 168]. In an analogous manner, genetically fused surface proteins to BirA (biotinylation enzyme acceptor peptide) introduce additional sections, making NPs capable of binding to specific surface proteins (**Figure 2.5G**). Apart from covalent cross-linking methods, electrostatic interactions also could be employed to create bonding between cationic NPs and negatively charged cell surfaces (**Figure 2.5H**) [169]. Another method of non-covalent bonding is the anchoring of ligand-functionalized NPs to membrane receptors naturally present on the cell surface (**Figure 2.5E**), which may or may not be bio-interfering.

Inspired by the functional potentials of cells in our body, efforts have been directed to employ key players of such functions in nano-formulations to specific targets such as inflamed tissue [170] or a tumor tissue [65]. Such hybridization could be by extraction of key biomolecule negotiators or whole cell membrane (**Figure 2.5I**). These components as well as desired

synthetic NPs are then hybridized using filter extrusion (**Figure 2.5I**). An emerging approach for biohybridization is based on microfluidics which offers a robust tool for NPs synthesis in a reproducible fashion (**Figure 2.5J**) [165].

Biohybrid NPs potential in personalized medicine

From Personalized Medicine to Personalized Nanomedicine

The rapid development of high-throughput 'omics' technologies, including genomics, proteomics, transcriptomics, metabolomics, autoantibody-omics, opened the way for a new challenge in medicine: i.e., the personalized or precision medicine [171]. Personalized medicine consists in the tailoring of either the diagnosis, treatment or prevention of a disease based on the unique genetic profile of a patient. It results in the shift from a 'one-size-fits-all' approach, where all patients that are diagnosed with the same disease will receive the same treatment, to a 'personalized' approach, where a specific treatment is designed for a specific patient or group of patients [172]. Such an individualized approach aims at overcoming the limitations related to the conventional symptoms-oriented diagnosis and treatment of a disease, which include: i) focus on terminal symptoms, with low or no attention to risk factors; ii) broad description of a disease, without discriminating between diseases that may have similar symptoms but different pathophysiology; iii) lack of attention to the underlying mechanisms of the symptoms; and iv) use of common therapeutic targets without taking into consideration the heterogeneity and complexity of pathophysiologic determinants of specific diseases, i.e., tumor microenvironment for cancer diseases.

Nanomedicine, i.e., the application of nanotechnologies, as diagnostic and/or therapeutic tool, to achieve advances in healthcare by exploiting the more advantageous chemical, biological and physical properties of materials at the nanoscale, offered several solutions to overcome some of these limitations [6]. The development of nanotechnology introduced several advantages in

medicine, such as the possibility to i) overcome the solubility issues of hydrophobic actives, especially anti-cancer drugs, ii) increase the physicochemical stability of molecules sensitive to light, enzyme degradation, acid/basic degradation, iii) encapsulate hydrophobic, hydrophilic, and amphiphilic drugs, either alone or in combination, into the same nanocarrier, to obtain a synergistic action, and iv) modify the pharmacodynamic and pharmacokinetic properties of actives. From a biological standpoint, the use of nanotechnologies had the main scope of increasing the localization of the payload (either an active molecule or an imaging agent) to the diseased tissue, thus reducing its off-target accumulation and the resulting side effects, mainly in the context of anti-cancer therapies. The first-generation nanomedicines, of which the Doxil, the PEGylated liposomal formulation of doxorubicin, represents the first one marketed, exploited disease-related physiologic disfunctions, like an unbalance between oncotic and osmotic pressure, failure of lymphatic drainage, and leakiness of vasculature, which all together constitute the enhanced permeation and retention (EPR) effect, as drivers for their passive accumulation. However, the lack of active targeting properties of the first-generation nanomedicines represents the main limitation to their application to personalized nanomedicine. As a matter of fact, despite the EPR has been well described in mice, there is no relevant evidence of its role in humans [173]. In addition, EPR effect doesn’t take into account the genetic background of each patient and, even in the same patient, of the heterogeneity of the microenvironmental conditions that regulate each specific disease, cancer in particular. In this scenario, the possibility to selectively direct nanomedicines towards specific cell types or organs through the functionalization of their surface with targeting agents, makes them promising for personalized therapies.

The design and development of active targeting strategies determines the shift from

personalized medicine to personalized nanomedicine. Several approaches have been developed so far, most of them are based on i) peptides discovered via phage-display techniques, and ii) on antibody targeting, mainly using monoclonal antibodies, due to their ability to target specific molecules expressed by single cell types. Ideally, targeted nanomedicines can be designed according to the biological features of a patient, in terms of cell type overexpressed in the diseased tissue, individual immune response of a patient to a specific antigen, his/her blood protein profile and gene expression characteristics, over-time expression of specific patterns and their correlation with the progression of a disease, and can be tailored in order to predict the potential biological effects, i.e., fate and efficacy, after their interaction with biological components. However, although the expectations towards personalized nanomedicines are high, as also revealed by the number of targeted nanosystems developed and published so far, no targeted nanomedicines reached the market or are currently available for personalized medicine [174, 175].

A range of factors must be attributed to this gap: First of all, from a pharmaceutical standpoint, the single or multi-functionalization of carrier surface with targeting molecules increases the synthesis steps, as well as the purification procedures and the resulting characterization processes. If we add to this the costs related to the targeting agents, it is clearly evident how the development of personalized nanomedicines is neither affordable nor realistic with current technologies. From a biological standpoint, instead, the main hurdle for personalized nanosystems consists in patient's variability and heterogeneity, which require the development of nanotreatments specific for single patients or specific groups of patients. If from one side the high versatility of nanocarriers to be modified according to the genetic indications deriving from individual patients could make this strategy suitable for this scope, on the other

hand the nano-bio interactions, i.e., the formation of a protein corona, which strictly depends on the surface chemistry of nanocarriers, thus affecting their biodistribution, cytotoxicity, and immunotoxicity properties, have to be taken into account [176, 177]. The role of the new biological identity of nanomedicines once systemically injected received overall scant attention yet, thus rendering not predictable their fate once in the bloodstream. To overcome these limitations, the design of experimental procedures that favor the study of physicochemical properties of nanomedicines in biologic conditions plays an important role toward their clinical translation. Lastly, from a regulatory standpoint, personalized nanomedicines land in a field that misses specific regulations, mainly regarding the quality control and safety assessment [178]. Moreover, technological/pharmaceutical concerns have to be considered, such as i) the evaluation of the properties of personalized nanomedicines after bulk production, which requires the development of appropriate characterization techniques, ii) standardization methods of surface density of targeting ligands per each formulation, iii) optimization of the number of targeting agents on the surface of nanocarriers and their impact on the physical stability of the final formulation.

Personalized Bio-Nanomedicine: one size doesn't fit all

Biohybrid, bio-inspired, or biomimetic NPs have recently emerged as last-generation nanomedicines bestowed with immune compatibility and intrinsic capability to negotiate the biological barriers [99]. Regardless of the hybridization method, biohybrid NPs present a biological identity that recapitulates the one of a cell or, more appropriately considering the size, of an extracellular vesicle (EV), i.e., exosomes. However, what makes biohybrid NPs unique is their intrinsic biological activity, even without being loaded with a pharmacologically active molecule. As a matter of fact, Zhang and coworkers showed the intrinsic properties of biohybrid

NPS deriving from RBC membranes to sequestrate endotoxins, like lipopolysaccharide, toxin B, thus working as sponges with the ability to clean up the blood [179-181]. Molinaro ad coworkers, instead, by using the membrane proteins of leukocytes combined with synthetic, biocompatible phospholipids, created a biohybrid NP able to increase the expression of anti-inflammatory genes, while reducing that of the pro-inflammatory ones, when systemically administered in both localized LPS-induced ear inflammation [5] and inflammatory bowel disease models [182]. With that said, the use of biological components that originate from cells or cell fragments opens a new scenario in nanomedicine, i.e., personalized bio-nanomedicine. From a technological/pharmaceutical standpoint, this approach offers several advantages with respect of both second-generation NPs and EV-based strategies, since it combines their advantages while overcoming the disadvantages, such as: i) recapitulation of the biological complexity of cell membranes on the carrier's surface; ii) control of physical parameters of the final formulation (that is, diameter, surface charge, and size homogeneity); iii) control of the loading and retention of chemically different molecules (that is, hydrophilic, amphiphilic and lipophilic drugs, peptides, proteins, and genetic material); iv) establishment of standardized protocols for their reproducible and scalable preparation; v) control over storage and shelf-life properties of biohybrid NPs by tailoring, for instance, their lipid or polymer composition in order to modulate the colloidal properties, particularly the surface charge; vi) one-step synthesis procedure, which avoids complex, costly, and time-consuming post-synthesis purification processes.

From a biological standpoint, while monoclonal antibodies or peptides can be used to personalize the targeting properties of a synthetic carrier, without obviating, however, their immunogenic potential, biohybrid nanocarriers used in an autologous context should reduce the

risk of an immunogenic response. In fact, pre-clinical studies involving the use of RBC and WBC-derived biohybrid NPs revealed no activation of either an inflammatory or immunogenic response following to their repeated administrations [5, 183]. In addition, this approach overcomes the concerns about EVs isolation, like low yield rate and efficiency (EVs' recovery percentage is often <50%), susceptibility to contamination, which make the process challenging for clinical translation [184].

Challenges in clinical translation of biohybrid NPs

After the development of a novel therapeutic for humans, its pharmaceutical classification and the regulatory aspects of manufacturing, application, and safety have to be addressed. Currently, the development of nanomedicines evolves faster than regulations do, thus leaving a lack of guidelines, considering also that traditional regulations do not fully cover nanoproducts [185, 186]. From what above reported, biohybrid NPs belong to the middle ground between synthetic NPs, i.e., the first/second-generation NPs, and the biological ones, i.e., EV-based NPs. While from a pharmaceutical standpoint this difference is important in terms of manufacturing, storage, and costs, from a regulatory standpoint, biohybrid NPs may be considered, as the EVs, biopharmaceuticals [187]. This category, in fact, includes "medicines that contain one or more active molecules made by or derived from a cell". The potential classification of biohybrid NPs under the class of biopharmaceuticals is important to further identify the regulatory issues, and envision the potential hurdles in terms of manufacturing, storage and costs regulations. We will try to provide in this section a background of the regulations the biohybrid NPs may be subjected to and the challenges for their clinical translation.

Regulatory issues

Paradoxically, despite the lack of specific regulations makes the clinical translation of nanoproducts for personalized nanomedicine challenging [186], the existence of regulatory frameworks for EV-based therapeutics in Europe, Australia and United States about their manufacturing and clinical trials [188], may represent an advantage for the clinical translation of biohybrid NPs. The following aspects have to be considered:

1) Identification of a mechanism of action, which can be due to the payload, to the membrane or the set of receptors on NP surface, or both. This will determine the pharmaceutical classification of the biohybrid NPs according to the International Society for Extracellular Vesicles, as well as the regulations of their characterization and quality control.

2) Evaluation of the safety. Several criteria have to be considered, among them the source of starting material (i.e., autologous, allogeneic or xenogeneic), degree of cell source manipulation in vitro, donor and recipient safety.

3) Physical and biological characterization. Manufacturing technique and standardization, purity, storage conditions, composition, presence of contaminants, quali-quantitative analysis.

4) *In vivo* biological analysis. Aspects such as pharmacodynamics, pharmacokinetics, biodistribution, safety pharmacology and toxicology (from general toxicity to immunogenicity and immunotoxicology) need to be investigated.

Manufacturing

One of the main hurdles that nanomedicines have to face during the clinical translation process from the development phase in the lab to the market consists in the identification of manufacturing protocols that ensure their reproducibility and scalability. In the specific case of biohybrid NPs, there is another level of difficulty represented by their biological component, which requires the addition to the standard physicochemical characterization of the molecular

one. It has to be taken into account that nanomaterials physicochemical and molecular properties usually differ when they are produced in bulk. In addition, the manufacturing of biohybrid NPs under current good manufacturing procedures dictates a rigid control over the physicochemical and molecular parameters, including composition, structure, surface area, charge, and functionality, size distribution, presence and surface density of markers, purity and presence of contaminants. From the manufacture standpoint, this opens two levels of attention:

1. The design of biohybrid NPs should involve the simplest platform/procedure possible. In this context, microfluidic methods offered a valuable tool for the scalable, reproducible, high-throughput fabrication of nanomedicines, including biomimetic nanovesicles. Moreover, despite the biological component represents the 'functional' part of the final nanoproduct, bottom-up synthetic strategies are always strongly recommended compared to the top-down ones, since they allow for a higher degree of precision over the final formulation and are more cost-effective.
2. The characterization of biohybrid NPs-based formulations requires appropriate infrastructure, adequate technical equipment, trained personnel and a quality management system, in compliance with good laboratory, manufacturing, and clinical practice.

Stability and Storage

Among the requirements that have to be considered for the successful translation of a product from the bench to the market, its pharmaceutical stability in storage conditions represents one of the most important. The transition from nanomedicine to bio-hybrid nanomedicine may have strong repercussions also in this context. Added to the standard requirements (e.g., for example, absence of degradation or aggregation of nanomaterials, maintenance of original diameter, size distribution and surface charge, preservation of payload content and integrity), novel characterization analyses will have to be carried out to ensure the

preserved biological activity of bio-hybrid NPs after storage, including biological integrity of proteins/receptors on carrier surface and their correct orientation [189]. The eventuality that personalized bio-hybrid nanomedicines will require to use the formulations right after they are synthesized should be considered in terms of technical and infrastructure feasibility and costs effectiveness. This may involve pharmaceutical companies to work back-to-back with hospitals in order to make treatments immediately available on daily basis, particularly in the cases when the biological component of the bio-hybrid NP comes from patients' RBCs or WBCs, for instance. In the scenario in which bio-hybrid NPs can be manufactured ahead of time and used for a specific patient, instead, standard storage techniques, i.e., freeze-drying, which is the most common, will have to be adapted to avoid the triggering of instability phenomena. The lack of standardized procedures for EVs' storage underlines the importance of the problem. As general guidelines, the use of isotonic buffers may prevent pH shifts during freeze-drying and storage procedures [188]. In addition, applied technologies, reagents and storage containers have to be validated in order to prevent any unexpected interaction with bio-hybrid NPs. Lastly, functional analyses and potency assays will have to validate the biological functionality of bio-hybrid NPs after storage.

Costs

Personalized nanomedicine is a multidisciplinary field where chemistry, physics, engineering, biology, toxicology, medicine, clinics, pharmacy converge. Surely, the cost-effectiveness of this approach represents one of the main limitations to its clinical translation. Compared to traditional therapies, personalized nanomedicines represent less than 1% of total drug patents per year, thus justifying the economic risk associated to their development [190]. Two main aspects have to be taken into account before personalized bio-inspired nanomedicine

reaches the market, i.e., i) the evaluation of the effective costs of manufacturing, and ii) the economic risk related to their development.

From what above mentioned, personalized nanomedicine implies elevated costs of manufacturing, maybe not acceptable for the pharmaceutical market. Those costs are mainly related to the manufacturing, reagents (particularly regarding the targeting agents, like monoclonal antibodies for instance), post-synthesis purification, infrastructure for physicochemical and biological characterization, and GMP-related procedures, including quality control. With respect to the economic risk, instead, it will be fundamental to demonstrate a real advantage of using bio-hybrid NPs compared to conventional treatments, which would justify novel investments in the field by pharmaceutical companies. Overall, bio-hybrid NPs can be considered as novel generation personalized nanomedicines. Pharmaceutical market will need to adapt its strategic lines towards personalized medicine. The key players for the successful translation of this approach to the market will involve the effective scientific divulgation internal and external stakeholders, as well as non-scientific communities, the realization of new economical strategies, such as the ones based on risk sharing schemes between pharmaceutical industry and consumers, and the identification of a field of application, such as for example the orphan diseases, due to the lack of current therapies [186].

Biomaterials Approach in Immunoengineering

Although implantable medical devices are critical players in several health-related products, functional integration of biomaterials are compromised by many challenges including foreign body responses (FBR) [191-193]. FBR initiates with an early inflammatory response against the implanted biomaterial, which progresses to chronic inflammation, granulation tissue, fibrous capsule formation, and rejection of the implant [194-196]. Controlling such responses using immunomodulation strategies leads to the development of implantable devices that could function for a longer periods in the body [191, 193]. One approach to regulate the immune response against implants is to use immunomodulatory biomaterials. These implants could regulate and/or reprogram immunocytes through different strategies including surface modification [197, 198], drug eluting systems [199], size and shape modulations [200], and stiffness induce modulations [201, 202]. Immunomodulatory approaches are currently under investigation, and demonstrate desirable efficacy to treat different disorders including chronic inflammation to autoimmune diseases [203, 204].

Adaptive immunity is considered as a main player in generating long-term immune response against implants [205, 206], with Dendritic Cells (DCs) and macrophages being key players in organizing hyper-inflammation through activation of T cells [207-210]. In fact, DCs are known as major antigen presenting cells (APCs), acting as a bridge between the innate and adaptive immune systems [211]. Furthermore, DCs are not only critical for the induction of immune responses but are also important for generating immunological tolerance, giving them a double edge sword to orchestrate immune responses [209, 212]. Therefore, much efforts have been devoted to reprogram DCs as therapeutic targets [213-218].

This review outlines the current knowledge on DCs role in host responses to the biomaterials and discuss in detail how physical and chemical properties of biomaterial could direct DCs responses. We begin with a brief introduction to the immune cell interaction with a biomaterial. Next, we discuss in detail DCs interaction with the biomaterial, DCs role in the activation of the adaptive immune system and T cells polarization, and how DCs recognize biomaterials with integrins and toll-like receptors (TLRs). Then, we describe how tolerogenic DCs are generated, how adsorbed proteins on the biomaterial surface determine DCs response, and we finally introduce some applications of biomaterial-based DCs immunomodulation.

Biomaterial-Immune cells interaction

Biomaterials implantation in the body is usually requires a surgical procedure. This procedure damages the veins and lead to blood-biomaterial interaction, which leads to an acute inflammatory response. After implantation, blood plasma components such as free ions, proteins (e.g. albumin, fibronectin, laminin and collagen) are adsorbed on the surface of biomaterial. Such adsorption is affected by physical and chemical properties of the biomaterial, such as size, topography, roughness, surface chemistry, and surface energy [219-221]. Therefore, biomaterials surface determines the type and conformation of adsorbed proteins which lead to the formation of different biomaterial-associated molecular patterns (BAMPs), inducing specific-BAMP immune responses. As BAMP partly specifies the extent of immune response, surface modification methods are used to the formation of a specific BAMP to restrict the immune responses [208, 222].

Upon BAMP formation, approximately four hours after implantation, the innate immune cells adhere to the biofilm, which triggers their response [208, 223]. Unlike BAMP which generates exogenous signals and leads to immunogenicity, the danger-associated molecular

pattern (DAMP) is released through ECM destruction and host cells necrosis during surgery and implantation/administration, which alerts the immune system [224, 225]. The DAMP, usually named alarmin, is equivalent to an endogenous BAMP which includes heat shock proteins, high mobility group box 1 (HMGB1) proteins, ATP, heparan sulfate, and uric acid [224]. PAMPs and DAMPs are identified through Pattern Recognition Receptors (PRRs) which include Toll-like receptors (TLRs) and c-type lectins, which are mainly expressed in macrophages and DCs.[226, 227] Identification of DAMPs and BAMPs lead to the release of the proinflammatory cytokines including IL-1β, IL-6, IL-12, and TNF-α, inducing chemotaxis of other cells [228] (**Figure 2.6**). The extent of the injury during implantation, implantation site, physicochemical properties of biomaterial, and the extent of provisional matrix formation determine the amount of DAMPs release and the formation of special BAMPs. Such parameters specify the extent of immune response like acute and chronic inflammations.

Acute inflammation is usually due to the presence of neutrophils and degranulation of mast cells that allow histamine secretion. M2 subtype of macrophage are known to play a role in resolving acute inflammation in approximately one week, and failure in resolution leads to the activation of the adaptive immune system to isolate the biomaterial from the tissue. When the innate immune cells fail in phagocytosis of the biomaterial, chronic inflammation, granulation tissue, foreign body reaction, and fibrous capsule formation occur [207]. Specifically, DCs adhere to the formed BAMP through their integrin receptors and identify the BAMP and DAMP through PRRs. These processes lead to the maturation of DCs, enabling them to capture antigens, migrate to the lymph nodes and interact with T cells [229, 230]. The obtained antigens are loaded inside the acidic vesicles, loaded on to major histocompatibility complex (MHC) and presented to the T cells [228, 231] (**Figure 2.7**). After DCs migration to the lymph nodes, the $CD4^+$ T cells

will detect the antigens loaded on MHC II, further polarizing T lymphocytes into effector types. Activation of Th1 subunit of $CD4^+$ T cells leads to the production of cytokines like Interferon-ɣ (IFN-ɣ) and IL-2, while the Th2 subset is involved in the production of IL-4, IL-5, IL-10, IL-13 and also IgG, IgA, IgE from B cells. It is revealed that Th2 inhibits the production of IFN-ɣ.

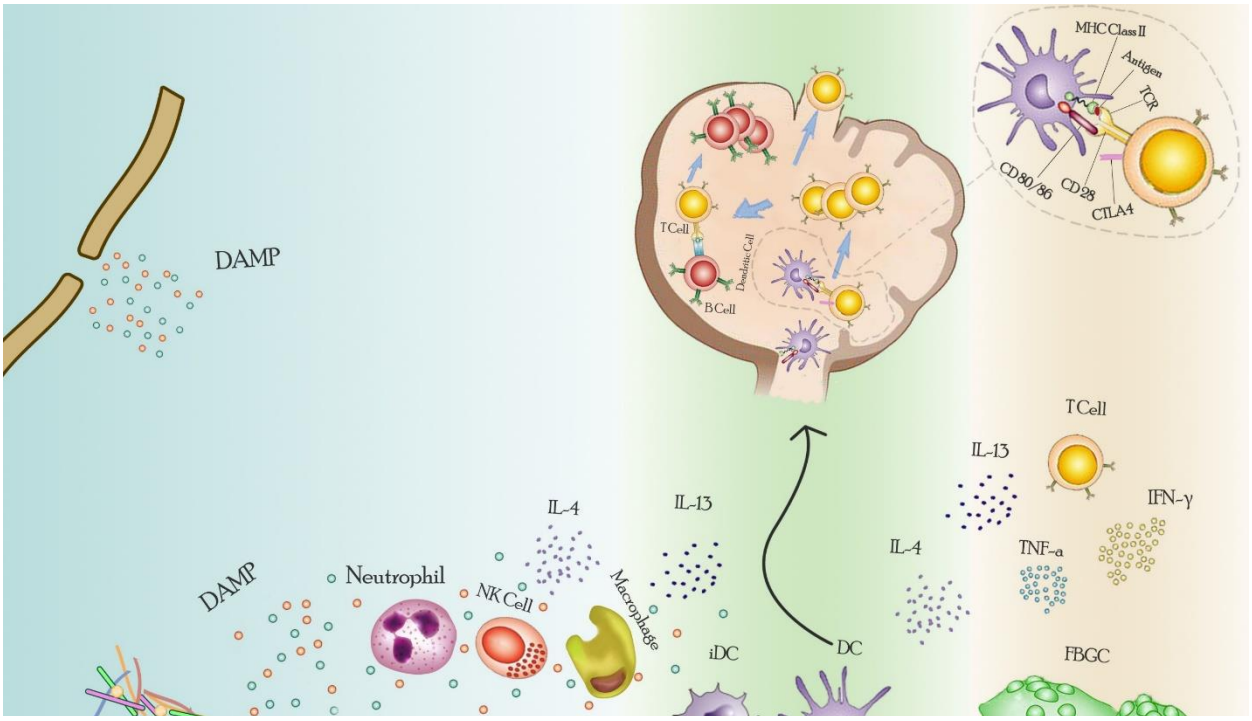

Figure 2.6. Schematic of DCs and other immune cells interaction with implanted biomaterial. Biomaterial implantation is associated with cell necrosis and ECM destruction and consequently DAMP generation. After four hours of implantation, BAMP is formed on the biomaterial surface; so, innate immune cells are able to adhere to the biomaterial surface. DC adhesion triggers its maturity which by identifying the BAMP and DAMP is completed. maturation of DC leads to an increase in the expression of stimulatory and co-stimulatory markers; consequently, DC can migrate to the lymph node and interact with T cells to activate them. Then, T cells migrate to the implanted site and secret inflammatory cytokine such as IL-4 and IL-13, which in turn increase

Following the same order, the Th17 subset also leads to the production of IL-17, IL-21, and IL-22 (**Figure 2.7**).

$CD8^+$ T cells detect the loaded antigens in MHC I. The activation of T cells is accomplished by two signal; the interaction between T cell receptor (TCR) with MHC molecules

provides the first signal [228]. Sustained signaling through TCR interaction with MHCs leads to the activation of some signal transduction pathways which in turn lead to the activation of the nuclear transcription factor. It has been demonstrated that the absence of the second signal leads to T cells polarization into tolerance, clone incompetent or deletion [232]. Therefore, the second signal is required which is provided by the interaction of CD80 (B7.1)/CD86 (B7.2), expressed on DCs, with CD28 expressed on T cell. It is proposed that CD28 co-stimulation is mediated by activation of downstream signaling pathway of TCR [233]. Consequently, the activated T cells are colonized and interact with B cells to activate them. Therefore, B cells undergo colonization and cause an intensity in innate immune responses through pathogen-specific antibodies production [228, 234, 235].

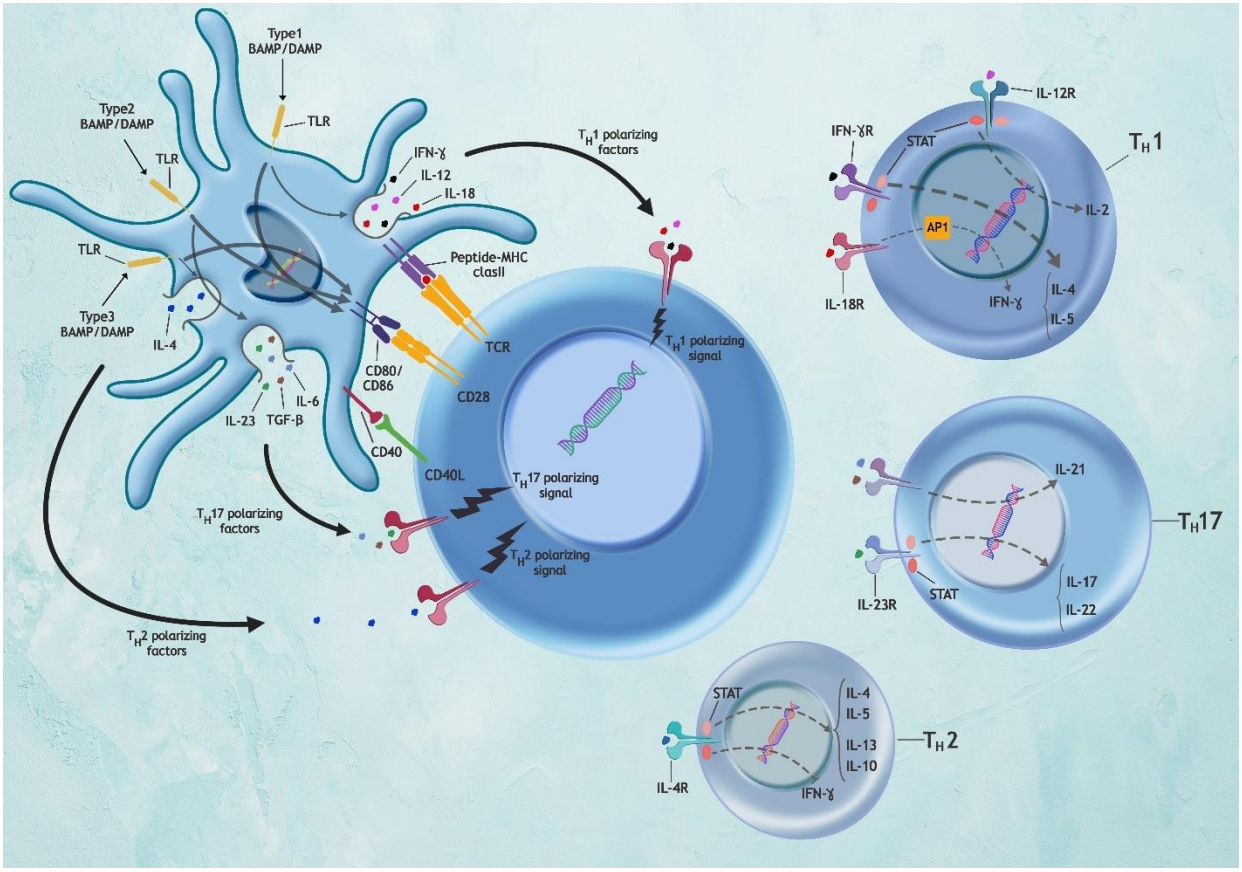

Figure 2.7. Downstream signaling cascades induced by BAMP and DAMP. Different downstream signaling pathways of TLRs are activated, leading to the secretion of different type of cytokines. secretion of IL-12, IL-18, and IFN-ɣ polarize CD4+ T

cells to Th1, and secretion of IL-2, IL-4, and IL-5 from such cell. CD4+ polarization to Th17 is done through IL-6, IL-23, and TGF-B. Th17 is responsible for the secretion of IL-17, IL-21, and IL-22. secretion of IL-4 from DCs leads to the polarization of CD4+ to Th2. Th2 activation is associated with the release of IL-4, IL-5, IL-10, and IL-13 and also inhibition of IFNγ secretion.

DC-Biomaterial interaction

The surface properties of the biomaterial determine the adhesion and activation of DCs. Similar to macrophages, hydrophilic/hydrophobic properties of the biomaterials surface determine DCs' adherence (and activation). Higher hydrophobic properties, for example, increases the adsorption of proteins that support DCs' adhesion, maturation, and immune activation. Hydrophilic surfaces lead to the adsorption of proteins that limit DCs' adhesion and maturation (**Figure 2.8**). For instance, Albumin, Fibronectin, and Vitronectin adhere to hydrophilic surfaces much higher than hydrophobic surfaces. In contrast, Fibrinogen and IgG2 have higher affinity to hydrophobic surfaces. Hydrophobic vs. hydrophilic properties of a surface are directly related to the surface chemistry, which could be manipulated through changing the surface functional groups. For instance, increasing the surface oxygen concentration makes the surface more hydrophilic, which reduces the maturation of DCs, and immune passivation. In contrast, carbon makes the surface more hydrophobic, increases DCs' adhesion-promoting proteins adsorption, DCs maturation, and immune activation, respectively (**Figure 2.8**).

In response to biomaterials, DCs migrate to lymph nodes to activate T cells. Upon migration and activation around the biomaterial's vicinity, T cells secrete IL-4 and IL-13, leading to upregulation of mannose receptors on macrophages. Such upregulation induces the infusion of macrophages and formation of the foreign body giant cells (FBGCs), and consequently, fibrous capsule formation [236-238]. Furthermore, it has been demonstrated that FBGCs could reduce the pH around the biomaterial implantation site, which in turn results in the degradation of biomaterial surface [207, 239].

Due to such an orchestrating role between innate and adaptive immunity, generating tolerogenic DCs could dampen such inflammatory responses against biomaterials [240]. There is a growing body of evidence showing that a wide variety of methods could be applied to modify physical and chemical properties of biomaterial to modulate DCs mature state. Investigation of the biomaterial-DCs interaction will pave our way for designing safe biomaterials in tissue engineering and improving vaccine delivery for immunotherapy [241]. To better understand the biomaterial-DCs interactions, we start by reviewing the different types of DCs. We then describe the type of interactions occur between biomaterials and DCs. And finally, we discuss the activation of DCs and their migration to organize adaptive immunity with some applications.

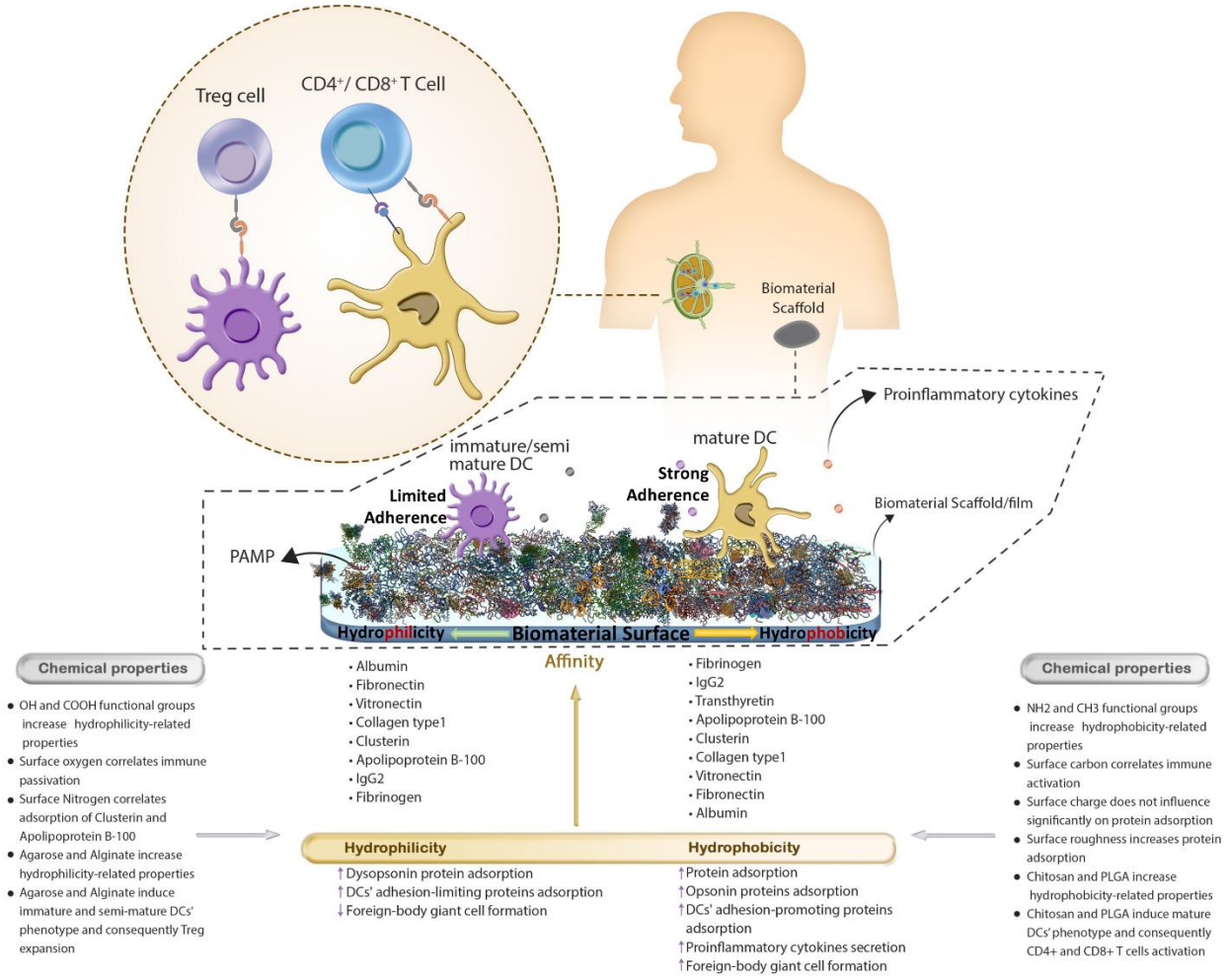

Figure 2.8. Biomaterials surface properties influence the DCs' response. Hydrophobicity increases the adsorption of some proteins that support DCs' adhesion, maturation, and immune activation. On the other hand, a biomaterial surface with higher hydrophilicity adsorbs proteins that limit DCs' adhesion and maturation. For instance, Albumin, Fibronectin, and Vitronectin adhere to hydrophilic surfaces much higher than hydrophobic surfaces. In contrast, Fibrinogen and IgG2 have higher affinity to hydrophilic surfaces. Hydrophobic vs. hydrophilic properties of a surface are directly related to the surface chemistry, which could be manipulated through changing the surface functional groups. For instance, increasing the surface oxygen concentration makes the surface more hydrophilic, which reduces the maturation of DCs, and immune passivation. In contrast, carbon makes the surface more hydrophobic, increases DCs' adhesion-promoting proteins adsorption, DCs maturation, and immune activation, respectively.

Subtypes of DC

DCs are usually categorized based on their lineage to Myeloid and Plasmacytoid types [242, 243]. The Plasmacytoid DCs (PDCs) are similar to plasma cells with some Myeloid DCs (MDC) features. PDCs, previously known as interferon-producing cells, could release IFNα

[244-246]. Unlike MDCs, myeloid antigens like CD11c, CD33, and CD11b are not expressed in PDCs, while GMDP markers CD123 (IL-3R) and CD45RA are expressed. It is shown that PDCs are equipped to the TLR7, TLR9, and interferon regulatory factors 7 (IRF7) which is the main transducer of type 1 interferon production to fight against acute and chronic viruses infection [242, 243, 247].

MDCs are categorized in two subsets of MDC-1 and MDC-2. MDC-1 is the main stimulant of T cells, and MDC-2 contributes in preventing wound infections. MDCs-1 is found in the blood, among resident DCs in lymph nodes, spleen, bone marrow, non-lymphoid tissues, skin, lung, intestine, and liver. It is shown that MDC-1 is potentially capable to present antigens by MHC I to activate CD8+ T cells, and also contribute in promoting Th1 responses through IL-12 production [242, 244]. Furthermore, MDC-1 is known as a major producer of type 3 interferon and expresses TLR3, TLR7, TLR9, and TLR10. MDC-2 is mainly found in blood, tissues, and lymphoid organs, and are involved in the wide range of immune response to foreign bodies. MDC-2 express a wide variety of receptors such as TLR2, TLR4, TLR5, TLR6, and TLR8, NOD-like receptor 2, leucine-rich repeat-containing protein 1 (NLRP1), NLRP3, Neuronal apoptosis inhibitory protein (NAIP), Dectin-2, and Dectin-1 [242].

Some other types of DCs such as Follicular DCs (FDCs) do not have a hematopoietic origin. These types of DCs do not express MHC II, arise from mesenchymal cells, and are located in lymphoid follicles [248]. FDCs play vital role in B-cell activation and affinity maturation of antibodies [249].

DCs in biomaterial recognition

DCs are able to undergo both the inflammatory and tolerogenic phenotypes [228]. DCs are initially immature, relatively immobile and star-shaped, which enables them to become active

upon capturing antigens.[250] After implantation of the biomaterial, the DCs interact with the adsorbed proteins on biomaterials surface through their receptors on the membrane [223].

Molecules that support DCs adhesion are known as cell adhesion molecules. Most of such cell adhesion molecules are the members of the four Selectin, Cadherin, Integrin and the large Immunoglobulin protein family [251]. It is revealed that, among those four families, integrins play a vital role in DCs function and also gained interest as a potential therapeutic target [252]. We therefore focus more on the role of integrins in the biomaterials induced inflammatory response.

Integrins in biomaterial recognition

Integrins are heterodimer proteins containing α and β chains connected to each other through noncovalent binding. There are 18 and 8 different subfamilies of α and β, respectively, that form at least 24 different types of integrins [253-255]. Integrins constitute the most versatile family of cell adhesion molecules in terms of structure and function, which led integrins to contribute in inflammation, innate and adaptive immunity, homeostasis, wound healing, and tissue morphogenesis [254-256]. Integrins on the surface of cells are first receptors adhering to the extracellular matrix proteins, adjusting cellular functions such as proliferation and differentiation. Leukocytes express a specific subfamily of integrin named β_2-integrin consisting of $\alpha_L\beta_2$ (CD11a), $\alpha_M\beta_2$ (CD11b), $\alpha_X\beta_2$ (CD11c), $\alpha_D\beta_2$ (CD11d). The intracellular adhesion molecules-1 (ICAM-1), -2, -3, and -5 are members of the immunoglobulin family and constitute the most important ligand for CD11a [252, 255, 256]. The sequences of CD11b and CD11c are highly similar and they share some ligands such as i3b, ICAM-1, and fibrinogen [257, 258]. CD11d binds to ECM proteins including vitronectin, plasminogen, fibrinogen, and CYr61 [257]. The CD11a and CD11b contribute to the leukocytes' migration to the inflammation site [256].

CD11a is required for a wide range of cell-cell interactions like T-B cells and T cells-DCs. Among leukocyte integrins, CD11a is expressed in most lymphocytes and DCs, while CD11b is mostly expressed in neutrophils, therefore, in some diseases like heart failure and stroke where neutrophils are important, CD11b antagonist molecules are used while in diseases like rheumatoid arthritis, psoriasis and organ transplantation rejection where lymphocytes and DCs are involved, CD11a antagonists are usually used [256].

β1-integrins are highly expressed on macrophage, while β2-integrins are expressed more on DCs, compared to β1-integrin [259]. β_2-integrin families mediate DCs adherence to the BAMP [256]. Following adhesion, the DCs maturation process begins, which is accompanied by morphological changes and also changes in the expression of receptors; for example, leads to an increase in the expression of C-C chemokine receptor 7 (CCR7), stimulatory molecules like HLA/MHC, co-stimulatory molecules like CD40, CD80, CD86, and the release of pro-inflammatory cytokines [252, 260].

Integrin markers are considered as a therapeutic target for controlling the host responses because their blocking leads to reduction in the adhesion of immune cells. Zaveri et al assessed the role of CD11b in macrophage response to microparticles and bulk material. They used macrophage derived from CD11b knockout (KO) mice to limit chronic inflammation and increase the functional life of implanted materials. Their results showed that absence of CD11b reduces the macrophage potential in polystyrene microparticles phagocytosis. Furthermore, they found that CD11b absence leads to the reduction in foreign body response to subcutaneously implanted polyethylene terephthalate, and a thinner foreign body capsule was formed in comparison to wild type (WT) [261] In line with this, Zaveri et al used CD11b KO mice to study the effect of CD11b in the macrophage response to implant-derived wear particles, ultra-high

molecular weight polyethylene (UHMWPE) microparticles. They found that deficient or blocked CD11b leads to the reduction in the macrophage phagocytosis and inflammatory cytokine secretion. Furthermore, their results demonstrated that lack of CD11b reduces the osteolysis compared to WT, by using calvarial osteolysis model.

The lesser the attachment of DCs to the biomaterial surface, the lower the DCs' maturation which in turn reduces immune responses. β_2-integrin subfamily plays a critical role in DCs maturation on the biomaterials surface. It is reported that DCs maturity on poly lactic-co-glycolic acid (PLGA) film is reduced by β_2-integrin blocking. Furthermore, β_2-integrin was found in biomaterial-adherent DCs podosomes in contact with PLGA surface [252]. Therefore, the biomaterials surface that limits β_2-mediated adhesion leads to the reduction of DCs response. Following by DCs adhesion, PRRs (especially by TLRs) recognize the BAMP.

Toll-like receptors in biomaterial recognition

Interaction of TLR with BAMP leads to recognition of the physical and chemical diversities in biomaterials. Upon TLRs interaction with DAMP and BAMP myeloid differentiation primary response 88 (MYD88) and its downstream pathways get activated. Triggering downstream pathways of MYD88 give rise to the activation of the interferon regulatory factor 5 (IRF5), IRF7, IRF3, activator protein 1 (AP-1), and nuclear factor-κB (NF-κB) [209, 262]. TLRs 1, 2, 4, 5 and 6 are expressed on the cell surface while 3, 7, 8, 9 are expressed cytoplasmically [263, 264]. DCs express all 10 type of TLRs, providing them with the capability to detect a wide range of materials or pathogens and act as a potent activator of adaptive immunity.

All TLRs on membranes are of the type I glycoproteins, expressed on macrophages, DCs, neutrophils, mucosal epithelial cells, and endothelial cells. Such receptors interact with BAMP

and DAMP and activate the signaling pathways like NF-κB leading to an increase in phagocytosis, secretion of proinflammatory cytokines, expression of co-stimulatory molecules like CD80 and CD86, and an increase in antigen presentation through the MHC [265]. It has been demonstrated that TLR4 are responsible for expression of co-stimulatory molecules in response to DAMP and BAMP stimulation. Precisely, TLR4-mediated activation of TRIF-related adapter molecule (TRAM) recruits the TIR-domain-containing adapter-inducing interferon-β (TRIF) and TRIF3. Activating the TANK Binding Kinase 1 (TBK1) and IKKα, by TRIF3, results in phosphorylation of IRF3 and IRF7, and consequently expression of co-stimulatory molecules, IFN-α, and IFN-β (**Figure 2.9**). Each one of the TLRs has its unique ligands that allow them to detect countless materials, viruses and bacteria, for instance, the bacteria cell wall is identified by five TLRs named TLRs 1, 2, 4, 5, and 6, which are extracellular TLRs (**Table 2.1**).

TLR4 can identify several unrelated structural ligands, like thermal shock proteins, liposaccharides (LPS) in the gram-negative bacteria walls, fibronectin, and fibrinogen.[263, 264, 266, 267] When HSP60 is released from the cells in response to imposed stress, it acts as a dangerous signal in innate immunity and leads to inflammatory responses [209]. Necrosis leads to secretion of the alarmins, identified as the unique activators of DCs and non-unique activators of the adaptive immune system [209, 263]. Interacting alarmins with the cells expressing PRRs cause alarmin-TLRs ligation followed by NF-κB pathway activation and proinflammatory cytokines secretion like TNF-α, IL-1β and IL-6, migration of other cells to the region, and an inflammatory microenvironment [268]. Furthermore, TLR4 possesses more ligands than other TLRs; therefore, due to its high capability in substances recognition is considered as a therapeutic target in immunomodulation [269].

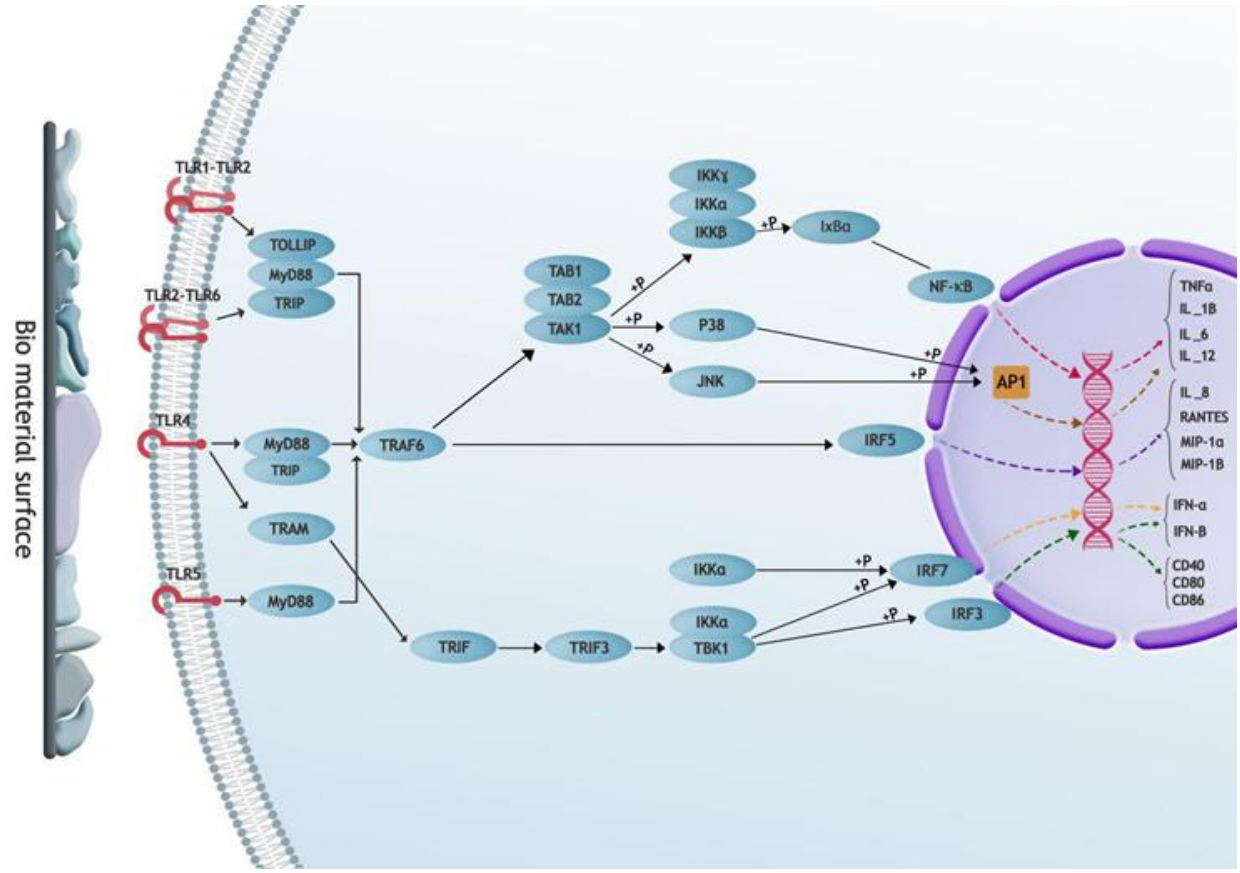

Figure 2.9. TLRs signaling pathway during interaction with BAMP. Upon TLRs interaction with BAMP and DAMP MYD88 is activated and interact with other adapter proteins like Toll-interacting protein (TOLLIP)and Toll/interleukin-1 receptor domain-containing adapter protein (TRIAP) to activate TNFR-associated factor 6 (TRAF6). TRAF6 with TAK1-binding protein 1 (TAB1) and TAB2 activate other cytoplasmic protein, TGF-β-activated kinase 1(TAK1), which in turn by phosphorylation of IKK family, P38, and c-Jun N-terminal kinases (JNK) lead to the activation of NF-κB and AP-1. Activation of NF-κB and AP-1, and direct activation of IRFF5 by TRAF6, resulted in the expression of cytokines and chemokines. In an independent pathway, TRAM pthway results in phosphorylation of IRF3 and IRF7, which are involved in the expression of co-stimulatory molecules, IFN-α, and IFN-β.

TLRs 1, 2, and 6 identify the wall components of gram-positive bacteria like the lipoprotein and peptidoglycans, while TLR5 identifies the Flagellin bacteria. TLR3, 7, 8, 9, and 10 are intracellular receptors among which TLR3 identifies double-stranded RNA, and TLR7 and 8 identify single-stranded RNA (**Table 2.2**) [226, 263, 270-272].

Table 2.1 Analysis of the extracellular TLRs

TLR	Immunocytes Expressing	Corresponded ligands	Ref.
TLR2/TLR1	Ne, Mo, MΦ, DC, B, T	Triacyl lipopeptides	[264, 271-273]
TLR2/TLR6	Ne, Mo, MΦ, DC, B, T	Diacyl lipopeptides, lipoteichoic acid, Heat shock proteins (HSP 60, 70), High mobility group protein (HMGB1),	[264, 271-274]
TLR4	Ne, Mo, MΦ, DC	Lipopolysaccharide (LPS), High concentration of endogenous ligands, such as heat shock proteins (HSP60 and HSP70), the extra domain A of fibronectins, oligosaccharides of hyaluronic acid, Heparan sulfate and fibrinogen.	[226, 264, 265, 270-274]
TLR5	Ne, Mo, MΦ, DC, T	Flagellin	[226, 264, 265, 270-274]

Ne: Neutrophil, Mo: monocyte, MΦ: Macrophage, DC: Dendritic Cell, B: B cells, T: T cells

In this context, applying TLRs antagonist such as monoclonal antibodies (mAb) and aptamers could be considered as a promising approach in modulating immune response.

Table 2.2 Analysis of the intracellular TLRs

TLR	Immunocytes Expressing	Corresponded Ligands	Ref.

TLR3	DC, B, T	dsRNA	[226, 264, 265, 270, 271, 273, 274]
TLR7	Ne, Mo, MΦ, DC, B	ssRNA, imidazoquinolines	[226, 264, 265, 270-274]
TLR8	Ne, Mo, MΦ, DC	ssRNA, imidazoquinolines	[226, 264, 265, 270-274]
TLR9	Ne, DC, B, T	CPG DNA, Chromatin IG complex	[226, 264, 265, 270-274]
TLR10	Ne, DC, B	Listeria monocytogenes	[274, 275]

AP177 antagonist aptamer was demonstrated to inhibits the activation of NF-κB activation through TLR2 stimulation. It was shown that AP177 inhibit 90% of NF-κB activity which is induced through PAM3CSK4 stimulation, a TLR1/2 agonist, while only inhibits 44% of NF-κB activity through FSL-1 stimulation, a TLR2/6 agonist. Moreover, results indicated that such aptamer inhibits 56-61% of NF-κB activity by stimulation via bacterial components such as LPS. Consequently, they concluded that AP-177 would be able to regulate TLR2-mediated immune response and restrict a wide range of TLR2 agonist molecules activity [276].

DCs migration

After the antigen experience and maturity, DCs migrate towards the lymph nodes [277]. DCs maturation is associated with an increase in CCR7 expression, which in turn leads to an increase in DCs' movement [250]. Interaction of CCR7 with its ligand (CCL21), expressed on

the surface of the lymphatic endothelial cells, leads DCs to migrate to the lumen of the lymph vessels through haptotaxis. Then, their traverse through the lymph flow to the lymph nodes and passively enter the subcapsular sinus (**Figure 2.10**) [250, 277-280]. In this migration, once more, by applying CCR7, DCs enter the parenchyma of the lymph node where a receptor named ACKR7 binds to CCL19 and CCL21. The receptor ACKR4 is placed on the subcapsular sinus ceiling of the lymph node, thus, by occupying CCL19 and CCL21 on the ceiling, a concentration gradient of CCL21 is formed on the lymph nodes paracortex which leads to DCs migration towards the T-rich region where DCs interact with T cells [250].

Molecular Candidates to Induce Tolerogenic DCs

DC act as a double-edged sword and could induce the immune activation or tolerance. DCs could restrict the immune responses by providing both peripheral and central tolerance. Such restriction is imposed through inducing T cells anergy and regulatory T cells (Treg) expansion in the peripheral tolerance and T cell elimination in the central tolerance. The tolDCs phenotype is characterized through the low-level expression of the CD86 and CD80 markers. Therefore, tolDCs are not able to induce the second signal in order to activate T cells, while they would be able to present antigen. In such cells, the level of IL-10 secretion increases, while the secretion of inflammatory cytokines such as IL-6, IL-1β, and IL-12p70 decrease [281]. TolDCs are considered as a therapy in autoimmune diseases, rejection of transplantation, and biomaterials implantation. Some of the proposed mechanisms are applied for in vitro generating tolDCs to be administered to the patient to induce tolerance for therapeutic purposes [216, 282-285].

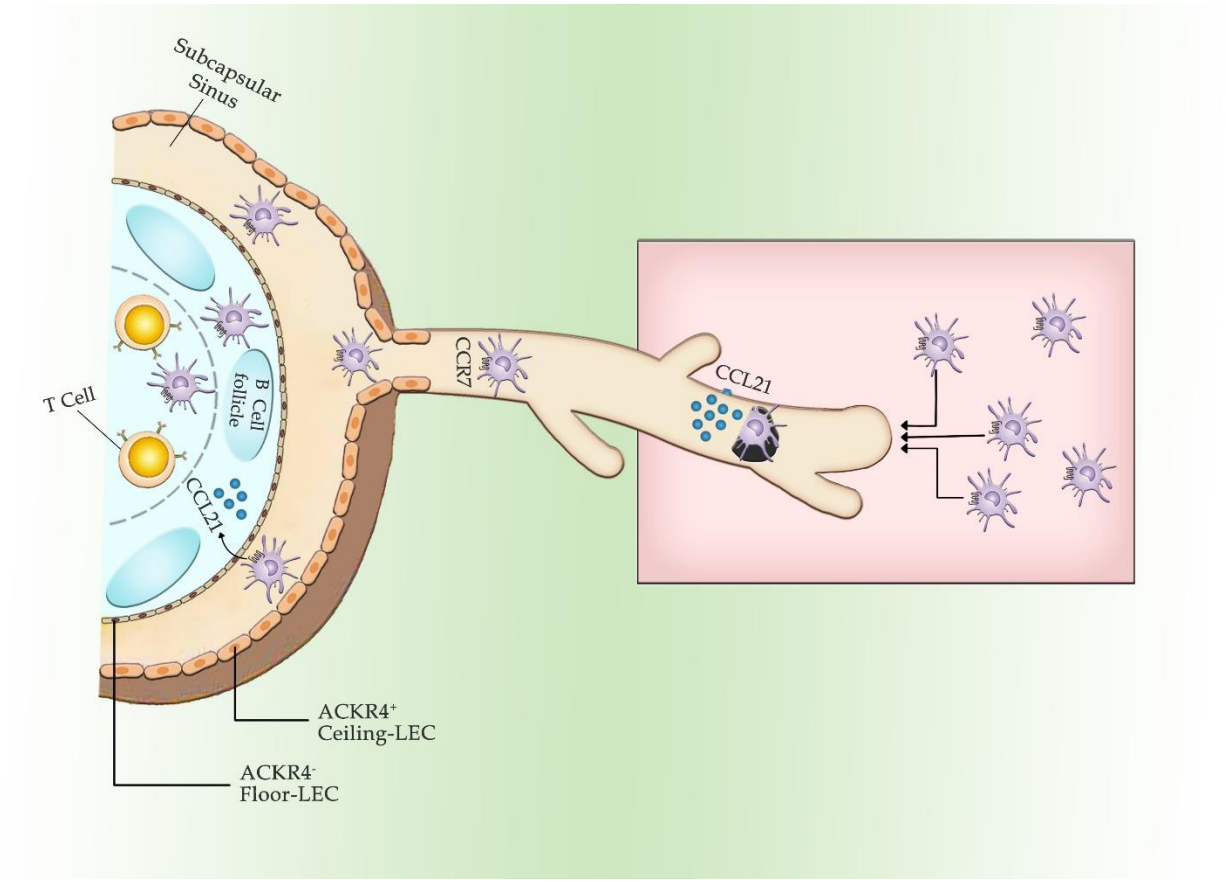

Figure 2.10. Basic principle of DCs migration. After the recognition process and maturity, DCs migrate towards the lymph nodes. DCs maturation is associated with an increase in CCR7 expression, which in turn leads to an increase in DCs' movement. Interaction of CCR7 with its ligand c-c chemokine ligand 21 (CCL21), expressed on the surface of the lymphatic endothelial cells, make DCs migrate to the lumen of the lymph vessels through haptotaxis. Then, their traverse through the lymph flow to the lymph nodes and passively enter the subcapsular sinus.

In a normal condition, DCs induce tolerance mainly through three different pathways. DCs induces Treg generation through IL-10 secretion. Upon Treg interaction with DCs, MHC II molecules on DCs surface are removed by Tregs in a process called trogocytosis. Trogocytosis is known to reduce the DCs capacity for T cell activation (**Figure 2.11**) [286]. The interaction of program cell death-1 (PD-1) on DCs with program cell death ligand -1 (PD-L1) on T cells inhibits T cell activation. Moreover, the binding of CTLA-4 on T cells to CD80/CD86 on DCs instead of CD28 highly contributes to inhibition of T cell activation.

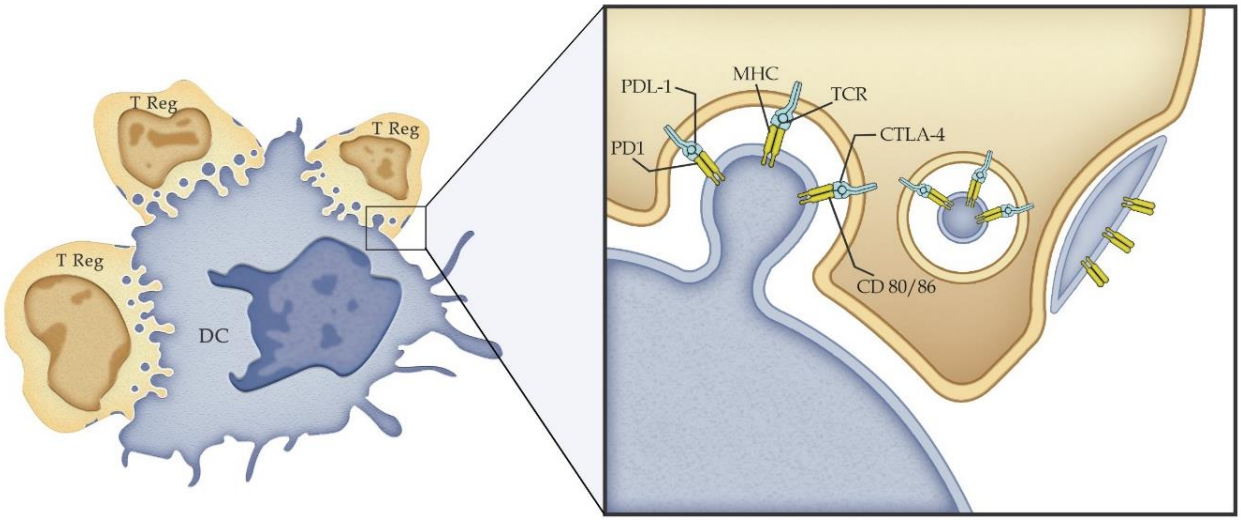

Figure 2.11. Interaction between DCs and Tregs. Antigen-specific Treg cells strongly bind to DCs and capture the cognate MHCII from DCs surface. It also facilitates the acquisition of B7 ligands in proximity.

IL-10 leads to the downregulation of MHC II, CD80, and CD86.[284, 287] Bok et al. argue that the generated tolDCs through IL-10 are more potent than generated tolDCs through dexamethasone, vitamin D3, TGF-β, and rapamycin in inducing tolerance. They reported that the generated tolDCs through TGF-β and dexamethasone act similar to the mature DCs in cytokines secretion and T cells stimulation. The generated tolDCs through rapamycin possess low ability in cytokines secretion while being a powerful stimulator for T cells. The tolDCs generated through IL-10 have considerable potential in tolerance induction, high ability in IL-10 secretion and low ability in T cells activation [288].

Deoxyspergualin (DSG) is an immunosuppressive drug and is applied in generating tolDCs. The 15-DSG is considered as the NF-κB inhibitor that inhibits pro-inflammatory cytokines secretion and DCs maturation. DCs maturation has been shown to be impaired via $F(Ab)_2$ immunotoxin ($F(Ab)_2$ IT) and 15-DSG. Such formulation has prevented the rejection of renal allografts in Rhesus macaques. Results indicated that 15 days administration of $F(Ab)_2$ IT

with 15-DSG reduced the transplant rejection by 87% [289]. With respect to the 1-10 mm diameter range biomaterials, Jhunjhunwala et al applied PLGA microparticles to deliver rapamycin to the DCs, by loading the rapamycin in microparticles (Ramps) of PLGA with 3.4 μm diameter. Addition of rapamycin loaded PLGA particles reduced the expression of DCs activation markers, including MHC II, CD40, and CD86. Due to the controlled-release properties of Ramps, even 4 days after DCs uptake the Ramps, DCs were able to reduce T cells activation. Nonetheless, soluble rapamycin failed to reduce T cells activation in the same 4 days period [283]. While this was not a direct biomaterial-based immunomodulation, but it infers that biomaterials could be used to regulate or extend the immunomodulatory effects of molecules. Variety of these molecules are in the literature. For instance, stimulation of human peripheral blood monocytes with granulocyte-macrophage colony-stimulating factor (GM-CSF) and IL-4 leads to the polarization of induced DCs (iDC). Due to the transient polarization, $1,25(OH)_2D_3$ (vitD3) could be used to prevent the iDCs' repolarization to the mDCs. Following that, the expression of CD1a, CD80, and CD40 in such cells is reduced, with no effect on the ability of IL-10 production [290]. In another study, vitD3 was found to restricts the full differentiation of monocytes to iDCs and macrophages. Although, DCs morphology did not change in the presence of vitD3, the CD86 and CD16 markers were not expressed on DCs and the expression of CD1a and CD14 were decreased and increased, respectively. The vitD3 inhibits the expression of CD40 and CD86 leading to a reduction in the ability of DCs to stimulate T cells. It was concluded that vitD3 modulate the immune response in the first step through inhibiting the DCs differentiation and maturation [285].

Administrating the agonist and antagonist of immune cells, especially the APCs like DCs, is one the most widely used immunoengineering approaches to obtain therapeutic outcomes.

According to the DCs functional mechanism, CD86 and CD80 are always considered as therapeutic targets in autoimmune diseases, tumors treatment, biomaterials implantations, and allograft transplantation [291]. The interaction of CD40, expressed on DCs, with CD40L, expressed on T cells, leads to upregulation of costimulatory molecules and secretion of cytokines like IL-6, IL-10, IL-12, and TNF-α [292]. Administration of CD40 antagonist mAb (ch5D12) together with CD86 antagonist mAb (chFUN-1) has shown to prevent kidney transplant rejection in a Rhesus monkey [293]. Animal groups intravenously received ch5D12 alone or combination of ch5D12 with chFUN-1. Both the protocols prevent the transplant rejection until the treatments was stopped with no side effects[293], and animals treated with the combination of mAbs did not survive longer than the animals treated with a high dose of ch5D12. The in vitro consumption of CP-870-893 mAb, a fully human CD40 agonist IgG2 mAb, results in apoptosis of tumor cells and a defect in tumor growth. Assessments on 29 patients with advanced solid tumors revealed partial responses in four cases and a definitive treatment response in one case. Noteworthy that these treatments are associated with side effects. Muromonab anti-CD3 has been used to prevent renal allograft transplant rejection, but it is accompanied with side effects that occur following infusion and lead to cytokine release syndrome (CRS) [294].

The ipilimumab as a specific antagonists antibody for CTLA-4 can suppress tumor cells, while having a series of side effects like rash and hepatitis [295]. Intravenously injection of Theralizumab (TGN1412), a superagonist monoclonal antibody for CD28, into 6 healthy male volunteers led to severe complications like induction of proinflammatory cytokines accompanied with a headache, nausea, diarrhea, hypertension, kidney failure, lung injury and severe and unexpected destruction of lymphocytes [296]. In another case, administration of specific CD40L mAb led to thromboembolic complications [297].

In addition to mAbs, aptamers could be used as active immunomodulatory molecules. The advantages of aptamer vs. mAb could be: 1) Synthesizing aptamers is cheaper, 2) Aptamers remain more stable at room and higher temperatures, 3) They are smaller than antibodies, 4) They may be less immunogenic, and 5) Aptamers may in some cases possess more inhibitory potency compared to antibodies [298, 299]. To fabricate aptamers, Gold and Tuerk developed the Systematic Evolution of Ligands by EXponential enrichment (SELEX) process, where oligonucleotides with a length of 30 to 40 bases were able to make a specific connection to proteins and [300-302]. With the advances in molecular sciences and the foundation of the specific aptamers SELEX technique, specific aptamers have been isolated for many targets including nucleic acids, amino acids, sugars, and their polymers, as well as mineral compounds and cell markers.

Aptamers could be used in blocking the active domain of immune-reactive molecules. RNA aptamers have been developed to block the internal domain of CD11a, which reduces cell adhesion to the leukocytes. Mechanistically, this aptamer prevents the signal transduction resulting from ICAMs and CD11a interaction. Authors further identified four aptamers against CD11a named TR-d20, TR-D28, TR-D31, and D42. Their work revealed that TR-d20, TR-D28, and TR-D31 are able to detect the CD11a with a high specificity [303]. Pastor et al identified two aptamers of CD28Apt2 and CD28Apt7. The monomeric state of the former could block the interaction of CD28 with CD80/CD86, which prevents the co-stimulatory signals transmission. Therefore, such aptamer strongly inhibits the proliferation of lymphocytes and induces T cells anergy. This aptamer could be effective in drug delivery systems for autoimmune diseases and reduce the rejection of biomaterial implantation or allogeneic transplant. Interestingly, they found that this aptamer in its dimeric state (unlike its monomeric state) acts as an agonist.

CD28Apt7 aptamer acts as an agonist that it can be considered as an appropriate candidate for promoting anti-tumor effects [291]. The TLR9 receptor activation leads to the anti-inflammatory responses and inflammation control in Sjogren's syndrome. Geffen et al identified the BL70-40 agonist aptamer which upon binding to the TLR9 leads to NF-κB activation. This activation increases the saliva and enhances the anti-inflammatory responses in the salivary glands to reduce the Ache's activity [304].

Proteins in DCs responses

Upon the biomaterial implantation in a physiological environment, the rapid blood-material interaction gives rise to the adsorption of proteins such as albumin, fibrinogen, fibronectin, laminin, collagen, vitronectin [223]. The protein adsorption initially is based on their diffusion, which can be influenced by different protein parameters like concentration in the implanted region, the size, the mobility, and more importantly their affinity to the surface. In this process, gradually, protein with more affinity would be substituted with the proteins with less affinity [207, 223]. DCs commonly adhere to adsorbed proteins through their β2-integrin receptors, so the type and conformation of proteins induce different responses like the maturity of DCs which leads to the activation of the adaptive immune system, or tolerogenic responses (**Figure 2.8**). The potential of adsorbed proteins to induce DCs maturation and activation of the adaptive immune system is assessed [207, 223, 252, 305, 306]. Brand et al showed that ECM proteins highly contribute in the DCs maturation, moreover, β_1-integrin leads to DCs adhesion to the adsorbed collagen type I followed by the maturity of DCs, and ultimately the expression of stimulatory and co-stimulatory molecules [307]. In the same context, Kohl et al suggested that monocyte-derived DCs and CD34+ stem cell-derived DCs use $\alpha_5\beta_1$ and $\alpha_6\beta_1$ integrins to adhere to the laminin and fibronectin, respectively.

According to [208, 257], fibrinogen adsorption leads to inflammatory response, while, adsorption of fibronectin and vitronectin contribute to the regulation of inflammatory responses. Furthermore, fibronectin and vitronectin are well-known ligands for β_1-integrin and fibrinogen is known as a β_2-integrin ligand, while the expression level of β_1-integrin in comparison to that of β_2-integrin is significantly lower in DCs. Therefore, surface engineering to direct the adsorption of the proteins like fibronectin, vitronectin, and collagen type I, which restrict the β2-mediated adhesion of DCs could contribute in the reduction of the DCs maturity. Such findings indicate that adsorbed proteins on biomaterial play crucial roles in the DCs responses [305]. Sigal et al reported a correlation between protein adsorption and wettability, where a surface with less wettability adsorbs more proteins. Moreover, they reported that large and small proteins have higher binding affinities to hydrophobic surfaces, while larger ones also get adsorbed to all the tested surfaces irrespective of the surface wettability [221]. It is proposed that hydrophobic biomaterials are recognized by TLRs as danger signals and trigger DCs activation [260, 308, 309]. Therefore, as DCs key adhesion molecule is β_2-integrin, it could be concluded that hydrophobic surfaces trigger an immune response by promoting DCs adhesion and maturation (**Figure 2.8**).

Protein adsorption on the microparticles surfaces also determines the immune response. It has been shown that protein adsorption on drug carriers impose a significant effect on phagocytosis by DCs. For instance, human serum albumin and IgA adsorption on the microparticles' surface give rise to reduction in the identification and phagocytosis through DCs [310, 311]. Thiele et al found that adsorption of α_2-human serum glycoprotein (α_2GP) on the microparticles' surface can increase the phagocytosis process [311]. Lee et al assessed the effect of biomaterials' surface on the interaction of the $\alpha_5\beta_1$ integrin of the K562 cell surface with

fibrinogen. Their results indicate that the adsorbed protein on hydrophilic surfaces in relation to hydrophobic surface has more binding with integrin, supporting more binding to K562 cells, and is subject to the following pattern: $COOH \approx CH_3 \approx NH_2 < OH$. They found that the orientation and conformation of adsorbed fibrinogen on the surface with a negative charge may result in the formation of stronger bonds with $\alpha_5\beta_1$ receptors. The fibrinogen's bond with $\alpha_5\beta_1$ has lower strength on the surface with COOH functional group compared to OH [312]. In a similar study, Lee et al showed that albumin adsorption increases by surface hydrophobicity, which corresponds to other reports [313]. Tanahashi et al found that the positive charge in the hydrogel can significantly increases the adsorption of vitronectin [222].

Tsuruta et al reported that polymers with hydroxyl functional group could incorporate water molecules at the surface and form a mesh-like structure. The mesh structure further entraps protein molecules into their entangled structure. Tendency of COOH to fibrinogen is higher than CO_2CH_3 and CH_3OH, thus, they concluded that protein adsorption without any change in the conformation on the polymer surface depends on free water fraction level [314].

DCs responses to different biomaterials

In addition to high contribution in immune responses, DCs are critical for the induction of immunological tolerance. To assess the different biomaterials' effects on DCs responses, Shokouhi et al cultured the DCs with different kind of materials like alginate, poly (D, L-lactic acid-co-glycolic acid), (RG503), and poly (L-lactic acid-co-trimethylene carbonate), (LT706) and found that such materials induce different levels of DCs maturation and surface markers expression. Moreover, they found that the hydrophobic materials, in comparison with hydrophilic, induce the release of more cytokines and chemokines, and that the TLRs could recognize the hydrophobic section of biological molecules as alarms [260].

In a similar study, Roger and Babensee showed that PLGA and chitosan films induce DCs maturation, by measuring the cytokines secretion and CD86 expression, while they did not observe this phenomenon in hyaluronic acid and agarose films. They assessed the importance of material type as an effective parameter in the level of DCs adhesion to BAMP. They found that DCs on the surface of PLGA film polarized into mature morphology. DCs adhered more on PLGA, while the DCs on the tissue culture polystyrene surface remained spherical with less adhesion. Blocking β_2-integrin with mAb reduced the maturation of DCs on either tissue culture polystyrene or PLGA.

Applications of biomaterial-based DCs immunoengineering

In this section, we briefly will review some of the applications of DCs immunoengineering through biomaterials approach. While at its infancy, materials-based immunomodulation has a promising future in the health industry. Dental implants, drug eluding biomaterials, transplantation devices, wound healing patches, anti-wrinkle injectables, biosensors, beauty and other medical implants could potentially be the market for immunomodulatory biomaterials. For example, Induction of tolDCs is known to promote osteointegration through improving the osteogenic differentiation. Zheng et.al investigated the surface effect of Titanium implant on the osteointegration and DCs maturation. Early osteogenic differentiation of MC3T3-E cells was tested on different Titanium surfaces including pretreatment (PT), sandblasted/acid-etched (SLA) and modified SLA (modSLA) treated Titanium surfaces. PT and SLA surfaces were hydrophobic with the contact angle of 109.9° and 77.4°, respectively, while the modSLA surface was hydrophilic (contact angle: 10°). modSLA surface had the highest concentration of surface oxygen (approximately 50%) and lowest concentration of carbon (32.74%) among other groups. The results implied that DCs cultured on

the modSLA surface, unlike PT and SLA surfaces, had a tolerogenic phenotype , which promoted osteogenic differentiation of MC3T3-E cells [240].

Microorganisms, such as bacteria, stick to and multiply on the surface of the tooth and in the pockets surrounding the tooth. This leads to an immune response, which causes an inflammatory disease, known as periodontitis. Sands et.al demonstrated that Tregs could be upregulated via injection of alginate loaded with GM-CSF and thymic stromal lymphopoietin (TSLP), intradermally into periodontitis tissue. They further showed that controlled local delivery of GM-CSF and TSLP from alginate hydrogel significantly increased tolDCs numbers in local lymph nodes, resulting in the enrichment of periodontal tissue with Tregs and IL-10, which in turn reduce inflammation [315]. Interestingly, adoptive transfer of tolDC has shown significant improvement in the rodent model of type 1 diabetes. Besin et.al showed that DCs in the presence of TSLP possessed a tolerogenic phenotype. Subcutaneous transplantation of TSLP-induced tolDCs in mouse model of autoimmune diabetes polarized T cells to the Treg and increase the production of IL-10 from Th2 cells. Only 25% of TSLP-tolDCs-injected mice developed diabetes starting at 18 weeks and maintained until 45 weeks, while 80% of control groups develop autoimmune diabetes [316]. Due to the challenges and costs associated with cell therapy, it could be of interest to develop a controlled-release biomaterial with capabilities to induce tolDCs, and the efficacy of the implant in reversing or delaying the occurrence of autoimmune diabetes. Interestingly, PLGA nano and microparticles loaded with GM-CSF, TGFβ, and insulin as an autoantigen, could induce tolDCs. This material boosted Tregs in pancreatic lymph node and spleens, increased PD-1 on CD4+ and CD8+ T lymphocytes, and reversed hyperglycemia for up to 100 days in autoimmune diabetes mouse model [317].

One of the recent avenues in immunoengineering is to use body's endogenous cells to reprogram other cells in the host. Artificial DCs/APCs (aAPCs) are one example of immunotherapy approach for autoimmune diseases and transplantation. The aAPC has been developed by coupling tolerance-inducer molecules to the different types of bead-based platforms including polymeric beads, inorganic beads, and lipid-based beads [318]. Shen et.al used a latex bead aAPCs, while H-2K^{b} peptide and apoptosis-inducing anti-Fas monoclonal antibody covalently coupled onto the bead surface. Administration of these beads depleted alloantigen (H-2K^{b})-specific T cells and prolong graft survival in a mouse model of alloskin transplantation. After transplantation of Full-thickness dorsal skin from male C57BL/6 mice (H-2K^{b}) to male BALB/c mice (H-2K^{d}) the prepared complex was injected intravenously. The prepared complex significantly depleted the antigen-alloreactive T cells and prolonged the graft survival without impairing overall immune responsiveness including antitumor responses [319].

Inflammatory Response Against Implanted Biomaterials

The past decade has witnessed huge advances in designing hybrid scaffolds for tissue engineering. Many novel technologies from synthetic biomaterial designs, scaffolds originated from extracellular components, bio-hybridization of naturally occurring glycolipids, proteins, and peptides with synthetic material to more futuristic technologies such as 3D printing have been advanced during this time. One aspect of some tissue engineered scaffolds is partly attempting to provide the host niche with a functional part to replace a diseased or defunct tissue. Successful implantation requires the compatibility of the scaffold with the host immunity and functionally integrate with the body. In this chapter, we will first review the current understanding of the scaffold's interaction with the host immunity. We then will briefly introduce the concept of bio-integration. Future developments in tissue engineering scaffolds are

partly focused on the capability of implants to regulate the local immune response as well as their potential to integrate with the host's body.

Macrophages in the forefront of immune response against implants

More than 0.5 million types of medical devices have entered the market according to FDA and Medtech Europe estimates [320]. More than a million cardiovascular devices are implanted each year [321], and 10 million dental implant procedures are performed [322]. Knee and hip arthroplasty procedures are exceeding 1 million per year only in the USA [323]. Five to ten million women worldwide have been reported to have artificial breast implants by 2011 [324]. Tissue engineered scaffolds are generally recognized as safe and bio-inert, but their utility has yet to be demonstrated on a larger scale. The first clinical trial tissue engineered grafts was initiated in 2015 (RegenVox study), which was later withdrawn on 2018 (clinicaltrails.gov).

It is noteworthy that grafts could trigger an immune response (immunogenic), interact with the host without causing an immune response (antigenic) or interact with the host following by immune reaction (immunoantigenic) [325]. Multiple factors including material type, size and shape [326, 327], location of the graft [328], and surgery procedures could influence such an immune response.

In this chapter we will focus on the myriad of events following by implantation of tissue engineered scaffolds. We then will briefly introduce the concept of biointegration. The interdisciplinary research within tissue engineering and immunology fields is one exciting trend in designing implantable scaffolds in the future.

Host immune reaction against implanted scaffolds

Long-term function and survival of implanted scaffolds requires absence of detrimental immune response [329]. For instance, glucose sensors fail to function up to their expected life-

time upon implantation and demonstrate erratic responses [330]. The immune response recently has been shown to be the main factor for signal inaccuracy in glucose measurements of continuous glucose monitors [331]. Understanding the evolution of immune response against implants is therefore of interest in tissue engineering field. In this section we attempt to review the myriad of immune system activation against implanted biomaterials.

Surgical procedure induces initial inflammation

In most cases, implantation of biomaterials is accompanied by injuries induced by surgical processes. Signals associated with wound formation prior to implantation call for innate immunity to act at the region. Surgical procedure initiates acute response recognized by the recruitments of macrophages and monocytes to the site of surgery, leading to the production of pro-inflammatory cytokines [328]. Non-hepatic systemic inflammatory responses, such as fever and tachycardia, are triggered by the release of tumor necrosis factor α (TNF-α) and interleukin 1β (IL-1β). TNF-α and IL-1β also stimulate the secretion of other cytokines, including IL-6 [332]. IL-6 regulates the hepatic acute response through the production of C-reactive proteins and other acute-phase proteins [333, 334].The release of proinflammatory cytokines and nitric oxide by macrophages and neutrophils can cause capillary leakage, providing even more leakage for the immune cells to localize around the inflamed area [335]. Clinically, the levels of IL-6 are also correlated with the severity of tissue trauma and the duration of surgery as well as the development of major complications [336, 337]. Laparoscopic procedures are associated with lower levels of IL-6 in comparison to open surgeries [338].

The disruption of microcirculation, which is the circulation of the blood in the terminal arterioles, capillaries, and venules, following surgery is also common and can lead to microvascular inflammation and vasoconstriction that reduces blood flow. At the site of

inflammation, leukocytes accumulate and adhere to the endothelial lining of blood vessels through adhesion molecules, such as selectins, CD11a/b/c, endothelial intercellular adhesion molecule 1 (ICAM-1), and vascular cell adhesion molecule 1 (VCAM-1), which increase the permeability of the blood vessels and disrupt their integrity [339]. Further, the attachment of polymorphonuclear cells (PMNCs) to the endothelium obstructs microcirculation and transcapillary fluid exchange. The combination of capillary leakage and disruption of microvascular environment results in serious vascular dysfunction that can lead to tissue damage as cells experience hypoxia and expose to progressive toxic metabolite accumulation [340].

Bacterial adhesion

Prior to implantation, tissue engineered scaffolds are prone to bacteria attachment. Increase in the number of implants application, such as catheters and prosthetics, correlate with the increasing rates of infection prevalence worldwide. For example, in 2014 Magill, S. S. et al. assessed that 25.6% of healthcare-associated infections in the United States were from device implants [341]. Infections can arise from implantation of biomaterials at surgical sites but is especially evident when the implant is exposed through an orifice, as external bacteria can penetrate the body [342]. A highly common infection-causing medical device is the urinary catheter, which alone, accounts for about 40% of the device-implant infections [343]. Such bacterial infections pose major complications as the implants are not able to be successfully integrated and normally functioning in the host body. In more severe cases, the patient may require device replacement or removal and can even suffer from bacterial resistance and persistence.

The surface of the implant serves as the attachment grounds for the proliferation of bacterial colonization. Device infections typically stem from the exposure of a body opening to

bacterial contamination during an implantation process. Following the implant, is the immediate attachment of extracellular matrix proteins that will result in the fimbria and hydrophobic adherence of bacteria onto the surface through the release of polysaccharide intercellular adhesin [344]. A new layer, known as biofilm, is eventually formed on top the biomaterial surface with the accumulation of microbial attachment and secretion of more extracellular polymeric substances [345]. The biofilm layer poses as a defense barrier for the microbes from inflammatory cells. The extracellular polymeric substances, consisting of exopolysaccharides, proteins, extracellular DNA (eDNA), etc., also act as media for the microbes to thrive, communicate, and exchange genes [346].

The transfer of genes between microbes and diversity in species introduces the concepts of immune response evasion and antibiotic resistance due to the variance in the gene sequences and phenotypes expressed; hence, the persistence of bacterial colonization [347]. Because bacteria can communicate and exchange genes within the biofilm, modern antibiotics are becoming less effective due to the microbes' adaptive abilities. Prosthetic implant infections can already be caused by many different types of bacteria (**Table 2.3**), and so, a particular type of infection is not limited to just a single bacterium, let alone a single strand of DNA, which is why bacterial infections are so difficult to treat [348].

As another form of survival, some microbes such as Staphylococcus Aureus, a species recognized in orthopedic infections, could occupy non-immune host cells as an evasion mechanism from inflammatory phagocytes and antibiotics [349]. Additionally, over time the microbe can trigger apoptosis of its host cell and thereby adhere to the implant. The trigger is accomplished by the bridge formation between staphylococcal fibronectin-binding protein

(FnBP) and α5β1 integrin on the host cell [350], which in turn increases the number of cell receptors to TNF-related apoptosis-inducing ligand and activates caspase 8 for apoptosis [351].

The high levels of bacterial attachment on its surface would be substituted by the host cells, as the process just a "race for space". Correspondingly, an increase in bacterial attachment, would correlate to a denser layer of biofilm [345]. Several factors such as the type of implant, level of invasiveness, and site of insertion play role in determining the severity of an infection [352].

Table 2.3. Major types of bacteria responsible for implant infection. Retrieved and recreated form ref [342] with permission. Copyright 2018, Nature Publishing Group.

Species	**Prevalence in medical device infections (%)**	**Prevalence in knee arthroplasty infections (%)**	**Prevalence in hip arthroplasty infections (%)**	**Prevalence in Infections involving external fixation (%)**	**Prevalence in Infections involving internal fixation (%)**	**Refs**
Staphylococcus aureus	31.7	21.1	22.2	54.5	47.8	[353]
	33.8	26.4	24.4	47.8	42.5	[354]
	13.0 (EU)[a]–31.0 (US)[a]	12.1 (EU)[a]–29.6 (US)[a]	13.6 (EU)[a]–32.6 (US)[a]	ND	ND	[355]
Coagulase-negative staphylococci	20.2 (US)[a]–39.3 (EU)[a]	21.7 (US)[a]–37.0 (EU)[a]	18.4 (US)[a]–40.7 (EU)[a]	33.8	33.8	[355]
Staphylococcus epidermidis	39.0	52.6	48.1	18.2	26.1	[353]
	31.5	41.8	43.6	15.2	21.9	[354]
Coagulase-negative staphylococci other than Staphylococcus epidermidis	11.6	ND	ND	ND	ND	[353]
	12.8	ND	ND	ND	ND	[354]

Streptococcus spp. and Enterococcus spp.	10.3 (US)[a]–14.5 (EU)[a]	10.3 (US)[a]–14.5 (EU)[a]	9.1 (US)[a]–12.1 (EU)[a]	ND	ND	[355]
Enterococcus faecalis	2.4	2.6	0.0	0.0	6.5	[353]
	4.4	0.5	3.5	8.7	5.3	[354]
Gram-negative bacteria	ND	4.5 (EU)[a]–6.4 (US)[a]	4.2 (EU)[a]–6.8 (US)[a]	ND	ND	[355]
Pseudomonas aeruginosa	6.1	10.5	3.7	18.2	4.3	[353]
	6.7	4.4	2.9	14.1	8.9	[354]
Escherichia coli	2.4	5.3	0.0	0.0	0.0	[353]
	1.6	ND	ND	ND	ND	[354]

EU: data from a European reference clinical setting; ND: not determined; US: data from a US reference clinical setting. [a]Infections after total arthroplasty.

Protein fouling further calls for immune response

Immediately after contact of biomaterials with tissue, biomaterial surface adsorbs proteins from interstitial fluid and blood [208]. Protein adsorption on biomaterial surfaces is followed by the competitive exchange of adsorbing and desorbing proteins. Based on this effect, proteins initially adsorbed on a surface are later on displaced by subsequently incoming proteins, which was first observed in 1960s by Vroman and Adams [356]. This protein fouling alters the composition of the proteinaceous coating of the biomaterial surface. Molecules in a protein mixture solution diffuse onto a surface at different rates. Proteins with lower molecular weight as well as highly concentrated proteins adsorb to the surface first and these proteins may later be replaced by other larger proteins or proteins with higher affinities but lower concentration [357].

Following the initial injury and implantation, proteins adsorb to the biomaterial surface in a process known as blood-material interactions, in which the coagulation systems, the complement system, the fibrinolytic system, the kinin-generating system, and platelets are activated by the initial vascular injury at the surgical site as we discussed earlier in this chapter [358-360] (**Figure 2.12A**). There are three main factors that affect protein adsorption:

characteristics of the proteins, physical properties of the biomaterial, and the environment of the implant site.

The blood plasma contains several types of proteins with various sizes, functions, and concentrations in the blood [361]. One of the most significant characteristics of proteins that affects protein adsorption is the type of interactive forces that cause proteins to attach to a surface. Because different proteins have different structures and properties [362], the bonds that they form with a biomaterial also vary. For example, a protein may engage in ionic interactions with a surface depending on its isoelectric point [363]. In a study that specifically examined bovine serum albumin (BSA), researchers found that BSA adsorbed to a biomaterial nearly 1000 times faster if the implant's surroundings did not match BSA's isoelectric points [364]. Therefore, proteins with an isoelectric point that is similar to physiological conditions adsorb to a surface less readily than proteins with higher or lower isoelectric points [363]. Other than a protein's isoelectric point, its intramolecular cross-linking pattern or rate of unfolding may affect the types of interactions the protein makes and its rate of adsorption [365].

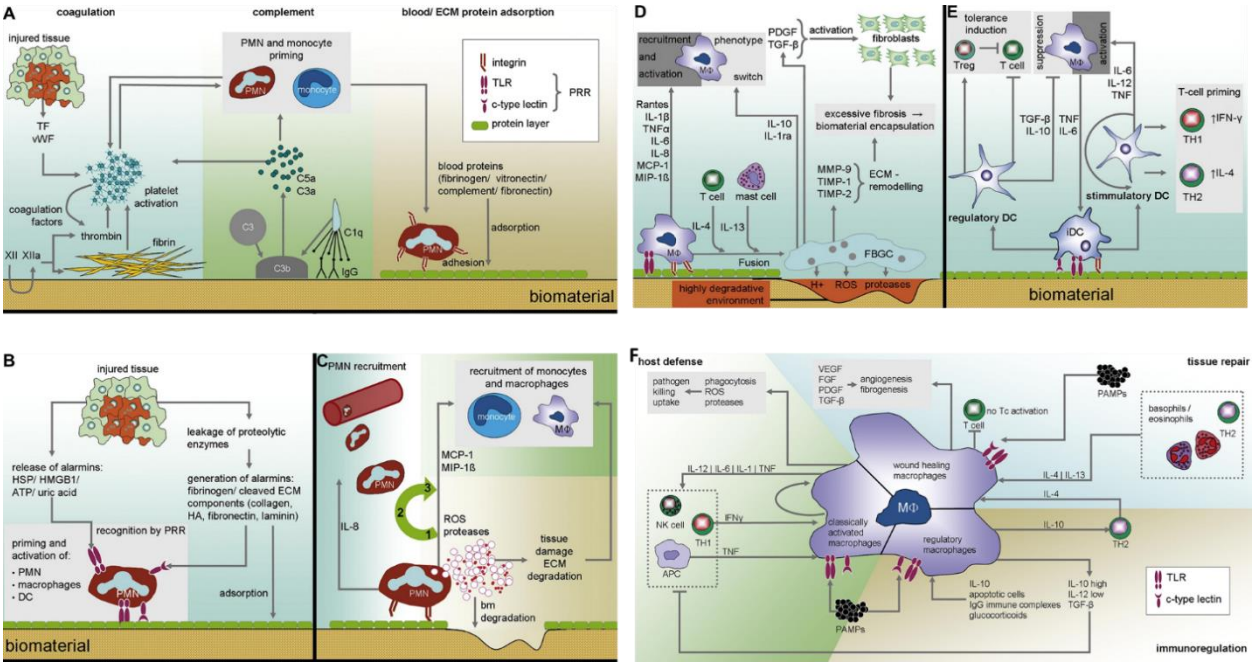

Figure 2.12. Myriad of immune response against implants. A) Following by protein adsorption onto biomaterials surface, coagulation cascade as well as complement and platelet adsorption initiate, resulting in activation of PMNCs cells, adjacent circulating monocytes, and resident macrophages. **B)** Damaged tissue further release alarmins, priming the immune cells for enhanced function by the engagement of pattern recognition receptors. **C)** The initial response (acute inflammatory response) is led by PMNCs cells, where they secrete proteolytic enzymes and ROS to digest the surface of implant. PMNCs cells sustain their influx and priming through secretion of IL-8. In later stage, PMNCs cells stop secreting IL8 to make transition from acute to chronic inflammation through secretion of cytokines that promote migration/recruitment and activation of circulating monocytes and resident macrophages, the key players of chronic inflammation. **D)** Sustained secretion of inflammatory mediators like TNFα, IL-6, and MCP-1 results in permanent activation of macrophages. Next, IL-4 and IL-13 cytokines induce the fusion of macrophages to foreign body giant cells, forming a degradative environment on the implant surface. Furthermore, foreign body giant cells induce remodeling of extracellular matrix and promote fibroblast activation culminating in extreme fibrosis. **E)** Dendritic cells also get activated by macrophage-secreted cytokines and engagement of pattern recognition receptors activate. Nature of the stimulus determines the maturation of dendritic cells to either immunogenic or tolerogenic subtypes, to amplify or suppress the inflammatory response, respectively. **F)** Based on their polarization, macrophages could enhance wound healing, immune dampening, or immune attack. It is accepted that macrophages regulate their functions based on biophysical/biochemical cues within their environment. Reprinted with permission from ref. [208] Copyright 2011, Elsevier.

The molecular weight of proteins is another determining factor in the rate of adsorption and the types of protein layers that are formed upon adsorption. The size of a protein affects its diffusion rate, which ultimately affects the rate of adsorption [363]. According to the Stokes-Einstein equation, the diffusion constant is inversely proportional to the radius of the protein [366]. Although some studies have proven that the Stokes-Einstein equation overestimates the

diffusion constant for several proteins, the inverse relationship between protein radius and diffusion constant presented by the equation is still valid [367]. Other than the seemingly instinctive information that smaller proteins diffuse faster, the size of proteins also affects how layers are aligned across the foreign material's surface. Larger proteins form multiple layers around a biomaterial, while smaller proteins usually adsorb as full or partial monolayers [368]. In a study comparing an array of proteins, researchers found that the number of layers that the proteins could form increased with molecular weight [369]. Assuming that the partition coefficient was fixed for all proteins, immunoglobulin M (IgM) (MW = 1000 kDa) was capable of occupying five layers, while albumin (MW = 66 kDa) only formed one [369]. Therefore, the size of the proteins that adsorb to a biomaterial not only correlates to their rate of protein adsorption, but also the thickness of the layers that the proteins form.

The concentration of protein in the blood plasma is also a significant variable that affects protein adsorption. Because blood plasma is an amalgam of proteins with varying concentrations [370], the proteins compete against each other to adsorb onto a surface. The diffusion rate of a protein is directly proportional to two values: the diffusion constant, which is the aforementioned value that depends on protein size, and the concentration of the individual protein in the solution [363]. As the concentration of a protein increases, its rate of diffusion across the plasma increases and the number of that protein adsorbed to the surface increases as well [371]. The concentration of each protein in the plasma also affects the protein layer formation around a biomaterial surface. When concentrated enough, proteins will arrange themselves on the material as closely as possible [372]. Therefore, a greater concentration of a certain protein will encourage its formation of a monolayer on a larger surface area of a biomaterial.

The orientation of proteins adsorbed onto a biomaterial surface influences the adsorption of subsequent proteins and ultimately the immune response. If proteins adsorb to a surface in a certain orientation, they limit the remaining surface area available for other proteins [363]. Consequently, this leads to other proteins adsorbing to the surface in different orientations or in smaller quantities than expected [363]. Protein orientation could also trigger the immune response. For instance, depending on how immunoglobulin G (IgG) adsorbs onto the surface of a biomaterial, bacterium, or even a nanomaterial (such as liposome), opsonization may occur [373].

Besides the characteristics of the proteins involved in adsorption, the physical properties of the biomaterial implant such as hydrophilicity also affect how fast and how effectively proteins may adsorb. The hydrophilicity of a biomaterial is an indirect measure of the presence of functional groups available for hydrogen bonds and charge within a material [374]. Hydrophobic and weakly hydrophilic biomaterials are known to attract more proteins than hydrophilic materials. This is because proteins must displace a larger amount of water molecules bound on the surface for hydrophilic biomaterials, thus requiring a greater amount of energy for proteins to adsorb [375]. The effects of hydrophilicity on protein adsorption can be proven further by observed changes in protein adsorption for biomaterials that are treated with hydrophilic coats on the surface. When hydrophilic polyelectrolyte films were coated over a biomaterial, the adsorption of blood plasma proteins was decreased by up to 20 times compared to the uncoated biomaterial [376].

Another category of factors that affects protein adsorption is the environment of the implant site. Although not as significant as the characteristics of the proteins and the biomaterial, the surroundings of the implant may affect how fast proteins adsorb to a foreign surface.

Physiological conditions that may affect protein adsorption include body temperature and pH. Temperature influences the kinetics of protein adsorption. Temperatures higher than body temperature accelerate the diffusion of proteins to the surface of the biomaterial implant [377]. It has been observed that the degree of BSA and fibrinogen adsorption on a temperature-responsive biomaterial at room temperature and 37 °C drastically influences the proteins adsorbed per unit of surface area [378]. While temperature affects the adsorption rate of most proteins, pH affects certain proteins by affecting their electrostatic state. As mentioned above, proteins adsorb more readily if the isoelectric point of a protein is different from the protein's surroundings [363]. If the implant site's pH is different from a specific protein's isoelectric point, that protein is more prone to engage in electrostatic interactions with a foreign substrate [377].

The thrombosis at the tissue/biomaterial surface forms the provisional matrix surrounding the scaffold [358]. Damaged tissue further release alarmins, priming the immune cells for enhanced function by the engagement of pattern recognition receptors (**Figure 2.12B**).

During the provisional matrix formation phase, both the classical and alternative pathways of the complement systems are activated as well as the coagulation cascade [379]. A fibrin matrix formed around the scaffold as C3b complement proteins deposit on the biomaterial surface, C3a and C5a complement proteins are released to recruit additional immune cells, and thrombocytes are activated through the coagulation system [360]. Fibrinogen, which is later converted into fibrin by thrombin [380], induces coagulation and the secretion of cytokines that further initiate the recruitment of immune cells [192]. It should be noted that fibrinogen could be deposited on materials surface based on the materials chemistry. Comparing the degree of phagocyte recruitment between polyester terephthalate films (PET) incubated with different amounts of fibrinogen, the PET sample that was exposed to more fibrinogen encountered more phagocytes than the sample that was exposed to less fibrinogen [381].

In addition, necrotic cells and damaged extracellular matrix release damage-associated molecular patterns (DAMP) that exacerbate the inflammation at the implanted site [382]. The implanted biomaterial also cause mast cells to degranulate, releasing histamine to promote diapedesis of inflammatory immune cells [383]. Ultimately, the provisional matrix serves as a framework for wound healing due to containing various cytokines, chemo-attractants, mitogens, growth factors and other substances that can increase microvascular permeability and modulate the activation/inhibition of immune cells.

The initial response (acute inflammatory response) is led by PMNCs cells, where they secrete proteolytic enzymes and reactive oxygen species (ROS) to digest the surface of implant. PMNCs cells sustain their influx and priming through secretion of IL-8. In later stage, PMNCs cells stop secreting IL8 to make transition from acute to chronic inflammation through secretion of cytokines that promote migration/recruitment and activation of circulating monocytes and resident macrophages, the key players of chronic inflammation (**Figure 2.12C**). Sustained secretion of inflammatory mediators like TNFα, IL-6, and MCP-1 results in permanent activation of macrophages. Next, IL-4 and IL-13 cytokines induce the fusion of macrophages to foreign body giant cells, forming a degradative environment on the implant surface. Furthermore, foreign body giant cells induce remodeling of extracellular matrix and promote fibroblast activation culminating in extreme fibrosis (**Figure 2.12D**). Dendritic cells also get activated by macrophage-secreted cytokines and engagement of pattern recognition receptors activate (**Figure 2.12E**). Nature of the stimulus determines the maturation of dendritic cells to either immunogenic or tolerogenic subtypes, to amplify or suppress the inflammatory response, respectively. Based on their polarization, macrophages could enhance wound healing, immune dampening, or immune attack. It is accepted that macrophages regulate their functions based on biophysical/biochemical cues within their environment (**Figure 2.12F**).

Following the formation of the provisional matrix, the acute inflammatory phase can last from minutes to days depending on the degree of damage from the surgery, the location of the implantation, and the level of provisional matrix formation [358]. The high levels of cytokines and chemo-attractants cause neutrophils, monocytes, and macrophages to migrate to the implanted scaffold. These phagocytic

cells can ingest cellular and extracellular matrix debris while secreting reactive oxygen and nitrogen species, proteinases, cytokines and chemokines that damage local tissues and recruit other immune cells [384-386]. Mast cells contribute to the phagocyte accumulation through histamine-mediated phagocyte recruitment [383, 387]. The severity of the acute response can be dampened through the administration of H1 and H2 histamine receptor antagonists, which reduces the buildup of inflammatory immune cells [387].

The initial acute response is followed by chronic inflammation that is characterized by the infiltration of mononuclear cells, such as monocytes and lymphocytes, and foreign body giant cells. Unless an infection occurs, chronic inflammation is resolved within 2 weeks [358]. The tissue repair process begins as macrophages, fibroblasts, keratinocytes, and other wound healing cells initiate the wound healing response.

Myriad of immune response following protein adsorption

The time frame of an immune response may vary depending upon many factors such as the size, shape, and surface properties of the implant (**Figure 2.13**)[388]. As mentioned earlier, upon the implantation of a biomaterial, the host's blood vessels are damaged. A specific type of immune response, known as the foreign body response, is subsequently initiated by the adsorption of proteins onto the implant and a thrombogenic surface is generated [358]. To repair the damaged blood vessels, coagulation begins as platelets are activated and form a mesh-like layer with the accompaniment of fibrin [381]. Bacteria then begin to adhere to the surface proteins and form a biofilm [389]. These initial reactions of coagulation and bacterial invasion collectively promote acute inflammation, otherwise known as the earliest stage of the immune response to an implant.

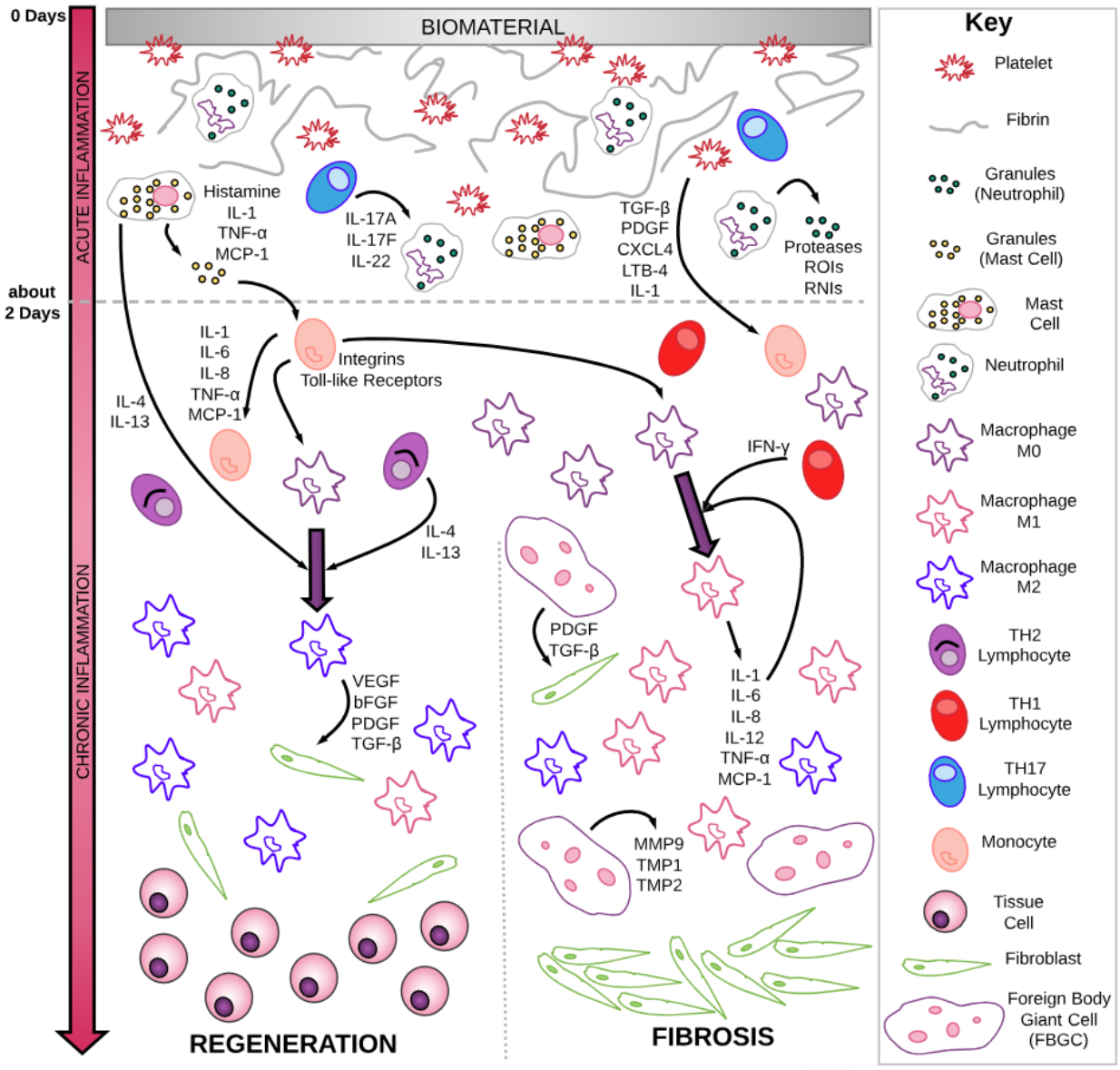

Figure 2.13 Overview of the Timeline for the Immune Response to a Biomaterial. Acute inflammatory response initiates by surgery pre-implantation. Second phase of inflammation occurs by absorption of proteins to the surface and the development of a provisional matrix. The matrix is loaded with platelets that plug the injured blood vessels, and also is a reservoir for growth factors and cytokines. This environment recruits PMNCs leukocytes and mast cells, typically known as acute inflammation phase. Further signaling molecules are subsequently secreted by the platelets and via degranulation of the neutrophils and mast cells, encouraging the recruitment macrophages to the site of implantation. The following stage is the chronic inflammatory phase defined by the presence of mononuclear cells. The secretion of factors (For instance MCP-1) signals further recruitment of peripheral blood monocytes that can differentiate into macrophages upon activation. During the initial phase of chronic inflammation, there is an increase in specific proinflammatory (M1) macrophages in the injured site. Stimulation by TH lymphocytes, the polarization of the macrophage population can change to a pro-healing phenotype (M2). Skewing macrophages from pro-inflammatory M1-type to pro-regenerative M2-type encourages the tissue regeneration at the implant site. However, M1-to-M2 polarization does not occur, the chronic inflammation phase will lead to fibrosis.

As the body's own version of self-defending soldiers, PMNCs Lymphocytes (PMNLs) including neutrophils are dispatched to constantly circulate and guard the body. As soon as the signals of a potential infection are sensed, Th17 lymphocytes immediately release IL-17 and CXCL8 to recruit inflammatory cells [390, 391]. The neutrophils are the first to be recruited to the site by quickly diffusing through the dilated blood vessels and begin attempting to phagocytose the implant [328, 392]. Often, these implants are too large for the neutrophils to engulf the foreign material. This prompts platelets to secrete growth factors, as well as, neutrophils and mast cells to degranulate into specific cytokines like IFN-γ and LPS [393]. These growth factors and cytokines then recruit macrophages and monocytes onto the battle site.

Recognized as the prime regulators of the response, macrophages are also a type of phagocyte that are responsible for not only the engulfment, but also the detection and antigen presentation of foreign entities [394]. Peripheral monocytes that are recruited to the implant site can also differentiate into macrophages upon activation [395]. After the macrophages' work in a normal wound healing process, fibroblasts would be drafted to repair and conclude the injury [396].

However, if aggravation from the inflammatory cells at an implant site persists, the process eventually diverges from normal wound healing. The next stage that follows is chronic inflammation [396]. If macrophages cannot proceed to engulf the foreign entities, they begin what is dubbed as "frustrated phagocytosis": a process in which many macrophages merge together, form a multinucleated foreign body giant cell (FBGC), and enclose the implant [394]. Instead of engulfing bits and pieces of the implant for the endo-lysosomal enzymes to catalyze, they secrete the enzymes into the interstitial space between the implant and FBGC. Finally, upon the activation of macrophages by IL-4 and IL-13 to stimulate the next step, the process

converges back to the normal wound healing process [397]. Fibroblasts are finally recruited and a granulation tissue around the implant forms with the deposition of collagen [397]. The dense, thick collagenous capsule immobilizes the functions of the implant, ultimately defeating its purpose.

Wound healing vs. scar formation

The process of how a wound heals is an important step for implant functional integration. Wound repair, or regeneration, consists of three stages: inflammation, new tissue formation, and remodeling [398]. To begin the sequence of acute wound healing, an inflammatory response occurs at the site of the injury. As mentioned above, the inflammatory response involves a cascade of events that begin with a fibrin clot and eventually lead to the restoration of the ECM [399]. Throughout the inflammatory response, a variety of cells including platelets and neutrophils are recruited to the wound area. Due to the recruitment of platelets, fibrin, neutrophils, and macrophages, hemostasis is restored and subsequent processes for wound healing is initiated. The inflammatory response occurs over the span of two to three days.

The second stage of wound healing, or new tissue formation, transpires over 2 to 10 days. This stage mainly consists of cell proliferation and migration [398]. After the bulk of the inflammatory response is concluded, keratinocytes migrate to the inner layer of the skin, known as dermis. Subsequently, angiogenesis occurs due to the positive regulation by the vascular endothelial growth factor A (VEGFA) and the fibroblast growth factor 2 (FGF2) [400]. The new capillaries formed from angiogenesis replace the fibrin matrix formed during the inflammatory response with granulation tissue. The structural repair of the wound is reinforced further via fibroblasts and myofibroblasts. Neighboring fibroblasts that are stimulated by macrophages

arrive at the wound area, and some differentiate into myofibroblasts. Fibroblasts and myofibroblasts then cooperate to produce an ECM. Along with the reconstruction of blood vessels and tissue, the keratinocytes that migrated also restore the barrier function of the epithelium.

The final and longest stage of wound healing is remodeling that can persist for a year or more. During most of this process, collagen is utilized as a medium to remodel and strengthen the injured skin. Most of the cells involved in the previous stages, which include macrophages and myofibroblasts, leave the wound site or go through apoptosis. Instead of the cells, the wound site is left with a mass that mainly consists of collagen and ECM proteins. Over the span of 6 – 12 months, remaining fibroblasts, macrophages, and endothelial cells collectively secrete matrix metalloproteinases (MMPs). MMPs convert the type III collagen backbone of the ECM into type I collagen [401, 402]. The degradation and reconstruction of the collagen backbone ultimately lead to a stronger repaired tissue.

If any phase during acute wound healing is interrupted, a nonhealing wound forms at the wound site [399]. As a result, the structure and function of the tissue at the wound will be not be optimal. The scars that form from the failure of acute wound healing can be classified as one of two categories: chronic wounds or post-injury pathological scars. Chronic wounds are defects in the skin's barrier caused by vascular insufficiency, diabetes mellitus, or effects from local pressure [399]. These scars usually occur on the lower part of the body [403]. For chronic wounds, the inflammatory response is prolonged [404]. Instead of the immune system progressing to the tissue formation stage of wound healing, there is a continuous competition between inflammatory and anti-inflammatory signals [405, 406]. One cause of the prolonged inflammation is a significant presence of proinflammatory cells, such as neutrophils and

macrophages, that delays healing [399]. Chronic wounds are often more critical than post-injury pathological scars.

Post-injury pathological scars consist of two types: hypertrophic scars and keloids. Hypertrophic scars occur after surgery or trauma, and they can regress spontaneously [399]. On the other hand, keloids do not regress spontaneously, and they are products of genetic predisposition [407]. The two types of pathological scars differ in their arrangement of collagen fiber and the extent of angiogenesis that occurs during scar formation. However, they share a similarity in that there is no optimal treatment for either one [408].

Although scar formation may not seem that significant because we encounter scars every day, fibrosis in certain areas can lead to additional complications that can be fatal. One example of an adverse effect of scarring in a specific region is pressure ulcers. These scars are a specific class of chronic wounds with a high mortality rate. To avoid further complications that may be critical to a patient's health, surgeons must monitor scar formation after the implant of a biomaterial.

Scar thickness and its effects

For biomaterials used within drug-delivery systems and tissue engineering, the thickness of a scar heavily impacts the biomaterial's effectiveness in carrying out its function. Biomaterials used in drug-delivery systems must utilize diffusive means in order to distribute drugs, as well as growth factors, to the surrounding local area [409]. Because the fibrous capsule can inhibit the diffusion of molecules from the implant into the body, it is evident that the thickness of a scar would impose a negative effect on implants.

Often times, the drug-eluting property of a stent that has been implanted into the body for the purpose of mediating the FBR will initially perform its job, but decline over time[410]. This

phenomenon occurs because the drug-eluting stent (DES) can delay the immune response, but not prevent it [110]. Before DES, bare metal stents (BMS) were developed because clinicians found that about 50% of their patients had to receive further angioplasty within the timeframe of 6 months [411]. These BMS were meant to keep the coronary artery open after the withdrawal of the PTCA balloon in angioplasty patients and reduced their number of clinical visits [412]. Despite these benefits, clinicians later found out that BMS were able to trigger a FBR that could result in additional narrowing of the artery [411]. As a result, scientists developed the DES. Ironically, Shuichi, et al. in 2013 found that the "accumulation of T lymphocytes tended to increase and that of macrophages increased significantly in the DES lesions compared with BMS lesions of the arteries"[413]. In other words, when comparing DES with BMS designs, DES seemed to have triggered a higher level of inflammation due to the higher prevalence of inflammatory cells at the implant site.

Recent understandings on immune cells activity against implants

Presence of Th17 Helper T-cells and recruitment of Neutrophils

Cellular-mediated immunity T-lymphocytes can be broken down into two subcategories: Cytotoxic (CD8+) and Helper (CD4+), where CD4+ can be further broken down into four subtypes: Th1, Th2, Th17, and Treg [390]. Th17 distinguishes itself from Th1 and Th2 in that it can participate in the phagocytosis process of microbes. The recruitment of neutrophils and the beginning of an immune response can either be indirectly induced by the release of IL-17A and IL-17F, or directly chemo-attracted by the release of CXCL8 (IL-8), from Th17 Helper T Cells [414].

Although current knowledge about Th17 lymphocytes is still relatively limited, Cappellano et. al have provided evidence to confirm the participation of Th17 lymphocyte during fibrous capsule formation. In their study, human peripheral blood mononuclear cells (PBMC)

was utilized to examine the foreign body response towards silicone breast implants in-vitro [415]. A chronic pro-inflammatory response is often induced by the implant's degradative silicone particulates [416]. Thus, capsular contracture, a frequent complication that arises with breast implants, is a variation of the fibrous scar tissue that forms because of the FBR. The capsular contracture tightly constricts around the breast implant until it becomes stiff and deformed [417]. The extent of the capsule formation depends upon many variables such as: the quantity of recruited inflammatory cells, whether the breast implants was silicone or saline, and time spans [418]. From immunohistochemical analyses on capsules of varying thickness, it was found that macrophages, fibroblasts, and activated CD4+ T-cells expressing CD25 and CD45RO markers, were prevalent at the breast implant surface [419]. Multiple analyses of flow cytometry on the capsule were also examined and a dominance of Th17 lymphocytes in comparison to regulatory T lymphocytes was observed, re-establishing the extent of capsule thickness and maintenance of suppressive activity [420].

3.2 Macrophages and their polarization

When migrated from the bloodstream into tissues, monocytes differentiate into macrophages [421]. The polarization of macrophages into a certain phenotype is highly dependent upon the specific microenvironment and conditions of their tissue location [422].

Unlike neutrophils, macrophages can be categorized into two functional subdivisions based on their activation pathway: M1 (Classical) and M2 (Alternative) [423]. M2 macrophages are then further distinguished into a diverse array of subtypes, such as: M2a, M2b, and M2c [424]. These macrophage subtypes are determined based on the gene transcription or protein expression of a set of M2 markers [425]. Full pathways responsible for macrophage activation could be found in **Figure 2.14**.

Pro-inflammatory M1 macrophages are responsible for initiating the immune response by aiding the neutrophils in degrading the biomaterial and phagocytosing microbes [425]. They are classically activated by intracellular microbes and cytokines, INF-γ and LPS [426]. As a defense mechanism, M1 macrophages have the ability to produce bacterial-toxic Nitric Oxide and secrete an expansive range of inflammatory cytokines[427].

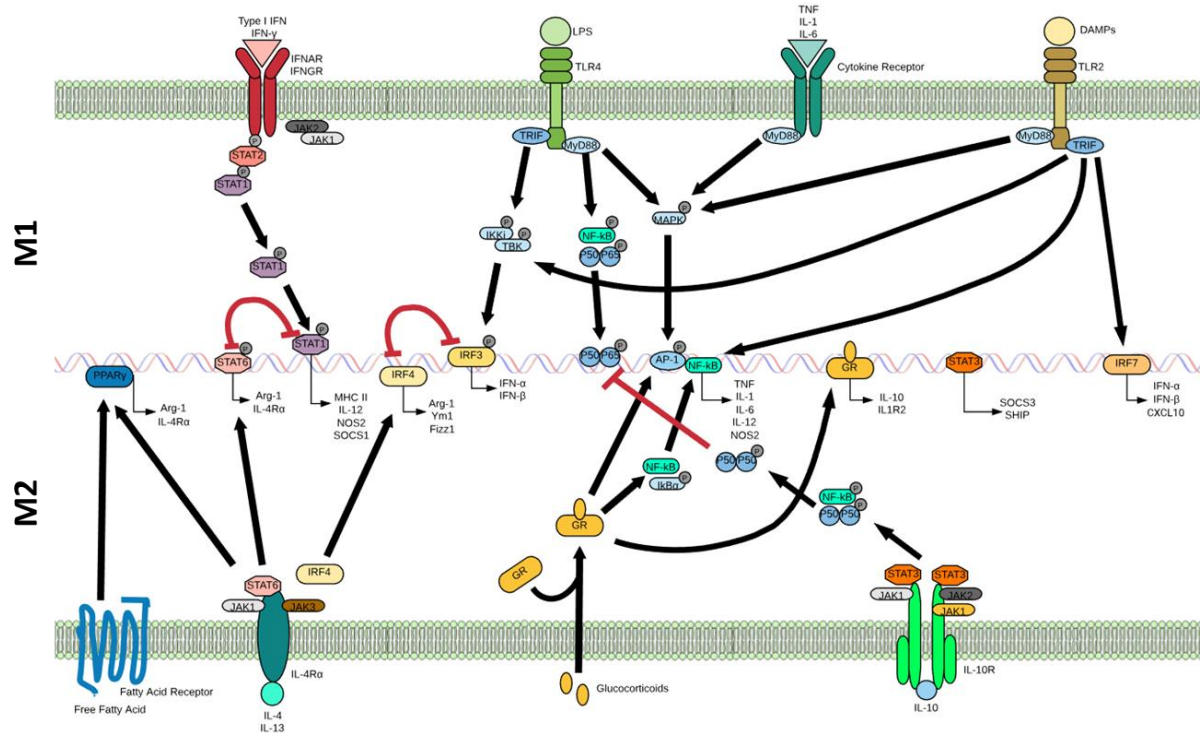

Figure 2.14. Signaling pathways regarding macrophage activation in the context of implants and biomaterials.

M1 macrophages: Macrophage phenotype skews towards M1 in response to stimulation by microbial products or pro-inflammatory cytokines. IFN-γ is the main the cytokine produced form Th1 cells that polarizes macrophages toward the M1 phenotype. IFN-γ receptor is formed of the IFNGR and IFNAR chains. The receptor recruits JAK1 and JAK2 adaptors which then lead to the activation of STAT1. IFN-γ elicits the expression programs of genes including MHC-II, IL-12, NOS-2 and SOCS-1. Bacterial moieties are recognized by pattern recognition receptors such as TLRs. TLR4 could be stimulated by LPS and other microbial ligands, leading to the induction of TRIF and MyD88 pathways. TRIF mediated pathway leads to the activation of a cascade of kinases, which finally leads to the activation of transcription factor IRF3. IRF3 regulates the production and secretion of type I interferon such as IFNα and IFNβ. Secreted type 1 interferons bind to IFNAR with consequent activation of the transcription factor STAT1. MyD88, second adaptor in response to activation of TLR4, triggers NF-kB pathway (p65 and p50), which is a key transcription factor related to polarization of M1 macrophage. MyD88 also activates AP-1 via MAPK signaling pathway. These pathways regulate a huge number of inflammatory genes including pro-inflammatory cytokines such as TNF, and IL-1β, IL-6, and IL-12, chemokines CCL2 (MCP-1), CXCL10 (IP-10), and CXCL11 (IP-9), co-stimulatory molecules, and antigen-processing molecules. DAMPs are endogenous ligands released by damaged or stressed tissues or cells to induce

sterile inflammatory response. DAMPs attached to the biomaterial surfaces strongly induced NF-κB/AP-1 transcription factor activity and pro-inflammatory cytokine secretion. DAMPs in their adsorbed conformations on material surfaces, may play an activating role in macrophage activation through TLR2 stimulation pathway, but not TLR4.

M2 macrophages: When IL-4, which is a Th2 produced cytokine, and IL-13 bind to the receptor IL-4Rα, M2 polarization is favored. This polarization occurs though several pathways, typically JAK1 and JAK3 signaling which further causing the activation and translocation of STAT6. Other transcription factors participated include IRF4 and PPARγ. STAT6, IRF4 and PPARγ regulate many of the genes associated with mouse M2 macrophages, Arg1, CD206 (or macrophaege mannose receptor 1, Mrc1), resistin-like-α (Retnla or Fizz1) and Ym1 (or chitinase 3-like 3, Chi3l3). Transcription factor PPARγ could also be activated by the binding of free fatty acids to fatty acid receptors. IL-10 that could be produced by all leukocytes binds to the IL-10 receptor, which is a heterodimer of IL10R1 and IL10R2. Ligation of IL-10R with IL-10 leads to the receptor auto-phosphorylation, arousing the activation of the transcription factor STAT3. The binding of STAT3 up-regulates the expression of SOCS3, mediating the suppression of pro-inflammatory cytokine signaling pathways.

Glucocorticoids are generated from the glucocorticoid hormones as a result from metabolism by cellular enzymes in macrophages. Owing to their lipophilic nature, they can diffuse through the membrane. Intracellular glucocorticoids bind the glucocorticoid receptor (GR), thus leading to the nuclear translocation of the complex. The complex directly binds DNA, promoting the transcription of anti-inflammatory genes such as IL-10 and IL1R2. Alternatively, GR complex can also interact with other transcription factors like NF-kB or AP-1.

Contrarily, M2 macrophages are considered to be anti-inflammatory and are alternatively activated by parasites, immune complexes, apoptotic cells, as well as, the exposure to cytokines such as IL-4, IL-13, and IL-10 [422]. M2 macrophages typically begin to accumulate after the levels of M1 macrophages begin to diminish as they are primarily responsible for inducing collagen production and fibrous capsule formation around the implanted biomaterial [428]. Apart from its role in the instigation of a fibrotic capsule, it can also defend against pathogens and clear apoptotic cells due to its high phagocytic nature. True to its anti-inflammatory nature, its other strength is in mitigating inflammatory response and promoting the wound healing process. Aside from its association with the inflammatory response, some other processes M2 macrophages partake in, include: tumor tissue growth, endocrine signaling, and organ morphogenesis [429].

As M2 macrophages are involved in a broad scope of processes, they are further sub-identified by their inductive stimuli and expression of cytokines (Table 2). M2a macrophages are activated by IL-4, IL-10 and IL-13, can release proteins like CD163 and Dectin-1, and are primarily involved with parasite phagocytosis [425, 430]. M2b macrophages are Type II

alternatively activated by LPS and immune complexes, but express IL-10, IL-1, IL-6 and TNF-α [427]. M2c are of an acquired deactivation in the sense of when an M1 macrophage deactivates its M1 gene transcription to polarize into an M2 macrophage [422]. M2c macrophages are stimulated by TGF-β and IL-10, but can express CD163, IL-21R, TLR1, TLR8 and CCL18 [431]. They are involved in the ECM deposition and tissue remodeling aspects of the immune response [431].

Table 2.4 Characteristics and functions of macrophages and neutrophils

	M1 Macrophage	**M2a Macrophage**	**M2b Macrophage**	**M2c Macrophage**	**Neutrophil**	Refs
Abundance in Blood	2–10% (Monocytes)				40–80%	[1]
Low Blood Count	Immunosuppression, bone marrow failure, chemotherapy (Monocytes)				Immunosuppression, bone marrow failure, chemotherapy	[2]
High Blood Count	Chronic infections, autoimmune diseases, leukemia (Monocytes)				Infection, inflammation, leukemia, intense exercise, stress, corticosteroids	[2]
Activation	Classical (Th1)	Alternative (Th2)	Type II Alternative	Acquired Deactivation	Th17	[3]
Transcription Factor	M1 differentiation promoted by IRF5	M2 differentiation suppressed by IRF5, but promoted by IRF4			Neutrophil migration is regulated by ATF3	[4], [6]
Stimuli	IFN-γ, LPS	IL-4, IL-10 and IL-13	IL-1, LPS and immune complexes	TGF-β IL-10	IL-17, IL-12, IL-21, IL-23, CXCL8	[5], [7]
Expression	IL-1β, IL-6, IL-12, IL-15, IL-23, TNF-α, CCR7, CD25, etc.	IL-4R and FcεR, Dectin-1, CD163, CD206, CD209	IL-10, IL-1, IL-6 and TNF-α	CD163, IL-21R, TLR1, TLR8, CCL18	Proteases, ROIs, RNIs	[5], [8]
Antigen Presentation	Yes -- Professional Antigen-Presenting Cell (MHC-II)				Can be induced -- Non-professional Antigen-Presenting Cell	[9]

Nitric Oxide Production	Yes	No, but produces trophic polyamines	No	No	No	[10]
Function	Killing of intracellular pathogens, pathogen phagocytosis, ECM degradation	Pathogen defense, clearing of apoptotic cells, mitigate inflammatory response, promote wound healing OTHER: organ morphogenesis, tissue turnover, and endocrine signaling			First inflammatory responders, pathogen phagocytosis	[8]

** CCR → C-C Chemokine Receptors
** ROIs & RNIs → Reactive Oxygen Intermediates & Reactive Nitrogen Intermediates

Immunoengineering scaffolds

Based on the discussions provided so far, immediately following by implantation of a tissue engineered scaffold, immune system initiates a complex myriad of negotiations with the scaffold itself, and in between its own cells. Being recognized as a foreign body, process of immune clearance begins to eradicate the scaffold, or encapsulate it within a scar-like fibrotic tissue. These series of events will initially impede the function of scaffold and eventually create a dysfunctional extra tissue. Current paradigm, not only in tissue engineering, but also in cancer therapy and implantable devices and nanotechnology fields is to make devices/biomaterials that are capable to negotiate with host immunity, be accepted as a self-domain, and finally integrate with the general system of the body [77]. In this context, multiple designs have been developed to be able to regulate the immune response in the adjacent environment of the implantation site.

There are multiple examples of recent developments in the axis of biomaterials-tissue engineering-immune-modulation. For instance, a scaffold could aid the repair of brain tissue following stroke. After stroke, an amplified immune and inflammatory response together with limited neuronal growth and angiogenesis results in a fibrotic cavity devoid of normal brain tissue [432]. Therefore, an ideal implantable scaffold could not only aid angiogenesis, but also

modulate the local inflammatory plethora. To formulate such an scaffold, used hyaluronic acid scaffolds loaded with heparin, which was shown to reduce the inflammation and induce neurogenesis and axonogenesis [432].

In the context of local immune-modulation, biomolecule negotiators are the forefront of biomaterials design. Headen et al. demonstrated that microgels presenting Fas ligand enhances the outcome of islet transplantation through elevation in the number of CD4+CD25+FoxP3+ regulatory T cells [129]. Fas ligand expression plays an important role in immune regulation. Tumor cells and immune privileged organs such as cornea express elevated levels of Fas ligand, through which the infiltrating T lymphocytes with Fas expression go through apoptosis through Fas-FasL interaction. When T lymphocytes get activated, they upregulate Fas, becoming more sensitive to Fas-FasL mediated apoptosis. Deficiency in such ligand interaction induces autoimmune pathologies in rodents and humans. Noteworthy that FasL could only induce apoptosis in activated lymphocytes when bound to its membrane and possess oligomeric form [433]. Matrix metalloproteinases can cleave FasL into a soluble molecule, attracting neutrophils.

Immune-modulatory biomaterial could be also used to regulate the host immunity against cancer. Effector T cells including CD4+ (T helper cells), CD8+ (cytotoxic T cells), memory T cells, and natural killer T cells facilitate tumour-killing processes through release of pro-inflammatory cytokines. On the other hand, regulatory T cells tend to regulate T cell immunity by suppressing effector T cells and releasing anti-inflammatory cytokines. Binding of T-cells surface negotiators such as PD-1, CTLA-4, and Fas to their complementary ligands on tumor cells is the central pathway by which effector T cell function is inhibited [434].

Even though immune-modulatory biomaterials are under investigation in the context of cancer, research expansion is needed in the field of tissue engineering. An ideal implantable scaffold could be considered as a live organ, where it not only functions the tasks it is supposed to, but also negotiates with the immediate host immune system to be recognized as self.

Biointegration of Scaffolds with the Host Body

As discussed earlier, for a tissue engineered scaffold to be fully functional, it must be integrated while keeping the host homeostasis. Not only this integration is in the context of immunological compatibility, but also functional integration. For instance, generally an implanted scaffold contains live cells, which need to experience same environment as endogenous cells. If the implanted tissue does not successfully integrate with the body's blood circulation and lymphatic drainage, cells will not survive, leading to an unfunctional tissue. Bio-integration thus could be defined as integration of an implanted scaffold within the adjacent bio-environment, where the scaffold could perform its function and communicate with other endogenous organs in an orchestrated manner. Failure of biointegration may lead to epithelial downgrowth, bacterial infection, and in rare cases, sepsis. Sepsis is known to be a life-threatening complication of an infection that can lead to many organ system failures. It occurs when the released chemokines in the bloodstream trigger an immune response throughout the entire body, rather than the site of inflammation alone. The rate of sepsis may increase due to drug-resistant bacteria, weakened immune systems, and older age of patients. Considering how most implants are meant to aid older patients and those with weaker immune systems, sepsis is a significant hindrance to implants.

Many elements are recognized so far for a successful biointegration. Apart from "nontoxic, nonimmunogenic, chemically inert/active, and acceptable by the human body" concepts in the immunological integration context, fibrous structures could aid biointegration because its morphology is more like that of an extracellular matrix. A fibrous structure would enhance cell attachment and proliferation, and delivery of cytokines and excretion of wastes. Another important aspect of biointegration is the successful angiogenesis, where the implanted tissue integrates with the main circulation system of the body to provide cells with required nutritients, oxygen, and hormones. Lymphatic drainage is also another critical aspect, where the implanted scaffold must be integrated with. Even though very critical, this concept has not been explored in detail thus far.

Conclusions and future perspective

The primary role of nanotechnology in drug delivery is to effectively deliver the drug to the desired target while maintaining its pharmacological activity. In this respect, various nanomaterials engineered to effectively be employed on the bench and beside. However, the extraordinary defense mechanism of our bodies recognizes, labels, informs members of immune system moieties, sequesters and eliminates them at the very early stage of their entrance into the body. This is the main impediment for efficient targeted drug delivery, which led the unsuccessful clinical outcomes of targeting delivery strategies.

In the quest for counteracting this phenomenon, one approach is to take advantage of bioinspired approaches. It is hypothesized that since many moieties in the body (such as RBCs, leukocytes, platelets and etc.) successfully negotiate with the immune system, they can be employed as the carrier for the therapeutic moieties. In this manner, variety of drugs and NPs, which their successful application normally suffers from their unfavorable biodistribution, low

pharmacokinetics, and harmful side effects, could be hybridized with recognized-to-body moieties to bypass the biological barriers.

Hybridizing synthetic materials (or drugs) with cell membrane biomaterials has shown an average of 10-fold enhancement in delivering the moieties to the favorable target. Recent technologies are therefore focused to improve the currently available biomimetic hybrids as one of the platforms for future drug delivery vesicles. Biomimetic hybrids reviewed in the present paper pave the way for the personalized medicine.

While at its infancy for the product development, the field of immunoengineering is rapidly gaining momentum to treat diseases associated with the immune system. Among variety of approaches, biomaterials/nanomaterials approaches have gained much attention. This review is a summary and a brief introduction to the interactions between DCs and materials. Better understanding such interactions may pave the way for future drug or device developments. The main conclusion is that DCs attachment and activation around biomaterials is tightly regulated by the surface properties of the biomaterials. In addition, DCs function could be regulated by variety of reagents including mAbs, aptamers, and synthetic drugs. Thus, biomaterials could be engineered to regulate DCs in two ways. 1) A drug-eluding or a controlled release hydrogel or any bio-nano-material that could reprogram the adjacent DCs. 2) Engineering biomaterials surface with immunoregulatory peptides/molecules as well as altering the surface functional group and hydrophobicity are other major methods to reprogram infiltrating DCs around biomaterials.

Regulating the DCs response via biomaterials could be used in many fields including tissue engineering, vaccine development, cancer immunotherapy, autoimmune disorders, allo- or xeno-graft rejections, biomaterial transplants, autoimmune and inflammatory based disorders.

Although this is a promising field of study, it requires further understanding of the biomaterial-DC interaction, functional mechanism of DCs, and DC biomarkers, both in protein and RNA levels.

References

1. Jiang, W., et al., *Designing nanomedicine for immuno-oncology.* Nature Biomedical Engineering, 2017. **1**: p. 0029.
2. Mahmoudi, M., et al., *Emerging understanding of the protein corona at the nano-bio interfaces.* Nano Today, 2016. **11**(6): p. 817-832.
3. Xu, R., et al., *An injectable nanoparticle generator enhances delivery of cancer therapeutics.* Nature Biotechnology, 2016. **34**: p. 414.
4. von Maltzahn, G., et al., *Nanoparticles that communicate in vivo to amplify tumour targeting.* Nature Materials, 2011. **10**: p. 545.
5. Molinaro, R., et al., *Biomimetic proteolipid vesicles for targeting inflamed tissues.* Nature materials, 2016. **15**(9): p. 1037-1046.
6. Blanco, E., H. Shen, and M. Ferrari, *Principles of nanoparticle design for overcoming biological barriers to drug delivery.* Nature biotechnology, 2015. **33**(9): p. 941-951.
7. Cedervall, T., et al., *Understanding the nanoparticle–protein corona using methods to quantify exchange rates and affinities of proteins for nanoparticles.* Proceedings of the National Academy of Sciences, 2007. **104**(7): p. 2050-2055.
8. Pelaz, B., et al., *Interfacing engineered nanoparticles with biological systems: anticipating adverse nano–bio interactions.* Small, 2013. **9**(9-10): p. 1573-1584.
9. Ferrari, M., *Frontiers in cancer nanomedicine: Directing mass transport through biological barriers.* Trends in Biotechnology, 2010. **28**(4): p. 181-188.
10. Khalid, A., et al., *Strategies for improving drug delivery: nanocarriers and microenvironmental priming.* Expert Opinion on Drug Delivery, 2017. **14**(7): p. 865-877.
11. Salvati, A., et al., *Transferrin-functionalized nanoparticles lose their targeting capabilities when a biomolecule corona adsorbs on the surface.* Nature Nanotechnology, 2013. **8**: p. 137.
12. Vroman, L., *Effect of Adsorbed Proteins on the Wettability of Hydrophilic and Hydrophobic Solids.* Nature, 1962. **196**: p. 476.
13. Chen, F., et al., *Complement proteins bind to nanoparticle protein corona and undergo dynamic exchange in vivo.* Nature Nanotechnology, 2016. **12**: p. 387.
14. Tenzer, S., et al., *Rapid formation of plasma protein corona critically affects nanoparticle pathophysiology.* Nat Nano, 2013. **8**(10): p. 772-781.
15. Lundqvist, M., et al., *Nanoparticle size and surface properties determine the protein corona with possible implications for biological impacts.* Proceedings of the National Academy of Sciences, 2008. **105**(38): p. 14265-14270.
16. Sahay, G., D.Y. Alakhova, and A.V. Kabanov, *Endocytosis of nanomedicines.* Journal of controlled release, 2010. **145**(3): p. 182-195.
17. Behzadi, S., et al., *Cellular uptake of nanoparticles: journey inside the cell.* Chemical Society Reviews, 2017. **46**(14): p. 4218-4244.
18. Mirshafiee, V., et al., *Impact of protein pre-coating on the protein corona composition and nanoparticle cellular uptake.* Biomaterials, 2016. **75**: p. 295-304.
19. Corbo, C., et al., *Unveiling the in Vivo Protein Corona of Circulating Leukocyte-like Carriers.* ACS Nano, 2017. **11**: p. 3262-3273.

20. Lesniak, A., et al., *Effects of the presence or absence of a protein corona on silica nanoparticle uptake and impact on cells.* 2012.
21. Digiacomo, L., et al., *An apolipoprotein-enriched biomolecular corona switches the cellular uptake mechanism and trafficking pathway of lipid nanoparticles.* Nanoscale, 2017. **9**(44): p. 17254-17262.
22. Lane, L.A., et al., *Physical chemistry of nanomedicine: understanding the complex behaviors of nanoparticles in vivo.* Annual review of physical chemistry, 2015. **66**: p. 521-547.
23. Verwey, E.J.W., *Theory of the Stability of Lyophobic Colloids.* The Journal of Physical and Colloid Chemistry, 1947. **51**(3): p. 631-636.
24. Derjaguin, B.V. and L. Landau, *Theory of the stability of strongly charged lyophobic sols and of the adhesion of strongly charged particles in solutions of electrolytes.* Acta physicochim. URSS, 1941. **14**(6): p. 633-662.
25. Schöttler, S., et al., *Protein adsorption is required for stealth effect of poly(ethylene glycol)- and poly(phosphoester)-coated nanocarriers.* Nature nanotechnology, 2016. **11**(February): p. 1-6.
26. Bertrand, N., et al., *Mechanistic understanding of in vivo protein corona formation on polymeric nanoparticles and impact on pharmacokinetics.* Nature Communications, 2017. **8**(1): p. 777.
27. Dai, Q., C. Walkey, and W.C.W. Chan, *Polyethylene Glycol Backfilling Mitigates the Negative Impact of the Protein Corona on Nanoparticle Cell Targeting.* Angewandte Chemie International Edition, 2014. **53**(20): p. 5093-5096.
28. Jokerst, J.V., et al., *Nanoparticle PEGylation for imaging and therapy.* Nanomedicine, 2011. **6**(4): p. 715-728.
29. Schlenoff, J.B., *Zwitteration: Coating Surfaces with Zwitterionic Functionality to Reduce Nonspecific Adsorption.* Langmuir, 2014. **30**(32): p. 9625-9636.
30. Groult, H., et al., *Phosphatidylcholine-Coated Iron Oxide Nanomicelles for In Vivo Prolonged Circulation Time with an Antibiofouling Protein Corona.* Chemistry-A European Journal, 2014. **20**(50): p. 16662-16671.
31. Pombo-García, K., et al., *Zwitterionic Modification of Ultrasmall Iron Oxide Nanoparticles for Reduced Protein Corona Formation.* ChemPlusChem, 2017. **82**(4): p. 638-646.
32. Cao, Z. and S. Jiang, *Super-hydrophilic zwitterionic poly(carboxybetaine) and amphiphilic non-ionic poly(ethylene glycol) for stealth nanoparticles.* Nano Today, 2012. **7**(5): p. 404-413.
33. Safavi-Sohi, R., et al., *Bypassing Protein Corona Issue on Active Targeting: Zwitterionic Coatings Dictate Specific Interactions of Targeting Moieties and Cell Receptors.* ACS Applied Materials & Interfaces, 2016. **8**(35): p. 22808-22818.
34. Pelaz, B., et al., *Surface Functionalization of Nanoparticles with Polyethylene Glycol: Effects on Protein Adsorption and Cellular Uptake.* ACS Nano, 2015. **9**(7): p. 6996-7008.
35. Gabizon, A., H. Shmeeda, and Y. Barenholz, *Pharmacokinetics of Pegylated Liposomal Doxorubicin.* Clinical Pharmacokinetics, 2003. **42**(5): p. 419-436.
36. Dong, Y., et al., *Lipopeptide nanoparticles for potent and selective siRNA delivery in rodents and nonhuman primates.* Proceedings of the National Academy of Sciences, 2014. **111**(11): p. 3955-3960.

37. Caracciolo, G., et al., *Lipid composition: a "key factor" for the rational manipulation of the liposome-protein corona by liposome design.* RSC Advances, 2015. **5**(8): p. 5967-5975.
38. Fleischer, C.C. and C.K. Payne, *Nanoparticle–Cell Interactions: Molecular Structure of the Protein Corona and Cellular Outcomes.* Accounts of Chemical Research, 2014. **47**(8): p. 2651-2659.
39. Aggarwal, P., et al., *Nanoparticle interaction with plasma proteins as it relates to particle biodistribution, biocompatibility and therapeutic efficacy.* Advanced Drug Delivery Reviews, 2009. **61**(6): p. 428-437.
40. Xu, M., et al., *How Entanglement of Different Physicochemical Properties Complicates the Prediction of in Vitro and in Vivo Interactions of Gold Nanoparticles.* ACS Nano, 2018. **12**(10): p. 10104-10113.
41. Zyuzin, M.V., et al., *Comprehensive and Systematic Analysis of the Immunocompatibility of Polyelectrolyte Capsules.* Bioconjugate Chemistry, 2017. **28**(2): p. 556-564.
42. Colapicchioni, V., et al., *Personalized liposome–protein corona in the blood of breast, gastric and pancreatic cancer patients.* The International Journal of Biochemistry & Cell Biology, 2016. **75**: p. 180-187.
43. Di Domenico, M., et al., *Nanoparticle-biomolecular corona: A new approach for the early detection of non-small-cell lung cancer.* Journal of Cellular Physiology, 2019. **234**(6): p. 9378-9386.
44. Hajipour, M.J., et al., *Personalized disease-specific protein corona influences the therapeutic impact of graphene oxide.* Nanoscale, 2015. **7**(19): p. 8978-8994.
45. Hellstrand, E., et al., *Complete high-density lipoproteins in nanoparticle corona.* FEBS Journal, 2009. **276**(12): p. 3372-3381.
46. Raesch, S.S., et al., *Proteomic and Lipidomic Analysis of Nanoparticle Corona upon Contact with Lung Surfactant Reveals Differences in Protein, but Not Lipid Composition.* ACS Nano, 2015. **9**(12): p. 11872-11885.
47. Bohne-Lang, A. and C.-W. von der Lieth, *GlyProt: in silico glycosylation of proteins.* Nucleic Acids Research, 2005. **33**(suppl_2): p. W214-W219.
48. Wan, S., et al., *The "Sweet" Side of the Protein Corona: Effects of Glycosylation on Nanoparticle–Cell Interactions.* ACS Nano, 2015. **9**(2): p. 2157-2166.
49. Tsoi, K.M., et al., *Mechanism of hard-nanomaterial clearance by the liver.* Nature Materials, 2016. **15**: p. 1212.
50. Walkey, C.D., et al., *Nanoparticle Size and Surface Chemistry Determine Serum Protein Adsorption and Macrophage Uptake.* Journal of the American Chemical Society, 2012. **134**(4): p. 2139-2147.
51. Tavares, A.J., et al., *Effect of removing Kupffer cells on nanoparticle tumor delivery.* Proceedings of the National Academy of Sciences, 2017. **114**(51): p. E10871.
52. Satchell, S.C. and F. Braet, *Glomerular endothelial cell fenestrations: an integral component of the glomerular filtration barrier.* American Journal of Physiology-Renal Physiology, 2009. **296**(5): p. F947-F956.
53. Curry, F.E. and R.H. Adamson, *Endothelial Glycocalyx: Permeability Barrier and Mechanosensor.* Annals of Biomedical Engineering, 2012. **40**(4): p. 828-839.
54. Kamaly, N., et al., *Nanomedicines for renal disease: current status and future applications.* Nature Reviews Nephrology, 2016. **12**: p. 738.

55. Longmire, M., P.L. Choyke, and H. Kobayashi, *Clearance properties of nano-sized particles and molecules as imaging agents: considerations and caveats.* Nanomedicine, 2008. **3**(5): p. 703-717.
56. Soo Choi, H., et al., *Renal clearance of quantum dots.* Nature Biotechnology, 2007. **25**: p. 1165.
57. Heldin, C.-H., et al., *High interstitial fluid pressure—an obstacle in cancer therapy.* Nature Reviews Cancer, 2004. **4**(10): p. 806-813.
58. Barua, S. and S. Mitragotri, *Challenges associated with penetration of nanoparticles across cell and tissue barriers: A review of current status and future prospects.* Nano Today, 2014. **9**(2): p. 223-243.
59. Kim, S.M., P.H. Faix, and J.E. Schnitzer, *Overcoming key biological barriers to cancer drug delivery and efficacy.* Journal of Controlled Release, 2017. **267**(Supplement C): p. 15-30.
60. Gaglia, J.L., et al., *Noninvasive mapping of pancreatic inflammation in recent-onset type-1 diabetes patients.* Proceeding National Academy of Science USA, 2016. **112**(7): p. 2139-2144.
61. Fu, W., et al., *Early window of diabetes determinism in NOD mice, dependent on the complement receptor CRIg, identified by noninvasive imaging.* Nature Immunology, 2012. **13**: p. 361–368.
62. Denis, M.C., et al., *Imaging inflammation of the pancreatic islets in type 1 diabetes.* Proceeding National Academy of Science USA, 2004. **101**(34): p. 12634-12639.
63. Dukhin, S.S. and M.E. Labib, *Convective diffusion of nanoparticles from the epithelial barrier toward regional lymph nodes.* Advances in Colloid and Interface Science, 2013. **199-200**(Supplement C): p. 23-43.
64. Sun, W., et al., *LEVERAGING PHYSIOLOGY FOR PRECISION DRUG DELIVERY.* Physiological Reviews, 2017. **97**: p. 189 –225.
65. Palomba, R., et al., *Biomimetic carriers mimicking leukocyte plasma membrane to increase tumor vasculature permeability.* Scientific Reports, 2016. **6**: p. 34422.
66. Engin, A.B., et al., *Mechanistic understanding of nanoparticles' interactions with extracellular matrix: the cell and immune system.* Particle and Fibre Toxicology, 2017. **14**(1): p. 22.
67. Chaudhuri, O., et al., *Extracellular matrix stiffness and composition jointly regulate the induction of malignant phenotypes in mammary epithelium.* Nature Materials, 2014. **13**: p. 970.
68. Wilhelm, S., et al., *Analysis of nanoparticle delivery to tumours.* Nature Reviews Materials, 2016. **1**: p. 16014.
69. Liu, H., et al., *Structure-based programming of lymph-node targeting in molecular vaccines.* Nature, 2014. **507**: p. 519.
70. Wang, C., et al., *In situ activation of platelets with checkpoint inhibitors for post-surgical cancer immunotherapy.* Nature Biomedical Engineering, 2017. **1**: p. 0011.
71. Liu, Y., Y.-c. Tseng, and L. Huang, *Biodistribution Studies of Nanoparticles Using Fluorescence Imaging: A Qualitative or Quantitative Method?* Pharmaceutical Research, 2012. **29**(12): p. 3273-3277.
72. Elci, S.G., et al., *Surface Charge Controls the Suborgan Biodistributions of Gold Nanoparticles.* ACS Nano, 2016. **10**(5): p. 5536-5542.

73. Dahlman, J.E., et al., *Barcoded nanoparticles for high throughput in vivo discovery of targeted therapeutics.* Proceeding National Academy of Science USA, 2017. **114**(8): p. 2060–2065.
74. Yaari, Z., et al., *Theranostic barcoded nanoparticles for personalized cancer medicine.* Nat Commun, 2016. **7**: p. 13325.
75. Yang, Y.-S.S., et al., *High-throughput quantitation of inorganic nanoparticle biodistribution at the single-cell level using mass cytometry.* Nature Communications, 2017. **8**: p. 14069.
76. Sharifi, S., et al., *Toxicity of nanomaterials.* Chemical Society Reviews, 2012. **41**(6): p. 2323-2343.
77. Mohammadi, M.R., et al., *PEG/Dextran Double Layer Influences Fe Ion Release and Colloidal Stability of Iron Oxide Nanoparticles.* Scientific Reports, 2018. **8**(1): p. 4286.
78. Arami, H., et al., *In vivo delivery, pharmacokinetics, biodistribution and toxicity of iron oxide nanoparticles.* Chemical Society Reviews, 2015. **44**(23): p. 8576-8607.
79. Sykes, E.A., et al., *Investigating the Impact of Nanoparticle Size on Active and Passive Tumor Targeting Efficiency.* ACS Nano, 2014. **8**(6): p. 5696-5706.
80. Sago, C.D., et al., *High-throughput in vivo screen of functional mRNA delivery identifies nanoparticles for endothelial cell gene editing.* Proceedings of the National Academy of Sciences, 2018.
81. Spitzer, Matthew H. and Garry P. Nolan, *Mass Cytometry: Single Cells, Many Features.* Cell, 2016. **165**(4): p. 780-791.
82. Kojima, Y., et al., *CD47-blocking antibodies restore phagocytosis and prevent atherosclerosis.* Nature, 2016. **536**: p. 86–90.
83. Duez, J., et al., *Mechanical clearance of red blood cells by the human spleen: Potential therapeutic applications of a biomimetic RBC filtration method.* Transfusion Clinique et Biologique, 2015. **22**(3): p. 151-157.
84. Theurl, I., et al., *On-demand erythrocyte disposal and iron recycling requires transient macrophages in the liver.* Nature Medicine, 2016. **22**: p. 945.
85. Fang, R.H., et al., *Cancer Cell Membrane-Coated Nanoparticles for Anticancer Vaccination and Drug Delivery.* Nano Letter, 2014. **14**(4): p. 2181-2188.
86. Guo, Y., et al., *Erythrocyte Membrane-Enveloped Polymeric Nanoparticles as Nanovaccine for Induction of Antitumor Immunity against Melanoma.* ACS Nano, 2015. **9**(7): p. 6918-6933.
87. Zhang, Y., et al., *Self-Assembled Colloidal Gel Using Cell Membrane-Coated Nanosponges as Building Blocks.* ACS Nano, 2017.
88. Kawabata, K., Y. Takakura, and M. Hashida, *The fate of plasmid DNA after intravenous injection in mice: involvement of scavenger receptors in its hepatic uptake.* Pharmaceutical Research, 1995. **12**(6): p. 825-30.
89. Lennox, K.A. and M.A. Behlke, *Chemical modification and design of anti-miRNA oligonucleotides.* Gene Therapy, 2011. **18**: p. 1111.
90. Kotterman, M.A., T.W. Chalberg, and D.V. Schaffer, *Viral Vectors for Gene Therapy: Translational and Clinical Outlook.* Annual Review of Biomedical Engineering, 2015. **17**(1): p. 63-89.
91. Kaczmarek, J.C., P.S. Kowalski, and D.G. Anderson, *Advances in the delivery of RNA therapeutics: from concept to clinical reality.* Genome Medicine, 2017. **9**(1): p. 60.

92. Yin, H., K.J. Kauffman, and D.G. Anderson, *Delivery technologies for genome editing.* Nature Reviews Drug Discovery, 2017. **16**: p. 387.
93. Yang, M., K. Sunderland, and C. Mao, *Virus-Derived Peptides for Clinical Applications.* Chemical Reviews, 2017. **117**(15): p. 10377-10402.
94. Li, W. and F.C. Szoka, *Non-viral gene therapy: polycation-mediated DNA delivery.* Pharmaceutical Research, 2007. **24**(3): p. 438–449.
95. McManus, J.J., J.O. Rädler, and K.A. Dawson, *Observation of a Rectangular Columnar Phase in a DNA−Calcium−Zwitterionic Lipid Complex.* Journal of American Chemical Society, 2004. **126**(49): p. 15966–15967.
96. Smith, T.T., et al., *In situ programming of leukaemia-specific T cells using synthetic DNA nanocarriers.* Nat Nano, 2017. **advance online publication**.
97. Whitehead, K.A., et al., *Degradable lipid nanoparticles with predictable in vivo siRNA delivery activity.* Nature Communications, 2014. **5**.
98. Yin, H., et al., *Non-viral vectors for gene-based therapy.* Nature Reviews Genetics, 2014. **15**: p. 541.
99. Parodi, A., et al., *Bio-inspired engineering of cell- and virus-like nanoparticles for drug delivery.* Biomaterials, 2017. **147**: p. 155-168.
100. Yoo, J.-W., et al., *Bio-inspired, bioengineered and biomimetic drug delivery carriers.* Nature reviews. Drug discovery, 2011. **10**(7): p. 521-35.
101. Lilavivat, S., et al., *In Vivo Encapsulation of Nucleic Acids Using an Engineered Nonviral Protein Capsid.* Journal of the American Chemical Society, 2012. **134**(32): p. 13152-13155.
102. Hernandez-Garcia, A., et al., *Design and self-assembly of simple coat proteins for artificial viruses.* Nature Nanotechnology, 2014. **9**: p. 698.
103. Butterfield, G.L., et al., *Evolution of a designed protein assembly encapsulating its own RNA genome.* Nature, 2017.
104. Rodriguez, P.L., et al., *Minimal "Self" Peptides That Inhibit Phagocytic Clearance and Enhance Delivery of Nanoparticles.* Science, 2013. **339**(6122): p. 971-975.
105. Tseng, D., et al., *Anti-CD47 antibody–mediated phagocytosis of cancer by macrophages primes an effective antitumor T-cell response.* Proceedings of the National Academy of Sciences, 2013. **110**(27): p. 11103-11108.
106. Tsai, R.K. and D.E. Discher, *Inhibition of "self" engulfment through deactivation of myosin-II at the phagocytic synapse between human cells.* The Journal of Cell Biology, 2008. **180**(5): p. 989.
107. Qie, Y., et al., *Surface modification of nanoparticles enables selective evasion of phagocytic clearance by distinct macrophage phenotypes.* Scientific Reports, 2016. **6**: p. 26269.
108. Chao, M.P., et al., *Therapeutic Antibody Targeting of CD47 Eliminates Human Acute Lymphoblastic Leukemia.* Cancer Research, 2011. **71**(4): p. 1374.
109. Chao, M.P., et al., *Extranodal dissemination of non-Hodgkin lymphoma requires CD47 and is inhibited by anti-CD47 antibody therapy.* Blood, 2011. **118**(18): p. 4890.
110. Edris, B., et al., *Antibody therapy targeting the CD47 protein is effective in a model of aggressive metastatic leiomyosarcoma.* Proceedings of the National Academy of Sciences, 2012. **109**(17): p. 6656-6661.

111. Gholamin, S., et al., *Disrupting the CD47-SIRPα anti-phagocytic axis by a humanized anti-CD47 antibody is an efficacious treatment for malignant pediatric brain tumors.* Science Translational Medicine, 2017. **9**(381).
112. Ring, N.G., et al., *Anti-SIRPα antibody immunotherapy enhances neutrophil and macrophage antitumor activity.* Proceedings of the National Academy of Sciences, 2017. **114**(49): p. E10578-E10585.
113. Gao, Q., et al., *Blockade of CD47 ameliorates autoimmune inflammation in CNS by suppressing IL-1-triggered infiltration of pathogenic Th17 cells.* Journal of Autoimmunity, 2016. **69**(Supplement C): p. 74-85.
114. Hu, C.-M.J., et al., *'Marker-of-self' functionalization of nanoscale particles through a top-down cellular membrane coating approach.* Nanoscale, 2013. **5**(7): p. 2664-2668.
115. Zou, W., J.D. Wolchok, and L. Chen, *PD-L1 (B7-H1) and PD-1 pathway blockade for cancer therapy: Mechanisms, response biomarkers, and combinations.* Science Translational Medicine, 2016. **8**(328): p. 328rv4.
116. Hamid, O., et al., *Safety and Tumor Responses with Lambrolizumab (Anti–PD-1) in Melanoma.* New England Journal of Medicine, 2013. **369**(2): p. 134-144.
117. Topalian, S.L., et al., *Safety, Activity, and Immune Correlates of Anti–PD-1 Antibody in Cancer.* New England Journal of Medicine, 2012. **366**(26): p. 2443-2454.
118. Pardoll, D.M., *The blockade of immune checkpoints in cancer immunotherapy.* Nature Reviews Cancer, 2012. **12**: p. 252.
119. Gordon, S.R., et al., *PD-1 expression by tumour-associated macrophages inhibits phagocytosis and tumour immunity.* Nature, 2017. **545**: p. 495.
120. Schmid, D., et al., *T cell-targeting nanoparticles focus delivery of immunotherapy to improve antitumor immunity.* Nature Communications, 2017. **8**(1): p. 1747.
121. Chen, G., et al., *Exosomal PD-L1 contributes to immunosuppression and is associated with anti-PD-1 response.* Nature, 2018. **560**(7718): p. 382-386.
122. Shirali, A.C., et al., *Nanoparticle Delivery of Mycophenolic Acid Upregulates PD-L1 on Dendritic Cells to Prolong Murine Allograft Survival.* American Journal of Transplantation, 2011. **11**(12): p. 2582-2592.
123. Ben Nasr, M., et al., *PD-L1 genetic overexpression or pharmacological restoration in hematopoietic stem and progenitor cells reverses autoimmune diabetes.* Science Translational Medicine, 2017. **9**(416).
124. Ansari, M.J.I., et al., *The Programmed Death-1 (PD-1) Pathway Regulates Autoimmune Diabetes in Nonobese Diabetic (NOD) Mice.* The Journal of Experimental Medicine, 2003. **198**(1): p. 63.
125. Brahmer, J.R., et al., *Safety and Activity of Anti–PD-L1 Antibody in Patients with Advanced Cancer.* New England Journal of Medicine, 2012. **366**(26): p. 2455-2465.
126. Robert, C., et al., *Nivolumab in Previously Untreated Melanoma without BRAF Mutation.* New England Journal of Medicine, 2014. **372**(4): p. 320-330.
127. Hughes, J., et al., *Precipitation of Autoimmune Diabetes With Anti-PD-1 Immunotherapy.* Diabetes Care, 2015. **38**(4): p. e55.
128. Barron, L., et al., *Cutting Edge: Mechanisms of IL-2–Dependent Maintenance of Functional Regulatory T Cells.* The Journal of Immunology, 2010. **185**(11): p. 6426.
129. Headen, D.M., et al., *Local immunomodulation with Fas ligand-engineered biomaterials achieves allogeneic islet graft acceptance.* Nature Materials, 2018. **17**(8): p. 732-739.

130. Yingling, J.M., K.L. Blanchard, and J.S. Sawyer, *Development of TGF-β signalling inhibitors for cancer therapy.* Nature Reviews Drug Discovery, 2004. **3**: p. 1011.
131. Casey, L.M., et al., *Conjugation of Transforming Growth Factor Beta to Antigen-Loaded Poly(lactide-co-glycolide) Nanoparticles Enhances Efficiency of Antigen-Specific Tolerance.* Bioconjugate Chemistry, 2017.
132. Hunter, Z., et al., *A Biodegradable Nanoparticle Platform for the Induction of Antigen-Specific Immune Tolerance for Treatment of Autoimmune Disease.* ACS Nano, 2014. **8**(3): p. 2148-2160.
133. Kuo, R., et al., *Peptide-Conjugated Nanoparticles Reduce Positive Co-stimulatory Expression and T Cell Activity to Induce Tolerance.* Molecular Therapy, 2017. **25**(7): p. 1676-1685.
134. Sugarman, J., et al., *Quantifying the importance of pMHC valency, total pMHC dose and frequency on nanoparticle therapeutic efficacy.* Immunology And Cell Biology, 2013. **91**: p. 350.
135. Clemente-Casares, X., et al., *Expanding antigen-specific regulatory networks to treat autoimmunity.* Nature 2016. **530**: p. 434–440
136. Stratigis, J.D., et al., *In Utero Injections of Nanoparticle Encapsulated Myelin Oligodendrocyte Glycoprotein Peptides Prevent Experimental Autoimmune Encephalopathy Via Central Tolerance.* Blood, 2017. **130**(Suppl 1): p. 4630.
137. Marcovina, S.M. and J.D. Morrisett, *Structure and metabolism of lipoprotein (a).* Current Opinion in Lipidology, 1995. **6**(3): p. 136-145.
138. Siuta-Mangano, P., K.W. Miller, and M.D. Lane, *Synthesis, processing, and secretion of hepatic very low density lipoprotein.* Journal of Cellular Biochemistry, 1984. **24**(2): p. 131–152.
139. Saka, H.A. and R. Valdivia, *Emerging Roles for Lipid Droplets in Immunity and Host-Pathogen Interactions.* Annual Review of Cell and Developmental Biology, 2012. **28**(1): p. 411-437.
140. Veglia, F., et al., *Lipid bodies containing oxidatively truncated lipids block antigen cross-presentation by dendritic cells in cancer.* Nature Communications, 2017. **8**(1): p. 2122.
141. Raman, R., et al., *Glycan–protein interactions in viral pathogenesis.* Current Opinion in Structural Biology, 2016. **40**(Supplement C): p. 153-162.
142. Mohammadi, M.R., et al., *Nanomaterials engineering for drug delivery: a hybridization approach.* Journal of Materials Chemistry B, 2017. **5**(22): p. 3995-4018.
143. Chen, S. and R. Chen, *A Virus-Mimicking, Endosomolytic Liposomal System for Efficient, pH-Triggered Intracellular Drug Delivery.* ACS Applied Materials & Interfaces, 2016. **8**(34): p. 22457-22467.
144. Kroll, A.V., et al., *Nanoparticulate Delivery of Cancer Cell Membrane Elicits Multiantigenic Antitumor Immunity.* Advanced Materials, 2017. **29**(47): p. 1703969-n/a.
145. Li, J., et al., *Biomimetic Platelet-Camouflaged Nanorobots for Binding and Isolation of Biological Threats.* Advanced Materials: p. 1704800-n/a.
146. Pearson, R.M., et al., *In vivo reprogramming of immune cells: Technologies for induction of antigen-specific tolerance.* Advanced Drug Delivery Reviews, 2017. **114**: p. 240-255.
147. Zanganeh, S., et al., *Iron oxide nanoparticles inhibit tumour growth by inducing pro-inflammatory macrophage polarization in tumour tissues.* Nat Nanotechnol, 2016. **11**(11): p. 986-994.

148. Guilliams, M. and C.L. Scott, *Does niche competition determine the origin of tissue-resident macrophages?* Nat Rev Immunol, 2017. **17**(7): p. 451-460.
149. Sindrilaru, A., et al., *An unrestrained proinflammatory M1 macrophage population induced by iron impairs wound healing in humans and mice.* J Clin Invest, 2011. **121**(3): p. 985-97.
150. Fuchs, A.-K., et al., *Carboxyl- and amino-functionalized polystyrene nanoparticles differentially affect the polarization profile of M1 and M2 macrophage subsets.* Biomaterials, 2016. **85**: p. 78-87.
151. Chen, E.Y., et al., *CD200 modulates macrophage cytokine secretion and phagocytosis in response to poly(lactic-co-glycolic acid) microparticles and films.* Journal of Materials Chemistry B, 2017. **5**(8): p. 1574-1584.
152. Parodi, A., et al., *Synthetic nanoparticles functionalized with biomimetic leukocyte membranes possess cell-like functions.* Nature Nanotechnology, 2012. **8**: p. 61.
153. Tsai, S., et al., *Reversal of Autoimmunity by Boosting Memory-like Autoregulatory T Cells.* Immunity, 2010. **32**(4): p. 568-580.
154. Gharagozloo, M., S. Majewski, and M. Foldvari, *Therapeutic applications of nanomedicine in autoimmune diseases: From immunosuppression to tolerance induction.* Nanomedicine: Nanotechnology, Biology and Medicine, 2015. **11**(4): p. 1003-1018.
155. Smith, D.M., J.K. Simon, and J.R. Baker Jr, *Applications of nanotechnology for immunology.* Nature Reviews Immunology, 2013. **13**: p. 592.
156. Hotaling, N.A., et al., *Biomaterial Strategies for Immunomodulation.* Annual Review of Biomedical Engineering, 2015. **17**(1): p. 317-349.
157. Baekkeskov, S., J.A. Hubbell, and E.A. Phelps, *Bioengineering strategies for inducing tolerance in autoimmune diabetes.* Advanced Drug Delivery Reviews, 2017. **114**(Supplement C): p. 256-265.
158. Melssen, M. and C.L. Slingluff, *Vaccines targeting helper T cells for cancer immunotherapy.* Current Opinion in Immunology, 2017. **47**(Supplement C): p. 85-92.
159. Singha, S., et al., *Peptide-MHC-based nanomedicines for autoimmunity function as T-cell receptor microclustering devices.* Nat Nanotechnol, 2017. **12**(7): p. 701-710.
160. Deeg, J., et al., *T Cell Activation is Determined by the Number of Presented Antigens.* Nano Letters, 2013. **13**(11): p. 5619-5626.
161. Hickey, J.W., et al., *Biologically Inspired Design of Nanoparticle Artificial Antigen-Presenting Cells for Immunomodulation.* Nano Lett, 2017. **17**(11): p. 7045-7054.
162. Patterson, D.M. and J.A. Prescher, *Orthogonal bioorthogonal chemistries.* Current Opinion in Chemical Biology, 2015. **28**(Supplement C): p. 141-149.
163. Stephan, M.T. and D.J. Irvine, *Enhancing cell therapies from the outside in: Cell surface engineering using synthetic nanomaterials.* Nano Today, 2011. **6**(3): p. 309-325.
164. Luk, B.T. and L. Zhang, *Cell membrane-camouflaged nanoparticles for drug delivery.* Journal of Controlled Release, 2015. **220**: p. 600-607.
165. Molinaro, R., et al., *Design and Development of Biomimetic Nanovesicles Using a Microfluidic Approach.* Advanced Materials, 2018. **30**.
166. Sletten, E.M. and C.R. Bertozzi, *Bioorthogonal Chemistry: Fishing for Selectivity in a Sea of Functionality.* Angewandte Chemie International Edition, 2009. **48**(38): p. 6974-6998.
167. Wang, H., et al., *Selective in vivo metabolic cell-labeling-mediated cancer targeting.* Nature Chemical Biology, 2017. **13**: p. 415.

168. Alvarez-Castelao, B., et al., *Cell-type-specific metabolic labeling of nascent proteomes in vivo.* Nature Biotechnology, 2017. **35**: p. 1196.
169. Anselmo, A.C., et al., *Delivering nanoparticles to lungs while avoiding liver and spleen through adsorption on red blood cells.* ACS Nano, 2013. **7**(12): p. 11129-11137.
170. Molinaro, R., et al., *Biomimetic proteolipid vesicles for targeting inflamed tissues.* Nature Materials, 2016. **15**: p. 1037-1046.
171. Chen, R. and M. Snyder, *Promise of personalized omics to precision medicine.* Wiley Interdisciplinary Reviews: Systems Biology and Medicine, 2012. **5**(1): p. 73-82.
172. Fornaguera, C. and J.M. García-Celma, *Personalized Nanomedicine: A Revolution at the Nanoscale.* Journal of Personalized Medicine, 2017. **7**(4).
173. Nichols, J.W. and Y.H. Bae, *EPR: Evidence and fallacy.* Journal of Controlled Release, 2014. **190**: p. 451-464.
174. Kamaly, N., et al., *Targeted polymeric therapeutic nanoparticles: design, development and clinical translation.* Chemical Society Reviews, 2012. **41**(7): p. 2971-3010.
175. Anselmo Aaron, C. and S. Mitragotri, *Nanoparticles in the clinic.* Bioengineering & Translational Medicine, 2016. **1**(1): p. 10-29.
176. Corbo, C., et al., *Personalized protein corona on nanoparticles and its clinical implications.* Biomaterials Science, 2017. **5**(3): p. 378-387.
177. Corbo, C., et al., *The impact of nanoparticle protein corona on cytotoxicity, immunotoxicity and target drug delivery.* Nanomedicine, 2015. **11**(1): p. 81-100.
178. Bregoli, L., et al., *Nanomedicine applied to translational oncology: A future perspective on cancer treatment.* Nanomedicine: Nanotechnology, Biology and Medicine, 2016. **12**(1): p. 81-103.
179. Wu, Z., et al., *Cell-Membrane-Coated Synthetic Nanomotors for Effective Biodetoxification.* Advanced Functional Materials, 2015. **25**(25): p. 3881-3887.
180. Thamphiwatana, S., et al., *Macrophage-like nanoparticles concurrently absorbing endotoxins and proinflammatory cytokines for sepsis management.* Proceedings of the National Academy of Sciences, 2017. **114**(43): p. 11488.
181. Luk, B.T. and L. Zhang, *Cell membrane-camouflaged nanoparticles for drug delivery.* Journal of Controlled Release, 2015. **220** p. 600-607.
182. Corbo, C., et al., *Engineered biomimetic nanovesicles show intrinsic anti-inflammatory properties for the treatment of inflammatory bowel diseases.* Nanoscale, 2017. **9**(38): p. 14581-14591.
183. Copp, J.A., et al., *Clearance of pathological antibodies using biomimetic nanoparticles.* Proceedings of the National Academy of Sciences, 2014. **111**(37): p. 13481.
184. Harting Matthew, T., et al., *Inflammation-Stimulated Mesenchymal Stromal Cell-Derived Extracellular Vesicles Attenuate Inflammation.* STEM CELLS, 2017. **36**(1): p. 79-90.
185. Bazile, D.V., *Nanotechnologies in Drug Delivery - An Industrial Perspective.* Journal of Drug Delivery Science and Technology, 2014. **24**(1): p. 12-21.
186. Zhang, X.-Q., et al., *Interactions of nanomaterials and biological systems: Implications to personalized nanomedicine.* Advanced Drug Delivery Reviews, 2012. **64**(13): p. 1363-1384.
187. Ilic, N., et al., *Examination of the Regulatory Frameworks Applicable to Biologic Drugs (Including Stem Cells and Their Progeny) in Europe, the U.S., and Australia: Part I—A Method of Manual Documentary Analysis.* STEM CELLS Translational Medicine, 2012. **1**(12): p. 898-908.

188. Lener, T., et al., *Applying extracellular vesicles based therapeutics in clinical trials – an ISEV position paper.* Journal of Extracellular Vesicles, 2015. **4**(1): p. 30087.
189. Lőrincz, Á.M., et al., *Effect of storage on physical and functional properties of extracellular vesicles derived from neutrophilic granulocytes.* Journal of Extracellular Vesicles, 2014. **3**(1): p. 25465.
190. Würmseher, M. and L. Firmin, *Nanobiotech in big pharma: a business perspective.* Nanomedicine, 2017. **12**(5): p. 535-543.
191. Gardner, A.B., et al., *Biomaterials-based modulation of the immune system.* BioMed research international, 2013. **2013**.
192. Vishwakarma, A., et al., *Engineering immunomodulatory biomaterials to tune the inflammatory response.* Trends in biotechnology, 2016. **34**(6): p. 470-482.
193. Chung, L., et al., *Key players in the immune response to biomaterial scaffolds for regenerative medicine.* Advanced Drug Delivery Reviews, 2017. **114**(Supplement C): p. 184-192.
194. Mohammadi, M.R., et al., *Biohybrid Nanoparticles to Negotiate with Biological Barriers.* Small, 2019. **15**(34): p. 1902333.
195. Mohammadi, M.R., et al., *7 - Scaffolds implanted: what is next?*, in *Handbook of Tissue Engineering Scaffolds: Volume One*, M. Mozafari, F. Sefat, and A. Atala, Editors. 2019, Woodhead Publishing. p. 127-152.
196. Mohammadi, R., et al., *33: Immunomodulatory Stem Cells to Alleviate the Foreign Body Response Against Implanted Biomaterials.* Transplantation, 2019. **103**(9S2).
197. Marzaioli, V., et al., *Surface modifications of silica nanoparticles are crucial for their inert versus proinflammatory and immunomodulatory properties.* International Journal of Nanomedicine, 2014. **9**: p. 2815.
198. Andorko, J.I. and C.M. Jewell, *Designing biomaterials with immunomodulatory properties for tissue engineering and regenerative medicine.* Bioengineering & translational medicine, 2017. **2**(2): p. 139-155.
199. Hamdy, S., et al., *Targeting dendritic cells with nano-particulate PLGA cancer vaccine formulations.* Advanced drug delivery reviews, 2011. **63**(10-11): p. 943-955.
200. Manolova, V., et al., *Nanoparticles target distinct dendritic cell populations according to their size.* European journal of immunology, 2008. **38**(5): p. 1404-1413.
201. Hubbell, J.A., S.N. Thomas, and M.A. Swartz, *Materials engineering for immunomodulation.* NATURE 2009. **462**: p. 449_460.
202. Shin, H., *Fabrication methods of an engineered microenvironment for analysis of cell–biomaterial interactions.* Biomaterials, 2007. **28**(2): p. 126-133.
203. Singh, A. and K. Roy, *Immuno-engineering: The Next Frontier in Therapeutics Delivery.* Advanced drug delivery reviews, 2017. **114**: p. 1.
204. Kelly, S.H., et al., *Biomaterial strategies for generating therapeutic immune responses.* Advanced drug delivery reviews, 2017. **114**: p. 3-18.
205. Sadtler, K., et al., *Divergent immune responses to synthetic and biological scaffolds.* Biomaterials, 2019. **192**: p. 405-415.
206. Chung, L., et al., *Interleukin-17 and senescence regulate the foreign body response.* bioRxiv, 2019: p. 583757.
207. Anderson, J.M., *In vitro and in vivo monocyte, macrophage, foreign body giant cell, and lymphocyte interactions with biomaterials*, in *Biological interactions on materials surfaces*. 2009, Springer. p. 225-244.

208. Franz, S., et al., *Immune responses to implants – A review of the implications for the design of immunomodulatory biomaterials.* Biomaterials, 2011. **32**(28): p. 6692-6709.
209. Babensee, J.E., *Interaction of dendritic cells with biomaterials.* Seminars in Immunology, 2008. **20**: p. 101–108.
210. Steinman, R.M., *The dendritic cell system and its role in immunogenicity.* Annual review of immunology, 1991. **9**(1): p. 271-296.
211. Demento, S.L., et al., *Pathogen-associated molecular patterns on biomaterials: a paradigm for engineering new vaccines.* Trends in biotechnology, 2011. **29**(6): p. 294-306.
212. Mebarek, N., et al., *Versatile polyion complex micelles for peptide and siRNA vectorization to engineer tolerogenic dendritic cells.* European Journal of Pharmaceutics and Biopharmaceutics, 2015. **92**: p. 216-227.
213. Hume, P.S., et al., *Strategies to reduce dendritic cell activation through functional biomaterial design.* Biomaterials, 2012. **33**: p. 3615_3625.
214. Kempf, M., et al., *Improved stimulation of human dendritic cells by receptor engagement with surface-modified microparticles.* drug targeting, 2003. **11**(1): p. 11-18.
215. Li, H., et al., *Efficient dendritic cell priming of T lymphocytes depends on the extracellular matrix protein mindin.* The EMBO journal, 2006. **25**(17): p. 4097-4107.
216. Penna, G. and L. Adorini, *1α, 25-dihydroxyvitamin D3 inhibits differentiation, maturation, activation, and survival of dendritic cells leading to impaired alloreactive T cell activation.* The Journal of Immunology, 2000. **164**(5): p. 2405-2411.
217. Spurrell, D.R., et al., *Vav1 Regulates the Migration and Adhesion of Dendritic Cells.* Immunology, 2009. **183**: p. 310_318.
218. Look, M., et al., *Nanogel-based delivery of mycophenolic acid ameliorates systemic lupus erythematosus in mice.* The Journal of clinical investigation, 2013. **123**(4): p. 1741-1749.
219. Keselowsky, B.G., D.M. Collard, and A.J. García, *Surface chemistry modulates fibronectin conformation and directs integrin binding and specificity to control cell adhesion.* Journal of Biomedical Materials Research Part A: An Official Journal of The Society for Biomaterials, The Japanese Society for Biomaterials, and The Australian Society for Biomaterials and the Korean Society for Biomaterials, 2003. **66**(2): p. 247-259.
220. Pelaz, B., et al., *Surface functionalization of nanoparticles with polyethylene glycol: effects on protein adsorption and cellular uptake.* ACS nano, 2015. **9**(7): p. 6996-7008.
221. Sigal, G.B., M. Mrksich, and G.M. Whitesides, *Effect of surface wettability on the adsorption of proteins and detergents.* Journal of the American Chemical Society, 1998. **120**(14): p. 3464-3473.
222. Tanahashi, K. and A.G. Mikos, *Protein adsorption and smooth muscle cell adhesion on biodegradable agmatine-modified poly(propylene fumarate-co-ethylene glycol) hydrogels.* 2003.
223. Schmidt, D.R., H. Waldeck, and W.J. Kao, *Protein Adsorption to Biomaterials*, in *Biological Interactions on Materials Surfaces: Understanding and Controlling Protein, Cell, and Tissue Responses*, D.A. Puleo and R. Bizios, Editors. 2009, Springer US: New York, NY. p. 1-18.
224. Bianchi, M.E., *DAMPs, PAMPs and alarmins: all we need to know about danger.* Journal of leukocyte biology, 2007. **81**(1): p. 1-5.

225. Tang, D., et al., *PAMPs and DAMPs: signal 0s that spur autophagy and immunity.* Immunological reviews, 2012. **249**(1): p. 158-175.
226. Akira, S. and H. Hemmi, *Recognition of pathogen-associated molecular patterns by TLR family.* Immunology letters, 2003. **85**(2): p. 85-95.
227. Hotaling, N.A., et al., *Biomaterial Strategies for Immunomodulation.* Annual Review of Biomedical Engineering 2015. **17**: p. 13.1–13.33.
228. Bracho-Sanchez, E., J.S. Lewis, and B.G. Keselowsky, *Biomaterials-based immunomodulation of dendritic cells*, in *Biomaterials in Regenerative Medicine and the Immune System*. 2015, Springer. p. 139-156.
229. Wieder, E., *Dendritic cells: a basic review.* International Society for Cellular Therapy, 2003.
230. Janeway Jr, C.A., et al., *Principles of innate and adaptive immunity.* 2001.
231. Dalgaard, J., et al., *Differential capability for phagocytosis of apoptotic and necrotic leukemia cells by human peripheral blood dendritic cell subsets.* Journal of leukocyte biology, 2005. **77**(5): p. 689-698.
232. Tai, Y., et al., *Molecular mechanisms of T cells activation by dendritic cells in autoimmune diseases.* Frontiers in pharmacology, 2018. **9**: p. 642.
233. Mak, T.W. and M.E. Saunders, *The immune response: basic and clinical principles*. 2005: Academic Press.
234. Dubey, C., M. Croft, and S.L. Swain, *Costimulatory requirements of naive CD4+ T cells. ICAM-1 or B7-1 can costimulate naive CD4 T cell activation but both are required for optimum response.* Immunology, 1995. **155**(1): p. 45-57.
235. Mueller, D.L., M.K. Jenkins, and R.H. Schwartz, *Clonal expansion versus functional clonal inactivation: a costimulatory signalling pathway determines the outcome of T cell antigen receptor occupancy.* Annual review of immunology, 1989. **7**(1): p. 445-480.
236. McNally, A.K. and J.M. Anderson, *Interleukin-4 induces foreign body giant cells from human monocytes/macrophages. Differential lymphokine regulation of macrophage fusion leads to morphological variants of multinucleated giant cells.* The American journal of pathology, 1995. **147**(5): p. 1487.
237. DeFife, K.M., et al., *Interleukin-13 induces human monocyte/macrophage fusion and macrophage mannose receptor expression.* The Journal of Immunology, 1997. **158**(7): p. 3385-3390.
238. McNally, A.K. and J.M. Anderson, *Phenotypic expression in human monocyte-derived interleukin-4-induced foreign body giant cells and macrophages in vitro: Dependence on material surface properties.* Journal of Biomedical Materials Research Part A, 2015. **103**(4): p. 1380-1390.
239. Haas, A., *The phagosome: compartment with a license to kill.* Traffic, 2007. **8**(4): p. 311-330.
240. Zheng, X., et al., *Effect of Different Titanium Surfaces on Maturation of Murine Bone Marrow-Derived Dendritic Cells.* Scientific Reports, 2017. **7**: p. 41945.
241. Zhu, F.-j., et al., *Role of Dendritic Cells in the Host Response to Biomaterials and Their Signaling Pathways.* Acta biomaterialia, 2019.
242. Collin, M. and V. Bigley, *Human dendritic cell subsets: an update.* Immunology, 2018. **154**(1): p. 3-20.
243. Shortman, K. and Y.-J. Liu, *Mouse and human dendritic cell subtypes.* Nature Reviews Immunology, 2002. **2**(3): p. 151.

244. Collin, M., N. McGovern, and M. Haniffa, *Human dendritic cell subsets.* Immunology, 2013. **140**(1): p. 22-30.
245. Liu, Y.-J., *IPC: professional type 1 interferon-producing cells and plasmacytoid dendritic cell precursors.* Annu. Rev. Immunol., 2005. **23**: p. 275-306.
246. McKenna, K., A.-S. Beignon, and N. Bhardwaj, *Plasmacytoid dendritic cells: linking innate and adaptive immunity.* Journal of virology, 2005. **79**(1): p. 17-27.
247. Honda, K., et al., *IRF-7 is the master regulator of type-I interferon-dependent immune responses.* Nature, 2005. **434**(7034): p. 772.
248. Denzer, K., et al., *Follicular dendritic cells carry MHC class II-expressing microvesicles at their surface.* The Journal of Immunology, 2000. **165**(3): p. 1259-1265.
249. Kranich, J. and N.J. Krautler, *How Follicular Dendritic Cells Shape the B-Cell Antigenome.* Frontiers in Immunology, 2016. **7**: p. 225.
250. Worbs, T., S.I. Hammerschmidt, and R. Forster, *Dendritic cell migration in health and disease.* Nat Rev Immunol, 2017. **17**(1): p. 30-48.
251. Freemont, A. and J. Hoyland, *Cell adhesion molecules.* Clinical molecular pathology, 1996. **49**(6): p. M321.
252. Rogers, T.H. and J.E. Babensee, *The role of integrins in the recognition and response of dendritic cells to biomaterials.* Biomaterials, 2011. **32**: p. 1270_1279.
253. Kapp, T.G., et al., *Integrin modulators: a patent review* Expert opinion, 2013. **23(10)**: p. 1273-1295.
254. MacPherson, M., et al., *Leukocyte beta2-integrins; genes and disease.* Journal of Genetic Syndromes and Gene Therapy, 2013. **4**(6).
255. Albelda, S.M. and C.A. Buck, *Integrins and other cell adhesion molecules.* The FASEB Journal, 1990. **4**(11): p. 2868-2880.
256. Shimaoka, M. and T.A. Springer, *Therapeutic antagonists and conformational regulation of integrin function.* Nature reviews. Drug discovery, 2003. **2**(9): p. 703.
257. Schittenhelm, L., C.M. Hilkens, and V.L. Morrison, *β2 integrins as regulators of dendritic cell, monocyte, and macrophage function.* Frontiers in immunology, 2017. **8**: p. 1866.
258. Yakubenko, V.P., S.P. Yadav, and T.P. Ugarova, *Integrin αDβ2, an adhesion receptor up-regulated on macrophage foam cells, exhibits multiligand-binding properties.* Blood, 2006. **107**(4): p. 1643-1650.
259. Ammon, C., et al., *Comparative analysis of integrin expression on monocyte-derived macrophages and monocyte-derived dendritic cells.* Immunology, 2000. **100**(3): p. 364-369.
260. Shokouhi, B., et al., *The role of multiple toll-like receptor signalling cascades on interactions between biomedical polymers and dendritic cells.* Biomaterials, 2010. **31**: p. 5759_5771.
261. Zaveri, T.D., et al., *Integrin-directed modulation of macrophage responses to biomaterials.* Biomaterials, 2014. **35**(11): p. 3504-3515.
262. Hu, P.-P., *Recent Advances in Aptamers Targeting Immune System.* Inflammation, 2017. **40**: p. 295_302.
263. Portou, M., et al., *The innate immune system, toll-like receptors and dermal wound healing: A review.* Vascular pharmacology, 2015. **71**: p. 31-36.
264. Akira, S., S. Uematsu, and O. Takeuchi, *Pathogen recognition and innate immunity.* Cell, 2006. **124**(4): p. 783-801.

265. Terhorst, D., et al., *The role of toll-like receptors in host defenses and their relevance to dermatologic diseases.* American journal of clinical dermatology, 2010. **11**(1): p. 1-10.
266. Hodgkinson, C.P., K. Patel, and S. Ye, *Functional Toll-like receptor 4 mutations modulate the response to fibrinogen.* Thrombosis and haemostasis, 2008. **100**(2): p. 301-307.
267. Millien, V.O., et al., *Cleavage of fibrinogen by proteinases elicits allergic responses through Toll-like receptor 4.* Science, 2013. **341**(6147): p. 792-796.
268. Dąbrowska, A.M. and R. Słotwiński, *The immune response to surgery and infection.* Central-European journal of immunology, 2014. **39**(4): p. 532.
269. Mukherjee, S., S. Karmakar, and S.P.S. Babu, *TLR2 and TLR4 mediated host immune responses in major infectious diseases: a review.* Brazilian Journal of Infectious Diseases, 2016. **20**(2): p. 193-204.
270. Akira, S. and K. Takeda, *Toll-like receptor signalling.* Nature reviews immunology, 2004. **4**(7): p. 499-511.
271. Takeda, K. and S. Akira, *Toll-like receptors in innate immunity.* International immunology, 2005. **17**(1): p. 1-14.
272. Uematsu, S. and S. Akira, *Toll-Like receptors (TLRs) and their ligands*, in *Toll-like receptors (TLRs) and innate immunity*. 2008, Springer. p. 1-20.
273. Taghavi, M., et al., *Role of pathogen-associated molecular patterns (PAMPS) in immune responses to fungal infections.* European journal of pharmacology, 2017. **808**: p. 8-13.
274. Shah, M.P., et al., *Toll-like receptors: A double edge sword.* Journal of Interdisciplinary Dentistry, 2013. **3**(2): p. 57.
275. Kawasaki, T. and T. Kawai, *Toll-Like Receptor Signaling Pathways.* Frontiers in Immunology, 2014. **5**(461).
276. Chang, Y.-C., et al., *Identification and characterization of oligonucleotides that inhibit Toll-like receptor 2-associated immune.* Faseb, 2009. **23**: p. 3078–3088.
277. Randolph, G.J., J. Ochando, and S. Partida-Sánchez, *Migration of dendritic cell subsets and their precursors.* Annu. Rev. Immunol., 2008. **26**: p. 293-316.
278. Martín-Fontecha, A., et al., *Regulation of dendritic cell migration to the draining lymph node.* Journal of Experimental Medicine, 2003. **198**(4): p. 615-621.
279. Ohl, L., et al., *CCR7 governs skin dendritic cell migration under inflammatory and steady-state conditions.* Immunity, 2004. **21**(2): p. 279-288.
280. Yoneyama, H., K. Matsuno, and K. Matsushima, *Migration of dendritic cells.* International journal of hematology, 2005. **81**(3): p. 204-207.
281. van Rijt, L.S., et al., *Essential role of dendritic cell CD80/CD86 costimulation in the induction, but not reactivation, of TH2 effector responses in a mouse model of asthma.* Journal of Allergy and Clinical Immunology, 2004. **114**(1): p. 166-173.
282. Morelli, A.E. and A.W. Thomson, *Tolerogenic dendritic cells and the quest for transplant tolerance.* Nature reviews. Immunology, 2007. **7**(8): p. 610.
283. Jhunjhunwala, S., et al., *Delivery of rapamycin to dendritic cells using degradable microparticles.* Journal of Controlled Release, 2009. **133**(3): p. 191-197.
284. Müller, G., et al., *Interleukin-10-treated dendritic cells modulate immune responses of naive and sensitized T cells in vivo.* Journal of investigative Dermatology, 2002. **119**(4): p. 836-841.

285. Piemonti, L., et al., *Vitamin D3 affects differentiation, maturation, and function of human monocyte-derived dendritic cells.* The Journal of Immunology, 2000. **164**(9): p. 4443-4451.
286. Akkaya, B., et al., *Regulatory T cells mediate specific suppression by depleting peptide–MHC class II from dendritic cells.* Nature immunology, 2019: p. 1.
287. Suciu-Foca, N., P. Berloco, and R. Cortesini, *Tolerogenic dendritic cells in cancer, transplantation, and autoimmune diseases.* Human immunology, 2009. **70**(5): p. 277-280.
288. Boks, M.A., et al., *IL-10-generated tolerogenic dendritic cells are optimal for functional regulatory T cell induction—a comparative study of human clinical-applicable DC.* Clinical immunology, 2012. **142**(3): p. 332-342.
289. Thomas, J.M., et al., *Peritransplant tolerance induction in macaques: Early events reflecting the unique synergy between immunotoxin and Deoxyspergualin 1, 2.* Transplantation, 1999. **68**(11): p. 1660-1673.
290. Canning, M.O., et al., *1-alpha, 25-Dihydroxyvitamin D3 (1, 25 (OH)(2) D (3)) hampers the maturation of fully active immature dendritic cells from monocytes.* European Journal of Endocrinology, 2001. **145**(3): p. 351-357.
291. Pastor, F., et al., *CD28 Aptamers as Powerful Immune Response Modulators.* Molecular Therapy—Nucleic Acids, 2013. **2**: p. 1_9.
292. van Kooten, C. and J. Banchereau, *Functional role of CD40 and its ligand.* International archives of allergy and immunology, 1997. **113**(4): p. 393-399.
293. Haanstra, K.G., et al., *Prevention of kidney allograft rejection using anti-CD40 and anti-CD86 in primates.* Transplantation, 2003. **75**(5): p. 637-643.
294. Hansel, T.T., et al., *The safety and side effects of monoclonal antibodies.* Drug Discovery, 2010. **9**: p. 325_338.
295. Weber, J., *Anti–CTLA-4 antibody ipilimumab: case studies of clinical response and immune-related adverse events.* The oncologist, 2007. **12**(7): p. 864-872.
296. Suntharalingam, G., et al., *Cytokine Storm in a Phase 1 Trial of the Anti-CD28 Monoclonal Antibody TGN1412.* medicine, 2006. **355**: p. 1018-28.
297. Mirabet, M., et al., *Platelet pro-aggregatory effects of CD40L monoclonal antibody.* Molecular Immunology, 2008. **45**: p. 937–944.
298. Jayasena, S.D., *Aptamers: an emerging class of molecules that rival antibodies in diagnostics.* Clinical chemistry, 1999. **45**(9): p. 1628-1650.
299. Thiviyanathan, V. and D.G. Gorenstein, *Aptamers and the next generation of diagnostic reagents.* PROTEOMICS-Clinical Applications, 2012. **6**(11-12): p. 563-573.
300. Balamurugan, S., et al., *Surface immobilization methods for aptamer diagnostic applications.* Anal Bioanal Chem, 2008. **390**: p. 1009_1021.
301. Zhou, G., et al., *Aptamers: A promising chemical antibody for cancer therap.* Oncotarget, 2016. **7**: p. 13446_13463.
302. Gold, L., *SELEX: how it happened and where it will go.* Journal of molecular evolution, 2015. **81**(5-6): p. 140-143.
303. Blind, M., W. Kolanus, and M. Famulok, *Cytoplasmic RNA modulators of an inside-out signal-transduction cascade.* Proceedings of the National Academy of Sciences, 1999. **96**(7): p. 3606-3610.
304. Gilboa-Geffen, A., et al., *Activation of the Alternative NFkB Pathway Improves Disease Symptoms in a Model of Sjogren's Syndrome.* PLoS ONE, 2011. **6**(12).

305. Acharya, A.P., et al., *Adhesive substrate-modulation of adaptive immune responses.* Biomaterials, 2008. **29**: p. 4736–4750.
306. Keselowsky, B.G., D.M. Collard, and A.J. García, *Surface chemistry modulates fibronectin conformation and directs integrin binding and specificity to control cell adhesion.* Journal of Biomedical Materials Research Part A, 2003. **66**(2): p. 247-259.
307. Brand, U., et al., *Influence of extracellular matrix proteins on the development of cultured human dendritic cells.* Immunology, 1998. **28**: p. 1673–1680.
308. Jones, J.A., et al., *Proteomic analysis and quantification of cytokines and chemokines from biomaterial surface-adherent macrophages and foreign body giant cells.* Journal of Biomedical Materials Research Part A: An Official Journal of The Society for Biomaterials, The Japanese Society for Biomaterials, and The Australian Society for Biomaterials and the Korean Society for Biomaterials, 2007. **83**(3): p. 585-596.
309. Shankar, S.P., et al., *Dendritic cell responses to self-assembled monolayers of defined chemistries.* Journal of Biomedical Materials Research Part A, 2010. **92**(4): p. 1487-1499.
310. Torché, A.-M., et al., *PLGA Microspheres Phagocytosis by Pig Alveolar Macrophages: Influence of Polyvinyl alcohol) Concentration, Nature of Loaded-Protein and Copolymer Nature.* Journal of drug targeting, 1999. **7**(5): p. 343-354.
311. Thiele, L., et al., *Competitive adsorption of serum proteins at microparticles affects phagocytosis by dendritic cells.* Biomaterials, 2003. **24**(8): p. 1409-1418.
312. Lee, M.H., et al., *Effect of biomaterial surface properties on fibronectin–a5b1 integrin interaction and cellular attachment.* Biomaterials, 2006. **27**: p. 1907–1916.
313. Lee, J.H. and H.B. Lee, *A wettability gradient as a tool to study protein adsorption and cell adhesion on polymer surfaces.* Biomaterials Science, 2015. **4**: p. 467_481.
314. Ishihara, K., et al., *Why do phospholipid polymers reduce protein adsorption?* Biomedical materials research a, 1998: p. 323_330.
315. Sands, R.W., et al., *Tuning Cytokines Enriches Dendritic Cells and Tregs in the Periodontium.* Journal of Periodontology, 2020.
316. Besin, G., et al., *Thymic Stromal Lymphopoietin and Thymic Stromal Lymphopoietin–Conditioned Dendritic Cells Induce Regulatory T-Cell Differentiation and Protection of NOD Mice Against Diabetes.* Diabetes, 2008. **57**(8): p. 2107-2117.
317. Lewis, J.S., et al., *Dual-Sized Microparticle System for Generating Suppressive Dendritic Cells Prevents and Reverses Type 1 Diabetes in the Nonobese Diabetic Mouse Model.* ACS Biomaterials Science & Engineering, 2019. **5**(5): p. 2631-2646.
318. Du, W., et al., *Enhanced proangiogenic potential of mesenchymal stem cell-derived exosomes stimulated by a nitric oxide releasing polymer.* Biomaterials, 2017. **133**: p. 70-81.
319. Shen, C., et al., *Killer artificial antigen-presenting cells deplete alloantigen-specific T cells in a murine model of alloskin transplantation.* Immunology letters, 2011. **138**(2): p. 144-155.
320. Feldman, M.D., et al., *Who is Responsible for Evaluating the Safety and Effectiveness of Medical Devices? The Role of Independent Technology Assessment.* Journal of General Internal Medicine, 2008. **23**(1): p. 57-63.
321. McIntyre, W.F. and J.S. Healey, *Cardiac implantable electronic device infections: From recognizing risk to prevention.* HeartRhythm, 2017. **14**: p. 846–847.
322. Andersen, O.Z., et al., *Accelerated bone ingrowth by local delivery of strontium from surface functionalized titanium implants.* Biomaterials, 2013. **34**(24): p. 5883-5890.

323. Osmon, D.R., et al., *Diagnosis and Management of Prosthetic Joint Infection: Clinical Practice Guidelines by the Infectious Diseases Society of Americaa.* Clinical Infectious Diseases, 2013. **56**(1): p. e1-e25.
324. Eaves, I.I.I.F. and F. Nahai, *Anaplastic Large Cell Lymphoma and Breast Implants: FDA Report.* Aesthetic Surgery Journal, 2011. **31**(4): p. 467-468.
325. Wiles, K., et al., *The Host Immune Response to Tissue-Engineered Organs: Current Problems and Future Directions.* Tissue Engineering Part B: Reviews, 2015. **22**(3): p. 208-219.
326. Veiseh, O., et al., *Size- and shape-dependent foreign body immune response to materials implanted in rodents and non-human primates.* Nature Materials, 2015. **14**: p. 643.
327. Najdahmadi, A., J.R.T. Lakey, and E. Botvinick, *Structural Characteristics and Diffusion Coefficient of Alginate Hydrogels Used for Cell Based Drug Delivery.* MRS Advances, 2018. **3**(40): p. 2399-2408.
328. Rezaa Mohammadi, M., et al., *Immune response to subcutaneous implants of alginate microcapsules.* Materials Today: Proceedings, 2018. **5**(7, Part 3): p. 15580-15585.
329. Jafarkhani, M., et al., *Strategies for directing cells into building functional hearts and parts.* Biomaterials Science, 2018. **6**(7): p. 1664-1690.
330. Helton, K.L., B.D. Ratner, and N.A. Wisniewski, *Biomechanics of the Sensor-Tissue Interface—Effects of Motion, Pressure, and Design on Sensor Performance and the Foreign Body Response—Part I: Theoretical Framework.* Journal of Diabetes Science and Technology, 2011. **5**(3): p. 632-646.
331. Xie, X., et al., *Reduction of measurement noise in a continuous glucose monitor by coating the sensor with a zwitterionic polymer.* Nature Biomedical Engineering, 2018.
332. Baigrie, R.J., et al., *Systemic cytokine response after major surgery.* BJS, 1992. **79**(8): p. 757-760.
333. Baumann, H. and J. Gauldie, *The acute phase response.* Immunology Today, 1994. **15**(2): p. 74-80.
334. Hildebrandt, U., et al., *Granulocyte elastase and systemic cytokine response after laparoscopic-assisted and open resections in Crohn's disease.* Diseases of the colon and rectum, 1999. **42**(11): p. 1480-6.
335. Bateman, R.M., M.D. Sharpe, and C.G. Ellis, *Bench-to-bedside review: Microvascular dysfunction in sepsis –hemodynamics, oxygen transport, and nitric oxide.* Critical Care, 2003. **7**(5): p. 359-373.
336. Cruickshank, A.M., et al., *Response of Serum Interleukin-6 in Patients Undergoing Elective Surgery of Varying Severity.* Clinical Science, 1990. **79**(2): p. 161.
337. Shenkin, A., et al., *The serum interleukin 6 response to elective surgery.* Lymphokine research, 1989. **8**(2): p. 123-127.
338. Kloosterman, T.C., et al., *Unimpaired immune functions after laparoscopic cholecystectomy.* Surgery, 1994. **115**(4): p. 424-8.
339. E, F., L. K, and A. KE, *Rapid leukocyte accumulation by "spontaneous" rolling and adhesion in the exteriorized rabbit mesentery.* Int J Microcirc Clin Exp 1991, 2006.
340. Ni Choileain, N. and H. Redmond, *Cell response to surgery.* Archives of Surgery, 2006. **141**(11): p. 1132-1140.
341. Magill, S.S., et al., *Multistate Point-Prevalence Survey of Health Care–Associated Infections.* The New England journal of medicine, 2014. **370**(13): p. 1198-1208.

342. Arciola, C.R., D. Campoccia, and L. Montanaro, *Implant infections: adhesion, biofilm formation and immune evasion.* Nature Reviews Microbiology, 2018. **16**(7): p. 397-409.
343. Tambyah, P.A., *Catheter-associated urinary tract infections: diagnosis and prophylaxis.* International Journal of Antimicrobial Agents, 2004. **24**: p. 44-48.
344. Garnett, J.A. and S. Matthews, *Interactions in Bacterial Biofilm Development: A Structural Perspective.* Current Protein & Peptide Science, 2012. **13**(8): p. 739-755.
345. Donlan, R.M., *Biofilms: Microbial Life on Surfaces.* Emerging Infectious Diseases, 2002. **8**(9): p. 881-890.
346. Wilton, M., et al., *Extracellular DNA Acidifies Biofilms and Induces Aminoglycoside Resistance in Pseudomonas aeruginosa.* Antimicrobial Agents and Chemotherapy, 2016. **60**(1): p. 544-553.
347. Proctor, R.A., et al., *Small colony variants: a pathogenic form of bacteria that facilitates persistent and recurrent infections.* Nature Reviews Microbiology, 2006. **4**: p. 295.
348. Song, Z., et al., *Prosthesis Infections after Orthopedic Joint Replacement: The Possible Role of Bacterial Biofilms.* Orthopedic Reviews, 2013. **5**(2): p. e14.
349. Josse, J., F. Velard, and S.C. Gangloff, *Staphylococcus aureus vs. Osteoblast: Relationship and Consequences in Osteomyelitis.* Frontiers in Cellular and Infection Microbiology, 2015. **5**: p. 85.
350. Fowler, T., et al., *Cellular invasion by Staphylococcus aureus involves a fibronectin bridge between the bacterial fibronectin-binding MSCRAMMs and host cell β1 integrins.* European Journal of Cell Biology, 2000. **79**(10): p. 672-679.
351. Alexander, E.H., et al., *Staphylococcus aureus - induced tumor necrosis factor - related apoptosis - inducing ligand expression mediates apoptosis and caspase-8 activation in infected osteoblasts.* BMC Microbiology, 2003. **3**: p. 5-5.
352. Rello, J., et al., *Epidemiology and Outcomes of Ventilator-Associated Pneumonia in a Large US Database.* Chest, 2002. **122**(6): p. 2115-2121.
353. Montanaro, L., et al., *Scenery of Staphylococcus implant infections in orthopedics.* Future Microbiology, 2011. **6**(11): p. 1329-1349.
354. Arciola, C.R., et al., *Etiology of Implant Orthopedic Infections: A Survey on 1027 Clinical Isolates.* The International Journal of Artificial Organs, 2005. **28**(11): p. 1091-1100.
355. Aggarwal, V.K., et al., *Organism Profile in Periprosthetic Joint Infection: Pathogens Differ at Two Arthroplasty Infection Referral Centers in Europe and in the United States.* J Knee Surg, 2014. **27**(05): p. 399-406.
356. Vroman, L. and A.L. Adams, *Findings with the recording ellipsometer suggesting rapid exchange of specific plasma proteins at liquid/solid interfaces.* Surface Science, 1969. **16**: p. 438-446.
357. Hirsh, S.L., et al., *The Vroman effect: Competitive protein exchange with dynamic multilayer protein aggregates.* Colloids and Surfaces B: Biointerfaces, 2013. **103**: p. 395-404.
358. Anderson, J.M., A. Rodriguez, and D.T. Chang, *Foreign body reaction to biomaterials.* Seminars in Immunology, 2008. **20**(2): p. 86-100.
359. Gorbet, M.B. and M.V. Sefton, *Biomaterial-associated thrombosis: roles of coagulation factors, complement, platelets and leukocytes.* Biomaterials, 2004. **25**(26): p. 5681-5703.

360. Andersson, J., et al., *Binding of C3 fragments on top of adsorbed plasma proteins during complement activation on a model biomaterial surface.* Biomaterials, 2005. **26**(13): p. 1477-1485.
361. Anderson, L. and N.G. Anderson, *High resolution two-dimensional electrophoresis of human plasma proteins.* Proceedings of the National Academy of Sciences, 1977. **74**(12): p. 5421.
362. Adkins, J.N., et al., *Toward a Human Blood Serum Proteome.* Molecular & Cellular Proteomics, 2002. **1**(12): p. 947.
363. Dee, K.C., D.A. Puleo, and R. Bizios, *Protein-Surface Interactions.* An Introduction to Tissue-Biomaterial Interactions, 2003: p. 37-52.
364. McUmber, A.C., T.W. Randolph, and D.K. Schwartz, *Electrostatic Interactions Influence Protein Adsorption (but Not Desorption) at the Silica–Aqueous Interface.* The Journal of Physical Chemistry Letters, 2015. **6**(13): p. 2583-2587.
365. Andrade, J.D., *Principles of Protein Adsorption.* Surface and Interfacial Aspects of Biomedical Polymers, 1985. **2**: p. 1-80.
366. Tyn, M.T. and T.W. Gusek, *Prediction of diffusion coefficients of proteins.* Biotechnology and Bioengineering, 1990. **35**(4): p. 327-338.
367. Koutsopoulos, S., et al., *Controlled release of functional proteins through designer self-assembling peptide nanofiber hydrogel scaffold.* Proceedings of the National Academy of Sciences of the United States of America, 2009. **106**(12): p. 4623-4628.
368. Noh, H. and E.A. Vogler, *Volumetric interpretation of protein adsorption: Partition coefficients, interphase volumes, and free energies of adsorption to hydrophobic surfaces.* Biomaterials, 2006. **27**(34): p. 5780-5793.
369. Krishnan, A., C.A. Siedlecki, and E.A. Vogler, *Traube-Rule Interpretation of Protein Adsorption at the Liquid−Vapor Interface.* Langmuir, 2003. **19**(24): p. 10342-10352.
370. Anderson, N.L. and N.G. Anderson, *The Human Plasma Proteome.* Molecular & Cellular Proteomics, 2002. **1**(11): p. 845.
371. Fang, F. and I. Szleifer, *Kinetics and Thermodynamics of Protein Adsorption: A Generalized Molecular Theoretical Approach.* Biophysical Journal, 2001. **80**(6): p. 2568-2589.
372. Kao, P., et al., *Volumetric Interpretation of Protein Adsorption: Interfacial Packing of Protein Adsorbed to Hydrophobic Surfaces from Surface-Saturating Solution Concentrations.* Biomaterials, 2011. **32**(4): p. 969-978.
373. Corbo, C., et al., *Unveiling the in Vivo Protein Corona of Circulating Leukocyte-like Carriers.* ACS Nano, 2017. **11**(3): p. 3262-3273.
374. Thevenot, P., W. Hu, and L. Tang, *SURFACE CHEMISTRY INFLUENCE IMPLANT BIOCOMPATIBILITY.* Current topics in medicinal chemistry, 2008. **8**(4): p. 270-280.
375. Cha, P., et al., *Interfacial Energetics of Protein Adsorption from Aqueous Buffer to Surfaces with Varying Hydrophilicity.* Langmuir, 2008. **24**(6): p. 2553-2563.
376. Wong, S.Y., et al., *Drastically Lowered Protein Adsorption on Microbicidal Hydrophobic/Hydrophilic Polyelectrolyte Multilayers.* Biomacromolecules, 2012. **13**(3): p. 719-726.
377. Rabe, M., D. Verdes, and S. Seeger, *Understanding protein adsorption phenomena at solid surfaces.* Advances in Colloid and Interface Science, 2011. **162**(1): p. 87-106.
378. X, C., et al., *Temperature dependent activity and structure of adsorbed proteins on plasma polymerized N-isopropyl acrylamide.* Biointerphases, 2006.

379. Lin, T.-h., et al., *Chronic inflammation in biomaterial induced periprosthetic osteolysis: NF-κB as a therapeutic target.* Acta biomaterialia, 2014. **10**(1): p. 10.1016/j.actbio.2013.09.034.
380. Litvinov, R.I. and J.W. Weisel, *What Is the Biological and Clinical Relevance of Fibrin?* Seminars in thrombosis and hemostasis, 2016. **42**(4): p. 333-343.
381. L, T. and E. JW, *Fibrin(ogen) mediates acute inflammatory responses to biomaterials.* The Journal of Experimental Medicine, 1993. **178**(6): p. 2147-2156.
382. Bennewitz, N.L. and J.E. Babensee, *The effect of the physical form of poly(lactic-co-glycolic acid) carriers on the humoral immune response to co-delivered antigen.* Biomaterials, 2005. **26**(16): p. 2991-2999.
383. Tang, L., T.A. Jennings, and J.W. Eaton, *Mast cells mediate acute inflammatory responses to implanted biomaterials.* Proceedings of the National Academy of Sciences of the United States of America, 1998. **95**(15): p. 8841-8846.
384. Henson, P.M., *The Immunologic Release of Constituents from Neutrophil Leukocytes.* The Journal of Immunology, 1971. **107**(6): p. 1547.
385. Nimeri, G., et al., *The influence of plasma proteins and platelets on oxygen radical production and F-actin distribution in neutrophils adhering to polymer surfaces.* Biomaterials, 2002. **23**(8): p. 1785-1795.
386. Patel, J.D., T. Krupka, and J.M. Anderson, *iNOS-mediated generation of reactive oxygen and nitrogen species by biomaterial-adherent neutrophils.* Journal of Biomedical Materials Research Part A, 2006. **80A**(2): p. 381-390.
387. Zdolsek, J., J.W. Eaton, and L. Tang, *Histamine release and fibrinogen adsorption mediate acute inflammatory responses to biomaterial implants in humans.* Journal of Translational Medicine, 2007. **5**(1): p. 31.
388. Sheikh, Z., et al., *Macrophages, Foreign Body Giant Cells and Their Response to Implantable Biomaterials.* Materials, 2015. **8**(9).
389. Garrett, T.R., M. Bhakoo, and Z. Zhang, *Bacterial adhesion and biofilms on surfaces.* Progress in Natural Science, 2008. **18**(9): p. 1049-1056.
390. Tari, K., et al., *Biology of TH17 Cells and Their Role in Inflammatory Diseases.* IBBJ, 2015. **1**(2).
391. Kopan, C., et al., *Approaches in Immunotherapy, Regenerative Medicine, and Bioengineering for Type 1 Diabetes.* Frontiers in Immunology, 2018. **9**: p. 1354.
392. Gould, S., *Innate Immunity: the First Line of Defence.* Scientific American Blog Network, 2014.
393. Theoharides, T.C., et al., *Mast cells and inflammation.* Biochimica et Biophysica Acta, 2012. **1822**(1): p. 21-33.
394. Lim, J.J., S. Grinstein, and Z. Roth, *Diversity and Versatility of Phagocytosis: Roles in Innate Immunity, Tissue Remodeling, and Homeostasis.* Frontiers in Cellular and Infection Microbiology, 2017. **7**: p. 191.
395. Lodge, A., *Difference Between Monocytes and Macrophages.* Astarte Biologics, 2017.
396. Sinno, H. and S. Prakash, *Complements and the Wound Healing Cascade: An Updated Review.* Plastic Surgery International, 2013. **2013**: p. 146764.
397. Koh, T.J. and L.A. DiPietro, *Inflammation and wound healing: The role of the macrophage.* Expert reviews in molecular medicine, 2011. **13**: p. e23-e23.
398. Gurtner, G.C., et al., *Wound repair and regeneration.* Nature, 2008. **453**: p. 314.

399. Eming, S.A., P. Martin, and M. Tomic-Canic, *Wound repair and regeneration: Mechanisms, signaling, and translation.* Science translational medicine, 2014. **6**(265): p. 265sr6-265sr6.
400. Werner, S. and R. Grose, *Regulation of Wound Healing by Growth Factors and Cytokines.* Physiological Reviews, 2003. **83**(3): p. 835-870.
401. Lovvorn, H.N., et al., *Relative distribution and crosslinking of collagen distinguish fetal from adult sheep wound repair.* Journal of Pediatric Surgery, 1999. **34**(1): p. 218-223.
402. Yager, D.R., et al., *Wound Fluids from Human Pressure Ulcers Contain Elevated Matrix Metalloproteinase Levels and Activity Compared to Surgical Wound Fluids.* Journal of Investigative Dermatology, 1996. **107**(5): p. 743-748.
403. Bergan, J.J., et al., *Chronic Venous Disease.* New England Journal of Medicine, 2006. **355**(5): p. 488-498.
404. Eming, S.A., et al., *Interrelation of immunity and tissue repair or regeneration.* Seminars in Cell & Developmental Biology, 2009. **20**(5): p. 517-527.
405. Eming, S.A., et al., *Differential Proteomic Analysis Distinguishes Tissue Repair Biomarker Signatures in Wound Exudates Obtained from Normal Healing and Chronic Wounds.* Journal of Proteome Research, 2010. **9**(9): p. 4758-4766.
406. Beidler, S.K., et al., *Inflammatory cytokine levels in chronic venous insufficiency ulcer tissue before and after compression therapy.* Journal of vascular surgery, 2009. **49**(4): p. 1013-1020.
407. Canady, J., et al., *Fibrosing connective tissue disorders of the skin: Molecular similarities and distinctions.* Journal of Dermatological Science, 2013. **70**(3): p. 151-158.
408. Reish, R.G. and E. Eriksson, *Scars: A Review of Emerging and Currently Available Therapies.* Plastic and Reconstructive Surgery, 2008. **122**(4).
409. Coelho, J.F., et al., *Drug delivery systems: Advanced technologies potentially applicable in personalized treatments.* The EPMA Journal, 2010. **1**(1): p. 164-209.
410. Yu, T., V.J. Tutwiler, and K. Spiller, *The Role of Macrophages in the Foreign Body Response to Implanted Biomaterials.* Biomaterials in Regenerative Medicine and the Immune System, 2015: p. 17-34.
411. Driscoll, P., *Complications Related to Implantation of Coronary Stents.* MedMarket Diligence, 2009.
412. Kiran, U. and N. Makhija, *Patient with Recent Coronary Artery Stent Requiring Major Non Cardiac Surgery.* Indian Journal of Anaesthesia, 2009. **53**(5): p. 582-591.
413. Yoneda, S., et al., *Late-phase inflammatory response as a feature of in-stent restenosis after drug-eluting stent implantation.* Coronary Artery Disease, 2013. **24**(5).
414. Pelletier, M., et al., *Evidence for a cross-talk between human neutrophils and Th17 cells.* Blood, 2010. **115**(2): p. 335.
415. Cappellano, G., et al., *Immunophenotypic characterization of human T cells after in vitro exposure to different silicone breast implant surfaces.* PLOS ONE, 2018. **13**(2): p. e0192108.
416. Backovic, A. and D. Wolfram, *Silicone mammary implants – Can we turn back the time?* Experimental Gerontology, 2007. **42**(8): p. 713-718.
417. JP, M., et al., *Determination of silicon in breast and capsular tissue from patients with breast implants performed by inductively coupled plasma emission spectroscopy. Comparison with tissue histology.* American Journal of Clinical Pathology, 1997: p. 236-46.

418. Wick, G., et al., *The Immunology of Fibrosis.* Annual Review of Immunology, 2013. **31**(1): p. 107-135.
419. Dolores, W., et al., *Cellular and molecular composition of fibrous capsules formed around silicone breast implants with special focus on local immune reactions.* Journal of Autoimmunity, 2004. **23**(1): p. 81-91.
420. Wolfram, D., et al., *T Regulatory Cells and TH17 Cells in Peri–Silicone Implant Capsular Fibrosis.* Plastic and Reconstructive Surgery, 2012. **129**(2).
421. Pittet, M.J., M. Nahrendorf, and F.K. Swirski, *The journey from stem cell to macrophage.* Annals of the New York Academy of Sciences, 2014. **1319**(1): p. 1-18.
422. Wermuth, P.J. and S.A. Jimenez, *The significance of macrophage polarization subtypes for animal models of tissue fibrosis and human fibrotic diseases.* Clinical and Translational Medicine, 2015. **4**: p. 2.
423. Martinez, F.O. and S. Gordon, *The M1 and M2 paradigm of macrophage activation: time for reassessment.* F1000Prime Reports, 2014. **6**: p. 13.
424. Chinetti-Gbaguidi, G. and B. Staels, *Macrophage polarization in metabolic disorders: functions and regulation.* Current Opinion in Lipidology, 2011. **22**(5): p. 365-372.
425. Rőszer, T., *Understanding the Mysterious M2 Macrophage through Activation Markers and Effector Mechanisms.* Mediators of Inflammation, 2015. **2015**: p. 816460.
426. Mosser, D.M. and X. Zhang, *Activation of Murine Macrophages.* Current protocols in immunology / edited by John E. Coligan ... [et al.], 2008. **CHAPTER**: p. Unit.
427. Benoit, M., B. Desnues, and J.-L. Mege, *Macrophage Polarization in Bacterial Infections.* The Journal of Immunology, 2008. **181**(6): p. 3733.
428. Kzhyshkowska, J., et al., *Macrophage responses to implants: prospects for personalized medicine.* Journal of Leukocyte Biology, 2015. **98**(6): p. 953-962.
429. Jetten, N., et al., *Anti-inflammatory M2, but not pro-inflammatory M1 macrophages promote angiogenesis in vivo.* Angiogenesis, 2014. **17**(1): p. 109-118.
430. Villa, A., et al., *Estrogens, Neuroinflammation, and Neurodegeneration.* Endocrine Reviews, 2016. **37**(4): p. 372-402.
431. Heusinkveld, M. and S.H. van der Burg, *Identification and manipulation of tumor associated macrophages in human cancers.* Journal of Translational Medicine, 2011. **9**: p. 216-216.
432. Nih, L.R., et al., *Dual-function injectable angiogenic biomaterial for the repair of brain tissue following stroke.* Nature Materials, 2018. **17**(7): p. 642-651.
433. O' Reilly, L.A., et al., *Membrane-bound Fas ligand only is essential for Fas-induced apoptosis.* Nature, 2009. **461**: p. 659.
434. Wang, H. and D.J. Mooney, *Biomaterial-assisted targeted modulation of immune cells in cancer treatment.* Nature Materials, 2018.

CHAPTER 3

Mesenchymal Stem Cells Derived Exosomes as Nanotherapeutics in Autoimmune Disorders

Abstract

More than 0.4 million people in U.S. are suffering from and Multiple Sclerosis (MS), which is an autoimmune disease targeting central nervous system (CNS). Mesenchymal stem cells (MSCs) are currently under investigation to treat MS, however, their therapeutic mechanism is not yet clear. To shed light on therapeutic mechanisms of transplanted stem cells and develop exosome-based nanotherapeutics in treating autoimmune diseases, we assessed the effect of exosomes secreted from human umbilical cord derived MSCs in treating MS using an experimental autoimmune encephalomyelitis (EAE) mouse model. We found that intravenous administration of MSC-derived exosomes i) reduced the mean clinical score of EAE mice compared to PBS control, ii) decreased neuroinflammation and infiltration of CD4+IFNγ (Th1) and CD4+IL-17+ (Th17) T cells into the CNS of EAE mice, and iv) upregulated the number of CD4+CD25+FoxP3+ regulatory T cells (Tregs) within the spinal cords of EAE mice. This observation suggested that MSC-derived exosomes exert their therapeutic efficacy, in part, through immunomodulation of T-lymphocytes. These results not only shed light on stem cell therapeutic mechanism, but also provide evidence that MSC-derived exosomes can potentially serve as cell-free therapies in creating a tolerogenic immune response to treat autoimmune disorders. Therefore, we further tested MSC-Exosome efficacy in mouse model of T1D.

Keywords: Autoimmunity; Multiple Sclerosis (MS); Type 1 Diabetes (T1D);

Mesenchymal Stem Cells (MSCs); Extracellular vesicles; Immunoengineering.

Introduction

Stem cells hold great promise for treating some of the most devastating diseases. MSCs are currently being investigated in over 730 clinical trials, including treating autoimmune diseases [1,2]. Unfortunately, preclinical studies and clinical trials using MSCs have produced mixed outcome, which in part is due to the incomplete understanding of their mechanisms of action (MOA) [2]. One particular puzzle in the MSC field is that following systemic transplantation, MSCs are quickly entrapped in the lung vasculature bed due to their big size with typically less than 1% of MSCs reach and engraft at the target sites [3], yet therapeutic effects are often observed [4-6]. Current paradigm attributes MSC's therapeutic functions mainly to paracrine factors [1,2]. We reasoned that extracellular vesicles (EVs) generated by transplanted cells in situ could be a mechanism by which stem cells contribute to tissue remodeling and regeneration in distant sites *in vivo* [7]. Indeed, several recent studies demonstrated EVs can modulate the immune system through multiple mechanisms [8-11] and MSC-derived EVs possess therapeutic functions [12-18].

To develop EVs as novel cell-free therapeutics and shed light on their potential roles in stem cell's effects *in vivo*, we evaluated exosomes released from MSCs (MSC-Exo) in treating devastating autoimmune diseases including multiple sclerosis (MS). MS is an inflammatory disease of the central nervous system (CNS) resulting in demyelination, neuronal injury and loss, and eventually neurological disability [19], [20], which currently is a significant burden on the healthcare system [21]. Specifically, therapeutic effects of exosomes derived from native MSC (Native-Exo) or MSC activated by IFNγ (IFNγ-Exo) in an experimental autoimmune encephalomyelitis (EAE) model [22] were evaluated and their main cellular and molecular

mechanisms were investigated. We found that systemic injection of IFNγ-Exo resulted in sustained clinical recovery with enhanced improvement in motor skills, reduction in neuroinflammation and reduced demyelination in EAE mice. In addition, we observed increased number of CD4+CD25+FOXP3+ regulatory T cells (Tregs) while reduced number of total macrophages/microglia and proinflammatory T cells within the spinal cords of IFNγ-Exo treated animals. Additionally, co-culture of IFNγ-Exo with activated PBMC cells reduced PBMC proliferation and levels of proinflammatory Th1 and Th17 cytokines including IL-6, IL-12p70, IL-17AF, and IL-22 yet increased level of immunosuppressive cytokine indoleamine 2,3-dioxygenase (IDO). IFNγ-Exo could also induce Tregs *in vitro* in murine splenocyte culture, likely mediated by a third-party accessory cell type.

Our findings from using MSC exosomes on MS treatment have led us to speculate their therapeutic effect on other autoimmune diseases including Type 1 Diabetes (T1D). Pathology of T1D has multiple aspects in common with MS. Type-1 diabetes (T1D) is an autoimmune disease in which the immune system attacks and destroys pancreatic β cells, therefore necessitating that patients receive insulin injections to regulate their blood glucose [23,24]. Around 3 million adults and children in the U.S. are estimated to suffer from T1D, and the number is anticipated to exceed 5 million by 2050. While the reasons behind T1D pathogenesis is not completely defined yet, its immunopathology is known to be the main aspect of the disease onset. Following by infiltration of CD11c+ dendritic cells and macrophages, pathogenic T cells infiltrate and could be detected around islets. Through further damage of the islets, self-antigen will release into the circulation, leading to disease progression. In Non Obese Diabetic (NOD) mice as well as peripheral blood of T1D patients, both major histocompatibility complexes (MHC) I and II restricted T cells that react with islet antigens have been identified. In most cases, these T cells

have been demonstrated to recognize islet autoantigens like those seen by autoantibodies (such as insulin, glutamic acid decarboxylase (GAD) and zinc transporter 8 (ZnT8)). There is convincing evidence that a variety of cytotoxicity-inducing molecules (for example, the TNFα, perforin, and granzyme B) are critical in pathogenesis of T1D mediated by both the CD4+ and CD8+ T cells [25]. The identification of IL-17-producing T helper 17 cells raised the possibility that this population (and the associated IL-23 cytokine) may be involved in the disease. Since our preliminary findings suggest that MSC exosomes have immunosuppressive effects on activated T cells, we further hypothesized that they could play suppressive role in a T1D model.

1. Materials & Methods

Isolation and characterization of MSC exosomes

To isolate exosomes, conditioned media from MSCs cultured for 3 days under IFNγ stimulation or native condition (without stimulation) went through serial ultracentrifugation and the exosome pellet was resuspended in phosphate-buffered saline (PBS) and kept at -80 °C before use. Isolated exosomes were re-suspended in PBS, mixed with 1X RIPA (Cell signaling technologies, USA) buffer and sonicated for five minutes, three times, with vortexing in between. Protein contents were measured using a BCA protein assay kit (Thermo Scientific Pierce, Rockford, IL, USA).

Volumes corresponding to 25 μg of protein from isolates were separated on a gradient precast polyacrylamide gel (Mini-PROTEAN®; Bio-Rad laboratories, Hercules, CA, USA). Samples were then transferred onto a nitrocellulose membrane which was then blocked with 5% Blotting Grade Blocker Non-Fat Dry Milk (Bio-Rad Laboratories) in Tris-buffer saline (TBS) for two hours. Membrane was then incubated with primary antibodies against Calnexin (1:1000; clone H-70; Santa Cruz Biotechnology, Santa Cruz, CA, USA), Galectin-1/LGALS1 (D608T)

Rabbit mAb (Cat# 12936), HSP70 (D69) Rabbit (Cat# 4876), TSG101 (1:1000; clone 4A10; Abcam, Cambridge, UK) and CD81 (1:800; clone H-121; Santa Cruz Biotechnology) dissolved in 0.25% Blotting Grade Blocker Non-Fat Dry Milk in TBS-Tween (TBST) overnight at 4 ºC, after which the membrane was washed with TBST for 10 minutes, three times.

EAE induction and progression

Female C57BL/6J mice, 6 to 8 weeks old, were purchased from Charles River laboratories Inc. (San Diego, USA). All animals were housed in pathogen-free conditions and treated according to the guidelines of the Animal Ethical Committee of University of California, Irvine. Mice were immunized with complete Freund adjuvant (IFA; Difco, Detroit, MI) containing 4 mg/mL Mycobacterium tuberculosis (strain H37Ra; Difco) and 200 μg MOG35-55 (AnaSpec, CA, USA).

To induce EAE, female C57BL/6J mice were immunized with complete Freund's adjuvant (CFA), MOG35-55, and pertussis toxin (Sigma-Aldrich)(injected 400 ng on days 0 and 2) and approximately 15-20 days later, mice displayed the peak of the disease showing complete paralysis of the tail and hind limbs with flattened posture. Native and IFNγ-MSC (1 million) and their respective exosomes (150 μg) were injected intravenously (iv) at the peak of the disease. Each mouse was graded blinded every other day and assigned a clinical score ranging from 0 to 4: No obvious changes in motor function compared to non-immunized mice (Score 0), tip of tail is limp (Score 0.5), limp tail (Score 1.0), limp tail and hind leg inhibition (Score 1.5), limp tail and weakness of hind legs (Score 2.0), limp tail and dragging of hind legs (Score 2.5), limp tail and complete paralysis of hind legs (Score 3.0), limp tail and complete paralysis of hind legs and partial front leg paralysis (Score 3.5), mouse is minimally moving around the cage and is minimally alert (Score 4.0). Mice were followed for at least 40 days following immunization.

Cytokine Secretion Analysis

Peripheral blood mononuclear cells (PBMCs) were isolated from buffy coats from healthy, anonymous blood donors (UCI institute for clinical and transitional science) by density gradient centrifugation (Ficoll-Pague plus, GE Healthcare). Cells activation was then conducted using DynaBeads® with 1:1 ratio, and some samples were co-cultured with exosomes. For Luminex assay, 50 µl of PBMC culture supernatants were collected and either frozen at -80 °C or immediately analyzed using a human custom ProcartaPlexTM (11plex, ThermoFisher Scientific, Vienna, Austria) with Luminex MAGPIX®. Results were then reported as Mean Fluorescence Intensity (MFI). To measure inflammatory cytokines in spinal cords, we harvested the supernatant after cell isolations of spinal cords. Supernatant solutions (100 µl) were then immediately kept in -80 °C and thawed immediately before performing the Luminex assay.

Flow cytometry

For flow cytometry experiments on T cells isolated from various organs, lymph nodes, spleen, and spinal cords of mice were removed and kept in ice cold RPMI supplemented with 10% heat inactivated FBS and 1% antibiotics. Cells were then collected by homogenization using cell strainer, which was then centrifuged at 500×g for 5 min, prior to RBC lysis with ACK buffer. Lymphocytes were then collected using Percoll® media density gradient centrifugation and subsequently stained for T cell subsets mentioned in the manuscript using the following antibodies: BV605 IL17 (CAT#: 506927), PE-IFNγ (CAT#: 505807), BV785 CD4 (CAT#: 317441), BV510 CD25 (CAT#: 302639), all purchased from Biolegend. Another wash step was performed before running the samples using a FACSAria (BD Bioscience) and data was analyzed using FlowJo Software (Tri Star, Ashland, OR, USA).

2. Results and Discussion

MSC exosomes improve functional outcomes in EAE

We first sought to examine MSC exosome's therapeutic effect in treating multiple sclerosis in a well-established EAE model. To induce EAE, female C57BL/6J mice were immunized with

complete Freund's adjuvant (CFA), MOG_{35-55} peptide, and pertussis toxin (injected on days 0 and 2) (**Fig. 3.1A**). Approximately 15-20 days later, mice displayed the peak of the disease showing complete paralysis of the tail and hind limbs with flattened posture. Each mouse was graded every other day and assigned a clinical score ranging from 0 to 4, where 0 represent healthy wild type (WT) and 4 represents dead mice. Exosomes derived from IFNγ activated MSCs (IFNγ-Exo) were infused intravenously (i.v.), as schematically shown in **Fig. 3.1A**. A dose of approximately 150 μg (or 1×10^9 particles, which was derived from 5-7 million MSCs) per mouse was used because a lower dose (30 μg) was shown to be less potent (**Fig. 3.1B**) and higher doses than 150 μg are impractical due to the inefficiencies in exosome preparation. While the focus of this study is exosome, native and IFNγ stimulated MSCs (1 million) were also included as control groups as we aim to compare exosome's efficacy to MSCs'. A single injection of IFNγ-Exo (n=6) at the peak of the disease (Day 18) resulted in a mean clinical score of 1.2 ± 0.3 at day 40, which is a significant improvement ($p < 0.001$) compared with PBS control (n=6) (mean clinical score of 2.9 ± 0.6) (**Fig. 3.1B**). Native-Exo (n=6) also ameliorated the disease but to a lesser extent than IFNγ-Exo with the mean clinical score of 2.2 ± 0.5 ($p < 0.05$). Comparison of exosomes with their MSC counterparts showed similar efficacy in EAE model. IFNγ treated MSCs (N=6) showed comparable clinical scores (1.5 ± 0.6; *n.s.*) to that of IFNγ-Exo (1.2 ± 0.3). Similarly, native MSCs (n=6) displayed comparable clinical scores (2.1 ± 0.4; *n.s.*) compared to Native-Exo (2.2 ± 0.5). We acknowledge that due to their small size and the enrichment steps, we are able to administer higher dosages of exosomes (based on the number of MSCs from which they were derived) compared to the MSC controls in this set of studies, demonstrating an advantage of exosome-based therapeutics. Despite the dosage

difference, the comparability in efficacy between MSCs and their exosomes suggests that exosomes could be considered as a surrogate treatment to the cell therapy.

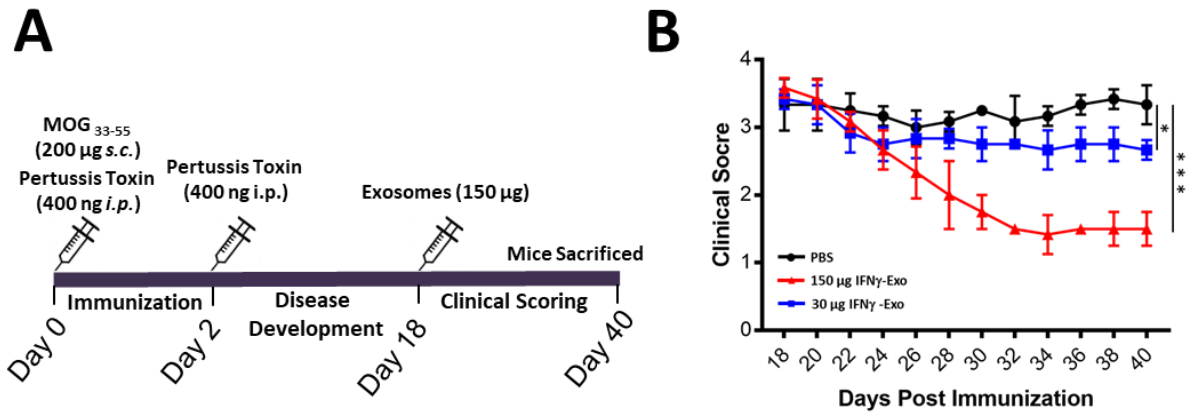

Figure 3.13. MSC-Exo improve clinical scores in EAE mice. A) Schematic representation of procedure to induce EAE and treatments (exosomes or MSCs) that mice received at day 18 followed by clinical scoring till day 40. Two different doses of **B)** Two doses of B) Two doses of exosomes were used to analyze the clinical efficacy and results compared against the PBS control. Mann-Whitney t-tests were used to determine the p values. (*$p < 0.05$; ***$p < 0.001$) [26].

Reduction of infiltrating CD4+ T cells into spinal cords and upregulation of Tregs

T-cell infiltration into the CNS is another hallmark of neuroinflammation, particularly in MS. Therefore, we also assessed the T-cell infiltration into the spinal cord of EAE mice using flow cytometry. For this set of experiments, whole spinal cords from each animal were excised and strained to harvest the cells. As shown in **Figures 3.2A, B,** and **C** significant reduction in the number of infiltrated CD4+ (n=3; 77.3 ± 24 cells per spinal cord; $p < 0.01$) into the spinal cords of IFNγ-Exo treated mice was observed compared to PBS control (n=3; 263.3 ± 38.1 cells per spinal cord). IFNγ-Exo exhibited a superior effect in reducing the number of infiltrated CD4+ compared to Native-Exo group (77.3 ± 24 vs 165.3 ± 12.5 cells per spinal cord; $p < 0.01$). Moreover, infiltration of the CD8+ cells was also dramatically reduced in IFNγ-Exo group (n=3) compared to PBS (n=3) control (44 ± 11.5 vs 260 ± 129 cells per spinal cord; $p < 0.05$) (Fig. 2E). In this case, Native-Exo group (n=3) exhibited a comparable effect (46 ± 7.5 cells per spinal

cord) in CD8+ cell reduction into spinal cords compared to the IFNγ-Exo group. The number of infiltrated CD4+ and CD8+ in the WT animals was almost undetectable.

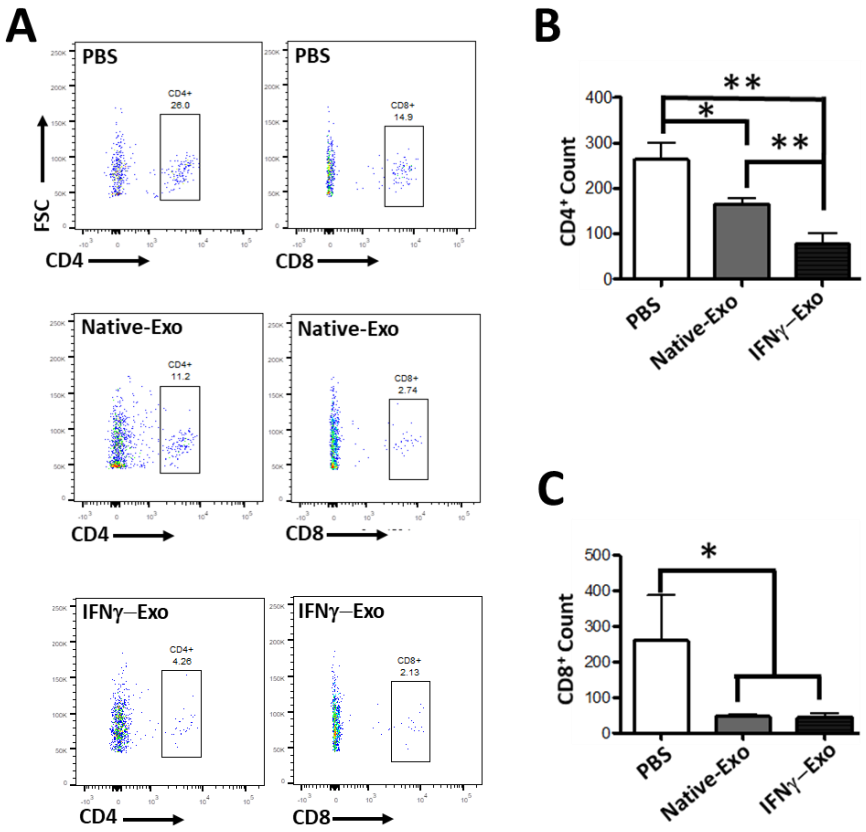

Figure 3.14. MSC exosomes treated mice showed reduced number of infiltrated T cells in spinal cords of EAE mice. A) Representative flow cytometry plots of CD4+ and CD8+ T cells within spinal cords. **B, C)** Flow cytometry quantification of spinal cords stained for infiltrated $CD4^+$ and $CD8^+$ T-cells, respectively. Unpaired t tests were used to determine p values (n=3; *$p < 0.05$; **$p < 0.01$) [26].

Recent evidences have suggested several proinflammatory T cell subsets including Th1 and particularly Th17 cells are key drivers in EAE [27,28]. We thus sought to characterize potential effect of our exosomes on Th1 and Th17 responses in the spinal cord. Flow cytometry analyses of mouse spinal cord cells showed that while the percentage of CD4+IFNγ+ T cells (Th1) (n=3, from 0.38±0.25% in PBS treated to 0.13 ± 0.12% in IFNγ-Exo treated) and CD4+IL-17+ T cells

(Th17) (n=3, from 0.52±0.4% in PBS treated to 0.14± 0.09% in IFNγ-Exo treated) decrease in the IFNγ-Exo treated mice, the difference was not significant (**Figure 3.3A, B**).

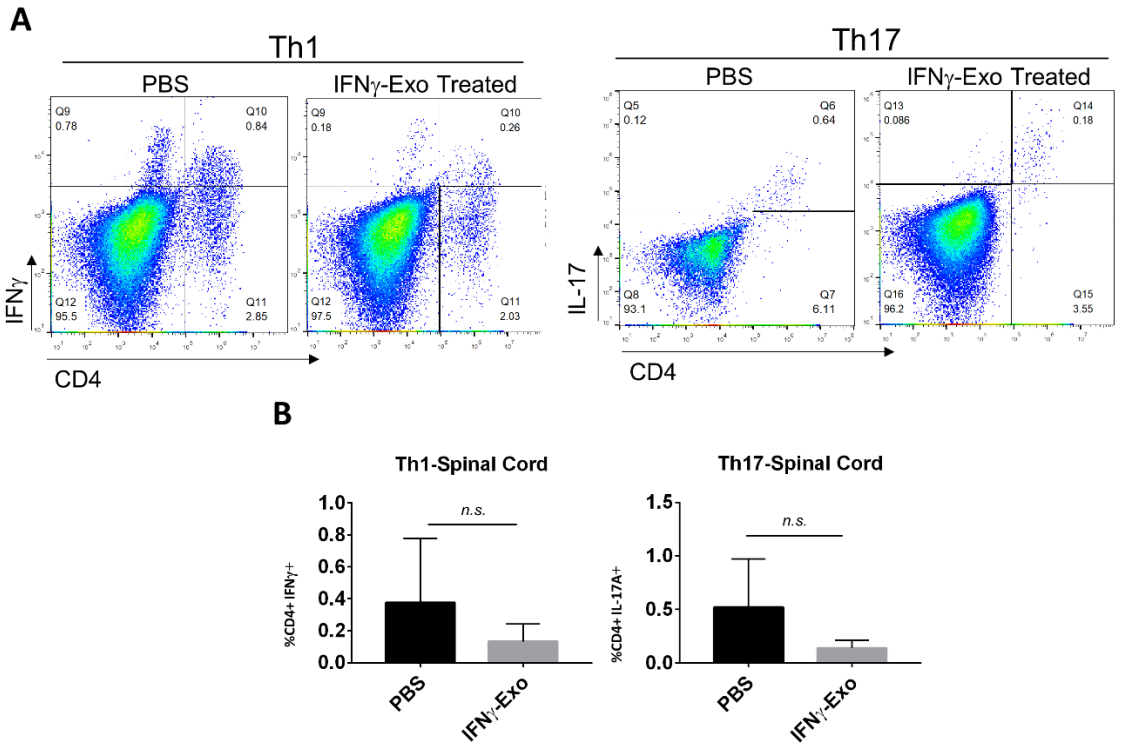

Figure 3.15. A) Representative flow cytometry plots and their quantification for spinal cords of PBS (n=3) and IFNγ-Exo (n=3) treated EAE mice, gated for CD4+IFNγ+ and CD4+IL-17A+ as representatives of Th1 and Th17, respectively. **B)** Plots are quantified for Th1/Th17. Unpaired t-tests were used to determine *p* values. (**p* < 0.05; ***p* < 0.01) [26].

In our initial study, we chose to inject exosomes on Day 18 post immunization, which is the peak of the disease and therefore represents an established disease stage. We reason that if MSC-derived exosomes work by suppressing the pro-inflammatory cells and cytokines, we might need to intervene at an earlier timepoint during the inflammatory induction phase in order to produce optimal therapeutic outcome. Indeed, it has been known that inflammatory T cells infiltrate the CNS and mediate inflammation prior to the onset of clinical symptoms of EAE[29-31]. Moreover, we hypothesize that increasing the number of exosome injections could further attenuate inflammation. While systematically optimizing treatment timing and number of injections is beyond the scope of the present work, we performed a pilot study where we

transplanted two doses of MSC-derived exosomes at earlier timepoints on day 12 and 14 post immunization (**Figure 3.4A**), which is known to be during the T cell inflammatory induction phase[30]. While it exhibited comparable treatment efficacy with respect to clinical score reduction (**Figure 3.4B**) and similar trends of total CD4+ T cell reduction and Treg increase in the spinal cord compared to the previous regimen of single injection on day 18, intervention with multiple injections at earlier timepoints showed a significant reduction of the Th17 cells (**Fig. 3.5A, B**). Th17 cells have recently been demonstrated to be a key player in EAE [27,28]. This data warrants future work to continue to optimize treatment timing and number of injections so we can better understand the evolving molecular and cellular heterogeneity as the disease progresses and eventually stratify patients and treatment regimens to achieve desirable outcomes [32].

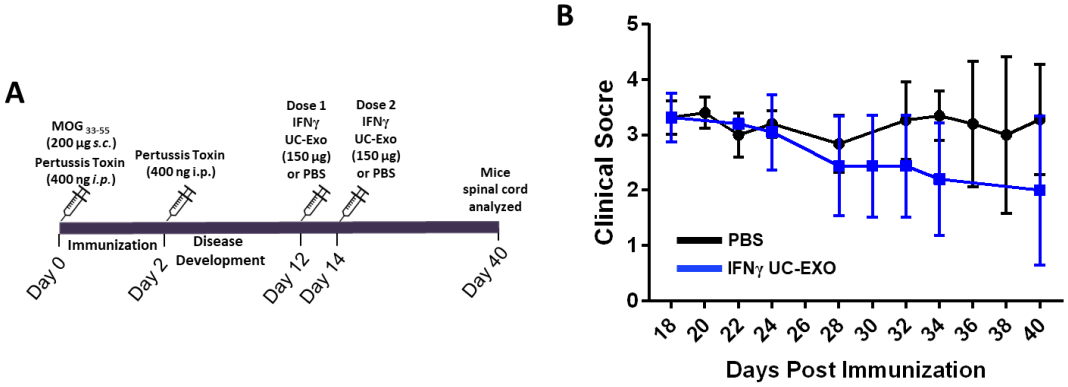

Figure 3.16. A) Schematic representation of early intervention procedure to treat EAE mice. IFNγ activated UC-MSC derived Exosomes (IFNγ-Exo) or PBS were injected i.v. to mice at days 12 and 14 (before disease peak). **B)** Clinical scoring was conducted from day 18 till day 40 after immunization [26].

In our previous study [26], we found that injected exosomes infiltrate into spleen and spinal cord within hours of injection. We therefore reasoned that within days after exosome injection, exosomes should have affected the immunopathology of the EAE mice.

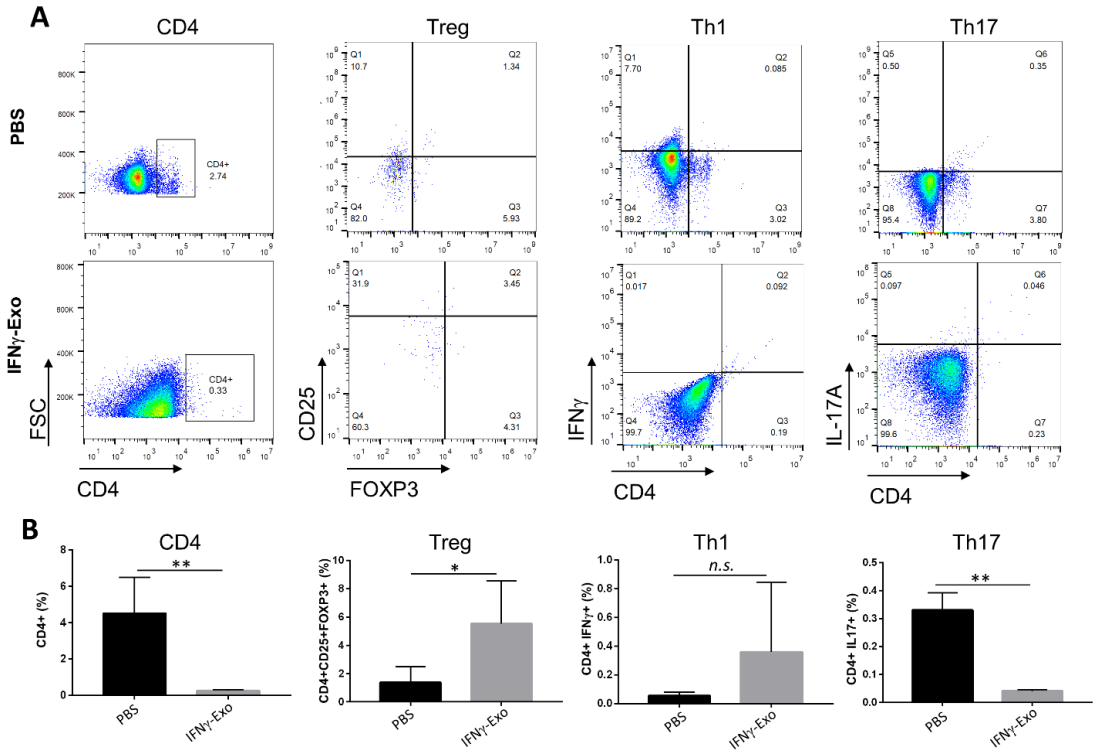

Figure 3.5. A**)** Representative flow cytometry plots and their quantification for spinal cords of PBS (n=3) and IFNγ-Exo (n=3) treated mice, gated for CD4, Th1, Th17, and Treg, and B) their corresponding quantifications. Unpaired t-tests were used to determine p values. (*$p < 0.05$; **$p < 0.01$) [26].

IFNγ-Exo Influences the immunopathology of EAE

To further understand the MoA of exosomes therapy, we attempted to understand the immune pathology of treated EAE mice. We particularly focused on the Treg/Th1/Th17 axis in circulation (blood), lymphoid organs (spleen and lymph nodes) and spinal cords. We chose to study T cells subsets in these organs as several studies have demonstrated the key role of Th1/Th17/Treg axis in these organs for the occurrence of MS pathology [33-35]. **Figure 3.6** describes some of the events that lead to pathogenesis of MS. Upon establishment of the central tolerance in the thymus, autoreactive T cells are eliminated prior to entry into the periphery. In case some autoreactive cells escape the central tolerance, then the peripheral tolerance controls the possible autoreactivity. If the peripheral tolerance malfunctions (e.g. through reduction in the presence or function of Tregs), autoreactive T cells could be activated in the periphery and

polarize into effector T cells. Such issues with the tolerance as well as genetic and environmental factors including pathogens and some constituents contribute to the immune response. Once entered into the blood stream, Th1, Th17, CD8+, B cells, and innate immune cells infiltrate into the central nervous system (CNS), leading to neuronal damage and MS pathology. Upon entrance into the CNS, CD4+ T cells get re-activated by antigen presenting cells and secreting IFNγ (by Th1 cells) and IL17 (by Th17 cells), leading to the recruitment of monocytes into the CNS and exacerbating inflammatory response. Inflammation further escalates by CD4+ T cells through epitope spreading. Main pathogenic T cells that are differentiated in the CNS are Th1 and Th17 cells, skewing away the differentiation of T cells into Th2.

Currently, some treatments have received clinical approvals. For instance, multiple IFNβ-based therapies have been approved to treat relapsing forms of MS. While its MoA is not yet fully understood, some investigations have reported that IFNβ inhibits cell infiltration to the CNS, interferes with antigen presentation, and modulate the Th17 response [28,33,36]. Simplistically, MS starts with the infiltration of autoreactive T cells into the CNS, promoting local inflammation and differentiation of Th1/Th17 cells that damage the CNS, which then causes symptomatic MS including the loss of motor function. Better understanding of the immune-pathology of MS has led a general move toward early treatment and many multicenter studies are planning to compare early intensive treatment rather than conventional later stage treatments [37].

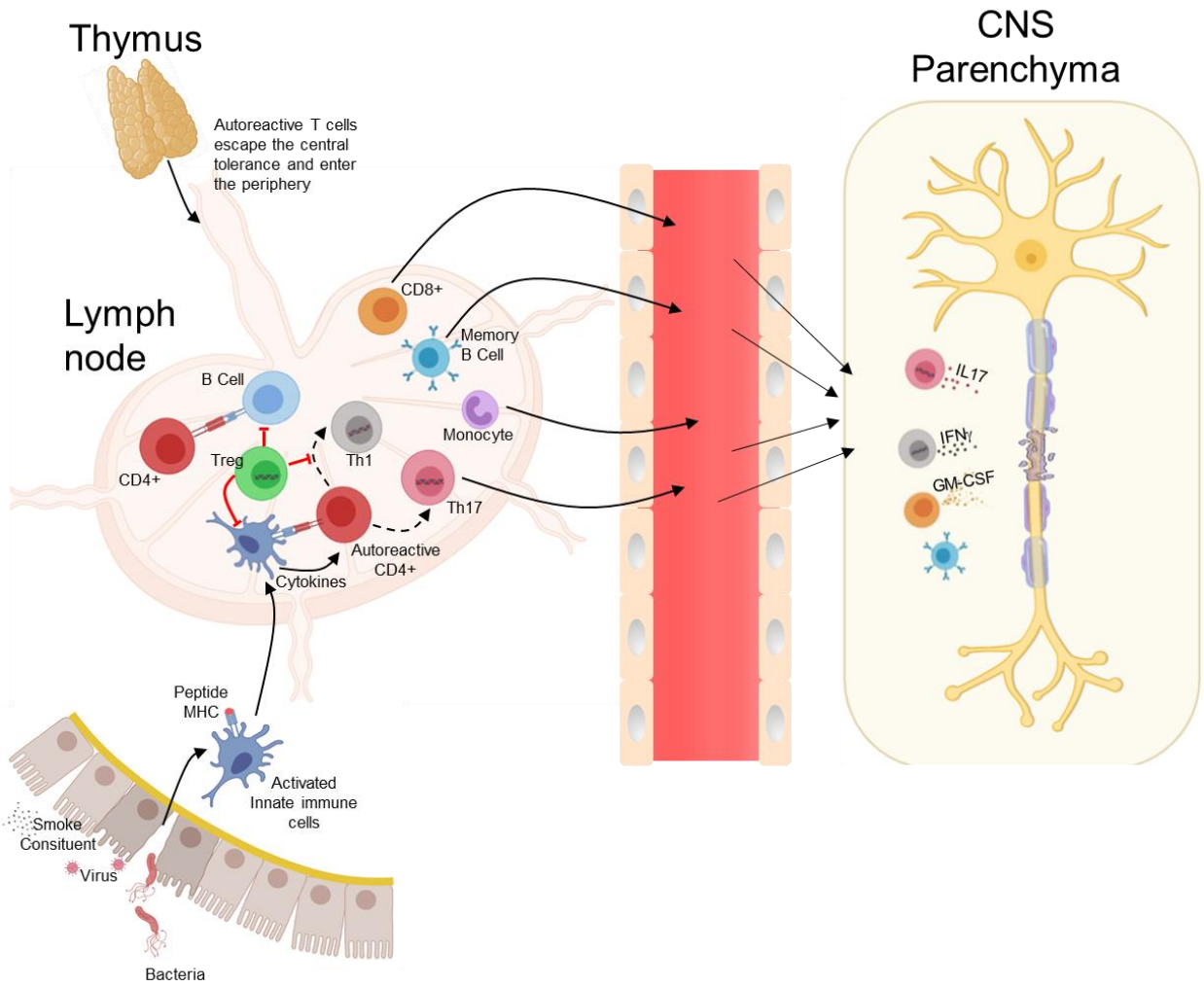

Figure 3.6. Brief Summary on Immune Response in Multiple Sclerosis (MS). In the thymus, autoreactive T cells are eliminated in the establishment of central tolerance. If some autoreactive cells escape, then the peripheral tolerance controls autoreactivity. If such tolerance malfunctions (e.g. through reduction in the presence or function of Tregs), autoreactive T cells could be activated in the periphery and polarize into effector T cells. In the case of MS, issues with the tolerance as well as genetic and environmental factors including pathogens and some constituents contribute to the immune response. Once entered the blood stream, Th1, Th17, CD8+, B cells, and innate immune cells infiltrate into the central nervous system (CNS), leading to neuronal damage and MS pathology.

In line with this trend, we speculated whether MSC-exosome administration could prevent/reduce the T cells activation and infiltration into the CNS. Thus, we chose to conduct an early intervention treatment, where MSC exosomes were injected prior to the severe paralysis of EAE mice, and when the T cells infiltration into the CNS are still in progress. We next immune-profiled T cells subsets that are important in MS pathology an investigated the MSC exosomes efficacy in T cells activation and infiltration.

Due to the immunopathological events occurred in the first 2 weeks of EAE induction, we further attempted to characterize the regulatory vs. pathological T cells in mice relevant organs including blood, spleen, lymph node, and spinal cord 2 days after the early intervention (**Figure 3.7A**).

Figure 3.7B shows that the population of CD4+ T cells in the IFNγ-Exo significantly upregulated in the mice blood (p = 0.0014) and CD8+ cells also upregulated, although not statistically significant (p = 0.0813). Like our observations when spinal cord T cells were analyzed at day 40, there was a significant reduction in CD4+ and CD8+ T cells population within the spinal cords of IFNγ-Exo treated EAE mice compared to PBS controls (**Figure 3.7C**). No difference was found for spleen and lymph nodes T cells population (**Figures 3.7D, E**). We next sought to analyze the sub-populations of T cells within the analyzed organs **(Figure 3.7A**).

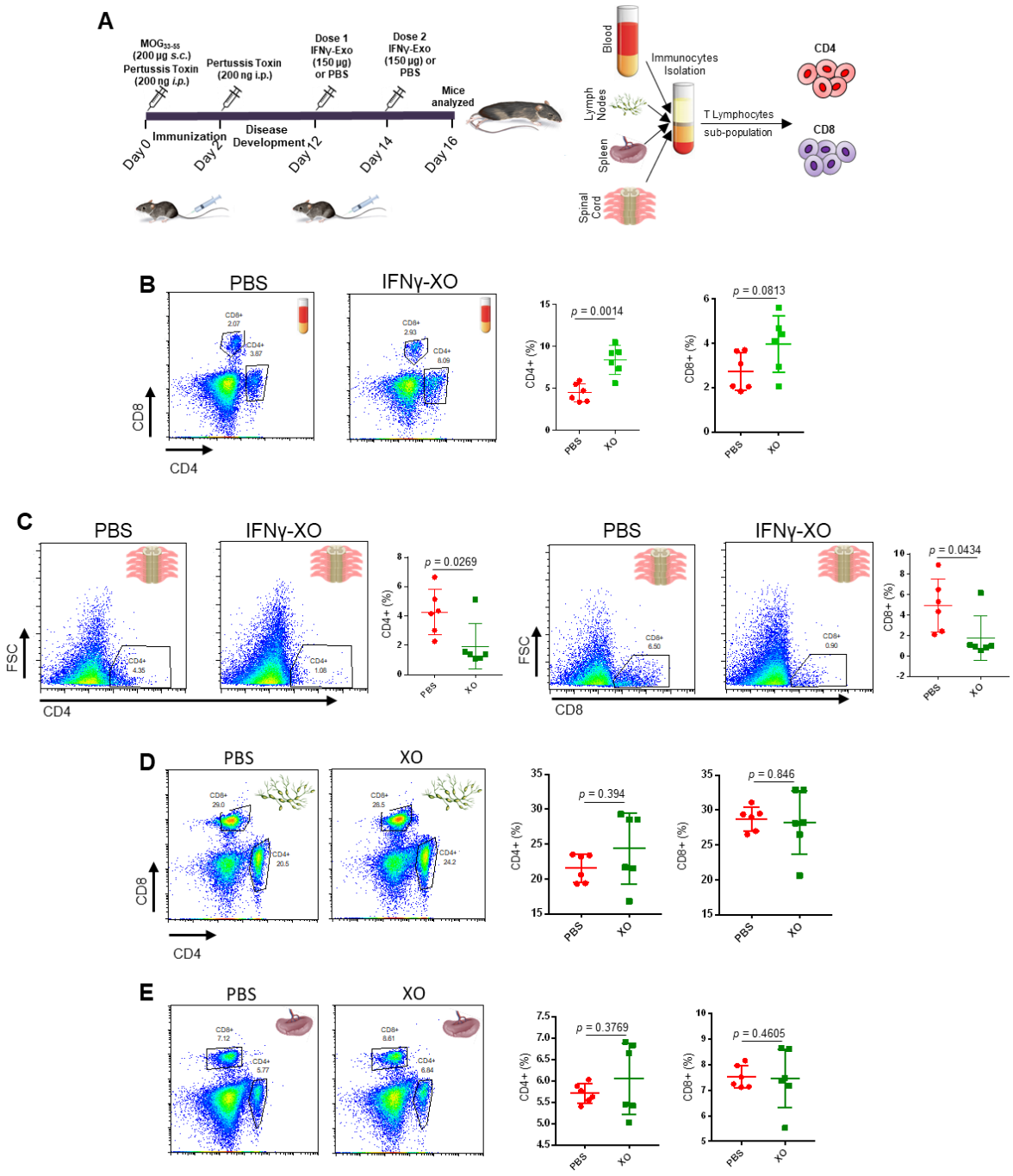

Figure 3.7. Effect of early intervention on the Multiple Sclerosis immunopathology of EAE mouse model. A) Schematic representation of early intervention procedure to treat EAE mice. IFNγ activated UC-MSC derived Exosomes (IFNγ-Exo) or PBS were injected i.v. to mice at days 12 and 14 (before disease peak, n=3 for each group). Bloods, Lymph Nodes, Spleens, and Spinal Cords were collected from both mice groups, immunocytes were isolated, and CD4+ or CD8+ T ;ymphocytes were quantified using flow cytometry. B) The population of CD4+ Lymphocytes significantly upregulated in the mice blood (p = 0.0014) and CD8+ cells also upregulated, although not statistically significant (p = 0.0813). C) Both CD4+ and CD8+ T lymphocytes were downregulated within mice spinal cords (p = 0.0269 and p= 0.0434, respectively). D,

E) In the lymph nodes and spleens, there were no significant difference between CD4 or CD8 population between PBS or IFNγ-Exo treated mice.

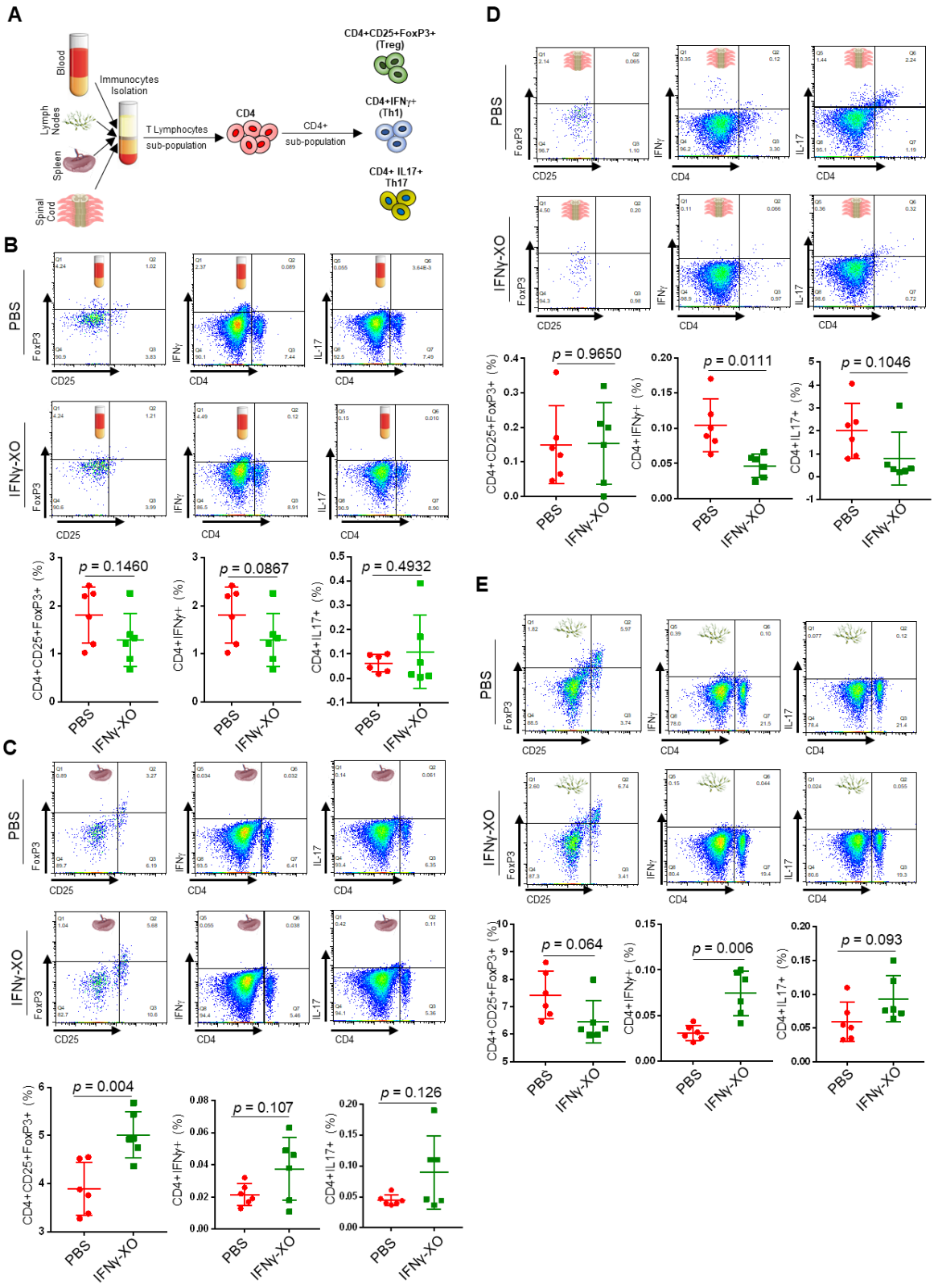

Figure 3.8. The effect of early intervention on Treg, Th1, and Th17 subpopulations in bloods, spleens, lymph nodes, and spinal cords of EAE mouse model. A) Schematic representation of T cells sub-population that were analyzed to quantify

the immunosuppressive effects of IFNγ-Exo on EAE mice. Results were compared against PBS control. B) Analysis of blood revealed no difference between T cells subtypes. C) While the Th1 and Th17 subpopulations in the spleen of mice injected with PBS or IFNγ-Exo were not different, CD4+CD25+FoxP3+ Tregs were upregulated in the spleens of IFNγ-Exo injected mice (p = 0.004). D) Th1 cells within the spinal cord reduce in the IFNγ-Exo injected group (p = 0.011), while Th17 cells show slight reduction (p = 0.1046). E) In the lymph nodes of IFNγ-Exo injected mice, there were slightly fewer Tregs (p = 0.064), more Th1 (p = 0.006) and Th17 (p = 0.093) cells.

Analysis of T lymphocytes sub-populations in the blood revealed no difference between PBS or of IFNγ-Exo treated EAE mice (**Figure 3.8B**). While the Th1 and Th17 subpopulations in the spleen of mice injected with PBS or IFNγ-Exo were not different, **Figure 3.8C** demonstrates that CD4+CD25+FoxP3+ Tregs were upregulated in the spleens of IFNγ-Exo injected mice (p = 0.004). Due to the biodistribution of exosomes into the spleens after i.v. injection (**Figure 3.9**), it could be concluded that exosomes localize to spleens, where they could induce or recruit Tregs. Recent evidences have suggested several proinflammatory T cell subsets including Th1 and particularly Th17 cells are key drivers in EAE [27,28]. We thus sought to characterize potential effect of our IFNγ-Exo on Th1 and Th17 responses in the spinal cord (**Figure 3.8D**). Th1 cells within the spinal cord reduce in the IFNγ-Exo injected group (p = 0.011), while Th17 cells show slight reduction (p = 0.1046). Lastly, in the lymph nodes of IFNγ-Exo injected mice, there were slightly fewer Tregs (p = 0.064), more Th1 (p = 0.006) and Th17 (p = 0.093) cells (**Figure 3.8E**). It should be noted that reduction of Th1 and Th17 in the lymph nodes of mice treated with IVIg has been reported to be linked to the therapeutic efficacy [35]. However, such results have been reported in the 9th day of EAE development. The IVIg was given from the day 0 (disease induction) till day 9, as opposed to our analysis which was conducted on day 16 [35]. Such time-point differences may partly explain the absence of Th1 and Th17 cells in the lymph nodes in our study.

To further reveal mechanisms underlying exosome-mediated effect in neurologic function in EAE, we next investigated the fate and biodistribution of administered exosomes. In

this set of experiments, Native-Exo was labeled with DiR, a lipophilic dye that is commonly used for in vivo and ex vivo imaging.[38] DiR itself was also included as a negative control. EAE and healthy mice were administered with the same number of DiR-exosomes as we did for previous treatment studies. For each experimental group, the mice were sacrificed at 24 h after the exosome injection and freshly dissected tissues were analyzed immediately for the fluorescence signal using IVIS imaging system. Exosomes were mostly found in the liver and spleen of healthy and EAE mice (**Figure 3.9A**).

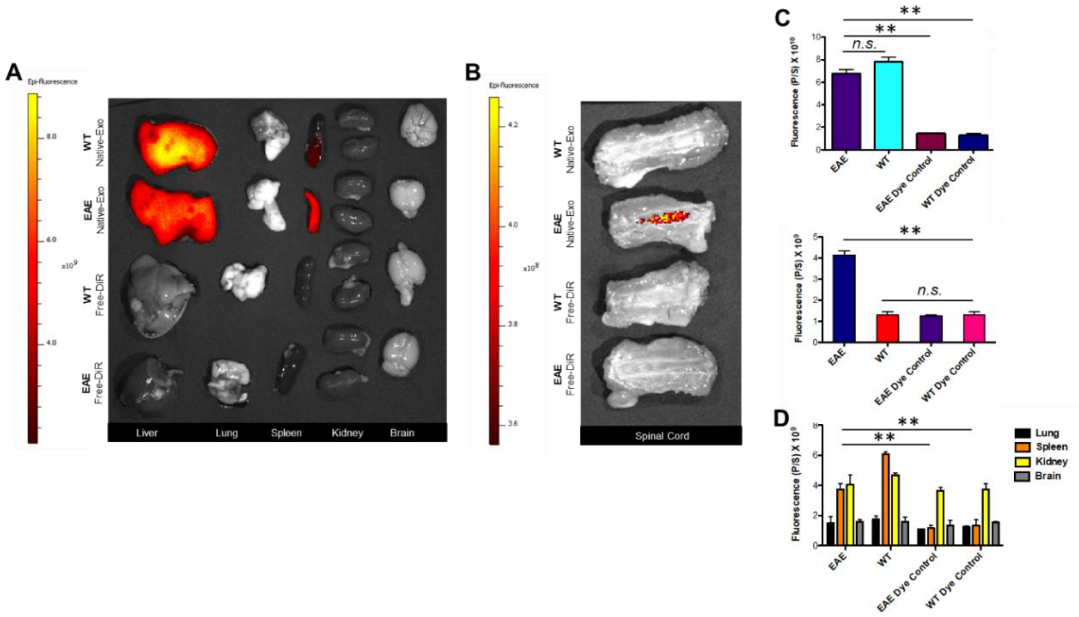

Figure 3.17. Biodistribution of Native-Exo in vivo. A) Representative IVIS images of different organs harvested at 3 hours following i.v. infusion of DiR labeled Native-Exo into healthy and EAE mice. Control groups received DiR dye alone (EAE-DiR, WT-DiR) to determine the background. B) Representative IVIS images of spinal cords 3 hours post injection of DiR labeled Native-Exo. C, D) Quantification of the fluorescent signal in different organs including liver, spleen, kidney, brain and lung at 3 hours following infusion of DiR labeled Native-Exo. (n=3; **p < 0.01). E) Quantification of the fluorescent signal in spinal cords at 3 hours post injection of DiR labeled Native-Exo. (n=3; *p < 0.05; **p < 0.01). Unpaired t-tests were used to determine p values.

It is also worthwhile to note that little signal was observed in lungs of exosome-treated animals, suggesting that exosomes, unlike MSCs, can bypass small lung vasculature bed owing to their

small size. Importantly, dye labeled IFNγ-Exo was observed in spinal cords of EAE, but not healthy animals, at 3 h following administration (**Figure 3.9B, C, D**),

IFNγ-Exo suppress T cell proliferation in vitro.

As we mentioned above, T cells play a central role in both mediating and regulating MS pathophysiology, and efforts to develop therapeutic strategies for MS have often focused on understanding factors that mediate T cell function[36]. As we observed a reduction of neuroinflammation and an induction of tolerance in exosome-treated EAE mice *in vivo*, we next sought to further confirm exosome-mediated immunomodulatory effects *in vitro*. To examine if MSC exosomes suppress T-cell activation *ex vivo*, carboxyfluorescein succinimidyl ester (CFSE)-labeled human peripheral blood mononuclear cells (PBMCs) were activated with anti-CD3/CD28 Dyna® beads (1:1 ratio) and further cultured with or without IFNγ-Exo and Native-Exo. Both Native-Exo and IFNγ-Exo suppressed activation of the gated T cells, with IFNγ-Exo being considerably more suppressive (**Figure 3.10**). These results are consistent with previous reports where the ability of MSC-derived exosomes to suppress T cell activation and proliferation was evaluated [12,15,16]. It is well established that MSC can suppress PBMC activation and proliferation in cocultures mainly through secreted immunomodulatory or immunosuppressive cytokines including IDO, IL-10, PGE2, TSG6, and TGFβ [1,2,39,40]. We further sought to understand the underlying pathways responsible for the effect of exosomes on the PBMC proliferation. Interestingly, IDO level in the PBMC coculture was significantly increased in the presence of IFNγ-Exo. IDO is an immunosuppressive enzyme that enhances the catabolism of tryptophan to kynurenine; both depletion of tryptophan and accumulation of the toxic kynurenine are known to inhibit T cell proliferation [41]. As Th1 and Th17 cells play

important roles in the pathology of autoimmune disorders including MS/EAE[27,28], to further probe the MOA of MSC-derived exosomes in suppressing T cell induction to Th1/Th17 subtypes, we analyzed several key representative Th1 and Th17 cytokines in this MSC exosome/PBMC coculture experiment. We found that in the presence of MSC-derived exosomes, the levels of several proinflammatory Th1 and Th17 cytokines including notably IL-6 (Th17 cytokine), IL-12p70 (Th1), IL-17AF (Th17), IL-22 (Th17) were significantly reduced (**Figure 3.10**) and IFNγ (Th1) and TNFα (Th1) demonstrating a trend of decrease though not significant (**Figure 3.11**).

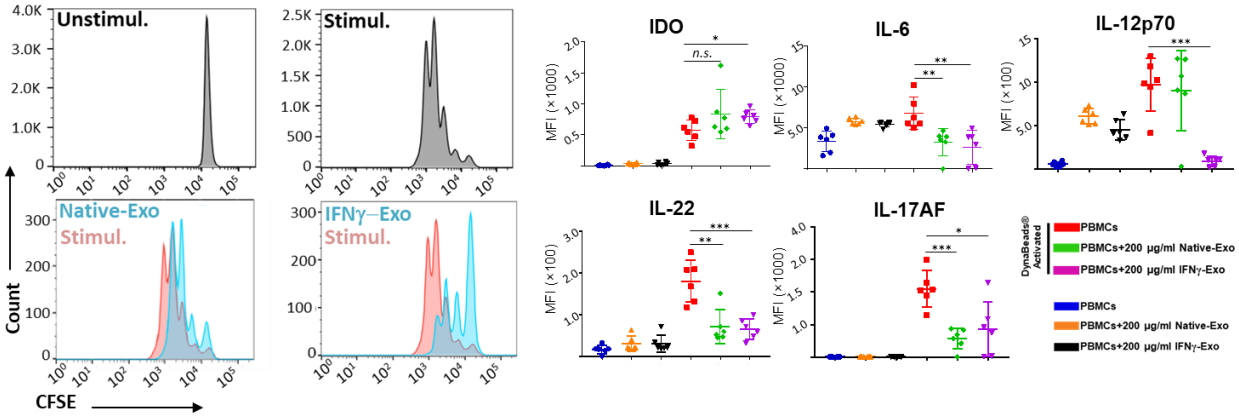

Figure 3.18. MSC-derived exosomes have immunosuppressive effects and induce Tregs *in vitro*. A) Human PBMCs were labeled with CFSE and stimulated for 4 d with Dyna® beads, in the absence or presence of exosomes produced by native or IFNγ-stimulated MSC. B) Addition of the MSC-derived exosomes to the PBMCs culture enhances the secretion of Indoleamine 2,3-dioxygenase (IDO), while reduces the secretion of IL-17AF, IL-22, IL-12p70, and IL-6 compared to activated PBMCs [26].

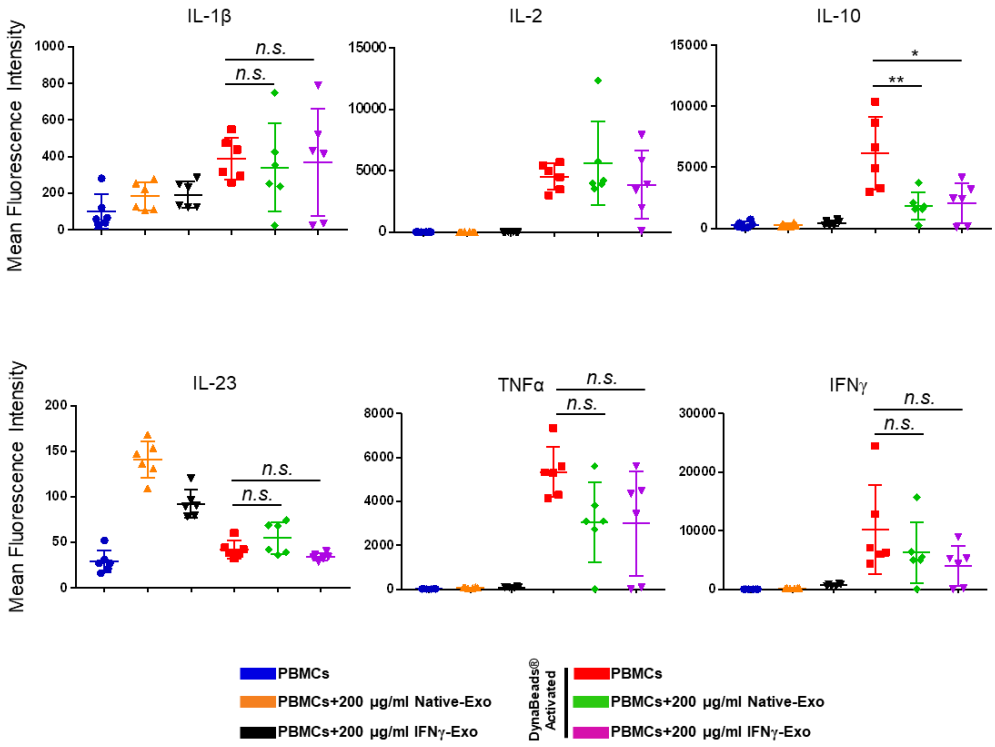

Figure 3.19. Human PBMCs stimulated for 4 d with Dyna® beads, in the absence or presence of exosomes produced by native or IFNγ-stimulated MSCs. Supernatants were harvested and secreted cytokine analyzed using Luminex MAGPIX™. Unpaired t-tests were used to determine *p* values. (*$p < 0.05$; **$p < 0.01$; ***$p<0.001$) [26].

Collectively, these data support the notion that MSC-derived exosomes can ameliorate EAE through, at least partly, by suppressing pathological T cell subset activation. This observation suggests that immunoregulatory effects of MSC derived exosomes could be further investigated in other autoimmune disorders.

Insights into the possible molecular mechanisms of exosome therapy

In our study, we found that a number of mRNAs are loaded by cells into exosomes which can potentially subsequently be delivered and translated into proteins in recipient cells. In particular, we previously found in our RNAseq analysis that IFNγ-Exo are highly enriched in several mRNAs with anti-inflammatory properties compared to Native-Exo [26]. Of particular

importance, for example, is IDO that has been widely demonstrated as a key player in MSC-mediated immunomodulation [42,43] and in the down-modulation of neuroinflammation in EAE [44,45]. Specifically, for any one million RNAs in our exosome preparation, there are 0 IDO transcripts in Native-Exo and approximately ~48 IDO transcripts in the IFNγ-Exo. We further demonstrated using RT-PCR that IDO mRNAs are present in full-length (**Figure 3.12A**). Together with our observation of increased IDO protein level in PBMC coculture with IFNγ-Exo, these evidences further support that the observed MSC-derived exosome's suppressive effect on PBMC proliferation could potentially be mediated, at least in part, by the transferred exosome IDO mRNA cargo to recipient PBMCs which are then translated and secreted into the medium. Finally, it should be noted that we found the presence of IFNγ in the exosomal preparations (**Figure 3.12B**). It is strongly recommended that upon addition of reagents or cytokines to the MSC cultures, exosomes collected from these media to be washed multiple times to remove the extra additives.

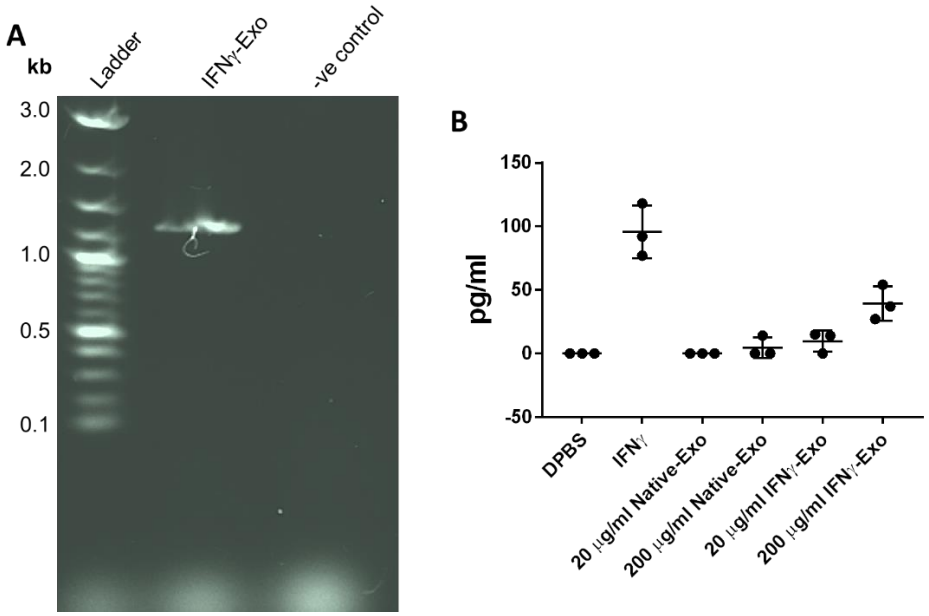

Figure 3.20. A) RT-PCR assay showed the presence of IDO1 mRNA within IFNγ-Exo. Resultant RT-PCR amplicons are approximately 1.2 kb, which is the size of full-length IDO-1 mRNA. B) ELISA assay was conducted to measure the residual IFNγ from the culture medium to the IFNγ-Exo [26].

This study facilitates the understanding of potential mechanisms by which MSCs exert therapeutic function. In the context of cell therapy, the majority of i.v.-infused MSCs get entrapped in filter organs without significantly homing to sites of injury, and yet they frequently exhibit therapeutic activity in numerous animal models [2]. The mechanisms to this puzzling phenomenon remain unclear. Our unpublished data showed that lung entrapped MSCs under physical and mechanical stresses could shed small vesicles to the circulation that could reach distant organs. Recent evidences suggest infused MSCs and their apoptotic products can be phagocytosed, which led to the generation of third-party phagocytes that ultimately mediate the observed immunomodulatory effects [4-6,46] The fact that MSC-derived exosomes can recapitulate MSC's efficacy in our EAE model and that their effects on T cells are mediated at least partly by third-party cells (e.g. macrophage) implies that transplanted MSCs could mediate their efficacy in vivo through secreted EVs, likely by first interfacing with APCs and phagocytes.[7,13,47-50]

Our data demonstrate that exosomes derived from IFNγ activated MSCs 1) suppress PBMC cell proliferation (likely through IDO), reduce proinflammatory cytokines and enhance induction of Tregs in vitro, 2) are distributed to the inflamed, but not healthy, spinal cords, reduce neuroinflammation and demyelination and improve functional outcomes in chronic EAE murine model. This study asserts that stem cell-derived exosomes can represent a viable approach to treat autoimmune and neurodegenerative disorders, which remains major unmet clinical needs. There are several potential advantages for the exploitation of exosomes as therapeutics and as vehicles for therapeutic delivery, compared to cells and conventional drug delivery systems (e.g., liposomes and nanoparticles): 1) the smaller size of exosomes allows reduced entrapment in small capillaries following systemic infusion, and potentially improves the therapeutic delivery to the diseased sites, 2) exosomes are expected to have significantly

longer shelf life, lower side-effects and other risks compared to cells because of their acellular status, 3) exosomes possess a complex mixture of factors targeting different therapeutic pathways and synergize to enhance therapeutic function compared to using individual factors, and 4) the natural cell origin of exosomes enhances our ability to genetically modify the cell of origin to produce exosomes with overexpressed agents for improved efficacy, biocompatibility and reduced immunogenicity.

We demonstrated that MSC exosomes showed potential to induce a tolerogenic immune response and therefore a sustained clinical recovery. Moreover, further MOA investigation on the reduction of Th17 cells and their associated proinflammatory cytokines can lead to development of exosome therapeutics that target disease pathways such as Th17 cytokines for patients who are refractory to the current treatment [27]. We demonstrated MSC-derived exosomes host a mixture of proteins and RNAs, some of which are implicated in anti-inflammatory, antigen presenting, or neuronal protection pathways. Future work will investigate individual markers (e.g. IDO) and dissect the cellular and molecular mechanisms to identify a panel of molecular markers that are responsible for exosome's therapeutic effect. This effort will allow us to 1) optimize exosome manufacturing and preparation processes to standardize potential batch-to-batch variations and develop quality control (QC) and release assays for clinical applications [51], and 2) engineer exosomes to overexpress selected candidates in the future to improve their efficacy [7,52]. Future work will also optimize treatment timing, especially at the onset of the disease, which might be more effective in attenuate inflammatory responses during the induction phase. It will also be interesting to further characterize how doses and number of injections affect outcomes, especially considering that increased doses in the MSC field have resulted in mixed outcomes,[53] presumably due to the host immune responses (e.g. antibodies) that were raised to

attenuate the therapy [54]. Intravenous infusion was chosen as administration route in this study due to its minimal invasiveness and convenience, however, other routes such as local injection of exosome [15] to inflamed spinal cords would be an interesting approach to explore in the future work to optimize their therapeutic outcome.

MSC Exosome therapy to prevent or delay the onset of Type 1 Diabetes

At least 24 million people in the United States are affected by autoimmune diseases, with $100 billion annual direct cost on health care. Type 1 Diabetes (T1D) for example, corresponds to more than 1.3 million individuals in the United States and expected to rise to 5 million people by 2050 [55]. Initial enthusiasm for treatment of T1D through islet transplantation via Edmonton Protocol was later subsided by a report from a multicenter clinical trial. Results from this worldwide study indicated that 16 of 44 patients with islet transplant became insulin-free for 1 year, and 10 patients experienced complete graft loss. Notably, although the short-term survival of the grafts is up to 80%, less than 20% of the grafted patients remain insulin-independent by 5 years [56]. These reports as well as the understanding of immune cells involvement against endogenous or exogenous islets led us to seek for therapies based on reprogramming patients' immune cells. Among myriad of immune cells, the role of macrophages in T1D development is controversial [57]. However, recent understandings show that they play a critical role in pathogenesis of T1D through involvement in pancreatic β cell death, upregulation of pro-inflammatory cytokines, production of reactive oxygen species (ROS), and enhanced T cell infiltration towards the pancreas. In addition, during acute inflammation, macrophages are first cells to accumulate at one side of the pancreatic islet at an early stage (2–3 weeks of age) [58]. However, little efforts have been attempted to reprogram the macrophages towards anti-inflammatory phenotype in the treatment of T1D. Here, we aim to reprogram the inflammatory

macrophages and T lymphocytes towards anti-inflammatory phenotype and investigate the outcomes in treatment of T1D following by islet transplantation.

Based on our observations on the EAE mouse model as well as in vitro evaluations, we hypothesized that MSC-Exo may show their immunoregulatory effects through both lymphocytes and leukocytes. NOD mice is a mouse model for T1D, which in many aspects mimic the pathology of T1D in humans, where immunocytes infiltration are the main pathological markers [59]. We expect that early intervention with two doses of MSC-Exo would alleviate the insulitis, leading to systemic prevention of T1D. Mice blood glucose, and body weight would be measured over-time and compared against PBS control. We therefore injected two doses of exosomes similar to EAE study (**Figure 3.13**)

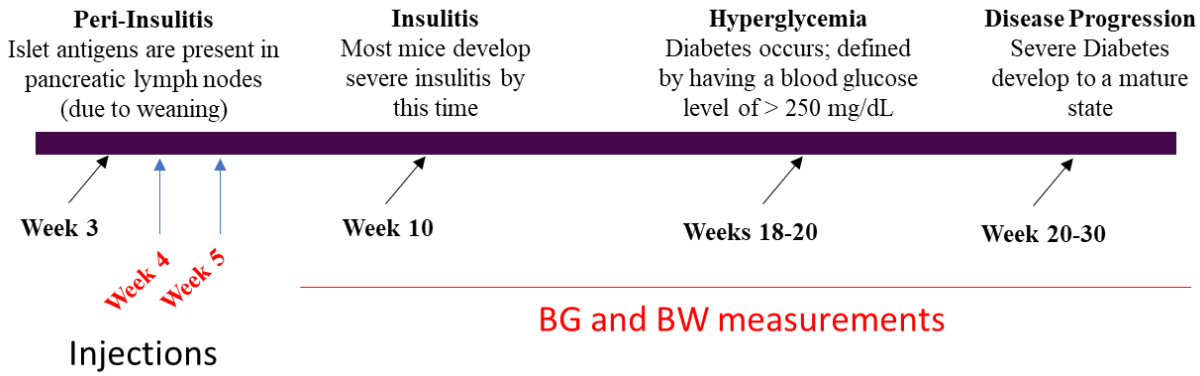

Figure 3.21. Study design to use MSC exosomes to prevent or delay the occurrence of T1D. Two dose injection of IFNγ-Exo prior to onset of immune-infiltration and blood glucoses and body weights were measured till hyperglycemia occurrence and persistence.

Blood glucose measurements prior and post diabetes occurrence revealed that our treatment, contrary to our preliminary hypothesis, does not delay or prevent the occurrence of hyperglycemia in NOD mouse model and no effect on the body weight changes (**Figure 3.14A, B**). We further attempted to test the efficacy of IFNγ-Exo on the survival of NOD mice.

While not statistically significant, we found that survival rates in mice injected with IFNγ-Exo are lower than that of PBS controls (**Figure 3.14C**).

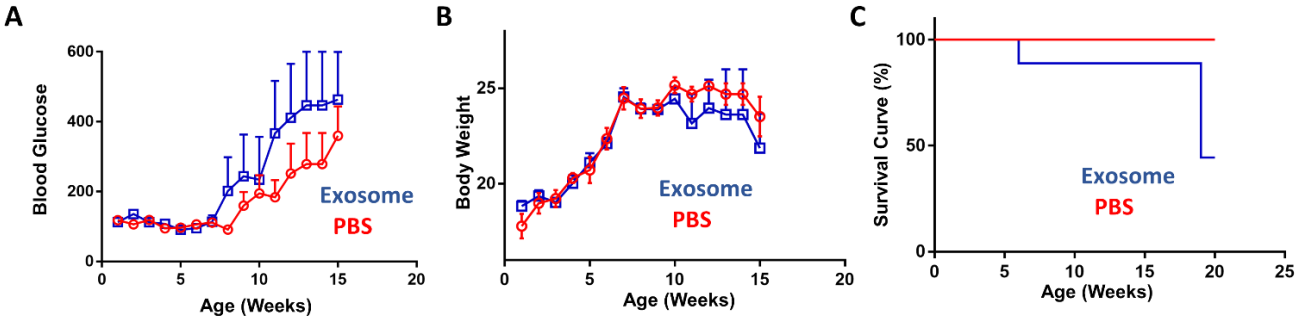

Figure 3.22. Injection of IFNγ-Exo had adverse results in the incidence of T1D. A) Injection of IFNγ-Exo not only did not delay the occurrence of hyperglycemia in NOD mouse models, but also induced hyperglycemia earlier than PBS control group (n = 5). B) Body weight changes were not significantly different between the PBS and IFNγ-Exo injected group, showing the lack of toxicity. C) While none of the PBS control NOD mice were died during the treatment period, 50% of the IFNγ-Exo injected NOD mice died by week 20 of the study.

Conclusions

This study facilitates the understanding of potential mechanisms by which MSCs exert therapeutic function. In the context of cell therapy, the majority of i.v.-infused MSCs get entrapped in filter organs without significantly homing to sites of injury, and yet they frequently exhibit therapeutic activity in numerous animal models.[2] The mechanisms to this puzzling phenomenon remain unclear. Our unpublished data showed that lung entrapped MSCs under physical and mechanical stresses could shed small vesicles to the circulation that could reach distant organs. Recent evidences suggest infused MSCs and their apoptotic products can be phagocytosed, which led to the generation of third-party phagocytes that ultimately mediate the observed immunomodulatory effects.[4-6,46] The fact that MSC-derived exosomes can recapitulate MSC's efficacy in our EAE model and that their effects on T cells are mediated at least partly by third-party cells (*e.g.* macrophage) implies that transplanted MSCs could mediate their efficacy *in vivo* through secreted EVs, likely by first interfacing with APCs and phagocytes.[7,13,47-50]

Our data demonstrate that exosomes derived from IFNγ activated MSCs 1) suppress PBMC cell proliferation (likely through IDO), reduce proinflammatory cytokines and enhance induction of Tregs *in vitro*, 2) are distributed to the inflamed, but not healthy, spinal cords, reduce neuroinflammation and demyelination and improve functional outcomes in chronic EAE murine model. This study asserts that stem cell-derived exosomes can represent a viable approach to treat autoimmune and neurodegenerative disorders, which remains major unmet clinical needs. There are several potential advantages for the exploitation of exosomes as therapeutics and as vehicles for therapeutic delivery, compared to cells and conventional drug delivery systems (*e.g.*, liposomes and nanoparticles): 1) the smaller size of exosomes allows reduced entrapment in small capillaries following systemic infusion, and potentially improves the therapeutic delivery to the diseased sites, 2) exosomes are expected to have significantly longer shelf life, lower side-effects and other risks compared to cells because of their acellular status, 3) exosomes possess a complex mixture of factors targeting different therapeutic pathways and synergize to enhance therapeutic function compared to using individual factors, and 4) the natural cell origin of exosomes enhances our ability to genetically modify the cell of origin to produce exosomes with overexpressed agents for improved efficacy, biocompatibility and reduced immunogenicity.

We demonstrated that MSC exosomes showed potential to induce a tolerogenic immune response and therefore a sustained clinical recovery. Moreover, further MOA investigation on the reduction of Th17 cells and their associated proinflammatory cytokines can lead to development of exosome therapeutics that target disease pathways such as Th17 cytokines for patients who are refractory to the current treatment.[27] We demonstrated MSC-derived exosomes host a mixture of proteins and RNAs, some of which are implicated in anti-inflammatory,

antigen presenting, or neuronal protection pathways. Future work will investigate individual markers (*e.g.* IDO) and dissect the cellular and molecular mechanisms to identify a panel of molecular markers that are responsible for exosome's therapeutic effect. This effort will allow us to 1) optimize exosome manufacturing and preparation processes to standardize potential batch-to-batch variations and develop quality control (QC) and release assays for clinical applications,[51] and 2) engineer exosomes to overexpress selected candidates in the future to improve their efficacy.[7,52] Future work will also optimize treatment timing, especially at the onset of the disease, which might be more effective in attenuate inflammatory responses during the induction phase. It will also be interesting to further characterize how doses and number of injections affect outcomes, especially considering that increased doses in the MSC field have resulted in mixed outcomes,[53] presumably due to the host immune responses (*e.g.* antibodies) that were raised to attenuate the therapy.[54] Intravenous infusion was chosen as administration route in this study due to its minimal invasiveness and convenience, however, other routes such as local injection of exosome[15] to inflamed spinal cords would be an interesting approach to explore in the future work to optimize their therapeutic outcome.

Lastly, the inefficacy of MSC derived exosomes therapy in a NOD autoimmune diabetic model could be further investigated from two different approaches. In the first approach, one could study the effect of residual IFNγ on the NOD mouse model through side-by-side analyses. The hypothesis here would be that due to the strong multi-potent inflammatory behavior of IFNγ, exosomes could not reduce the induction and severity of the inflammation. The second approach could be the time-poin study. Here we injected the exosomes in the initial stages of inflammatory response. It is highly recommended that exosomes be injected in different time points after week 6 of age, prior to the hyperglycemic incidence. Maybe exosomes are effective when the

inflammation is at its max, which occurs at later time-point in the NOD mouse model. Our results further show that MSC exosomes may have therapeutic efficacy, but due to the complexities in the molecular mechanisms, multiple side-by-side studies should be performed to optimize the therapy timeline.

References

1 Singer, N. G. & Caplan, A. I. Mesenchymal stem cells: mechanisms of inflammation. *Annu. Rev. Pathol.* **6**, 457-478, doi:10.1146/annurev-pathol-011110-130230 (2011).

2 Galipeau, J. & Sensébé, L. Mesenchymal Stromal Cells: Clinical Challenges and Therapeutic Opportunities. *Cell Stem Cell* **22**, 824-833, doi:https://doi.org/10.1016/j.stem.2018.05.004 (2018).

3 Fischer, U. M. *et al.* Pulmonary passage is a major obstacle for intravenous stem cell delivery: the pulmonary first-pass effect. *Stem Cells Dev.* **18**, 683-692, doi:10.1089/scd.2008.0253 (2009).

4 de Witte, S. F. H. *et al.* Immunomodulation By Therapeutic Mesenchymal Stromal Cells (MSC) Is Triggered Through Phagocytosis of MSC By Monocytic Cells. *STEM CELLS* **36**, 602-615, doi:10.1002/stem.2779 (2018).

5 Galleu, A. *et al.* Apoptosis in mesenchymal stromal cells induces in vivo recipient-mediated immunomodulation. *Science Translational Medicine* **9**, eaam7828, doi:10.1126/scitranslmed.aam7828 (2017).

6 Luk, F. *et al.* Inactivated Mesenchymal Stem Cells Maintain Immunomodulatory Capacity. *Stem Cells and Development* **25**, 1342-1354, doi:10.1089/scd.2016.0068 (2016).

7 Riazifar, M., Pone, E. J., Lotvall, J. & Zhao, W. Stem Cell Extracellular Vesicles: Extended Messages of Regeneration. *Annu Rev Pharmacol Toxicol* **57**, 125-154, doi:10.1146/annurev-pharmtox-061616-030146 (2017).

8 Thery, C., Ostrowski, M. & Segura, E. Membrane vesicles as conveyors of immune responses. *Nat. Rev. Immunol.* **9**, 581-593, doi:10.1038/nri2567 (2009).

9 Marino, J. *et al.* Donor exosomes rather than passenger leukocytes initiate alloreactive T cell responses after transplantation. *Science Immunology* **1**, aaf8759, doi:10.1126/sciimmunol.aaf8759 (2016).

10 Viaud, S. *et al.* Updated Technology to Produce Highly Immunogenic Dendritic Cell-derived Exosomes of Clinical Grade: A Critical Role of Interferon-γ. *Journal of Immunotherapy* **34**, 65–75 (2011).

11 Pusic, A. D., Pusic, K. M., Clayton, B. L. & Kraig, R. P. IFNgamma-stimulated dendritic cell exosomes as a potential therapeutic for remyelination. *J. Neuroimmunol.* **266**, 12-23, doi:10.1016/j.jneuroim.2013.10.014 (2014).

12 Shigemoto-Kuroda, T. *et al.* MSC-derived Extracellular Vesicles Attenuate Immune Responses in Two Autoimmune Murine Models: Type 1 Diabetes and Uveoretinitis. *Stem Cell Reports* **8**, 1214-1225, doi:https://doi.org/10.1016/j.stemcr.2017.04.008 (2017).

13 Lankford, K. L. *et al.* Intravenously delivered mesenchymal stem cell-derived exosomes target M2-type macrophages in the injured spinal cord. *PLOS ONE* **13**, e0190358, doi:10.1371/journal.pone.0190358 (2018).

14 Laso-García, F. *et al.* Therapeutic potential of extracellular vesicles derived from human mesenchymal stem cells in a model of progressive multiple sclerosis. *PLOS ONE* **13**, e0202590, doi:10.1371/journal.pone.0202590 (2018).

15 Bai, L. *et al.* Effects of Mesenchymal Stem Cell-Derived Exosomes on Experimental Autoimmune Uveitis. *Scientific Reports* **7**, 4323, doi:10.1038/s41598-017-04559-y (2017).
16 Fujii, S. *et al.* Graft-Versus-Host Disease Amelioration by Human Bone Marrow Mesenchymal Stromal/Stem Cell-Derived Extracellular Vesicles Is Associated with Peripheral Preservation of Naive T Cell Populations. *STEM CELLS* **36**, 434-445, doi:10.1002/stem.2759 (2018).
17 Silva, A. K. A. *et al.* Thermoresponsive Gel Embedded with Adipose Stem-Cell-Derived Extracellular Vesicles Promotes Esophageal Fistula Healing in a Thermo-Actuated Delivery Strategy. *ACS Nano* **12**, 9800-9814, doi:10.1021/acsnano.8b00117 (2018).
18 Lai, R. C., Yeo, R. W. Y., Tan, K. H. & Lim, S. K. Exosomes for drug delivery — a novel application for the mesenchymal stem cell. *Biotechnology Advances* **31**, 543-551, doi:https://doi.org/10.1016/j.biotechadv.2012.08.008 (2013).
19 Dendrou, C. A., Fugger, L. & Friese, M. A. Immunopathology of multiple sclerosis. *Nat Rev Immunol* **15**, 545-558, doi:10.1038/nri3871 (2015).
20 Ransohoff, R. M., Hafler, D. A. & Lucchinetti, C. F. Multiple sclerosis-a quiet revolution. *Nat Rev Neurol* **11**, 134-142, doi:10.1038/nrneurol.2015.14 (2015).
21 Hogancamp, W. E., Rodriguez, M. & Weinshenker, B. G. The epidemiology of multiple sclerosis. *Mayo Clin Proc* **72**, 871-878, doi:10.1016/S0025-6196(11)63504-0 (1997).
22 Constantinescu, C. S., Farooqi, N., O'Brien, K. & Gran, B. Experimental autoimmune encephalomyelitis (EAE) as a model for multiple sclerosis (MS). *Br J Pharmacol* **164**, 1079-1106, doi:10.1111/j.1476-5381.2011.01302.x (2011).
23 Herold, K. C., Vignali, D. A., Cooke, A. & Bluestone, J. A. Type 1 diabetes: translating mechanistic observations into effective clinical outcomes. *Nature reviews. Immunology* **13**, 243-256, doi:10.1038/nri3422 (2013).
24 Bluestone, J. A. *et al.* Type 1 diabetes immunotherapy using polyclonal regulatory T cells. *Sci Transl Med* **7**, doi:ARTN 315ra189
10.1126/scitranslmed.aad4134 (2015).
25 Bluestone, J. A., Herold, K. & Eisenbarth, G. Genetics, pathogenesis and clinical interventions in type 1 diabetes. *Nature* **464**, 1293, doi:10.1038/nature08933
https://www.nature.com/articles/nature08933#supplementary-information (2010).
26 Riazifar, M. *et al.* Stem Cell-Derived Exosomes as Nanotherapeutics for Autoimmune and Neurodegenerative Disorders. *ACS Nano* **13**, 6670-6688, doi:10.1021/acsnano.9b01004 (2019).
27 Wagner, C. A. & Goverman, J. M. Novel Insights and Therapeutics in Multiple sclerosis [version 1; referees: 3 approved]. *F1000Research* **4** (2015).
28 Johnson, M. C. *et al.* Distinct T cell signatures define subsets of patients with multiple sclerosis. *Neurology(R) neuroimmunology & neuroinflammation* **3**, e278-e278, doi:10.1212/NXI.0000000000000278 (2016).
29 Murphy, Á. C., Lalor, S. J., Lynch, M. A. & Mills, K. H. G. Infiltration of Th1 and Th17 cells and activation of microglia in the CNS during the course of experimental autoimmune encephalomyelitis. *Brain, Behavior, and Immunity* **24**, 641-651, doi:https://doi.org/10.1016/j.bbi.2010.01.014 (2010).
30 Caravagna, C. *et al.* Diversity of innate immune cell subsets across spatial and temporal scales in an EAE mouse model. *Scientific Reports* **8**, 5146, doi:10.1038/s41598-018-22872-y (2018).

31 Thakker, P. *et al.* IL-23 Is Critical in the Induction but Not in the Effector Phase of Experimental Autoimmune Encephalomyelitis. *The Journal of Immunology* **178**, 2589, doi:10.4049/jimmunol.178.4.2589 (2007).
32 Dennis, G., Jr. *et al.* Synovial phenotypes in rheumatoid arthritis correlate with response to biologic therapeutics. *Arthritis research & therapy* **16**, R90-R90, doi:10.1186/ar4555 (2014).
33 Carbajal, K. S. *et al.* Th Cell Diversity in Experimental Autoimmune Encephalomyelitis and Multiple Sclerosis. *The Journal of Immunology* **195**, 2552, doi:10.4049/jimmunol.1501097 (2015).
34 Kwong, B. *et al.* T-bet-dependent NKp46+ innate lymphoid cells regulate the onset of TH17-induced neuroinflammation. *Nature Immunology* **18**, 1117, doi:10.1038/ni.3816 https://www.nature.com/articles/ni.3816#supplementary-information (2017).
35 Othy, S. *et al.* Intravenous Gammaglobulin Inhibits Encephalitogenic Potential of Pathogenic T Cells and Interferes with their Trafficking to the Central Nervous System, Implicating Sphingosine-1 Phosphate Receptor 1–Mammalian Target of Rapamycin Axis. *The Journal of Immunology* **190**, 4535, doi:10.4049/jimmunol.1201965 (2013).
36 Fletcher, J. M., Lalor, S. J., Sweeney, C. M., Tubridy, N. & Mills, K. H. T cells in multiple sclerosis and experimental autoimmune encephalomyelitis. *Clin Exp Immunol* **162**, 1-11, doi:10.1111/j.1365-2249.2010.04143.x (2010).
37 Reich, D. S., Lucchinetti, C. F. & Calabresi, P. A. Multiple Sclerosis. *New England Journal of Medicine* **378**, 169-180, doi:10.1056/NEJMra1401483 (2018).
38 Merian, J., Gravier, J., Navarro, F. & Texier, I. Fluorescent nanoprobes dedicated to in vivo imaging: from preclinical validations to clinical translation. *Molecules* **17**, 5564-5591, doi:10.3390/molecules17055564 (2012).
39 François, M., Romieu-Mourez, R., Li, M. & Galipeau, J. Human MSC Suppression Correlates With Cytokine Induction of Indoleamine 2,3-Dioxygenase and Bystander M2 Macrophage Differentiation. *Molecular Therapy* **20**, 187-195, doi:https://doi.org/10.1038/mt.2011.189 (2012).
40 Tipnis, S., Viswanathan, C. & Majumdar, A. S. Immunosuppressive properties of human umbilical cord-derived mesenchymal stem cells: role of B7-H1 and IDO. *Immunology & Cell Biology* **88**, 795-806, doi:10.1038/icb.2010.47 (2010).
41 Meisel, R. *et al.* Human bone marrow stromal cells inhibit allogeneic T-cell responses by indoleamine 2,3-dioxygenase–mediated tryptophan degradation. *Blood* **103**, 4619, doi:10.1182/blood-2003-11-3909 (2004).
42 Chen, W. *et al.* Immunomodulatory effects of mesenchymal stromal cells-derived exosome. *Immunologic Research* **64**, 831-840, doi:10.1007/s12026-016-8798-6 (2016).
43 Murphy, M. B., Moncivais, K. & Caplan, A. I. Mesenchymal stem cells: environmentally responsive therapeutics for regenerative medicine. *Exp. Mol. Med.* **45**, e54, doi:10.1038/emm.2013.94 (2013).
44 Sakurai, K., Zou, J. P., Tschetter, J. R., Ward, J. M. & Shearer, G. M. Effect of indoleamine 2,3-dioxygenase on induction of experimental autoimmune encephalomyelitis. *J Neuroimmunol* **129**, 186-196 (2002).
45 Mbongue, J. C. *et al.* The Role of Indoleamine 2, 3-Dioxygenase in Immune Suppression and Autoimmunity. *Vaccines (Basel)* **3**, 703-729, doi:10.3390/vaccines3030703 (2015).

46 Braza, F. *et al.* Mesenchymal Stem Cells Induce Suppressive Macrophages Through Phagocytosis in a Mouse Model of Asthma. *STEM CELLS* **34**, 1836-1845, doi:10.1002/stem.2344 (2016).
47 Domenis, R. *et al.* Pro inflammatory stimuli enhance the immunosuppressive functions of adipose mesenchymal stem cells-derived exosomes. *Scientific Reports* **8**, 13325, doi:10.1038/s41598-018-31707-9 (2018).
48 Gonçalves, F. d. C. *et al.* Membrane particles generated from mesenchymal stromal cells modulate immune responses by selective targeting of pro-inflammatory monocytes. *Scientific Reports* **7**, 12100, doi:10.1038/s41598-017-12121-z (2017).
49 Song, Y. *et al.* Exosomal miR-146a Contributes to the Enhanced Therapeutic Efficacy of Interleukin-1β-Primed Mesenchymal Stem Cells Against Sepsis. *STEM CELLS* **35**, 1208-1221, doi:10.1002/stem.2564 (2017).
50 Zhang, B. *et al.* Mesenchymal stromal cell exosome–enhanced regulatory T-cell production through an antigen-presenting cell–mediated pathway. *Cytotherapy* **20**, 687-696, doi:https://doi.org/10.1016/j.jcyt.2018.02.372 (2018).
51 Reiner, A. T. *et al.* Concise Review: Developing Best-Practice Models for the Therapeutic Use of Extracellular Vesicles. *STEM CELLS Translational Medicine* **6**, 1730-1739, doi:10.1002/sctm.17-0055 (2017).
52 Armstrong, J. P. K., Holme, M. N. & Stevens, M. M. Re-Engineering Extracellular Vesicles as Smart Nanoscale Therapeutics. *ACS Nano* **11**, 69-83, doi:10.1021/acsnano.6b07607 (2017).
53 Bouffi, C., Bony, C., Courties, G., Jorgensen, C. & Noël, D. IL-6-Dependent PGE2 Secretion by Mesenchymal Stem Cells Inhibits Local Inflammation in Experimental Arthritis. *PLOS ONE* **5**, e14247, doi:10.1371/journal.pone.0014247 (2010).
54 Griffin, M. D., Ritter, T. & Mahon, B. P. Immunological Aspects of Allogeneic Mesenchymal Stem Cell Therapies. *Human Gene Therapy* **21**, 1641-1655, doi:10.1089/hum.2010.156 (2010).
55 http://www.jdrf.org.
56 Desai, T. & Shea, L. D. Advances in islet encapsulation technologies. *Nature Reviews Drug Discovery* **16**, 338–350 (2017).
57 Wa˚llberg, M. & Cooke, A. Immune mechanisms in type 1 diabetes. *Trends in Immunology* **34**, 583-591 (2013).
58 Navegantes, K. C. *et al.* Immune modulation of some autoimmune diseases: the critical role of macrophages and neutrophils in the innate and adaptive immunity. *J Transl Med* **15**, 36, doi:10.1186/s12967-017-1141-8 (2017).
59 Tan, T. G., Mathis, D. & Benoist, C. Singular role for T-BET+ CXCR3(+) regulatory T cells in protection from autoimmune diabetes. *P Natl Acad Sci USA* **113**, 14103-14108, doi:10.1073/pnas.1616710113 (2016).

CHAPTER 4

Controlled Release of Stem Cell Secretome Attenuates Inflammatory Response Against Implanted Biomaterials

Abstract

Inflammatory response against implanted biomaterials impairs their functional integration and induces medical complications in the host's body. To suppress such immune responses, one approach is the administration of multiple drugs to halt inflammatory pathways. This challenges patient's adherence and could cause additional complications such as infection. Alternatively, biologics that regulate multiple inflammatory pathways are attractive agents in addressing the implants immune complications. Secretome of Mesenchymal Stromal Cells (MSCs) is a multipotent biologic, regulating the homeostasis of lymphocytes and leukocytes. Here, it is reported that alginate microcapsules loaded with processed conditioned media (pCM-Alg) reduces the infiltration and/or expression of CD68+ macrophages likely through the controlled release of pCM. *In vitro* cultures revealed that alginate could dose-dependently induce macrophages to secrete TNFα, IL-6, IL-1β, and GM-CSF. Addition of pCM to the cultures attenuated the secretion of TNFα ($p = 0.023$) and IL-6 ($p < 0.0001$) by alginate or lipopolysaccharide (LPS) stimulations. Mechanistically, pCM suppressed the NfκB pathway activation of macrophages in response to LPS ($p < 0.0001$) *in vitro* and cathepsin activity ($p = 0.005$) in response to alginate *in vivo*. These observations suggest the efficacy of using MSC derived secretome to prevent or delay the host rejection of implants.

Keywords: foreign body response, mesenchymal stem (stromal) cells, secretome, exosomes, macrophages, alginate, inflammation

Introduction

Long-term biocompatibility and function of implanted scaffolds require absence of detrimental immune response [1]. The immune response that is also known as foreign body response (FBR) could be divided into sequential steps of tissue injury, immunocytes recruitment and adhesion, induction of myofibroblasts, and fibrotic capsule formation. Such events prevent the interaction of the implants with the surrounding microenvironment, leading to the non-functionality of the implants and complications in the host's body. A few examples that FBR creates issues for the implants are signal inaccuracy in glucose measurements of continuous glucose monitors [2-4], graft rejections of encapsulated pancreatic islets [5-8], and complications of breast implants that recently led FDA to recall BIOCELL textured breast implants from market.[9, 10] To alleviate such immune and fibrotic responses, multiple approaches have been described previously, including manipulation of size [5, 11, 12]. Shape [13, 14], surface characteristic,[15-18] and fabrication of devices with controlled release of anti-inflammatory agents.[6, 19, 20]

Inflammatory response against implanted biomaterials depend upon the structural and physiochemical properties of the material, where multiple signaling pathways are involved. [21-25] One example of FBR is the fibrotic cascade against implanted alginate microcapsules containing pancreatic islets for the glycemic control in Type 1 Diabetics. The onset of FBR is upon surgical procedure prior to transplantation, leading to neutrophils activation and migration.[26, 27] Inflammatory response further proceeds with the activation and recruitment of macrophages, B cells and T cells around microcapsules.[5, 21, 27, 28] Within weeks to months, immunocytes populate the surface of microcapsules, interfering the accessibility of insulin

outwards and of nutrients inwards the microcapsules. In the long-term, implants get encapsulated and fibrosed.

The result of this immune myriad is the non-functionality of the transplant known as graft failure. Thus, strategies have been developed to regulate the inflammatory response against alginate microcapsules for long-term efficacy of pancreatic islet transplantation.[19, 20, 29] Among different immunomodulatory approaches, alginate's surface engineering[29-31] and loading of alginate with immunomodulatory factors[19, 20] have been extensively described previously. It is therefore expected that a controlled-release biomaterial with releasing multi-potent anti-inflammatory agent may better shield the implants against the host immune-interactions to halt fibrotic cascade.

In this context, Mesenchymal Stromal Cells (MSCs) are known as multipotent cells that regulate variety of inflammatory pathways including NF-κB**,**[32] JAK/STAT,[33] MyD88,[34] PI3K/AKT[35] and PGE2 downstream pathways. [36] MSCs are under investigation in more than 700 clinical trials, mostly focused on inflammatory and autoimmune disorders. While their therapeutic mechanisms are remained to be fully elucidated, MSCs are suggested to exert their immunomodulatory characteristics partly through paracrine factors.[35, 37-42] Cumulated body of evidence suggests that secretome of MSCs has immunosuppressive and immunoregulatory potentials, interacting with different classes of immunocytes.[32, 38, 40] We thus prepared alginate microcapsules loaded with processed condition media (pCM) secreted from human Umbilical Cord Derived MSCs (pCM-Alg) and subcutaneously implanted into C57/BL6 (immunocompetent) mice. After two weeks, we removed and studied the explants of pCM-Alg as well as Ctrl-Alg microcapsules. We hypothesized that pCM will be released into the host's

microenvironment and dampens the inflammatory response against microcapsules (**Figure 4.1 a, b**).

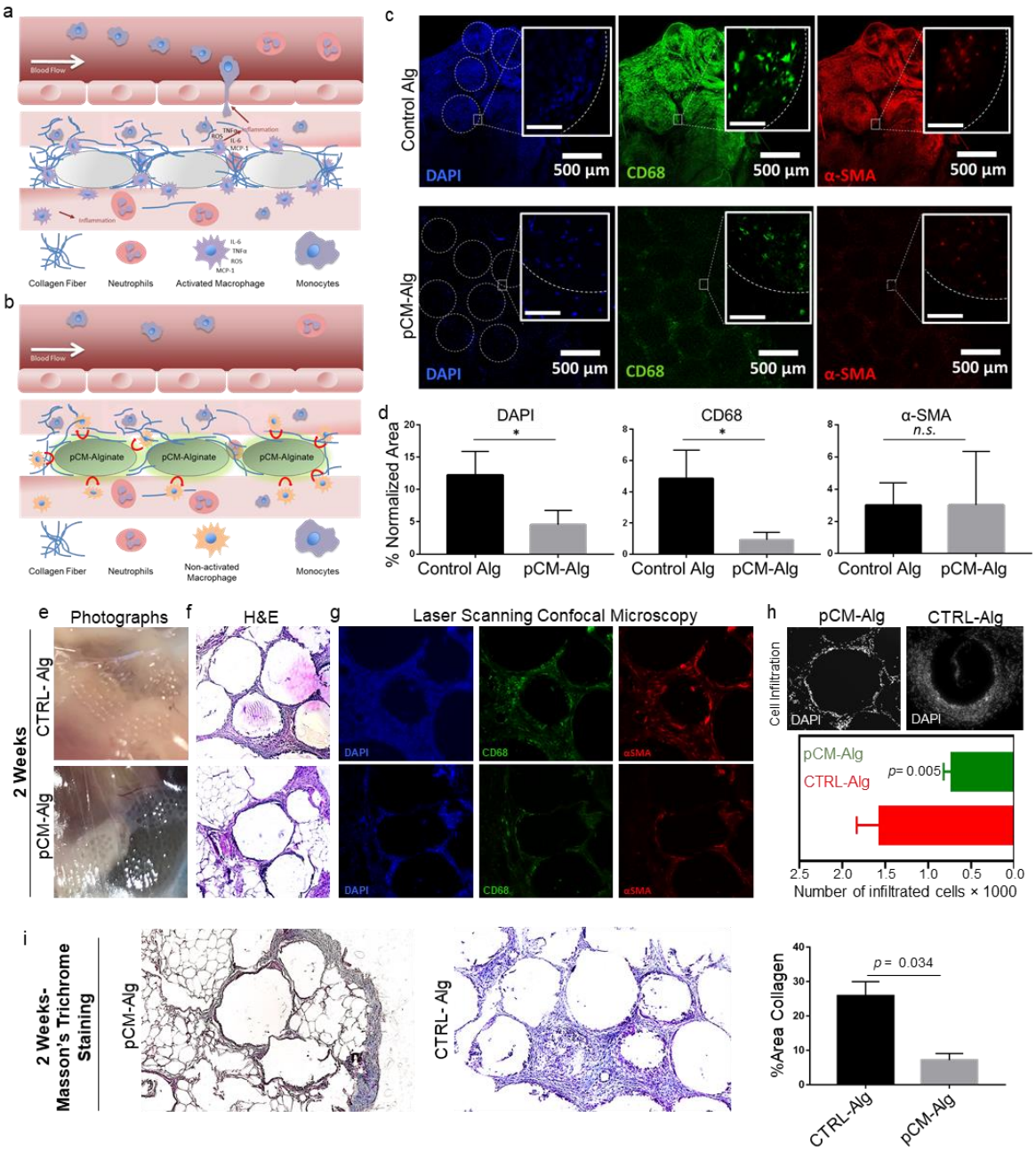

Figure 4.23. Cell infiltration around pCM-Alg is less than control microcapsules. Both control and pCM microcapsules were implanted subcutaneously in C57/BL6 mice. Two weeks after implantation, formed fibrotic tissues were extracted and analyzed for cell infiltration. Schematic representation of the reduction of inflammatory response in **a)** control alginates versus **b)** pCM-Alg microcapsules. **c)** Whole explants were analyzed for CD68 and α-SMA markers, and nuclei were counterstained with DAPI. Some capsules and magnified images (scalebar=50 µm) are marked for visual aid. **e)** Some of the microcapsules were imaged after 2 weeks of implantation and prior to explantation. Explants then fixed and sectioned into slices with 5 µ thickness. **f)** Tissue slides were stained with H&E and **g)** CD68 and α-SMA markers, and nuclei were counterstained with DAPI. Similar procedures and staining were also performed on microcapsules collected 4-weeks after implantation. **h)** Total cells infiltration was quantified using the counts of DAPI positive spots. **i)** Masson's Trichrome staining was used to quantify the collagen presence as a fibrotic marker, demonstrating the higher amount of collagen around CTRL-Alg microcapsules. In all experiments n=4, Unpaired t-test with Welch's correction, n.s. non-significant; *p<0.05)

Results and Discussions

To observe the difference in immune-profiles, we collected the whole-mount explants and stained for total cell infiltration as well as two FBR markers i.e. CD68+ (macrophages) and αSMA+ (alpha smooth muscle actin) cells (**Figure 4.1c**). To compare the number of cells, signal area was measured in similar magnifications and normalized by the total tissue area in the image. **Figure 4.1d** shows the quantification for the DAPI area, which indicates the reduction in total cell infiltration (n = 4, p = 0.015) around pCM-Alg (normalized area of DAPI % = 4.54% ± 2.25%, mean ± SD) compared to control (normalized area of DAPI% = 12.26% ± 3.64%). Normalized area of CD68+ macrophage also reduced from 4.86% ± 1.81% to 0.94% ± 0.47% (n = 4, p = 0.019) in control and pCM-Alg (**Figure 4.1d**). No difference in the αSMA+ cells between two groups were found (n = 4, p = 0.99; normalized area % = 3.01% ± 1.38% and 4.19% ± 3.3% for Ctrl-Alg and pCM-Alg, respectively).

We further sought to characterize and quantify the immune-profiles for both pCM-Alg and Ctrl-Alg microcapsules. We thus explanted microcapsules after 2 weeks implantation and sectioned the microcapsules for immunostaining. **Figure 4.1e** shows the images of fibrotic tissue captured prior to explantation, which were then micro-sectioned into 5-10 μm slices. We then stained the slices with H&E (**Figure 4.1f**) and conducted immunofluorescence (**Figure 4.1g**) to visualize the inflammatory milieu around microcapsules. These results suggest that, at least two weeks after implantation, total cell infiltration and CD68+ around pCM-Alg were lower than Ctrl-Alg. To further quantify cell infiltration around implants, we DAPI stained fibrotic tissues and counted each DAPI+ area as an individual cell using IMARIS software. Total cell infiltration around pCM-Alg was significantly lower (p = 0.005) around the pCM-Alg (722 ± 101) microcapsules compared to Ctrl-Alg (1562 ± 772) after 2 weeks of implantation (**Figure 4.1h**).

After the initial inflammatory response against the implants, fibroblasts get recruited around the inflammatory microenvironment. Fibroblasts are then responsible for final fibrous collagen and matrix protein deposition.[21] We therefore sought to quantify the collagen quantity around the microcapsules. **Figure 4.1i** demonstrates the Masson's Trichrome staining and quantification of collagen (blue staining). Using the imageJ software to quantify collagen (as described in **Methods** section), we found that there is significantly less collagen around the pCM-Alg microcapsules compared to CTRL-Alg ones (p = 0.0034). This result further suggests the less-fibrotic response around pCM-Alg microcapsules.

These results offer that, at least during the first 2 weeks after implantation, pCM-Alg alleviates the initial inflammatory response, whereby fewer total cells and CD68+ macrophages are infiltrated around alginate microcapsules. We further hypothesized that reduction of cell infiltration could be partly explained via the release of pCM to the surrounding microenvironment of microcapsules. Upon release, pCM dampens the local inflammation likely through interacting with infiltrating/adjacent immunocytes. To measure the release profile, we first quantified the protein amount encapsulated in pCM-Alg microcapsules and found that ~1000 pCM-Alg microcapsules contain 901.6 ± 143.9 μg/mL proteins. The encapsulated protein amount reduced to 197 ± 88.3 μg/mL after 48 h of incubation at 37 °C (**Figure 4.2a**), suggesting the overtime reduction of protein within pCM-Alg microcapsules. To speculate the protein release profile, we collected 0.5 mL of the media around pCM-Alg microcapsule and measured the protein content. **Figure 4.2b** shows the cumulative protein release, demonstrating the controlled release profile from pCM-Alg over 48 h (green line graph). These results in their totality suggest that pCM-Alg releases its protein content overtime.

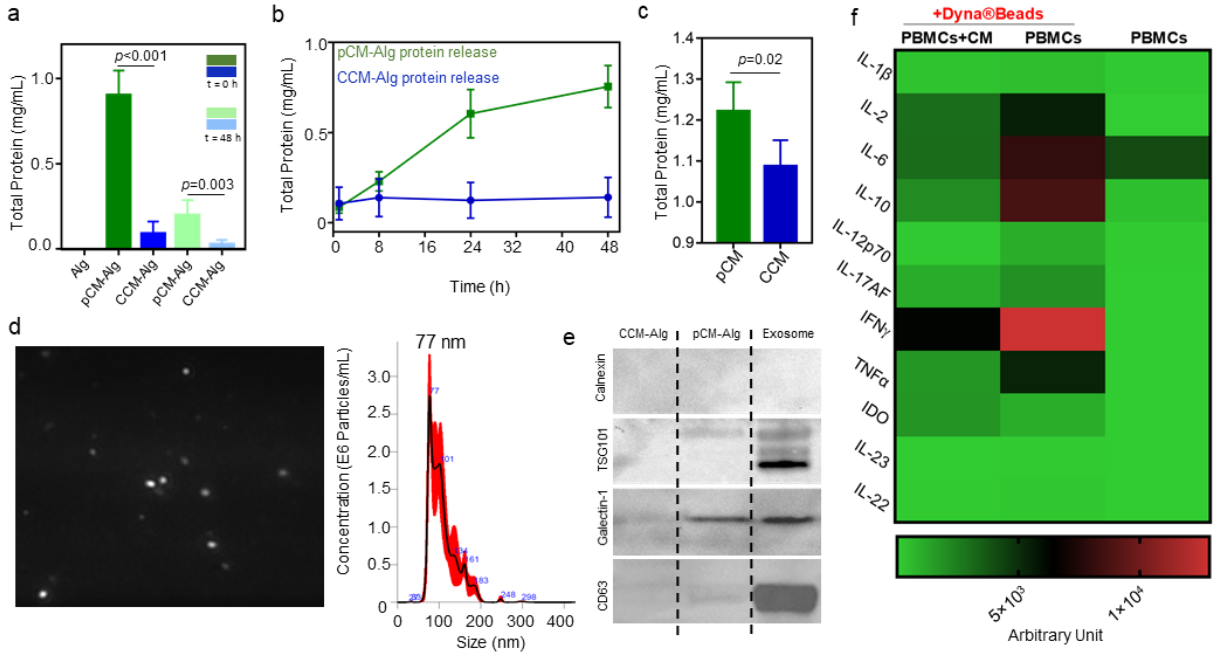

Figure 4.24. pCM-Alg microcapsules release immunomodulatory MSCs secretome *in vitro*. a) protein content of freshly prepared pCM-Alg is 901.6 ± 143.9 µg/mL per ~1000 microcapsules, which is higher than that of CCM-Alg (88.4 ± 72.3 µg/mL; $p < 0.001$). After 48 h of incubation, ~1000 pCM-Alg microcapsules retain 197 ± 88.3 µg/mL total protein, while CCM-Alg contains 27.6 ± 23.7 µg/mL ($p = 0.003$). **b)** total protein release for both pCM-Alg and CCM-Alg over 48 h, suggesting that proteins released from pCM-Alg are specific to MSC secretome rather that cell culture media. **c)** BCA assay was used to measure the protein amount in pCM and CCM, where pCM contains higher protein content (1.22 ± 0.10 mg/mL; $p = 0.02$) compared to culture media (1.08 ± 0.06 mg/mL). **d)** Proteins released form pCM-Alg at 8 h were collected and characterized for the exosome release. Nanoparticle Tracking analyses (NTA) and **e)** Western blotting were used to count and verify the released exosomes. In both cases, negative controls were proteins release from CCM-Alg at 8 h of incubation. **f)** To test the immunomodulatory effects of MSC secretome, Peripheral human Blood Mononuclear Cells (PBMCs) proliferation assay was conducted. PBMCs were activated by magnetic beads coated with anti-CD3 and anti-CD28 in the presence and absence of pCM for 4 days. Supernatants of cultures were isolated, and cytokines were analyzed. We found that addition of pCM to the activated PBMCs co-culture decreases the Mean Fluorescence Intensity of IL-6 (2.0-fold), IL-12p70 (4.7-fold), IFNγ (2.5-fold), TNFα (2.4-fold), and increases IDO (1.9-fold). Significance measurements were conducted by Unpaired t-test with Welch's correction.

The pCM (which is a processed conditioned media produced by MSCs) contains variety of proteins, which are coming from two separate sources. The first source is the proteins and growth factors in the cell culture media (CCM), and the second source is secreted factors from MSCs (secretome). In our previous experiments we demonstrated the release of proteins from pCM-Alg, however, we have not determined to what extend these proteins have originated from CCM or secretome. To gain a better understanding on the origin of the released proteins, we

prepared a new alginate formulation that incorporates CCM into alginate microcapsules (CCM-Alg). We then attempted to measure the protein release from CCM-Alg and compare it against pCM-Alg. **Figure 4.2a** shows the total protein content for ~1000 microcapsules of CCM-Alg (88.4 ± 72.3 μg/mL) was significantly lower than that of pCM-Alg (901.6 ± 143.9 μg/mL; $p < 0.001$). In a similar trend, **Figure 4.2a** shows that less proteins retained within CCM-Alg (27.6 ± 23.7 μg/mL) compared to that of pCM-Alg (197 ± 88.3 μg/mL; $p = 0.003$) after 48 h incubation. The ~10-fold more proteins encapsulated in pCM-Alg vs. CCM-Alg could suggest two possibilities: In a similar volume, either pCM contains ~10-fold more proteins compared to CCM, or alginate could retain ~10-fold more proteins of pCM compared to proteins of CCM. To investigate these possibilities, we first analyzed the protein amount in pCM and CCM. **Figure 4.2c** demonstrates the comparison between CCM and pCM, showing that pCM contains slightly higher amount of protein (1.22 ± 0.10 mg/mL; $p = 0.02$), compared to CCM (1.08 ± 0.06 mg/mL). Even though higher, the protein content within pCM does not justify a 10-fold difference in the protein content of pCM-Alg and CCM-Alg. It should be noted that pCM was obtained from a 2-days of sera free MSCs cultures, while CCM is obtained form 2-days of similar incubations but in the absence of MSCs.

We next sought to investigate the second possibility, which is hypothesizing that alginate could retain ~10-fold more pCM proteins compared to proteins of CCM. While many factors could affect more protein retention in pCM-Alg, we particularly hypothesized that proteins within pCM are larger than CCM proteins. Larger proteins then could not facilely diffuse out of microcapsules, leading to higher protein retention in pCM-Alg microcapsules. It is now widely demonstrated that the secretome of MSC contains variety of extracellular vesicles, [32, 38, 40] and these vesicles are hybrid structures of lipid, proteins, and genetic materials. Indeed, it is well

established that MSCs secrete variety of vesicles including apoptotic bodies,[43] microvesicles,[42] exosomes,[35] lipoprotein particles,[44] and ribonucleoproteins.[45] Interestingly, these vesicles could recapitulate the therapeutic benefits of MSCs, stimulating research and development of cell free therapy. [35, 46, 47] The presence of these vesicles within the pCM-Alg (but not CCM-Alg) may partly explain the higher protein retention in pCM-Alg microcapsules.

We then focused our experiments to test whether extracellular vesicles are entrapped within pCM-Alg and could be released from them. Since apoptotic bodies and microvesicles were removed in our pCM preparation,[35, 42] we particularly sought to investigate the exosomes release from the pCM-Alg. To test this possibility, we evaluated the released exosomes from pCM-Alg after 8 h of incubation. To observe and quantify the released exosomes from both pCM-Alg, and CCM-Alg, we conducted NTA analyses. **Figure 4.2d** shows the representative image of the vesicles captured via NTA, demonstrating the size of 107.6 ± 35.9 nm, matching the size range of exosomes in accordance with other reports.[35, 48, 49] No vesicle was observed in the released content of CCM-Alg (data not shown). To further confirm that the visualized vesicles are *bona fide* exosomes, the released cargo was characterized for exosomal markers using Western blotting. We found the presence of three well-established exosomal markers, TSG101,[35, 50] CD63,[46] and Galectin-1,[35] in pCM-Alg released content, while they were absent in the CCM-Alg released proteins (**Figure 4.2e**). We chose to represent 4 biomarkers, because based on Minimal Information for Studies of Extracellular Vesicles (MISEV), presence of 3 biomarkers and absence of one putative contaminant are minimally required to characterize the extracellular vesicles.[51] Since cell debris could also contaminate the condition media, we also checked Calnexin, which is the endoplasmic reticulum

contamination[42] in the released cargo, and it was not detectable in the released pCM and purified exosomes (**Figure 4.2e**). These results suggest that, at least part of the released proteins from pCM-Alg are exosomes secreted by MSCs. These exosomes then entrap within pCM-Alg microcapsules, and due to their large size (i.e. ~ 50-150 nm), there is a higher protein retention in pCM-Alg and a delay in outwards diffusion from pCM-Alg microcapsules (**Figures 4.2a, b**).

Thus far, we observed that pCM-Alg reduces the FBR response *in vivo* and releases the MSC secretome in a controlled fashion. We then hypothesized that released secretome would modulate the immune-milieu around the pCM-Alg, leading to the reduced cell infiltration. Our hypothesis stems in the MSCs capability to regulate the immune response in part through secretion of cytokines and extracellular vesicles.[32, 35, 40] Similar concept has been developed in previous studies, where CXCL12[6, 20] and GW2580[19] were incorporated within alginate microcapsules to alleviate the FBR. To examine the immunomodulatory effects of pCM on immunocytes, we conducted human Peripheral Blood Mononuclear Cells (PBMCs) proliferation assay and isolated the supernatants to measure the cytokine secretion. PBMCs were activated by magnetic beads coated with anti-CD3 and anti-CD28, which mimics the antigen presentation to T lymphocytes. We found that addition of pCM to the activated PBMCs culture decreases the Mean Fluorescence Intensity of IL-6 (2.0-fold), IL-12p70 (4.7-fold), IFNγ (2.5-fold), TNFα (2.4-fold), and increases IDO (1.9-fold), which are summarized in the **Figure 4.2f**. It is well documented that MSC can suppress PBMC proliferation in cocultures mainly through secretory molecules including IDO,[52] IL-10,[53, 54], PGE2,[55] TSG6,[56] and TGFβ.[57] Interestingly, the immunosuppressive effects of MSCs has been associated with their secretory molecules,[38, 39, 58] further supporting our results from the PBMC proliferation cytokine panel.

Myriad of immune activation and immunocytes infiltration have been reported following by alginate microcapsules implantation, with macrophages as central players to orchestrate such responses.[5, 21, 27] Failure in the resolution of macrophage inflammatory response to the implants could lead to chronic inflammation and complications. We therefore focused our experiments to better understand the immunoregulatory of pCM on activated macrophages. Macrophages could be activated through variety of agonists and pathways. We particularly designed our *in vitro* macrophage activation experiments to simulate the immunostimulatory properties of alginates to better replicate the *in vivo* inflammatory conditions caused by alginate implantation.

Two mechanisms have been described to explain the reasons for alginate-based inflammatory response. Some studies have suggested the presence of immunogens within alginate (such as lipopolysaccharide (LPS), lipoteichoic acid, and peptidoglycans) are the main inducers of inflammation.[59, 60] Others reported that such contaminations were undetectable in their alginate,[21, 26, 29] and linked the inflammatory response to the inherent properties of alginate. Alginate is a natural acidic polysaccharide extracted from marine brown seaweeds.[23, 24] It is composed of different blocks of β-(1, 4)-D-mannuronate (M) and its C-5 epimer α-(1, 4)-L-guluronate (G), and Guluronate oligosaccharide derived from alginate has been reported to readily activate macrophages partly through Toll-like receptor 4 (TLR4) signaling pathway.[23, 24] Either through presence of endotoxins or inherent ability of alginate to be immunogenic, TLR4 agonistic effect of alginate is one of the main shared immunostimulatory pathways among different reports. We therefore attempted to test whether pCM could resolve the immunogenicity of alginates and LPS against macrophages.

To test the immunosuppressive capabilities of pCM on myeloid lineage, we first tested whether pCM could inhibit the inflammatory response in both human- and murine-derived macrophages. We first attempted to test cytokine secretion from murine RAW 264.7 macrophages under stimulatory conditions. To stimulate macrophages, we used two doses of either alginate or LPS. Macrophages were stimulated with 0.125 or 1.250 mg/mL of ultrapure UPLVG alginate for 12 h and secreted cytokines were collected for the analysis. **Figure 4.3a** shows the schematic representation of experimental procedure, where macrophages were incubated with 0.125 or 1.250 mg/mL of UPLVG for 12 h in the presence or absence of pCM. We found that alginate significantly upregulates the secretion of TNFα and IL-6 in a dose dependent manner, and alginate also increases the production of IL-1β, and GM-CSF, while not statistically significant (**Figure 4.3b**). Furthermore, addition of pCM significantly reduces TNFα and IL-6 secretion from alginate-stimulated RAW macrophages (**Figure 4.3b**).

To further validate the immunomodulatory effect of pCM on macrophages, we tested the level of CD68 marker on macrophages. CD68 upregulation is one of the biomarkers for macrophage activation in response to inflammatory stimuli,[8, 61] including TLR4 stimulation.[62] From the cultures, macrophages were then collected and analyzed for the CD68 expression (**Figures 4.3c**). **Figure 4.3d** demonstrates the quantification of CD68+ population, revealing that CD68 is upregulated via both doses of UPLVG stimulation. CD68 expression on native RAW macrophages was 1.41% ± 0.60%, which 0.125 mg/mL alginate increased CD68 expression to 5.89% ± 0.35%, and addition of pCM reduced it to 2.71% ± 0.63% (p = 0.005). Moreover, 1.25 mg/mL alginate upregulated CD68 expression on RAW macrophages to 7.64% ± 2.1%, while addition of pCM to the culture reduced it to 2.91% ± 1.20% (p = 0.008). It should be noted that RAW cell line does not fully mimic the macrophage responses [63], however, in the

context of inflammatory response with various stimuli (such as LPS) and cytokine secretion, RAW cells are valuable for assessing macrophage responses [64, 65].

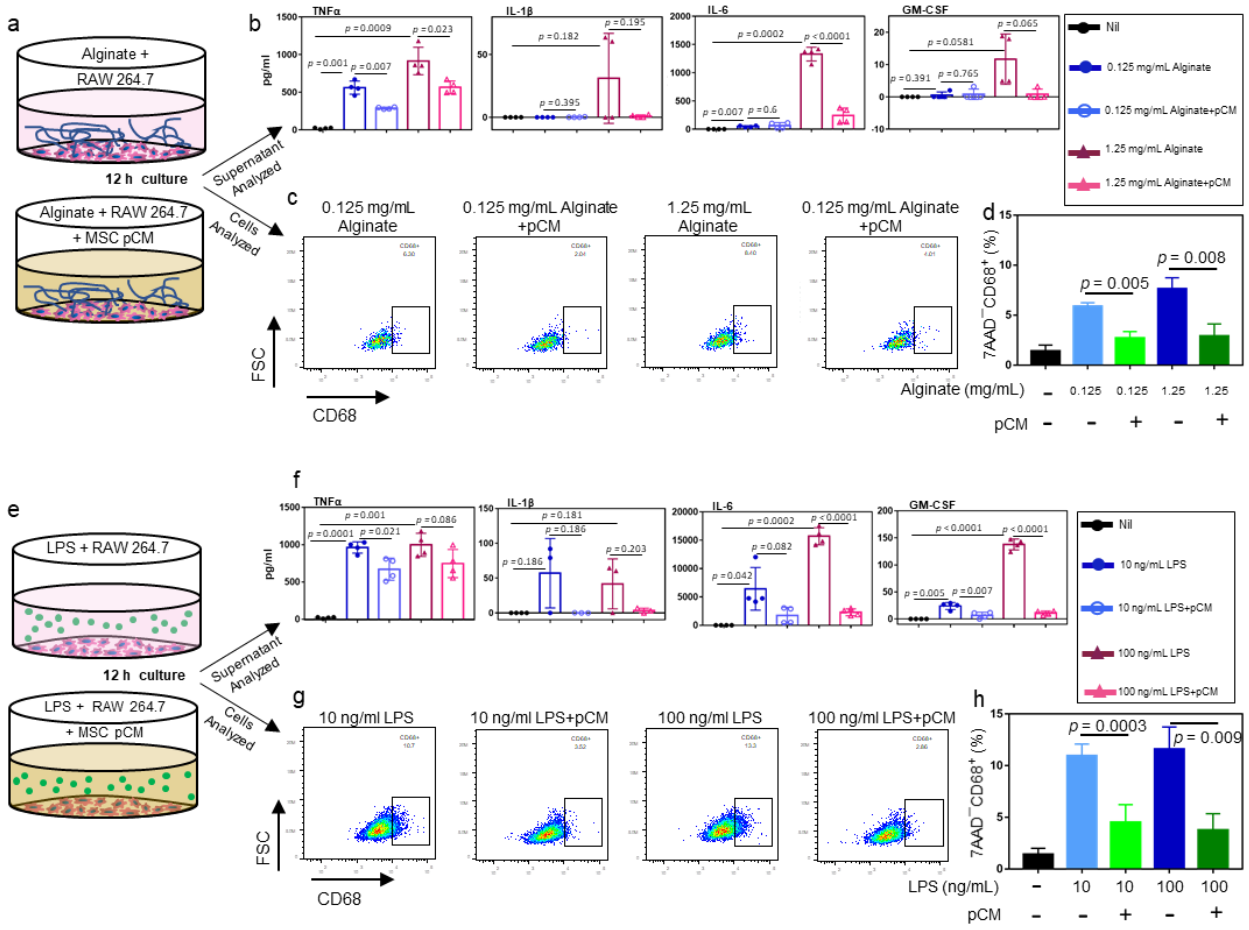

Figure 4.25. pCM reduces the inflammatory response in activated macrophages. a) Schematic representation of macrophages cultured with alginate in the presence and absence of pCM. **b)** addition of 0.125 or 1.25 mg/mL of alginate to the macrophages enhances the secretion of TNFα, IL-1β, and IL-6. Presence of pCM in the cultures significantly reduces the secretion of these cytokines. **c, d)** alginate upregulates the CD68 expression of RAW macrophages, while addition of pCM to the cultures reduces CD68 expression. CD68 expression on native RAW macrophages was 1.41% ± 0.60%. CD68 expression increased to 5.89% ± 0.35% in the presence of 0.125 mg/mL, while addition of pCM reduced it to 2.71% ± 0.63% (p = 0.005). Addition of 1.25 mg/mL alginate upregulated the CD68 expression to 7.64% ± 1.10%, while addition of pCM reduced it to 2.91% ± 1.20% (p = 0.008). **e)** schematic representation of macrophages cultured with LPS in the presence and absence of pCM. **f)** addition of 10 or 100 ng/mL of LPS to the RAW macrophages upregulates the secretion of TNFα, IL-1β, IL-6, and GM-CSF, and addition of pCM significantly reduces these secretions. **g, h)** CD68 expression for the culture with 10 ng/mL and 100 ng/mL LPS was 10.96% ± 3.93% and 11.59% ± 2.75%, respectively. Addition of pCM to the culture reduced the CD68 expression to 4.53% ± 1.39% for the former (p = 0.0003), and 3.78% ± 1.29% for the later (p = 0.009). Statistical analysis was done by unpaired t-test analyses with Welch's correction.

To test the validity of these observations under a more potent stimulatory conditions, we used LPS as a strong TLR4 agonist. **Figure 4.3e** shows the schematic representation of experimental procedure, where macrophages were incubated with 10 and 100 ng/mL of LPS for

12 h in the presence or absence of pCM. LPS activated macrophages with a similar trend as UPLVG, although the amount of cytokine secretion was higher via LPS activation (**Figure 4.3f**), and presence of pCM reduced the TNFα, IL-6, and GM-CSF cytokine secretion. These results suggest that pCM possesses immunomodulatory effects on murine macrophages when activation is partly through LPS stimulation. The CD68 expression for the culture with 10 ng/mL and 100 ng/mL LPS was 10.96% ± 3.93% and 11.59% ± 2.75%, respectively. Addition of pCM to the culture reduced the CD68 expression to 4.53% ± 1.39% for the former (p = 0.0003), and 3.78% ± 1.29% for the later (p = 0.009) (**Figure 4.3 g, h**).

These results in their totality suggest that pCM inhibits alginate- or LPS-induced activation of murine macrophages. We specifically have focused on macrophages due to their critical role in the long-term functionality of the implants. Macrophage depletion by clodrosome (liposomal clodronate) has shown to prevent fibrosis against alginate[19, 21] and poly(ethylene glycol)[66] implants. It is therefore concluded that the anti-fibrotic effect of pCM is partly due to their macrophage suppression.

Given that mouse biology doesn't always predictably model human biology, and to better understand some of the cellular pathways underlying the reduction of macrophage activation, we further pursued studying the interaction of pCM with human macrophages. Based on our earlier findings here, pCM dampens the secretion of inflammatory cytokines from macrophages that are hallmarks of NFκB pathway (i.e. IL-6, TNFα, GM-CSF, and IL-1β). It is also known that through agonistic interaction with TLR4, LPS activates an IKK complex, phosphorylating IκB proteins. Upon phosphorylation, IκB gets ubiquitinated, which liberates NF-κB/Rel complexes. Activated NF-κB/Rel complexes are further activated by post-translational modifications and translocate into nucleus to induce target gene expression, including IL-6, IL-1, and TNFα in

activated macrophages.[67] We particularly hypothesized that pCM downregulates/interferes with the activation of NFκB pathway. We therefore repeated the stimulation of macrophages in NFκB reporter THP-1 human cell lines, which are integration of an NFκB-inducible secreted embryonic alkaline phosphatase (SEAP) reporter construct. As a result, these cells could quantitatively measure NF-κB activation by determining the activity of SEAP.

We found that pCM reduces the NFκB activation in both 10 and 100 ng/mL LPS stimulation. **Figure 4.4a** shows the representative images of the SEAP activity (NFκB activation) as a result of 10 and 100 ng/mL LPS stimulation in the presence and absence of pCM. Luminescence count from IVIS imaging was quantified using equivalent regions on interest (**Figure 4.4b**), suggesting that pCM is a potent inhibitor of LPS induced NFκB activation. Same conditions were replicated, and signals were acquired using a plate reader, demonstrating a similar trend in the potency of pCM to inhibit NFκB activation (**Figure 4.4c**). Addition of pCM to the culture, reduced the luminescence counts of 10 ng/ml LPS activated THP-1 cells from 1084.2 ± 186.2 to 116.0 ± 66.5 ($p < 0.0001$).

Different pathways have been associated to biomaterials fibrosis including NFκB,[68-70] colony stimulating factor receptor,[19, 21] and JAK/STAT.[25, 71, 72] NFκB regulates multiple aspects of innate and adaptive immunity, and plays a critical role in regulating the function, activation, and survival of innate immunocytes and inflammatory T cells.[67] NFκB pathway has been reported in response to PDMS,[22] poly(ethylene glycol),[68] and alginate,[69] and reduction in NFκB has been correlated with reduced fibrosis.[22, 25] Similar to observations in the present study, other works have also reported the reduction in NFκB activation with secretome of MSCs.[32, 73, 74] We therefore could conclude that one mechanism by which

pCM-Alg demonstrates lower FBR is due to the reduction of NFκB activation of macrophage on, or around microcapsules.

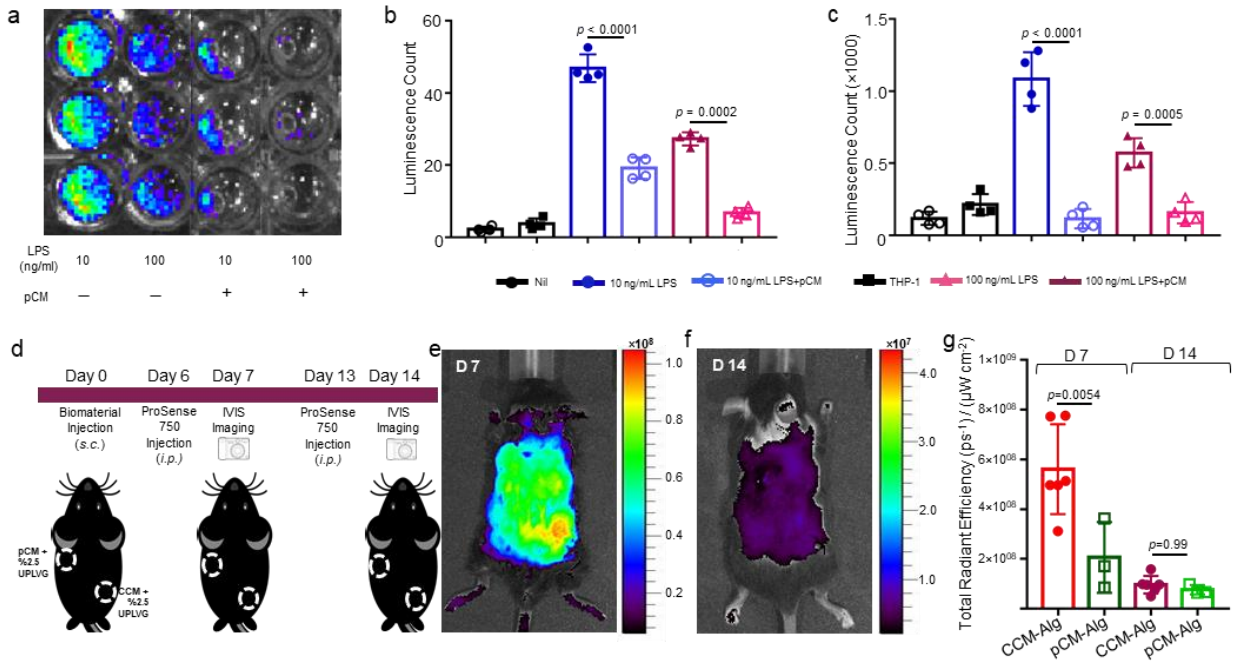

Figure 4.26. pCM reduces inflammatory response partly through regulation of NFκB pathway. a) representative IVIS images of the SEAP activity (NFκB activation) as a result of 10 and 100 ng/mL LPS stimulation in the presence and absence of pCM. **b)** luminescence count from IVIS imaging was quantified using equivalent regions on interest, suggesting that pCM is a potent inhibitor of LPS induced NFκB activation. **c)** Same conditions were replicated, and signals were acquired using a plate reader, demonstrating a similar trend in the potency of pCM to inhibit NFκB activation. For instance, addition of pCM to the culture, reduced the luminescence counts of 10 ng/ml LPS activated THP-1 cells from 1084.2 ± 186.2 to 116.0 ± 66.5 ($p < 0.0001$). **d)** Study timeline of cathepsin activity measurements in C57/BL6 mice. **e, f)** representative IVIS images at 7 and 4 d after implantation. g) total radiant efficiency was quantified, where 7 d after implantation, inflammatory response against pCM-Alg mixture (n=3; $2.06\times10^8 \pm 1.42 \times 10^8$) was significantly lower than that of CCM-Alg (n=6; $5.61\times10^8 \pm 2.06 \times 10^8$), which is the mixture of CCM and alginate. Data is presented as mean ± SD. Statistical analysis was done by unpaired t-test analyses with Welch's correction.

To further validate the anti-inflammatory effects on pCM-Alg *in vivo*, we quantified the induction of cathepsin activity around the implants. Cathepsin is a protease that breaks down proteins and peptides in order to eliminate a foreign substrate. Cathepsin activity measurement has been established as a robust method to evaluate the inflammatory response against implanted biomaterials *in vivo* [19, 29, 75]. Mechanistically, TLR4 stimulation of macrophages has shown to indirectly increase cathepsin activity.[76] Cathepsin expression of macrophages increases in

response to TLR4 agonist, however, mRNA expression of cathepsin does not change. In addition, neutralizing antibodies against IL-1β, TNFα, IFN-β could inhibit the cathepsin upregulation. Thus, augmented cathepsin activity is reported to be through involvement of secreted cytokines.[76]

We thus quantified the cathepsin activity 7 and 14 days after implantation of alginate (**Figure 4.4d, e, f**). To control the effect of culture media on the cathepsin activity measurements, we used our standard CCM addition to the 2.5% alginate solution. We found that 7 d after implantation, inflammatory response against pCM-Alg mixture (n=3; $2.06\times10^8 \pm 1.42 \times 10^8$) is significantly lower than that of CCM-Alg (n=6; $5.61\times10^8 \pm 2.06 \times 10^8$), which is the mixture of CCM and alginate (**Figures 4.4d, f**). Therefore, pCM could reduce the inflammatory response against alginate both *in vitro* and *in vivo*.

Conclusion

Our study offers a biohybrid formulation that reduces the inflammatory response against alginate microcapsules. This biohybrid scaffold takes advantage of immunosuppressive capabilities of MSC secretory factors, where loading alginate microcapsules with these factors reduces immune infiltration around microcapsules and decrease the cathepsin activity of alginate *in vivo*. We found that alginate induces inflammatory response in murine macrophages in a dose dependent manner, leading to secretion of TNFα, IL-6, IL-1β, and GM-CSF. Addition of pCM to the media reduces the macrophage activation in response to alginate ad LPS, both of which partly activate macrophages through TLR4 pathway.

The pCM-Alg platform benefits from facile preparation method, which could easily be scaled-up for high-throughput manufacturing processed. In addition, through its controlled-release nature, many drug delivery and tissue regeneration applications could be further explored

using pCM-Alg. Specifically, pCM-Alg could regulate the fibrotic response against the implants, where other parenchymal cells could be formed around the microcapsules (as shown in **Figures 4.1e, f**). This could encourage the tissue regeneration and wound healing around the pCM-Alg platform. Moreover, finding a molecular mechanism underlying the anti-inflammatory effects of secretome (and also extracellular vesicles secreted by stem cells) seem to be very tedious. This complexity mainly originates from the complexity and variety of molecules (including proteins, coding and non-coding RNAs, and lipids) present in the secretome and extracellular vesicles.[35, 42] To address this complexity, at least partly, we here propose that mechanisms underlying the effect of complex biologics could be characterized through their interactions with activated immunocytes. This interaction could be analyzed with RNAseq of immunocytes, establishing consistency and potency assays for complex biologics.

Materials and Methods

Isolation of UCMSCs and Exosomes

Umbilical cords were collected from UC Irvine Medical Center. The subject population included healthy pregnant women at full-term gestation (>37 weeks), maternal age 18-40 years old, who gave birth at UCI Medical Center. Any known complicated pregnancies were excluded from the collection. Umbilical cord derived Mesenchymal Stem Cells (UC-MSCs) were isolated according to the previously published method with some modifications. Briefly, UCs were washed with PBS under a sterile laminar flow cell culture hood and were cut longitudinally to remove blood vessels. Tissues were then cut into 2-3 mm^3 segments and incubated with 0.09% collagenase Type II (Sigma) for 45 minutes at 37 °C in a humidified incubator with 5% CO_2. After digestion, tissues were passed through a 100 μ mesh sized filters. Cells were then centrifuged at 300 ×g and 4 °C for 20 mins and resuspended in DMEM/F12 (Gibco)

supplemented with 10% FBS, 1% penicillin/streptomycin and 1% L-glutamine. Cells transferred to 175 cm^2 flasks and incubated at 37°C in a humidified atmosphere with 5% CO_2. Flasks were left undisturbed for 2-3 days, after which the medium was changed to remove non-adherent cells. Collected UCMSCs were then characterized based on The International Society of Cellular Therapy position on minimal criteria for defining multipotent MSCs [77]. This criteria states that MSCs are plastic-adherent cells in standard culture conditions, and express CD105, CD146 and CD90, while lack expression CD45, which is consistent with the UCMSCs isolated in our study (**Figure 4.5**).

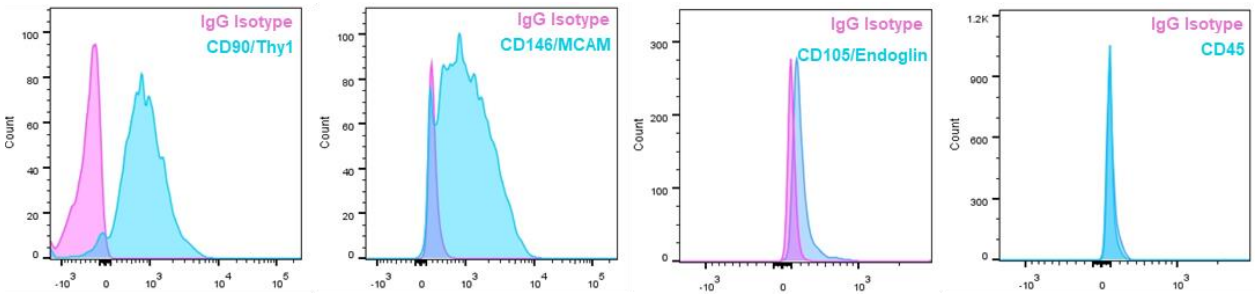

Figure 4.5. Umbilical Cord Derived Stem Cells (UCMSCs) Surface Biomarker. Cells were characterized for their surface markers, showing the expression of CD90/Thy1, CD146/MCAM, CD105/Endoglin, while cells are negative for CD45.

Collagen Quantification

To quantitatively compare the expression of collage in the fibrotic tissues around microcapsules, Masson's Trichrome Staining images were analyzed using a previously published method [78]. Using ImageJ software, images were formatted to RGB (Image →type), and image was separated into different colored sections using color deconvolution. Collagen (the blue color) was then separated into a new image using the task Image → Color→ Color Deconvolution → Masson Trichrome. To minimize possible noise levels, we adjusted the thresholds from 0 to 100 (Image→ Adjust→ Threshold). Next, using the region of interest manager (Analyze→ Tools→ ROI Manager), we drew a square around the entirety of the sample

using ImageJ's square tool. Measuring the area, the output was the area of the entire image as well as the percentage of that image that was blue and where collagen fibers were present.

Processing Condition Media

Umbilical cord derived MSCs (UCMSCs) were the source of MSCs in this study. We isolated and characterized UCMSCs (**Figure 4.5**), and these cells were the source of conditioned media use throughout the study. To prepare processed condition media (pCM), MSCs were expanded between passages 6-10. After reaching 70% confluency, fresh serum free media was added to the culture flasks and further cultured for 2 days. Collected media was then centrifuged at 300 ×g and 4 °C for 30 mins and 16500 ×g and 4 °C for 20 mins, which is known to remove dead cells and microvesicles. [35, 42] Supernatant were then collected and named as processed Conditioned Media (pCM), which was then stored at -80 °C until use. It should be noted that maximum storage time was less than 1 year.

Exosomes Isolation

As previously described,[35] conditioned media from cultures of MSC cells grown as described above were centrifuged at 300 ×g for 10 minutes. Supernatant was collected and transferred to ultracentrifuge tubes (Polyallomer Quick-Seal centrifuge tubes 25×89 mm, Beckman Coulter). Samples were then centrifuged in a Beckman Coulter ultracentrifuge (Optima L-90 K or Optima XE- 90 Ultracentrifuge, Beckman Coulter) for 20 minutes at 16,500 ×g (Type Ti 45, Beckman Coulter), to remove microvesicles. Supernatant was then carefully collected and centrifuged for 2.5 h with a Type 45 Ti rotor at 4 °C at 120,000×g. Exosome pellet was resuspended in PBS and stored at -80°C.

Alginate Microcapsules Preparation

UPLVG alginate (NovaMatrix®, Sandvika, Norway) were fabricated by dissolving 2.5% w/v in 0.9% sterile saline solution and mounted on an air-driven electrostatic microcapsule generator (Nisco Engineering Inc., Oslo, Norway). The alginate solution was added dropwise into a sterile filtered (0.22 μm) gelling solution composed of sterile 20 mM barium chloride and 25 mM HEPES solution to generate circular microcapsules of ~350 microns in diameter. Alginate microcapsules loaded with pCM (pCM-Alg) microgels were prepared by lyophilization technique overnight. Microcapsules were first centrifuged at 100 ×g and 4 ℃ for 5 mins. Supernatant was discarded and 500 μL of a 10% PEG 400 and 8% glycerol solution per 3000 microcapsules was added. Samples were then frozen at -80 ℃ for 4 h and lyophilized for 12 h. Lyophilized microcapsules were then rehydrated by pCM (or cell culture media) on a rocking plate at 4 ℃ for 4 h with constant agitation at 500 rpm. Next, pCM-Alg microcapsules washed with sterile saline solution in triplicate for 1 minute each. Ctrl-Alg and CCM-Alg microcapsules were also further subjected to these steps and rehydration step was conducted with sterile saline solution and sera free culture media, respectively.

Microscopy

Sections were then cut into 5 μm slices and blocked with 2% rat serum and 2% BSA. Slides were then stained with DAPI (1:1000), AlexaFluor® 647 anti-αSMA (1:200), and FITC anti-CD68 antibodies (1:200). Total area of DAPI, CD68, and α-SMA were quantified using ImageJ (NIH, USA) and compared between AI and control group using unpaired t-test with Welch's correction (*n.s.* non-significant, $*p < 0.05$). To quantitatively compare the number of infiltrated cells, signal area was measured in similar magnifications and normalized by the total tissue area in the image.

Controlled Release Studies

Both pCM-Alg and CCM-Alg microcapsules (~1000) were incubated at 37 °C in a humidified incubator with 5% CO_2 for 48 h. At indicated timepoints after co-incubation (i.e. 8, 24, and 48 h), 1 mL of the culture supernatant were collected and 1 mL of sterile DPBS was replaces. Isolated proteins were then measured for protein quantity, and exosomal content. The results from protein quantity analyses were then depicted as total protein release versus time. Collected media from the cultures were then subjected to exosome isolation kit (ExoQuick ULTRA EV Isolation Kit CAT#: EQULTRA-20A-1) and isolated exosomes were then frozen at -80 °C until analysis. To count and visualize released exosomes, Nanoparticle Tracking Analysis (NTA) was performed using the Nanosight system (NS300 Malvern instruments, USA). Exosomes were analyzed based on light scattering using an optical microscope aligned perpendicularly to the beam axis. Continuous syringe pump flow was adjusted to be 100 μL/minute. A 60 s video was recorded and subsequently analyzed using NTA software.

In vitro cultures and cytokine analyses

RAW 264.7 cells were purchased from ATCC (CAT# TIB-71) and NFκB reporter Luc-THP-1 human cell lines were purchased from InvivoGen (CAT#: thpl-nfkb) employed for downstream experiments of this study. Passages 5-10 were cultured in RPMI 1640 supplemented with 10% of heat inactivated FBS in the presence of 1% penicillin/streptomycin and 1% L-glutamine. Cells were then stimulated with 10 and 100 ng/mL of LPS (Invitrogen, CAT#: 50-112-2025). In addition to LPS, 0.125 and 1.25 mg/mL of alginate were used for stimulation. Stimulated and non-stimulated cells were then mixed with diluted pCM (50%). To eliminate the possibility of media and/or growth factor effect on our analyses, pCM was mixed with fresh culture media (1:1 ratio) and control media was prepared using culture media and sterile DPBS

(1:1 ratio). Control cells, LPS stimulated cells in the presence and absence of 50% pCM, and non-stimulated cells in the presence and absence of 50% pCM (100,000 cells for each condition) were cultured for 10-14 h at 37 °C in a humidified incubator with 5% CO_2. Next, both cells and supernatant were collected for flow cytometry and cytokine analyses, respectively. Supernatants were centrifuges at 2500 ×g and 4 °C for 5 mins and stored at -80 °C. Samples were then shipped on dry ice to Eve Technologies (Calgary, Canada), where cytokines were analyzed using Mouse Focused 10-Plex Discovery Assay (MDF10).

Peripheral blood mononuclear cells (PBMCs) were isolated from buffy coats from healthy, anonymous blood donors (UCI institute for clinical and transitional science) by density gradient centrifugation (Ficoll-Pague plus, GE Healthcare. Dynabeads Human T-Activator CD3/CD28 for T Cell Expansion and Activation was used with 1:1 ratio of PBMCs:Dynabeads. The pCM was mixed with fresh culture media (1:1 ratio) and control media was prepared using culture media and sterile DPBS (1:1 ratio). DynaBeads were then added to isolated PBMCs in the presence and absence of pCM. Supernatants were collected and Luminex assay was used to analyze the secreted cytokines. 50 µl of PBMC culture supernatants were collected and either frozen at -80 °C or immediately analyzed using a human custom ProcartaPlex (11plex, ThermoFisher Scientific, Vienna, Austria) with Luminex 77. Results were then reported as Mean Fluorescence Intensity (MFI).

Flow Cytometry

As describe earlier, RAW 264.7 cells were stimulated with either LPS (10 and 100 ng/mL) or alginate (0.125 and 1.25 mg/mL) in the presence and absence of 50% pCM. 100,000 cells for each condition were cultured for 10-14 h at 37 °C in a humidified incubator with 5% CO_2. Next, cells were collected and stained with 7AAD (1:1000) and CD68 (1:200).

Western blotting

1 mL of released proteins from pCM-Alg and CCM-Alg were collected and subjected to exosome isolation using (ExoQuick ULTRA EV Isolation Kit CAT#: EQULTRA-20A-1). Around 20 µg of the released proteins were mixed with 1X RIPA (Cell signaling technologies, USA) buffer and sonicated for five minutes, three times, with vortexing in between. Protein contents were measured using a BCA protein assay kit (Thermo Scientific Pierce, Rockford, IL, USA). Twenty-five µL of BSA standard or 25 µl of sample were transferred to a 96 well plate, and 200 ml working reagent was added. The plate was incubated for 30 minutes at 37 °C and absorbance was analyzed with a SpectraMax 384 Plus spectrophotometer at 562 nm and the SoftMax Pro software (Molecular Devices, 1311 Orleans Drive, Sunnyvale, CA, USA). 20 µg of protein from each sample was then separated on a gradient precast polyacrylamide gel (Mini-PROTEAN®; Bio-Rad laboratories, Hercules, CA, USA). Samples were then transferred onto a nitrocellulose membrane which was then blocked with 5% Blotting Grade Blocker Non-Fat Dry Milk (Bio-Rad Laboratories) in Tris-buffer saline supplemented with %0.1 Polysorbate 20 (TBST) overnight at 4 °C. Membrane was then washed with TBST incubated with primary antibodies against Calnexin (1:1000; clone H-70; Santa Cruz Biotechnology, Santa Cruz, CA, USA), Galectin-1/LGALS1 (D608T) Rabbit mAb (Cat# 12936), and TSG101 (1:1000; clone 4A10; Abcam, Cambridge, UK) dissolved in 0.25% Blotting Grade Blocker Non-Fat Dry Milk in TBST overnight at 4 ºC. Next, membrane was washed with TBST for 10 minutes, three times. Secondary antibodies (Calnexin: (1:2500) ECL anti-rabbit IgG horseradish peroxidase-linked F(ab')2 fragment (donkey, anti-rabbit); for TSG101: (1:2000) ECL anti-mouse IgG horseradish peroxidase-linked F(ab')2 fragment (sheep, anti-mouse); GE Healthcare, Buckinghamshire, UK) were diluted in 0.25% Blotting Grade Blocker Non-Fat Dry Milk in TBST and incubated for 1.5 hours. Membranes were analyzed with ECL Prime Western Blotting Detection (GE Healthcare)

and a VersaDoc 4000 MP (Bio-Rad Laboratories).

IVIS Imaging

NFκB reporter Luc-THP-1 human cell lines were (InvivoGen, San Diego USA) were used which are integration of an NFκB-inducible secreted embryonic alkaline phosphatase (SEAP) reporter construct. These cells are engineered THP-1 monocyte cell line by stable integration of an NF-κB-inducible Luc reporter construct. The levels of NF-κB-induced secreted luciferase in the cell culture supernatant are readily assessed with Quanti-Luc (CAT#: rep-qlc2). As a result, these cells could quantitatively measure NF-κB activation by determining the activity of SEAP. Cell were cultured in a phenol free media and supernatants (as described in the *in vitro* culture section of the methods) were collected. QUANT-Luc assay solution was added with a concentration of 1 mg/mL and incubated for 30 seconds. The resulted plate was then imaged in an IVIS imager (or VersaDoc 4000 MP). Exposure time was adjusted as 0.2 sec, field of view 12.5, f number 16, and binning factor of 4 were selected as optimized acquisition settings.

To evaluate the inflammatory response against alginate, live animal imaging was conducted using IVIS imager to measure the cathepsin activity.[75] Mouse were fed alfalfa free meal to eliminate the fluorescence background. To minimize the inflammatory response due to surgical procedure, and to characterize the inherent inflammatory response against alginate, 180 μL of %2.5 alginate was mixed with 20 uL of PBS, CCM, or pCM. Each sample was then subcutaneously injected into opposite diagonal spaces on the mid-back of the male C57/BL6 mice (**Figure 4 d**). Six days after injection, 100 uL of ProSense 750 FAST (NEV11171, PerkinElmer Inc.) was injected intraperitoneally 18-24 h prior to image capturing session.

Whole-body IVIS imaging was then performed, and signals were quantified using equivalent regions of interest. At days 7 and 14 mice were scanned by IVIS Spectrum system (Xenogen, Caliper LifeScience). The mice were anesthetized with 2% isoflurane and oxygen and maintained at 1.5% isoflurane throughout the procedure. The settings of the IVIS Spectrum system were Exposure = 9.0, Binning = Medium, F-Stop = 4, Excitation = 710 nm and Emission = 780 nm.

Animal Studies

All animal procedures were performed under approved University of California Irvine, Institutional Animal Care and Use Committee (Protocol #: AUP-17-241). Around 3000 of pCM-Alg or CTRL-Alg microcapsules were implanted subcutaneously into 12-16 weeks old C57/BL6 male mice for two weeks. The mice were anesthetized using 2% Isoflurane USP-PPC (Pharmaceutical partners of Canada, Richmond, ON, Canada). The mouse back hairs were shaved mouse skin sterilized using ENDURE 400 Scrub-Stat4 Surgical Scrub (chlorhexidine gluconate, 4% solution; Ecolab Inc., Minnesota, USA) and 70% ethanol. Surgical procedures were conducted under a sterile laminar flow hood and sterility measures were strictly upheld to minimize possible surgery-induced infection or severe inflammation. To implant the scaffolds, one 3-5 mm incision was cut on the dorsal upper section of each mouse. Around 3000 microcapsules were dispersed in 500 μL sterile PBS and injected into the subcutaneous pocket within bottom dorsal section of each mice. The incisions were then sutured using Surgipro II monofilament polypropylene 6–0 (Covidien, Massachusetts, USA) and sterilized with Betadine (a 10% povidone-iodine solution for skin disinfection) to prevent possible infections. Additionally, buprenorphine (as HCL) (0.03mg/ml; Chiron Compounding Pharmacy Inc. Guelph, ON, Canada) was added to water bottles in the cages as a pain reliever. All animals were then carefully monitored for 5 days as our standard post-operational procedure. Upon explantation,

capsules were fixed in 4% formaldehyde at 4 °C overnight and embedded in paraffin. Whole mount explants were also stained and embedded on poly-l-lysine coated glass slides for confocal microscopy.

Statistical Analysis

Data are plotted as mean ± standard deviation (SD) and analyzed with the software GraphPad Prism. Statistical analysis is conducted using unpaired t-test with Welch's correction (n = 3 or 4 as indicated per experiment). Differences were considered statistically significant if the *p-value < 0.05).

1. Jafarkhani, M., et al., *Strategies for directing cells into building functional hearts and parts.* Biomaterials Science, 2018. **6**(7): p. 1664-1690.
2. Xie, X., et al., *Reduction of measurement noise in a continuous glucose monitor by coating the sensor with a zwitterionic polymer.* Nature Biomedical Engineering, 2018.
3. McClatchey, P.M., et al., *Fibrotic Encapsulation is the Dominant Source of Continuous Glucose Monitor Delays.* Diabetes, 2019: p. db190229.
4. Helton, K.L., B.D. Ratner, and N.A. Wisniewski, *Biomechanics of the Sensor-Tissue Interface—Effects of Motion, Pressure, and Design on Sensor Performance and the Foreign Body Response—Part I: Theoretical Framework.* Journal of Diabetes Science and Technology, 2011. **5**(3): p. 632-646.
5. Veiseh, O., et al., *Size- and shape-dependent foreign body immune response to materials implanted in rodents and non-human primates.* Nature Materials, 2015. **14**: p. 643.
6. Alagpulinsa, D.A., et al., *Alginate-microencapsulation of human stem cell–derived β cells with CXCL12 prolongs their survival and function in immunocompetent mice without systemic immunosuppression.* American Journal of Transplantation, 2019. **19**(7): p. 1930-1940.
7. Mohammadi, M.R., et al., *7 - Scaffolds implanted: what is next?*, in *Handbook of Tissue Engineering Scaffolds: Volume One*, M. Mozafari, F. Sefat, and A. Atala, Editors. 2019, Woodhead Publishing. p. 127-152.
8. Mohammadi, R., et al., *33: Immunomodulatory Stem Cells to Alleviate the Foreign Body Response Against Implanted Biomaterials.* Transplantation, 2019. **103**(9S2).
9. https://www.fda.gov/consumers/consumer-updates/what-know-about-breast-implants.
10. *https://www.accessdata.fda.gov/scripts/cdrh/cfdocs/cfRes/res.cfm?ID=176159*.
11. Mohammadi, M.R., et al., *Biohybrid Nanoparticles to Negotiate with Biological Barriers.* Small, 2019. **15**(34): p. 1902333.
12. Hotaling, N.A., et al., *Biomaterial Strategies for Immunomodulation.* Annual Review of Biomedical Engineering, 2015. **17**(1): p. 317-349.
13. Mitrousis, N., A. Fokina, and M.S. Shoichet, *Biomaterials for cell transplantation.* Nature Reviews Materials, 2018. **3**(11): p. 441-456.

14. Bookstaver, M.L., et al., *Improving Vaccine and Immunotherapy Design Using Biomaterials.* (1471-4981 (Electronic)).
15. Zhang, L., et al., *Zwitterionic hydrogels implanted in mice resist the foreign-body reaction.* Nature Biotechnology, 2013. **31**: p. 553.
16. Jansen, L.E., et al., *Zwitterionic PEG-PC Hydrogels Modulate the Foreign Body Response in a Modulus-Dependent Manner.* Biomacromolecules, 2018. **19**(7): p. 2880-2888.
17. Yesilyurt, V., et al., *A Facile and Versatile Method to Endow Biomaterial Devices with Zwitterionic Surface Coatings.* Advanced Healthcare Materials, 2017. **6**(4): p. 1601091.
18. Headen, D.M., et al., *Local immunomodulation with Fas ligand-engineered biomaterials achieves allogeneic islet graft acceptance.* Nature Materials, 2018. **17**(8): p. 732-739.
19. Farah, S., et al., *Long-term implant fibrosis prevention in rodents and non-human primates using crystallized drug formulations.* Nature Materials, 2019. **18**(8): p. 892-904.
20. Chen, T., et al., *Alginate Encapsulant Incorporating CXCL12 Supports Long-Term Allo- and Xenoislet Transplantation Without Systemic Immune Suppression.* American Journal of Transplantation, 2015. **15**(3): p. 618-627.
21. Doloff, J.C., et al., *Colony stimulating factor-1 receptor is a central component of the foreign body response to biomaterial implants in rodents and non-human primates.* Nature Materials, 2017. **16**: p. 671.
22. Moore, L.B., et al., *Loss of monocyte chemoattractant protein-1 alters macrophage polarization and reduces NFkappaB activation in the foreign body response.* Acta Biomaterialia, 2015(1878-7568 (Electronic)).
23. Bi, D., et al., *Alginate enhances Toll-like receptor 4-mediated phagocytosis by murine RAW264.7 macrophages.* International Journal of Biological Macromolecules, 2017. **105**: p. 1446-1454.
24. Fang, W., et al., *Identification and activation of TLR4-mediated signalling pathways by alginate-derived guluronate oligosaccharide in RAW264.7 macrophages.* Scientific Reports, 2017. **7**(1): p. 1663.
25. Moore, L.B. and T.R. Kyriakides. *Molecular Characterization of Macrophage-Biomaterial Interactions*. in *Immune Responses to Biosurfaces*. 2015. Cham: Springer International Publishing.
26. Jhunjhunwala, S., et al., *Neutrophil Responses to Sterile Implant Materials.* PLOS ONE, 2015. **10**(9): p. e0137550.
27. Rezaa Mohammadi, M., et al., *Immune response to subcutaneous implants of alginate microcapsules.* Materials Today: Proceedings, 2018. **5**(7, Part 3): p. 15580-15585.
28. Sadtler, K., et al., *Divergent immune responses to synthetic and biological scaffolds.* Biomaterials, 2019. **192**: p. 405-415.
29. Vegas, A.J., et al., *Combinatorial hydrogel library enables identification of materials that mitigate the foreign body response in primates.* Nature Biotechnology, 2016. **34**: p. 345.
30. Ma, M., et al., *Development of Cationic Polymer Coatings to Regulate Foreign-Body Responses.* Advanced Materials, 2011. **23**(24): p. H189-H194.
31. Spasojevic, M., et al., *Reduction of the Inflammatory Responses against Alginate-Poly-L-Lysine Microcapsules by Anti-Biofouling Surfaces of PEG-b-PLL Diblock Copolymers.* PLOS ONE, 2014. **9**(10): p. e109837.

32. Su, V.Y.-F., et al., *Mesenchymal Stem Cell-Conditioned Medium Induces Neutrophil Apoptosis Associated with Inhibition of the NF-κB Pathway in Endotoxin-Induced Acute Lung Injury.* International journal of molecular sciences, 2019. **20**(9): p. 2208.
33. Vigo, T., et al., *IFN-γ orchestrates mesenchymal stem cell plasticity through the signal transducer and activator of transcription 1 and 3 and mammalian target of rapamycin pathways.* Journal of Allergy and Clinical Immunology, 2017. **139**(5): p. 1667-1676.
34. Chen, C.-P.M.D.P.D., P.-S.P.D. Tsai, and C.-J.M.D.P.D. Huang, *Antiinflammation Effect of Human Placental Multipotent Mesenchymal Stromal Cells Is Mediated by Prostaglandin E2via a Myeloid Differentiation Primary Response Gene 88-dependent Pathway.* Anesthesiology: The Journal of the American Society of Anesthesiologists, 2012. **117**(3): p. 568-579.
35. Riazifar, M., et al., *Stem Cell-Derived Exosomes as Nanotherapeutics for Autoimmune and Neurodegenerative Disorders.* ACS Nano, 2019. **13**(6): p. 6670-6688.
36. Yin, J.Q., J. Zhu, and J.A. Ankrum, *Manufacturing of primed mesenchymal stromal cells for therapy.* Nature Biomedical Engineering, 2019. **3**(2): p. 90-104.
37. Shigemoto-Kuroda, T., et al., *MSC-derived Extracellular Vesicles Attenuate Immune Responses in Two Autoimmune Murine Models: Type 1 Diabetes and Uveoretinitis.* Stem Cell Reports, 2017. **8**(5): p. 1214-1225.
38. Lai, R.C., et al., *Exosome secreted by MSC reduces myocardial ischemia/reperfusion injury.* Stem Cell Res., 2010. **4**(3): p. 214-222.
39. Timmers, L., et al., *Reduction of myocardial infarct size by human mesenchymal stem cell conditioned medium.* Stem Cell Research, 2008. **1**(2): p. 129-137.
40. Vizoso, F.J., et al., *Mesenchymal Stem Cell Secretome: Toward Cell-Free Therapeutic Strategies in Regenerative Medicine.* International journal of molecular sciences, 2017. **18**(9): p. 1852.
41. Carreras-Planella, L., et al., *Immunomodulatory Effect of MSC on B Cells Is Independent of Secreted Extracellular Vesicles.* Frontiers in Immunology, 2019. **10**: p. 1288.
42. Mohammadi, M.R., et al., *Isolation and characterization of microvesicles from mesenchymal stem cells.* Methods, 2019.
43. Riazifar, M., et al., *Stem Cell Extracellular Vesicles: Extended Messages of Regeneration.* Annual Review of Pharmacology and Toxicology, 2017. **57**(1): p. 125-154.
44. Vickers, K.C., et al., *MicroRNAs are transported in plasma and delivered to recipient cells by high-density lipoproteins.* Nature Cell Biology, 2011. **13**(4): p. 423-433.
45. Lasser, C., *Mapping Extracellular RNA Sheds Lights on Distinct Carriers.* Cell, 2019. **177**(1097-4172 (Electronic)).
46. Lankford, K.L., et al., *Intravenously delivered mesenchymal stem cell-derived exosomes target M2-type macrophages in the injured spinal cord.* PLOS ONE, 2018. **13**(1): p. e0190358.
47. Bai, L., et al., *Effects of Mesenchymal Stem Cell-Derived Exosomes on Experimental Autoimmune Uveitis.* Scientific Reports, 2017. **7**(1): p. 4323.
48. Shabbir, A., et al., *Mesenchymal Stem Cell Exosomes Induce Proliferation and Migration of Normal and Chronic Wound Fibroblasts, and Enhance Angiogenesis In Vitro.* Stem Cells and Development, 2015. **24**(14): p. 1635-1647.

49. Sun, Y., et al., *Human Mesenchymal Stem Cell Derived Exosomes Alleviate Type 2 Diabetes Mellitus by Reversing Peripheral Insulin Resistance and Relieving β-Cell Destruction.* ACS Nano, 2018. **12**(8): p. 7613-7628.
50. Zhao, J., et al., *Mesenchymal stromal cell-derived exosomes attenuate myocardial ischaemia-reperfusion injury through miR-182-regulated macrophage polarization.* Cardiovascular Research, 2019. **15**(1755-3245 (Electronic)).
51. Théry, C., et al., *Minimal information for studies of extracellular vesicles 2018 (MISEV2018): a position statement of the International Society for Extracellular Vesicles and update of the MISEV2014 guidelines.* Journal of Extracellular Vesicles, 2018. **7**(1): p. 1535750.
52. François, M., et al., *Human MSC Suppression Correlates With Cytokine Induction of Indoleamine 2,3-Dioxygenase and Bystander M2 Macrophage Differentiation.* Molecular Therapy, 2012. **20**(1): p. 187-195.
53. Nemeth, K., et al., *Bone marrow stromal cells attenuate sepsis via prostaglandin E(2)-dependent reprogramming of host macrophages to increase their interleukin-10 production.* Nat. Med., 2009. **15**(1): p. 42-49.
54. Del Fattore, A., et al., *Immunoregulatory Effects of Mesenchymal Stem Cell-Derived Extracellular Vesicles on T Lymphocytes.* Cell Transplantation, 2015. **24**(12): p. 2615-2627.
55. Bouffi, C., et al., *IL-6-Dependent PGE2 Secretion by Mesenchymal Stem Cells Inhibits Local Inflammation in Experimental Arthritis.* PLOS ONE, 2010. **5**(12): p. e14247.
56. Qi, Y., et al., *TSG-6 released from intradermally injected mesenchymal stem cells accelerates wound healing and reduces tissue fibrosis in murine full-thickness skin wounds.* J. Investig. Derm., 2013. **134**(2): p. 526-537.
57. English, K., et al., *Cell contact, prostaglandin E2 and transforming growth factor beta 1 play non-redundant roles in human mesenchymal stem cell induction of CD4+CD25Highforkhead box P3+ regulatory T cells.* Clinical & Experimental Immunology, 2009. **156**(1): p. 149-160.
58. Baraniak, P.R. and T.C. McDevitt, *Stem cell paracrine actions and tissue regeneration.* Regenerative Medicine, 2009. **5**(1): p. 121-143.
59. Paredes-Juarez, G.A., et al., *A Technology Platform to Test the Efficacy of Purification of Alginate.* Materials (Basel, Switzerland), 2014. **7**(3): p. 2087-2103.
60. Paredes-Juarez, G.A., et al., *The role of pathogen-associated molecular patterns in inflammatory responses against alginate based microcapsules.* Journal of Controlled Release, 2013. **172**(3): p. 983-992.
61. Tsukamoto, K., et al., *Synergically Increased Expression of CD36, CLA-1 and CD68, but Not of SR-A and LOX-1, with the Progression to Foam Cells from Macrophages.* Journal of Atherosclerosis and Thrombosis, 2002. **9**(1): p. 57-64.
62. Feng, H., I. Pyykkö, and J. Zou, *Involvement of Ubiquitin-Editing Protein A20 in Modulating Inflammation in Rat Cochlea Associated with Silver Nanoparticle-Induced CD68 Upregulation and TLR4 Activation.* Nanoscale Research Letters, 2016. **11**(1): p. 240.
63. Chamberlain, L.M., et al., *Phenotypic non-equivalence of murine (monocyte-) macrophage cells in biomaterial and inflammatory models.* Journal of Biomedical Materials Research Part A, 2009. **88A**(4): p. 858-871.

64. Saborano, R., et al., *Metabolic Reprogramming of Macrophages Exposed to Silk, Poly(lactic-co-glycolic acid), and Silica Nanoparticles.* Advanced Healthcare Materials, 2017. **6**(14): p. 1601240.
65. Kalluru, R., et al., *Poly(lactide-co-glycolide)-rifampicin nanoparticles efficiently clear BCG infection in macrophages and remain membrane-bound in phago-lysosomes.* Journal of Cell Science, 2013. **126**(14): p. 3043.
66. Haque, M.R., J.-H. Jeong, and Y. Byun, *Combination strategy of multi-layered surface camouflage using hyperbranched polyethylene glycol and immunosuppressive drugs for the prevention of immune reactions against transplanted porcine islets.* Biomaterials, 2016. **84**: p. 144-156.
67. Liu, T., et al., *NF-κB signaling in inflammation.* Signal Transduction and Targeted Therapy, 2017. **2**(1): p. 17023.
68. Amer, L.D., et al., *Inflammation via myeloid differentiation primary response gene 88 signaling mediates the fibrotic response to implantable synthetic poly(ethylene glycol) hydrogels.* Acta Biomaterialia, 2019.
69. Yang, D. and K.S. Jones, *Effect of alginate on innate immune activation of macrophages.* Journal of Biomedical Materials Research Part A, 2009. **90A**(2): p. 411-418.
70. Lawlor, C., et al., *Treatment of Mycobacterium tuberculosis-Infected Macrophages with Poly(Lactic-Co-Glycolic Acid) Microparticles Drives NFκB and Autophagy Dependent Bacillary Killing.* PLOS ONE, 2016. **11**(2): p. e0149167.
71. Moreno, J.L., et al., *IL-4 promotes the formation of multinucleated giant cells from macrophage precursors by a STAT6-dependent, homotypic mechanism: contribution of E-cadherin.* Journal of leukocyte biology, 2007. **82**(6): p. 1542-1553.
72. Mukherjee, S., et al., *Mesenchymal stem cell-based bioengineered constructs: foreign body response, cross-talk with macrophages and impact of biomaterial design strategies for pelvic floor disorders.* Interface Focus, 2019. **9**(4): p. 20180089.
73. van Buul, G.M., et al., *Mesenchymal stem cells secrete factors that inhibit inflammatory processes in short-term osteoarthritic synovium and cartilage explant culture.* Osteoarthritis and Cartilage, 2012. **20**(10): p. 1186-1196.
74. Liu, Y.-Y., et al., *Hypoxia-preconditioned mesenchymal stem cells ameliorate ischemia/reperfusion-induced lung injury.* PLOS ONE, 2017. **12**(11): p. e0187637.
75. Bratlie, K.M., et al., *Rapid biocompatibility analysis of materials via in vivo fluorescence imaging of mouse models.* PLoS One, 2010. **5**(4): p. e10032.
76. Creasy, B.M. and K.L. McCoy, *Cytokines regulate cysteine cathepsins during TLR responses.* Cellular Immunology, 2011. **267**(1): p. 56-66.
77. Dominici, M., et al., *Minimal criteria for defining multipotent mesenchymal stromal cells. The International Society for Cellular Therapy position statement.* Cytotherapy, 2006. **8**(4): p. 315-317.
78. Chen, Y., Q. Yu, and C.-B. Xu, *A convenient method for quantifying collagen fibers in atherosclerotic lesions by ImageJ software.* Int J Clin Exp Med, 2017. **10**(10): p. 14904-14910.

CHAPTER 5

Islet Xenotransplantation in Diabetic Mice using Stem Cell Derived Immunomodulatory Microcapsules

Abstract

Immune-based foreign body response (FBR) to biomaterials compromises the function of the implants and leads to medical complications. Here, we report a hybrid alginate microcapsule (AlgXO) that controllably releases exosomes derived from Umbilical Cord Mesenchymal Stem Cells (XOs). Upon release, XOs suppress the local immune-microenvironment and mitigate the FBR against alginate microcapsules, where xenotransplantation of rat islets encapsulated in AlgXO led to > 5 months euglycemia in immunocompetent mouse model of Type 1 Diabetes. AlgXO significantly reduced the immune response in subcutaneous and intraperitoneal sites, while non-inflammatory fibrosis was observed in the subcutaneous space. *In vitro* analyses revealed that XOs suppressed the proliferation of CD3/CD28 activated splenocytes and CD3+ T cells. Comparing suppressive potency of XOs in purified CD3+ T cells versus splenocytes, we found XOs more profoundly suppressed T cells in the splenocytes coculture, where a heterogenous cell population presents. XOs also suppressed CD3/CD28 activated human peripheral blood mononuclear cells (PBMCs) and reduced their inflammatory cytokine secretion including IL-2, IL-6, IL-12p70, IL-22, and TNFα. We further confirmed that XOs mechanism of action is likely through myeloid cells and they suppress both murine and human macrophages partly through interfering with NfκB pathway. We believe that through its local controlled

release of XOs, AlgXO is a platform that could alleviate the local immune response to implantable biomaterials.

Keywords: Xenotransplantation; Type 1 Diabetes; MSC; Exosome; Immunosuppression; Foreign Body Response

Introduction

Transplantation of therapeutic cells have offered treatments for variety of diseases, including, β-cells replacement therapies [1], bone-marrow transplantation [2], and Parkinson's disease [3,4]. Engineerability of cells and their responsiveness to the environmental cues make them living factories that deliver therapeutic agents on demand and with appropriate dosing. The promise of cell-based therapies is hampered by safe and effective transplantation method. Transplanted cells can elicit strong immune response, especially if originate from non-syngeneic sources. Administration of immunosuppressive regimen (i.e. the non-steroidal anti-inflammatory agents) has been proposed to mute such immune responses, however, this approach may lead to detrimental side-effects including hepatocellular, cardiac or renal toxicities [5], gastrointestinal ulceration, bleeding and microbial dysbiosis [6,7].

One notable example of therapeutic cell transplantation is the pancreatic islet transplantation to treat Type 1 Diabetes (T1D), which has stimulated ~50 years of research and clinical trials. Human trials on islet transplantation initiated with the Edmonton protocol, suggesting > 5 years efficacy in some cases [8,9]. However, adverse events through daily administration of immunosuppressive regimen as well as lack of allogeneic cell donors further compromised the clinical practice of Edmonton protocol [7]. Encapsulation of islets within a protective biomaterial has been considered to eliminate the chronic immunosuppression [10]. Dating back to the 80s, islet transplantation within alginate microcapsules were found to prolong the glycemic correction in diabetic rodents [11]. However, limited therapeutic efficacy and transient glycemic control have been reported in follow up human trials of islet transplantation within alginate microcapsules [10,12-14]. This suggests the restricted functionality of transplants

through islet death and/or loss of mass transfer inwards and outwards of microcapsules. Main reasons behind the graft failure are likely to be the islet necrosis (due to the lack of nutrients and oxygen accessibility within the microcapsules) [15], as well as immune-mediated pericapsular growth and fibrosis [16-22]. The latter is also known as foreign Body Response (FBR), which creates patients discomfort and variety of health complications [23-25].

Preventing the transplantation-led inflammatory response reduces pericapsular overgrowth and fibrosis. Many studies have demonstrated that islet transplantation within immune-modulator or immune-insulator microcapsules provide long-term euglycemia in immunocompetent diabetic rodents [1,20,26-28]. Various strategies have been employed to modulate and/or mute the local immune response against implants, including the surface bound immunomodulatory ligands [27], anti-biofouling surface modification [26,29,30], and controlled release of anti-inflammatory agents. The controlled-release (or drug eluding) biomaterials could hold and release variety of anti-inflammatory and/or immunomodulatory molecules overtime (e.g. dexamethasone [31], IL-4 [32], CSF-1R inhibitor [20], and CXCL12 [28,33]). There are two main possible drawbacks with some of the molecular target inhibitors. The first issue is the potential side effects associated with these agents. For instance, CSF1R inhibitors can elicit fatigue/asthenia, edema [34] and nonreversible grade 3 deafness [35], and CXCL12 causes toxicity in cerebrocortical neurons [36]. Other molecular targets such as TNFα inhibitors and anti-TGFβ compounds are also linked to variety of complications in clinical trials [37,38]. The second challenge with molecular inhibitors lies in their inability to regulate multitude of inflammatory pathways involved against biomaterials transplants, including NFκB [39-41], CSF1R [17,20], and JAK/STAT [42-44] pathways. Thus, it is speculated that the controlled release of agents that regulate multiple inflammatory pathways

is likely to better mute the inflammatory response against implants compared to agents that interfere with single targets.

In this context, Mesenchymal Stromal Cells (MSCs, also named as medicinal signaling cells) are recognized to regulate variety of inflammatory pathways including NFκB [45], JAK/STAT [46], MyD88 [47], PI3K/AKT [48] and downstream of PGE2 [49]. The current paradigm of MSC treatment is through paracrine factor, which could partly be attributed to exosomes (XOs) [49,50]. Indeed, XOs are recognized to recapitulate the properties as MSCs [48,51-54]. While detailed mechanisms behind immunomodulatory effects of XOs are not yet fully elucidated, hybridization of RNAs, proteins, and lipids in a single nanosized platform have provided them with the capability to interact with and regulate the function of macrophages [55], NK cells [56,57], B cells[58,59], and T-lymphocytes [60]. We thus hypothesized that encapsulation of XOs within alginate microcapsules (AlgXO) alleviates the FBR. Upon blocking the inflammation, we next hypothesized that transplantation of rat islets within AlgXO prolongs the function of transplanted islets in immunocompetent diabetic mice.

Islet xenotransplantation within AlgXO microcapsules delays the graft rejection

We first isolated XOs from umbilical cord derived MSCs (UC-MSCs) and characterized UC-MSCs and the size, number, and protein biomarkers of their XOs (described in **Materials & Methods** and **Figure 5.1**). Adherent cells were then characterized for surface markers to further confirm their MSC origin. **Figure 5.1a** shows that isolated cells have low expression of Stro-1, high expression CD90/Thy1, CD146/MCAM, CD105/Endoglin, CD166, CD44 while cells are negative for CD19, CD45 and CD106. Such expression profiles are consistent with previous

reports [61,62]. XOs were characterized according to an established protocol by International Society of Extracellular Vesicles, where CD63, TSG101, GAPDH, Galectin-1, and Hsp70 were present while and endoplasmic reticulum marker, Calnexin, was absent (**Figure 5.1b**).

We recently performed similar analyses for bone marrow derived MSC derived exosomes [48] and microvesicles [51], and found that Calnexin marker can be used as one of the markers to distinguish between exosomes and microvesicles as well as XOs purity. Comparing the Western blotting results from MSC derived MVs and MSC derived exosomes [48] suggest that calnexin and CD81 may potentially be used to distinguish between exosomes and MVs. XOs were visualized and quantified using NTA analysis, where $1.7 \times 10^{12} \pm 7.6 \times 10^{11}$ XOs/mL spherical particles with average diameter 105 ± 48 nm were isolated from ~ 150 to 190 million cultured MSCs in 100% confluency (**Figure 5.1c**).

XOs were labeled with anti-CD63-modified magnetic beads (Exosome Isolation CD63, Lot OK527, Life Technologies AS, Oslo, Norway) overnight with gentle agitation. The beads were washed with 1% exosome-depleted FBS in PBS and then incubated with human IgG (Sigma-Aldrich) for 15 minutes at 4°C. Following another washing step, the beads were incubated with PE-TGFβ, PE/Cy7-PD-L1 and APC/Cy7-MHCII or Isotype Controls (Biolegend, San Diego, USA) for 40 minutes with gentle agitation at room temperature. After another washing step, the samples were analyzed using a FACSAria (BD Bioscience) and data was processed using FlowJo Software (Tri Star, Ashland, OR, USA). Flow cytometry analysis of TGFβ, PD-L1, and MHCII expression on XOs bound to anti-CD63-coated beads demonstrated minimal expression of TGFβ-1 and MHCII, and the absence of PD-L1 (**Figure 5.1d**). We particularly sought to measure the expression of TGFβ-1 and PD-L1, as its expression on cancer

cells XOs has been suggested to play a critical role in the immune evasion of tumor microenvironment [63-65].

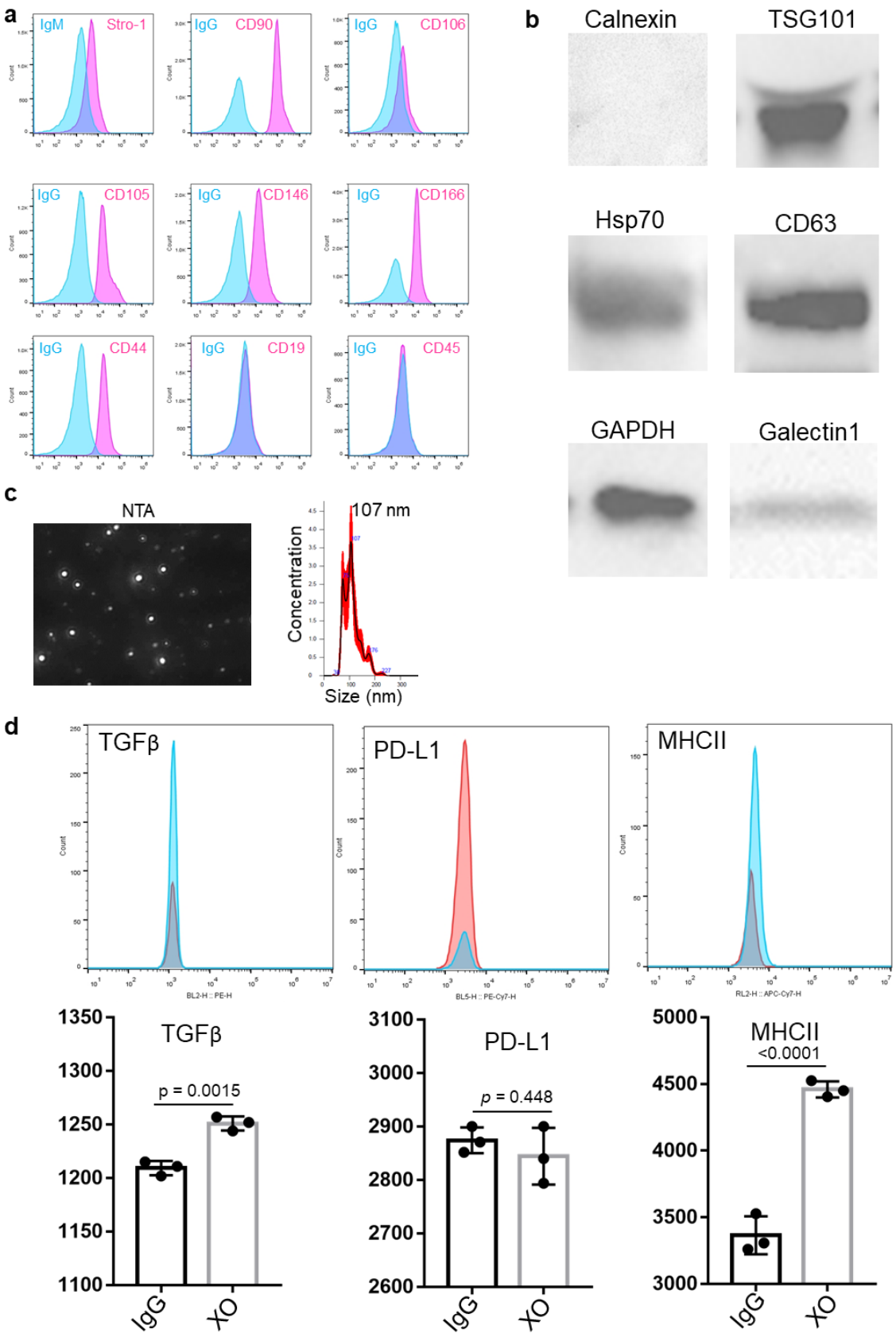
a
IgM
Stro-1
IgG
CD90
IgG
CD106
IgG
CD105
IgG
CD146
IgG
CD166
IgG
CD44
IgG
CD19
IgG
CD45
b
Calnexin
TSG101
Hsp70
CD63
GAPDH
Galectin1
c
NTA
107 nm
Concentration
Size (nm)
d
TGFβ
PD-L1
MHCII
BL2-H :: PE-H
BL5-H :: PE-Cy7-H
RL2-H :: APC-Cy7-H
TGFβ
p = 0.0015
PD-L1
p = 0.448
MHCII
<0.0001
IgG
XO

Figure 5.27. Umbilical Cord Derived Stem Cells (MSCs) and their secreted XOs characterization. **a)** Cells were characterized for their surface markers, showing the low expression of Stro-1, high expression CD90/Thy1, CD146/MCAM, CD105/Endoglin, CD166, CD44 while cells are negative for CD19, CD45 and CD106. Cells were then cultured as described in the Materials & Methods section, and XOs were isolated. **b)** Isolated XOs were then characterized using stablished biomarkers using Western blotting. XOs were positive for CD63, Galectin 1, TSG101, HSP70, Hsp70, and negative for and endoplasmic reticulum marker Calnexin. **c)** XOs possess spherical shape with the 105 ± 48 nm as an average size for maximum quantity of vesicles, based on NTA analyses. It should be noted that in average, 1.7 X 10^{12} ± 7.6 X 10^{10} XOs/mL were isolated from ~ 150 to 190 million cultured MSCs in 100% confluency. **d)** Flow cytometry analysis of TGFβ, PD-L1, and MHCII expression on XOs bound to anti-CD63-coated beads. Statistical significance is calculated through unpaired t-test with Welch's correction.

Two type of microcapsules were fabricated, which are regular Ba^{2+} cross-linked UPLVG microcapsules (CTRL) and AlgXO. To fabricate AlgXO, we loaded XOs inside alginate microcapsules (**Figure 5.2a**).

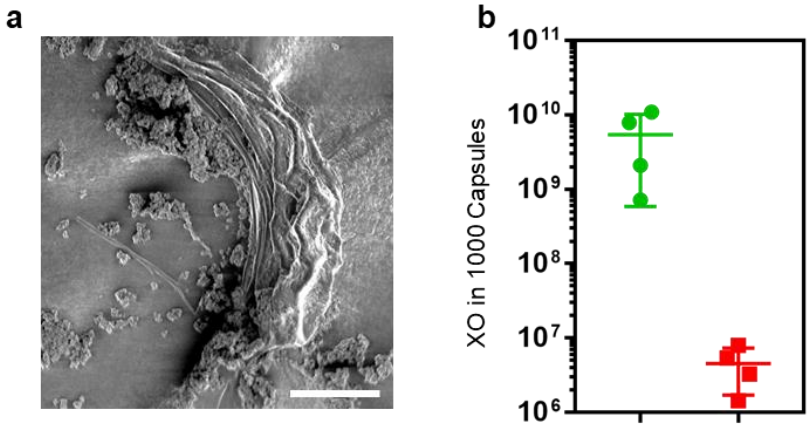

Figure 5.28. a) Freeze-Fractured Scanning Electron Microscopy of an AlgXO microcapsule, showing the encapsulated XOs within the microcapsules (Scale = 100 μm). **b)** total number of exosome encapsulated within ~1000 AlgXO microcapsules is 5.43 × 10^9 ± 4.84 × 10^9 using NTA analysis. (n = 4 separate preparation)

To quantify XOs within AlgXO, we dissolved microcapsules and collected XOs through ultracentrifugation (further described in **Materials & Methods** and **Figure 5.3**). Total number of XOs within ~1000 AlgXO was 5.43 × 10^9 ± 4.84 × 10^9 (n = 4), whereas XOs within CTRL microcapsules were below the detection limit of NTA (**Figure 5.2b**).

We then sought to investigate the functionality of islet transplantation within AlgXO microcapsules. Rat islets (1500 IEQ) were encapsulated either in AlgXO or CTRL microcapsules

and transplanted into the i.p. cavity of STZed C57/BL6 mice with a week-long established hyperglycemia (n = 5).

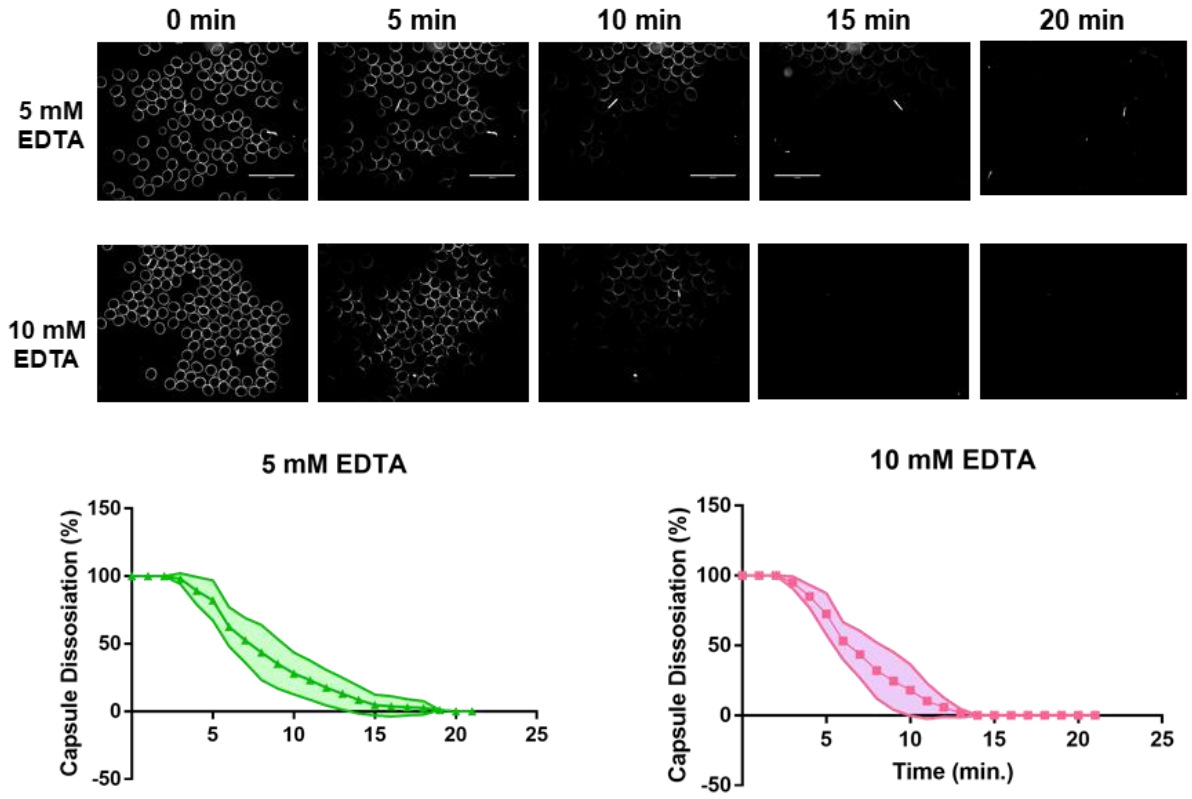

Figure 5.29. EDTA dissolves alginate microcapsules. CTRL microcapsules (n = 100) were dissolved in 5 or 10 mM EDTA, and microscopic images were taken in 1 min intervals using EVOS imaging system microscope.

To assure the purity and quality of rat islets from each isolation and minimize the batch to batch variations between islets, we conducted quality control for every batch (described in **Materials & Methods** and **Figure 5.4**).

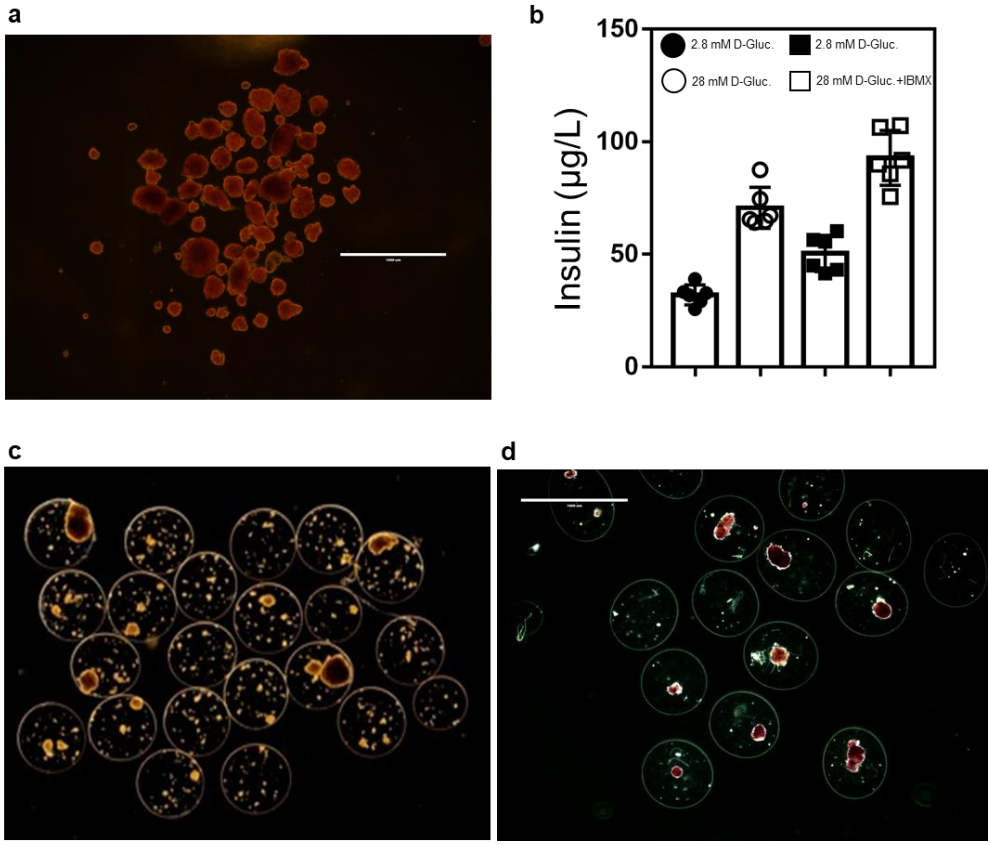

Figure 5.30. Islets quality control. After each islet isolation, we ran quality control measurements. a) DTZ staining to quantify the islet purity and count (947 ± 137 IEQ). **b)** Glucose Stimulation Insulin Release (GSIR) test is run to validate the functionality of the isolated islets. Encapsulated c) CTRL microcapsules and d) AlgXO microcapsules

Figure 5.5a shows that transplantation of rat islets within AlgXO provided euglycemia in diabetic mice for > 5 months, whereas the islets transplanted within CTRL microcapsules functionally failed to regulate mice hyperglycemia within a month. To assure that the glycemic correction is due to AlgXO transplants and not pancreatic regeneration in diabetic mice, we removed the AlgXO transplants after 105 days of transplantation by washing the i.p. cavity. Within 16 hours of graft removal, mice non-fasting blood glucose elevated and remained hyperglycemic (dashed green line, **Figure 5.5a**). To control the effect of AlgXO on the maintenance of hyperglycemia in the STZ mice, empty AlgXO microcapsules (*i.e.* without

pancreatic islets) were also transplanted into the i.p. cavity of STZed C56/BL6 mice, but they failed to reverse hyperglycemia (**Figure 5.6**). We particularly designed this experiment because a recent study had reported that intravenous injection of UC-MSCs derived XOs into STZ mice promoted expression and membrane translocation of glucose transporter 4, and reduced the hyperglycemic severity [66].

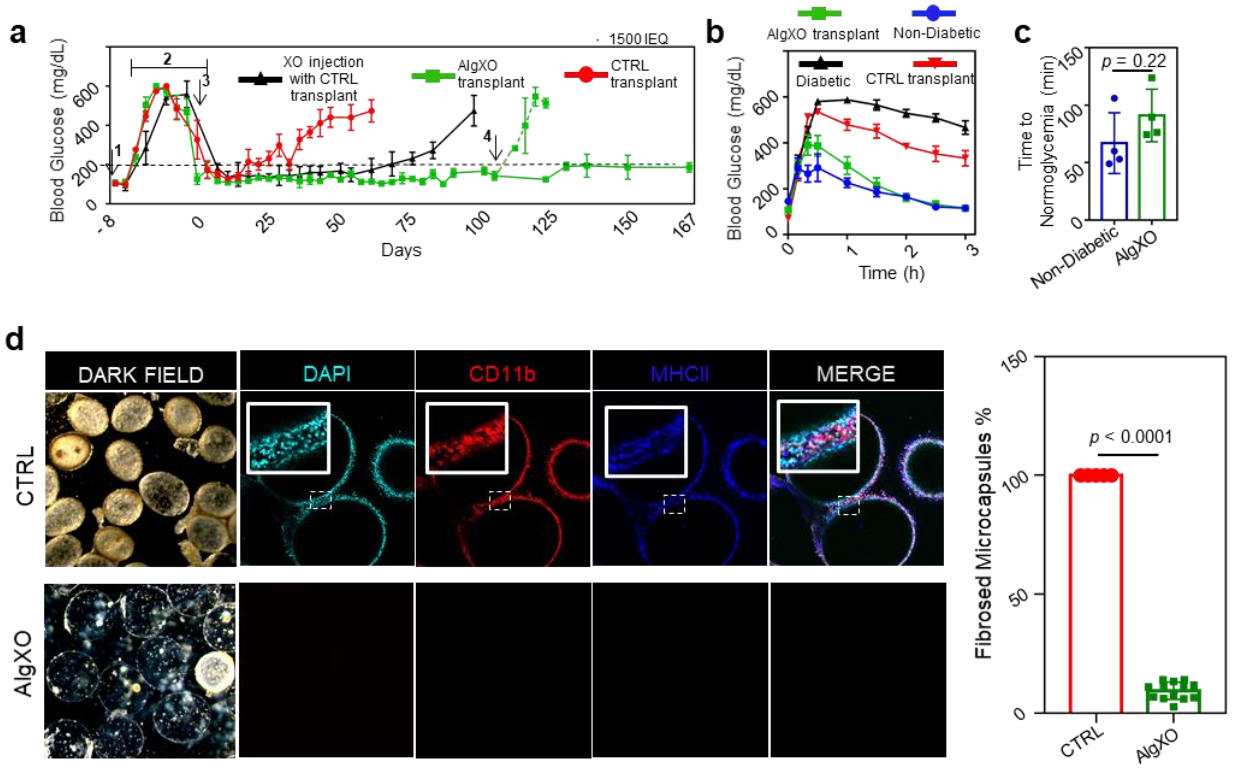

Figure 5.31. Islet xenotransplants within AlgXO reverses hyperglycemia in diabetic immunocompetent mice. a) Non-fasting blood glucose levels in C57/BL6 STZ mice (n = 5) shows that transplantation of 1500 IEQ rat islets within AlgXO provided euglycemia in diabetic mice for > 5 months, whereas the CTRL microcapsules failed in less than 1 month. To further confirm that the glycemic correction is merely due to transplants and not pancreatic regeneration in STZ mice, we washed the i.p. cavity of mice and removed the explants after 105 days of transplantation (n = 2). Within 18 hours of graft removal, mice blood glucose elevated and remained hyperglycemic for the rest of their lifetime (dashed green line). Separate i.p. transplantation of islets within CTRL microcapsules and XOs provided normoglycemia for ~70 days (black line) (n = 4). **b)** We further tested the efficacy of AlgXO transplants in response to oral glucose tolerance test (OGTT). One month after transplantation, similar to STZ mice (n = 3), CTRL microcapsules failed to regulate the glucose levels (n = 4), whereas AlgXO transplants successfully reversed hyperglycemia event induced by glucose challenge (n = 4), with similar trend as non-diabetic controls. **c)** The average time to reach normoglycemia after an OGTT for non-diabetic mice was 67 ± 26 minutes and for mice with AlgXO transplants was 91 ± 21 minutes (n = 4). It should be noted that blood glucose of 200 mg/dL was chosen as the threshold for normo- vs. hyper-glycemia. This suggest a slight delay in glucose response of mice received AlgXO transplants versus non-diabetic mice, while the difference was not statistically significant (p = 0.22). **d)** After one month, both CTRL and AlgXO (from 1500 IEQ group) transplants were removed through washing the i.p. cavity. Next, microcapsules were analyzed for the immune-infiltration (also known as pericapsular cell growth) with laser scanning confocal microscopy. Some cells were CD11b+ and some of the CD11b+ cells were expressing MHCII biomarker. All the collected CTRL microcapsules were found to have pericapsular cells attached to

the surface, while the percentage of AlgXO transplants with pericapsular growth was 9.4% ± 3.6%, which was significantly lower than CTRL transplants ($p < 0.0001$). Statistical significance is calculated through unpaired t-test with Welch's correction.

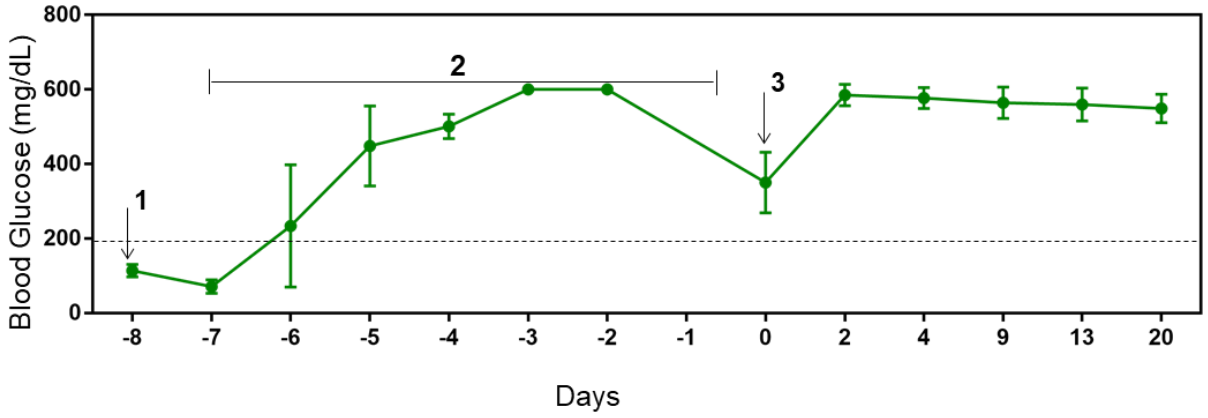

Figure 5.32. Transplantation of AlgXO microcapsules without islets failed to reverse hyperglycemia in STZ mice. Empty (without islets) AlgXO microcapsules could not reverse the hyperglycemia in diabetic mice.

We next asked whether the *in vivo* function of islet xenotransplants could be prolonged by administration of non-encapsulated XOs. We thus transplanted 1500 IEQ rat islets in CTRL microcapsules, and at the same time, injected (i.p.) $8.1 \times 10^9 \pm 7.3 \times 10^9$ XOs (n = 4). This dose was chosen to be consistent with the dose of XOs in AlgXO xenotransplant studies conducted earlier. Administration of non-encapsulated XOs at the time of islet transplantation in CTRL microcapsules extended the euglycemia in diabetic mice for 2 months (**Figure 5.5a**), although not as prolonged as AlgXO transplants. We further tested the efficacy of AlgXO transplants in response to oral glucose tolerance test (OGTT) after 1 month of transplantation (**Figure 5.5b**). After 30 mins of glucose challenge onset, the non-diabetic mice blood glucose reached to 291 ± 120 mg/dL (n = 4). During the same time, the blood glucose of mice transplanted with islets in AlgXO and CTRL microcapsules were 386 ± 91 mg/dL and 534 ± 9 mg/dL, respectively (n = 4). This number was 580 ± 28 mg/dL for diabetic mice (n = 3). We set the 200 mg/dL as the blood glucose threshold between diabetic (hyperglycemic) and non-diabetic (normoglycemic) mice. We then attempted to find the duration required for each mouse to reach 200 mg/dL after the

glucose challenge. Polynomials with degree 5 were assigned to the OGTT curve of every individual mice (**Figure 5.7a, b**), and time to normoglycemia was calculated based on the value of 200 for the polynomial functions. **Figure 5.5c** demonstrates that 67 ± 26 minutes is the average required time for non-diabetic mice to reach normoglycemia after an OGTT, and such duration was 91 ± 21 minutes for mice with AlgXO transplants. This suggest a slight delay in glucose response of mice received AlgXO transplants compared to non-diabetic mice, while the difference was not statistically significant (n = 4, p = 0.22). We believe that this delay is likely due to the diffusion of insulin/glucose outwards/inwards AlgXO microcapsules.

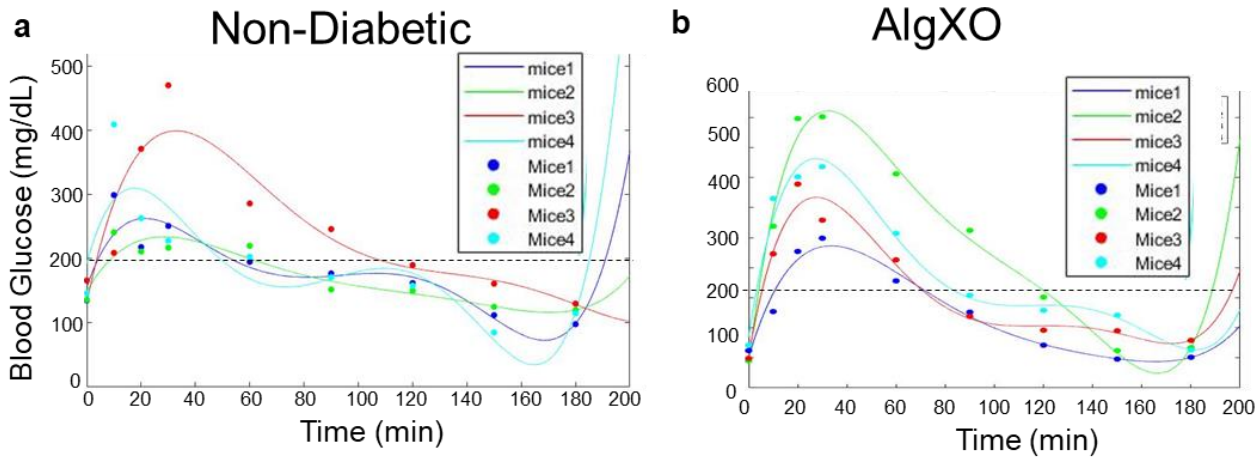

Figure 5.33. Polynomial regressions onto glucose challenge response. a) Polynomials with degree 5 were assigned to the OGTT curve of every individual mice of a non-diabetic group and **b)** AlgXO transplanted group (1500 IEQ). Small circles show the raw OGTT data and lines represent the assigned polynomial. Dashed line demonstrates the normoglycemic criterion (i.e. blood glucose < 200 mg/mL).

Clinical trials for islet transplantation have shown that allogeneic or xenogeneic source of islets affect the clinical efficacy, and have resulted in conflicting results. More specifically, although xenotransplantation in diabetic patients partially reduced hypoglycemic events, higher doses of xenogeneic islets were less effective [67,68]. We thus sought to understand whether such

observations could be replicated in our pre-clinical diabetic mice model, and we found that the xeno-islet dose is a critical determinant of the transplant therapeutic efficacy.

Clinical trials for islet allo- or xeno- transplantations have resulted in conflicting results. Although xenotransplantation in non-immunosuppressed diabetic patients was associated with some reduction in hypoglycemic events, there was a lack of correlation between the dosage of islets and the euglycemic efficiency outcome [67,68]. Results from this trial showed that the transplantation of 5000 IEQ/kg xeno-islets was associated with superior glycemic control and graft function compared to higher doses of xeno-islets (i.e. 15,000 or 20,000 IEQ/kg). Interestingly, a recent auto-transplantation clinical trial demonstrated a strong dose-response relationship between the islet dose and graft function [69]. This trial suggested that the islet graft failure was 25-fold more likely in patients transplanted with low dose (< 2000 IEQ/kg) islets versus higher doses (≥ 5000 IEQ/kg or more) [69]. To replicate such conflicting observations in a pre-clinical animal model, we sought to find whether islet dose influences the efficacy of islet transplantation in our study. We used a low dose (500 IEQ) and a high dose (5000 IEQ) islets transplanted within AlgXO and CTRL microcapsules. Islets (5000 IEQ) within AlgXO reversed hyperglycemia for about 80 days but failed to do so in longer periods. Surprisingly, 5000 IEQ islets within the CTRL microcapsules were not able to consistently reverse the hyperglycemia in STZ mice (**Figure 5.8a**). We further repeated the efficacy of AlgXO transplants in response to OGTT in the 5000 IEQ transplanted group and compared against non-diabetic control (**Figure 5.8b**). Polynomials with degree 5 were assigned to the OGTT curve of every individual mice (**Figure 5.8c**), and time to normoglycemia was calculated based on the value of 200 for the polynomial functions. **Figure 5.8d** demonstrates that the average time to reach normoglycemia

after an OGTT for mice with AlgXO transplants was 112 ± 32 minutes. This suggest a delay in glucose response of mice received AlgXO transplants versus non-diabetic mice ($p = 0.08$).

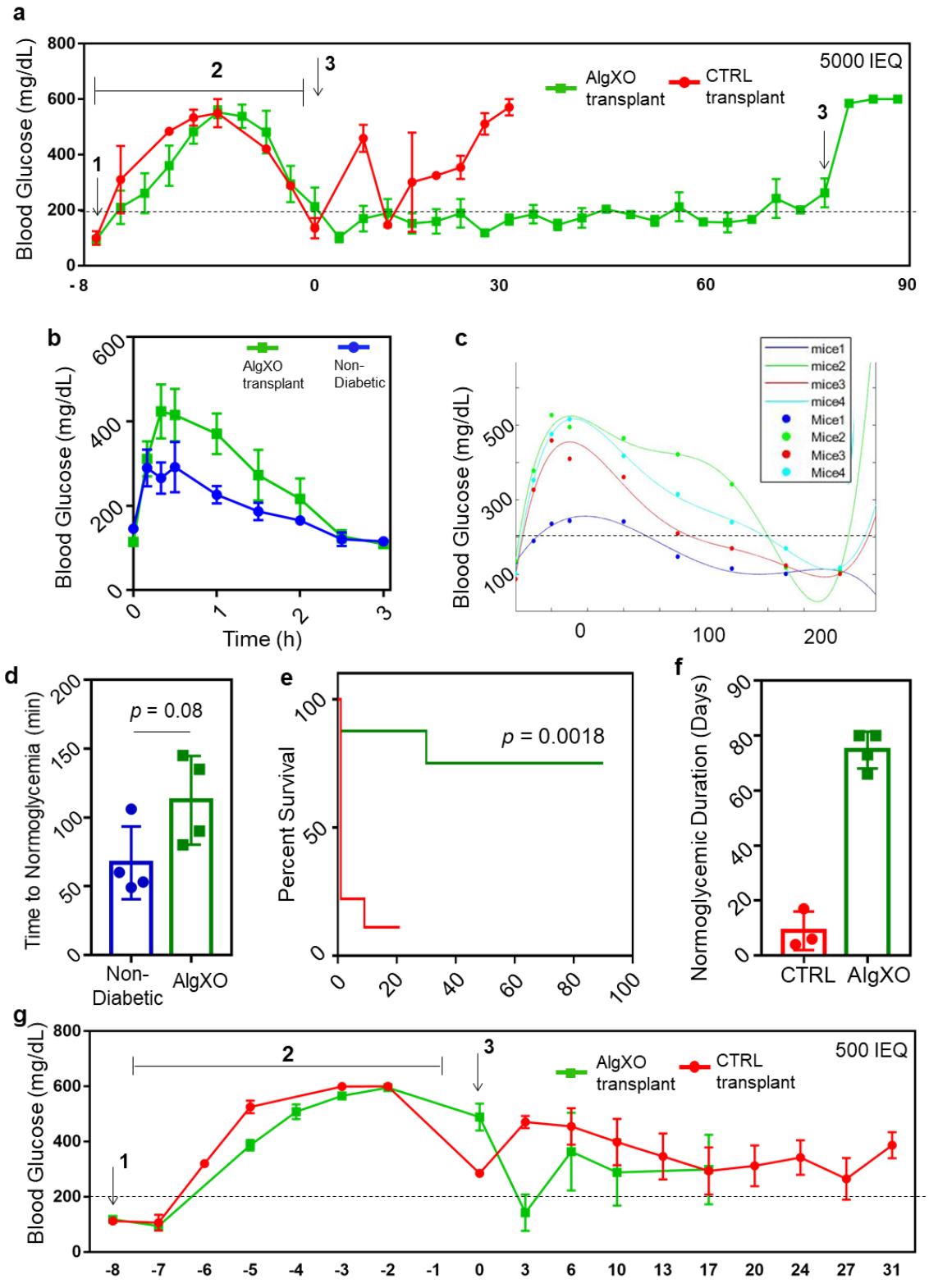

Figure 5.34. Dose study of islets xenotransplantation (i.e. 500 or 5000 IEQ islets) in immunocompetent STZ mice. a) In higher islet dosage (5000 IEQ), CTRL transplants failed to consistently reverse hyperglycemia in C57/BL6 STZ mice. However, AlgXO transplants reversed hyperglycemia for ~ 80 days. **b)** We further tested the efficacy of AlgXO transplants in response to

oral glucose tolerance test (OGTT). One month after transplantation, AlgXO transplants successfully reversed hyperglycemia event induced by glucose challenge with a similar trend as non-diabetic mice. **c)** Polynomials with degree 5 were assigned to the OGTT curve of every individual mice and equations were solved to find the average time needed for the mice blood glucose to reach 200 mg/dL after an OGTT. The average time to reach normoglycemia (i.e. 200 mg/dL) after an OGTT was 112 ± 32 minutes for mice transplanted with 5000 IEQ islet encapsulated in AlgXO. **d)** The average time to reach normoglycemia for non-diabetic mice was 67 ± 26 minutes. This suggest a slight delay in glucose response of mice received AlgXO transplants versus non-diabetic mice (p = 0.08). **e)** Mice received CTRL transplants with 5000 IEQ islets had low survivals, where 6 of 10 mice died within a day of transplantation, while only 1/7 mice receiving AlgXO transplants with 5000 IEQ islets died within one day of transplantation and 5 others remained alive till the end of the study (p = 0.0018, Long-rank (Mantel-Cox) test). **f)** Mice that received AlgXO transplants with 5000 IEQ isltes remained normoglycemic for 75 ± 7 days, while this duration for CTRL transplanted mice was 9 ± 7 days after transplantation. **g)** Lower dose islets (500 IEQ) was ineffective in euglycemic induction neither within CTRL nor AlgXO microcapsules. On the diagram, 1 shows the STZ induction, 2 shows the time for diabetes progression, and 3 shows the transplantation timepoints. On the diagram, 1 shows the STZ induction, 2 shows the time for diabetes progression, and 3 shows the transplantation timepoints. Statistical significance is calculated through unpaired t-test with Welch's correction.

In addition, 6 out of 10 diabetic mice that received 5000 IEQ islets within CTRL microcapsules died within a day of transplantation, while this ratio was 1 out of 8 for AlgXO group (**Figure 5.8e**, p = 0.0018). As a result, AlgXO microcapsules delayed the graft rejection and increased the normoglycemic duration in mice transplanted with high dose islets (**Figure 5.8f**); however, with less efficacy than medium dose of islets i.e. 1500 IEQ. We further tested lower dose of islets (500 IEQ), where neither the AlgXO nor the CTRL microcapsules were able to reverse hyperglycemia in the recipient mice (**Figure 5.8g**).

Our results in their totality suggest that AlgXO extends the functionality of islet xenotransplants > 5 months. We also found that the therapeutic effect of islet xenotransplants does not necessarily improve by elevating the dose, which could partly support the conflicting results in the dose studies of islet xenotransplants [67].

AlgXO reduces inflammation and fibrosis

We next sought to delineate possible mechanisms that prolonged the function of islet transplants within AlgXO microcapsules. In a broad context, two major players are widely

recognized in the long-term failure of microencapsulation technologies: 1) lack of nutrients and oxygen accessibility into the microcapsules, which leads to islet necrosis [15], and 2) and inflammatory-based foreign body response (FBR) within weeks of transplantation forms a dense fibrotic tissue around the microcapsules, blocking the function of islets [16-19]. To investigate possible mechanisms by which islets encapsulated within AlgXO provide longer glycemic correction, we factored both of these points [19-22].

In the early stage of transplantation, the health and viability of islets suffer from oxidative stress (likely within a week), and at later stages inflammatory-led fibrosis influences graft viability by constraining oxygen and metabolite diffusion into the microcapsules [19]. Recently, it has been demonstrated that MSC exosomes could relieve the β-cell apoptosis and destruction [66], and enhance islets survival under hypoxic conditions [70]. Thus, we speculated whether XOs enhance rat islets viability *in vitro*, and found that XOs (both 20 and 200 µg/mL doses) as well as AlgXO enhance the rat islets viability (**Figure 5.9**). It is therefore likely that AlgXO retains the encapsulated islets viability during early stages of transplantation.

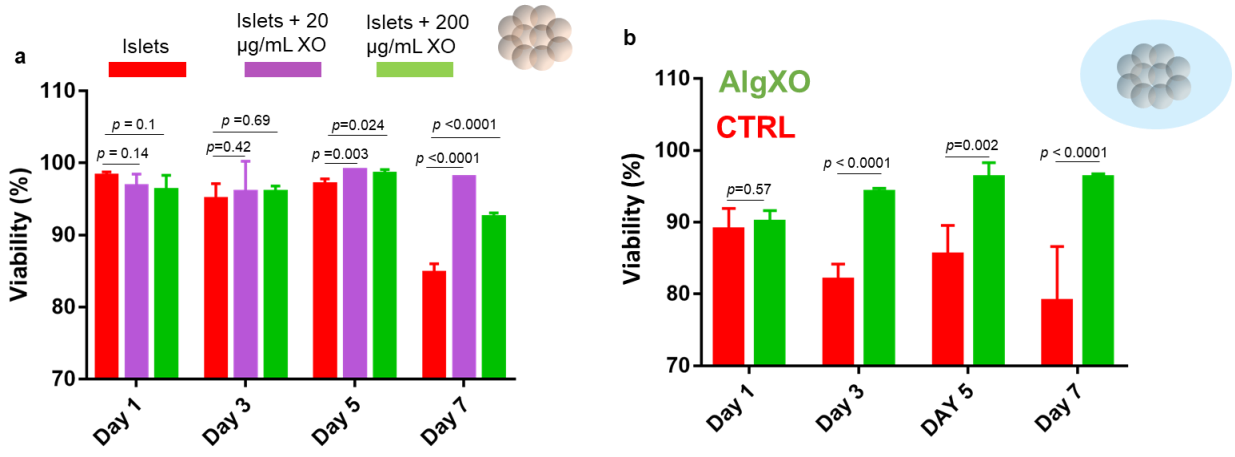

Figure 5.35. XOs enhance the viability of naked and encapsulated rat islets. a) Addition of 20 µg/mL and 200 µg/mL XOs to the islet cultures significantly enhances the viability of islets after 5 and 7 days of culture. It should be noted that viability was measured using Calcein AM (live cells) and propidium iodide (dead cells) staining. **b)** Starting from 3 days of islet encapsulation,

AlgXO enhances the viability of encapsulated islets within the first week of encapsulation. Statistical significance is calculated through unpaired t-test with Welch's correction.

In longer periods, however, inflammatory-led FBR further compromise the viability and functionality of the islets within microcapsules. Inhibition of inflammation-led fibrosis has been shown to provide long-term function of transplanted islets and euglycemia in diabetic rodents [1,19,20,26]. Having known the multi-potent anti-inflammatory properties of MSCs derived XOs [48,51-54], we hypothesized that encapsulation of rat islets within AlgXO microcapsules reduces the inflammatory response, leading to the long-term function of islets and glycemic control in immunocompetent diabetic mice. To investigate the inflammatory response against AlgXO and CTRL xenotransplants, we explanted both groups and analyzed for immune infiltration.

Since the 1500 IEQ CTRL transplants failed to function in about less than a month (**Figure 5.1a**), we explanted CTRL or AlgXO xenotransplants from mice at day 31 of the implantation. It should be noted that at this timepoint CTRL transplants failed to function in the OGTT experiment (**Figure 5.1b**). We next analyzed the pericapsular attachment around both microcapsules and observed that CTRL groups are covered with macrophages, while most of AlgXO explants were clear and transparent (**Figure 5.1d**). Noteworthy that 9% ± 3.6% of the microcapsules from AlgXO explants showed pericapsular cell attachment which were significantly lower than pericapsular cell attachment on CTRL explants (**Figure 5.1e**, $p < 0.0001$). Analyses of the subtypes that infiltrated around CTRL microcapsules revealed the presence of CD11b+ macrophages. At least in some locations, CD11b+ macrophages express MHCII+, as observed through co-localization of CD11b and MHCII markers. Macrophages generally express moderate levels of MHCII to regulate immune tolerance and local surveillance to maintain homeostatic immunity. However, macrophages will up-regulate MHCII expression

and antigen presentation capacity in a proinflammatory environment, where antigens presented to CD4+ lymphocytes.

We pursued our study to find out reasons for the different inflammatory response against AlgXO and CTRL transplants. Mounted evidence has delineated the immunogenicity of alginate polymer [16,18,29,71]. Such immunogenicity has been attributed to two separate mechanisms, which could also be viewed as complementary phenomena. First line of thoughts support that the presence of endotoxin contaminations within alginate are the main immunogens, including lipopolysaccharide (LPS), lipoteichoic acid, and peptidoglycans [72,73]. Through lack of endotoxin presence within the commercially purified alginate (such as the UPLVG in the present study), others have reported that even without endotoxins alginate may enhance immune response [17,26,74]. These reports suggest that such inflammatory response is likely due to the inherent nature of alginate. Guluronate oligosaccharide derived from alginate, for example, has been reported to readily activate macrophages partly through Toll-like receptor 4 (TLR4) signaling pathway [75,76]. While the exact mechanisms for such response is debated, resolving the inflammatory response against alginate microcapsules in unanimously reported to prevent or delay the fibrosis. In this context many groups have reported the long-term efficacy of islet transplantation within fibrosis-resistant devices [20,26,28,29,77].

To comprehensively compare the inflammatory response of AlgXO and CTRL microcapsules, we further focused on the empty microcapsules and the inflammatory response they induce *in vivo*. We transplanted ~3000 AlgXO or CTRL microcapsules into the subcutaneous space of C57/BL6 mice, and both microcapsules were explanted after 2 weeks (**Figure 5.10a**). A 2-weeks timepoint was selected, as it has been established as a suitable

timepoint to resolve and reflect both innate and adaptive immune system as well as fibrotic responses to implanted materials in C57/BL6 mice [16,17].

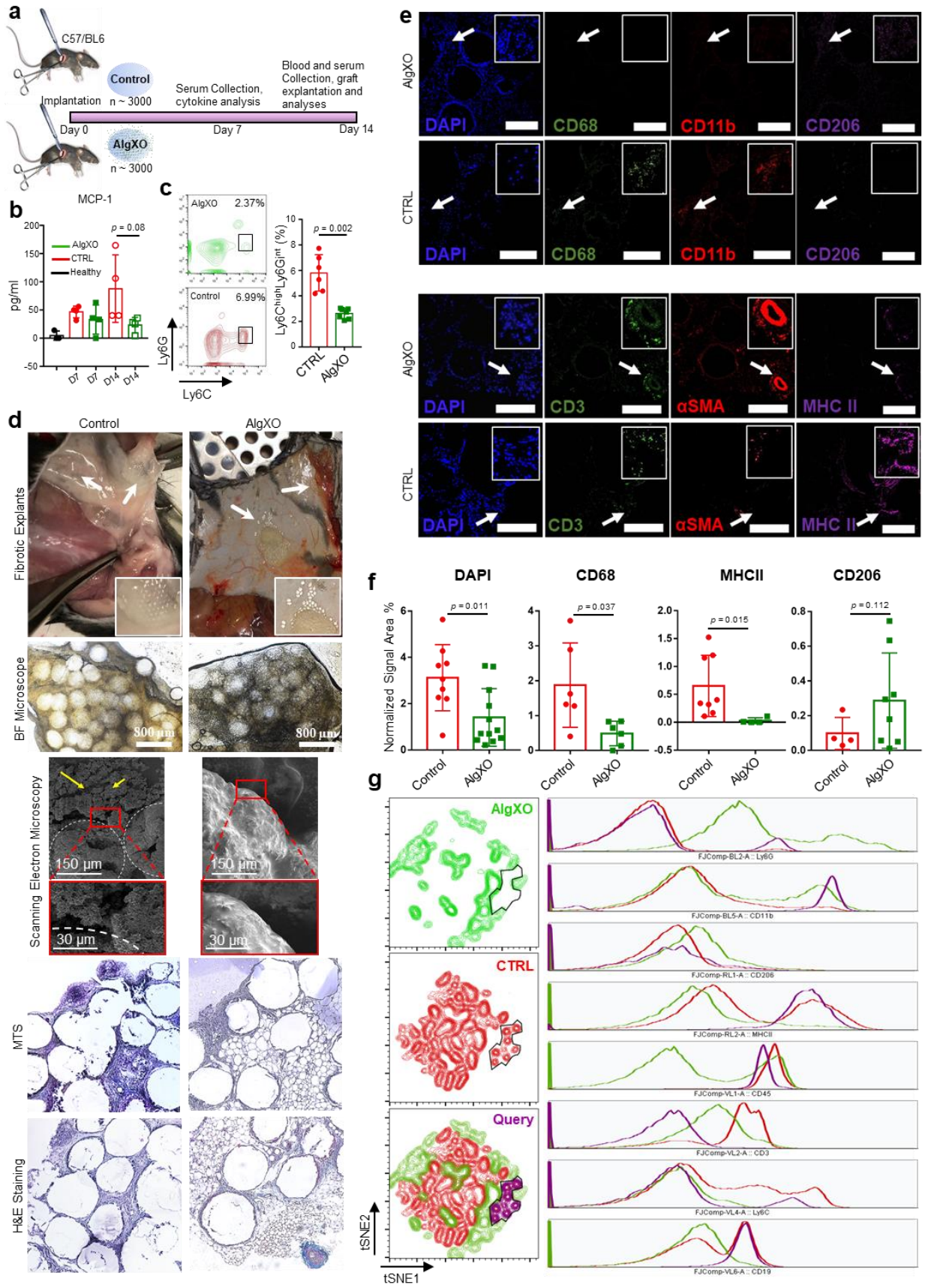
a
C57/BL6
Implantation
Control
n ~ 3000
AlgXO
n ~ 3000
Day 0
Day 7
Day 14
Serum Collection, cytokine analysis
Blood and serum Collection, graft explantation and analyses
b
MCP-1
p = 0.08
AlgXO
CTRL
Healthy
pg/ml
D7
D7
D14
D14
c
AlgXO
2.37%
Control
6.99%
Ly6G
Ly6C
Ly6C^high Ly6G^int (%)
p = 0.002
CTRL
AlgXO
d
Control
AlgXO
Fibrotic Explants
BF Microscope
800 µm
Scanning Electron Microscopy
150 µm
30 µm
MTS
H&E Staining
e
AlgXO
CTRL
DAPI
CD68
CD11b
CD206
CD3
αSMA
MHC II
f
DAPI
CD68
MHCII
CD206
Normalized Signal Area %
p = 0.011
p = 0.037
p = 0.015
p = 0.112
Control
AlgXO
g
AlgXO
CTRL
Query
tSNE1
tSNE2
FJComp-BL2-A :: Ly6G
FJComp-BL5-A :: CD11b
FJComp-RL1-A :: CD206
FJComp-RL2-A :: MHCII
FJComp-VL1-A :: CD45
FJComp-VL2-A :: CD3
FJComp-VL4-A :: Ly6C
FJComp-VL6-A :: CD19

Figure 5.36. AlgXO microcapsules show reduced fibrosis and inflammation after 2 weeks transplantation. a) Study design to compare and quantify the FBR response against AlgXO and CTRL microcapsules. Two weeks study was performed as this timeframe is suitable for resolving and reflecting both innate and adaptive immune system as well as fibrotic responses to implanted materials in C57/BL6 mice. Blood and sera were collected on days 7 and 14 for immunocytes and inflammatory cytokines analyses (n = 4). **b)** Two weeks after implantation, MCP-1 chemokine was more than 3.7-fold less for mice that had received AlgXO versus the ones transplanted with CTRL. **c)** CD45+CD11b+Ly6C^{high}Ly6G^{med} inflammatory monocytes were significantly lower (p = 0.002) in the blood of mice transplanted with AlgXO compared to CTRL (n = 3). **d)** While captured images from explants and their BF microscopy are similar, sections and scanning electron micrographs from two weeks explants show different immune-environment around microcapsules. White arrows show the localization of grafts and yellow arrows point to the cells infiltrated around microcapsules. **e, f)** Fixed fibrotic tissues were later sectioned and stained for sub-populations of immunocytes. Normalized areas of DAPI, CD68, and MHCII around explant microenvironments of AlgXO were significantly lower than CTRL microcapsules (n = 4). g) Total cells of fibrotic tissues were collected and stained for flow cytometry analyses of immunocytes subpopulation. tSNE plots further demonstrates the different immune-environment around AlgXO and CTRL explants. We further conducted a query on a subpopulation that is present on CTRL but absent in AlgXO immune-environment. This subpopulation is CD45+CD11b+CD19+MHCII+CD3-Ly6C-, which is likely to be the B cells sob-population. Statistical significance is calculated through unpaired t-test with Welch's correction.

At days 7 and 14 serum cytokines were also measured, reflecting the systemic inflammatory response, if any. Among 11 cytokine panels, there was no significant difference between serum cytokines of mice that were subcutaneously transplanted with AlgXO or CTRL (**Figure 5.10b** and **Figure 5.11**). While not statistically significant, the average amount of MCP-1 chemokine in the serum of mice transplanted with CTRL microcapsules for 2 weeks (87.8 ± 59.9 pg/mL) was ~3.7-fold higher than mice implanted with AlgXO microcapsules (23.3 ± 13.4 pg/mL). The difference between systemic MCP-1 led us to further study the circulatory inflammatory monocytes in response to AlgXO and CTRL transplants.

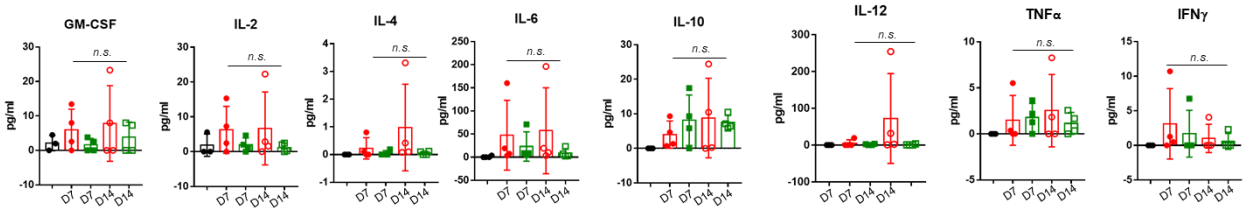

Figure 5.37. Blood cytokines analyses of mice received AlgXO or CTRL microcapsules. Mice serum was harvested from mice at days 7 and 14 after transplantation, showing no significant difference among groups. One-way ANOVA was conducted to measure the statistical difference. Wiled Type (WT) mice was also added to the groups as a negative control (n = 4, statistical significance is calculated through unpaired t-test with Welch's correction). Red: CTRL; Green: AlgXO, Black: Healthy

Detection of circulating microbial molecules or pro-inflammatory cytokines by bone marrow-resident cells leads to MCP-1 production to modulate the frequency of circulating

inflammatory monocytes [78]. MCP-1 is a chemokine that binds to CCR2 and mediates the recruitment of inflammatory ($Ly6C^{high}$) monocytes to the site of inflammation. We next sought to quantify the inflammatory monocytes in the mice's blood 2 weeks after implantation. **Figures 6.10c** shows the flow cytometry plots and their quantification of the inflammatory monocytes ($CD45+CD11b+Ly6C^{high}Ly6G^{med}$ [79]) subpopulation. $CD45+CD11b+Ly6C^{high}Ly6G^{med}$ in the mice transplanted with AlgXO (2.62% ± 0.4%) were significantly lower (n = 3, p = 0.002) compared to those monocytes in the blood circulation of CTRL microcapsules (5.8% ± 1.4%). These observations suggest that the AlgXO transplants are likely to reduce the systemic inflammatory response against regular alginate microcapsules.

The destination of circulating monocyte has been linked to the site of MCP-1 secretion [80-82], which is also a site of hyper-inflammation. In the present study, the transplant site is likely to be the main site of inflammatory response. We therefore sought to investigate the local inflammatory response around implants. Upon explantation procedure, we found that all detectable CTRL microcapsules have agglomerated into a pseudo tissue (**Figure 5.10d).** For AlgXO, while some microcapsules were remained intact and non-aggregated (shown with white arrows), the rest were entrapped in a pseudo tissue with multiple blood vessels around them. Pseudo tissues from both groups were isolated carefully not to contain endogenous tissues of mice. Bright Field microscopy demonstrated that both pseudo tissues have entrapped the microcapsule groups (**Figure 5.10d**). Under scanning electron microscopy evaluations, some microcapsules were detected (**Figure 5.10d**; white dashed line for visual guide of microcapsules) to be surrounded with rough microstructures and the AlgXO ones were entrapped in smooth structures. Tissues were sectioned into 5-10 μ slices and stained with H&E and Masson's Trichrome Staining (MTS). The fibrotic tissue formed around CTRL microcapsules

demonstrated the significant infiltration of mostly mononuclear cells, while such histology was not observed in AlgXO fibrotic tissues (**Figure 5.10d**).

To better compare the immune environment, we compared and quantified the cellular components that drive the fibrotic response. Both fibrotic tissues were stained for different immunocytes including macrophages (CD11b+ and CD68+), T cells (CD3+), pro-regenerative macrophages (CD206), antigen presenting cells (MHCII), and fibrotic marker of smooth muscle actin (αSMA). DAPI counterstaining was also used to count total cell infiltration within fibrotic tissues (**Figure 5.10e**). Total cell infiltration around microcapsules was significantly lower in AlgXO fibrotic tissues (p = 0.011). Similar trends were observed for CD68 (p = 0.037) and MHCII (p = 0.015). In contrast, there was no association between CD206 expression (p = 0.112). While these observations suggest the less immune-infiltrated milieu in AlgXO fibrotic microenvironment, the T cell sub population (CD3+) and fibrosis marker (αSMA) were found to be expressed more in AlgXO fibrotic microenvironment.

These mixed outcomes were against our initial hypothesis on the anti-inflammatory and/or anti-fibrotic response of AlgXO microcapsules *in vivo*. In particular, αSMA, which was highly expressed in the AlgXO microenvironment, is a marker for activated myofibroblasts that are responsible for downstream collagen deposition and fibrosis of implanted alginate microcapsules [17]. However, αSMA is also a contractile protein expressed in pericytes as well as in the vascular smooth muscle cells that surround arteries and arterioles [83]. In the histological observations, the αSMA cells were found to have a round structure consistent with blood vessel structure (**Figure 5.10e**). Next, we quantified the blood vessel formation and found that there is more blood vessel within the subcutaneous area (and around microcapsules) of AlgXO 2-weeks explants (**Figure 5.12**). We further isolated cells from fibrotic tissues and analyzed their

subpopulation using flow cytometry. There was significantly higher CD45+ cells (n = 4; $p < 0.0001$) collected from AlgXO fibrotic tissues (33.1% ± 8.0%) compared to control (83.0% ± 12.8%) (**Figure 5.12b**). Tissue sections were further analyzed for αSMA showing vasculature presence in the AlgXO fibrotic microenvironment, demonstrating a vascular-shaped microstructure (**Figure 5.12c, d**). These results in their totality suggest the presence of blood vasculature and less inflammatory milieu around AlgXO fibrotic tissues.

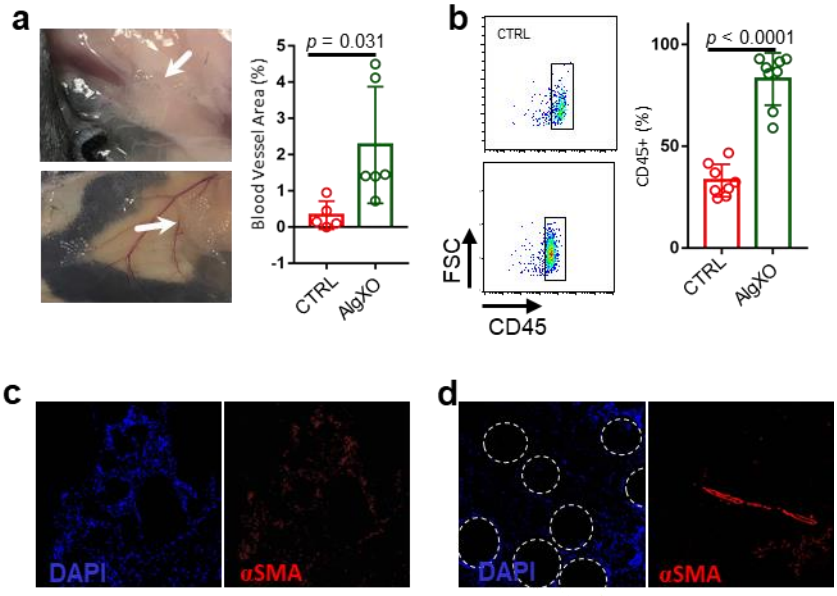

Figure 5.38. Vasculature present in the fibrotic tissue around AlgXO. a) Pictures from subcutaneous explants show presence of blood vessels in AlgXO fibrotic microenvironment. **b)** Flow cytometry analyses shows the presence of higher CD45+ cells ($p < 0.0001$) harvested from AlgXO fibrotic tissues (33.1% ± 8.0%) compared to control (83.0% ± 12.8%). **c)** αSMA (markers of blood vessels) were absent in CTRL fibrotic tissues compared to d) AlgXO. Statistical significance is calculated through unpaired t-test with Welch's correction.

To gain more holistic information on the fibrotic tissues around CTRL and AlgXO microcapsules, we compared the components of both microcapsules at the single cell level using flow cytometry. The tSNE plots in **Figure 5.10g** demonstrate highly segregated sub-populations for AlgXO and CTRL fibrotic tissues. We particularly queried the subpopulations that were absent in AlgXO but present in CTRL as shown in **Figure 5.10g** black line area (purple colored query). This subpopulation is CD45+CD11b+CD19+MHCII+CD3-Ly6C-, which is likely to be

the B cells sub-population. To further see the quantity of B cells in fibrotic microenvironments, we analyzed CD45+CD19+ B cells (**Figure 5.13a**). The CD45+CD19+ cells were remarkably less (n = 4, $p < 0.0001$) in AlgXO (0.9% ± 0.5%) compared to that of CTRL (22.5% ±5.1%). B lymphocytes play critical roles in the FBR against alginate microcapsules. In particular, B cells knockout as well as CXCL13 neutralization have been reported to dampen the FBR to implanted alginate microcapsules during a 2-weeks implantation period [17], which aligns with our observations in the present study. In addition to B cells, innate lymphoid cells and $\gamma\delta^+$ T cells leads to a chronic adaptive antigen dependent Th17 cell response [84]. In our study, we found that there was a higher quantity of CD3+ in AlgXO compared to CTRL ($p = 0.026$), which is likely due to the blood/blood vessels in the AlgXO microenvironment (**Figure 5.13b**). This could be further confirmed due to the vicinity of blood vessels with T cells (**Figure 5.10e**).

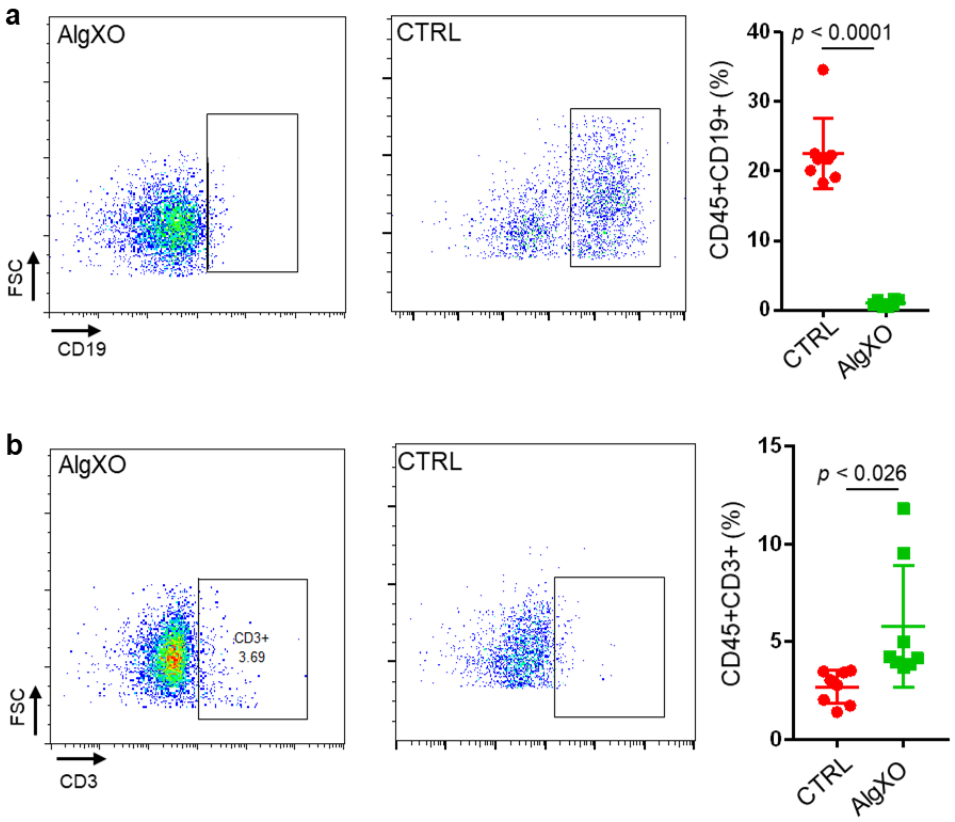

Figure 5.39. The percentage of **a)** B and **b)** T cells presence in the fibrotic Tissues around AlgXO and CTRL (n = 4). Statistical significance is calculated through unpaired t-test with Welch's correction.

We pursued the experiments to further investigate the anti-inflammatory properties of AlgXO microcapsules. Immune infiltration could be characterized with cell types present in the lavage around the inflamed area, particularly for biomaterials-based inflammation [1,26]. Live cells within the subcutaneous lavage were first analyzed for common lymphocyte marker (CD45). **Figure 5.14a, b** shows the percentage of CD45+ cells in lavage of CTRL implanted mice were 41.6% ± 4.2% and in the AlgXO implanted were 8.5% ± 5.2% (n = 4, $p < 0.0001$).

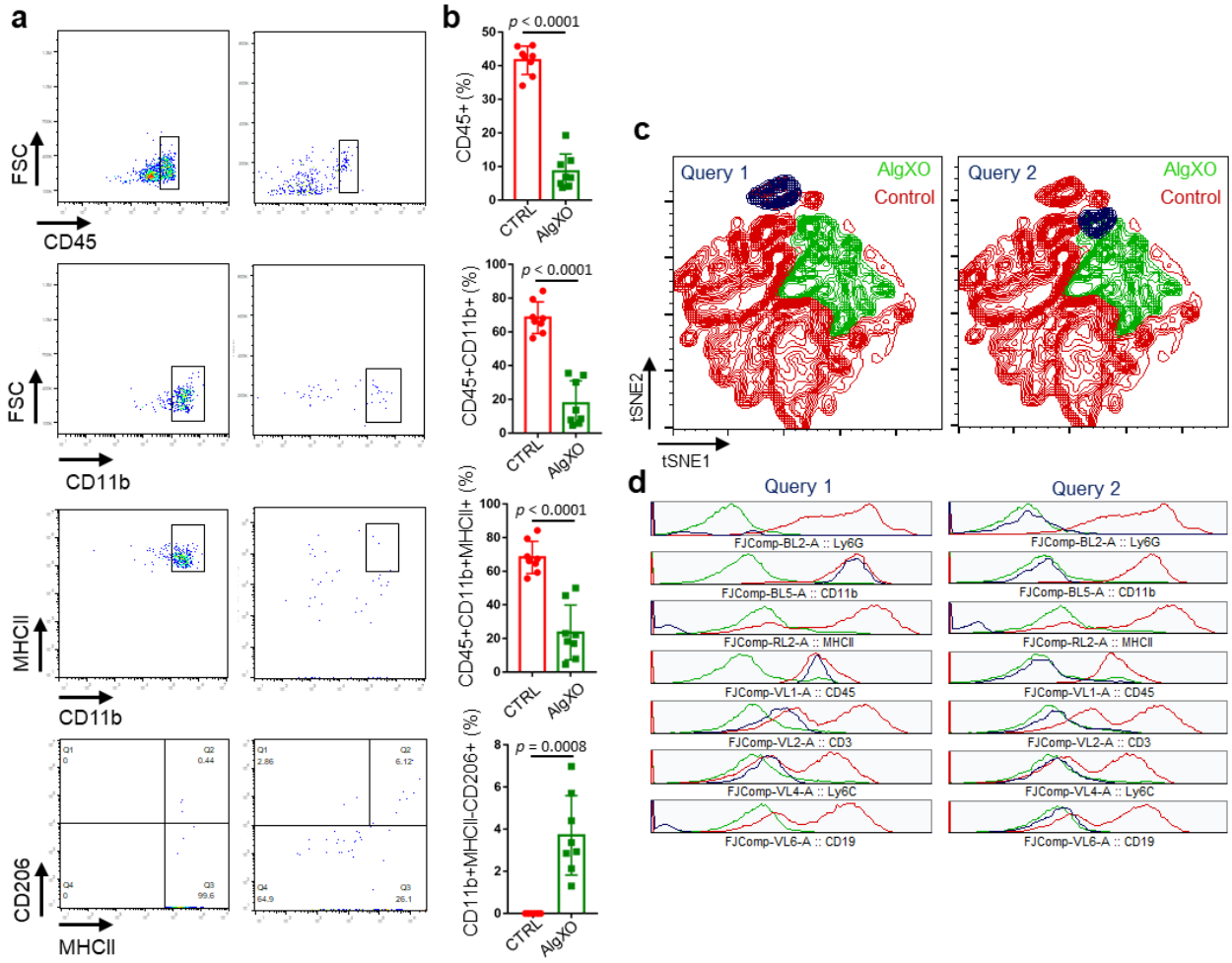

Figure 5.40. Flow cytometry analyses of lavage around microcapsules show distinct immunocytes population around AlgXO and CTRL microcapsules. a, b) Flow cytometry analyses demonstrates the total CD45+ population present around AlgXO is less than CTRL microcapsules. Similar trend was observed for CD11b+, CD11b+MHCII+, and CD11b+MHCII-CD206+ sub-populations. **c)** tSNE plots demonstrates the different cell environment present in the lavage collected from surrounding non/low adherent cells around AlgXO and CTRL explants. **d)** Two sub-populations were then analyzed for immune markers. Cells in Query 1 (gated on specific sub population present in CTRL but not in AlgXO) was CD45+CD11b+CD3-CD19-MHCII-Ly6C-Ly6G-, which is likely to be dendritic cells. Cells in Query 2 (gated on specific sub population present in AlgXO but not in CTRL) was CD45-CD11b-CD3-CD19-MHCII-Ly6C-Ly6G-, which is likely to be neither from myeloid or lymphoid origin. (n = 4, statistical significance is calculated through unpaired t-test with Welch's correction).

Sub-gating on CD45+ cells, the percentage of CD11b+ cells decreased from 68.4% ± 9.4% for CTRL to 17.6% ± 13.4% for AlgXO microcapsules ($p < 0.0001$). Around 68.2% ± 9.5% of CD11b+ cells are also expressing MHCII for CTRL, while this percentage is 23.5% ± 16.3% for AlgXO microcapsules ($p < 0.0001$). Interestingly, there was no detectable CD45+CD11b+MHCII-CD206+ (M2-like macrophages [85]) for CTRL, while this population was 3.7% ± 1.9% for lavage retrieved from the surrounding environment of AlgXO microcapsules ($p < 0.0001$). To gain a more holistic information on the lavage immune-profile, we compared the lavage components of both microcapsules at the cellular level through tSNE representation. **Figure 5.14c, d** show tSNE plots and two sub-populations that were analyzed for immune markers. Query 1 (gated on specific sub population present in CTRL but not in AlgXO) was CD45+CD11b+CD3-CD19-MHCII-Ly6C-Ly6G-, which is likely to be non-activated dendritic cells [86]. Query 2 (gated on specific sub population present in AlgXO but not in CTRL) showed the subpopulation of cells with CD45-CD11b-CD3-CD19-MHCII-Ly6C-Ly6G- markers, which are likely to be from neither myeloid nor lymphoid origin. These results in their totality supports the reduced-inflammatory response against AlgXO implants, while non-inflammatory tissues were formed around AlgXO. It should be noted that transplantation of 1500 IEQ rat islets within AlgXO or CTRL failed to regulate the dysglycemia when transplanted subcutaneously (**Figure 5.15**).

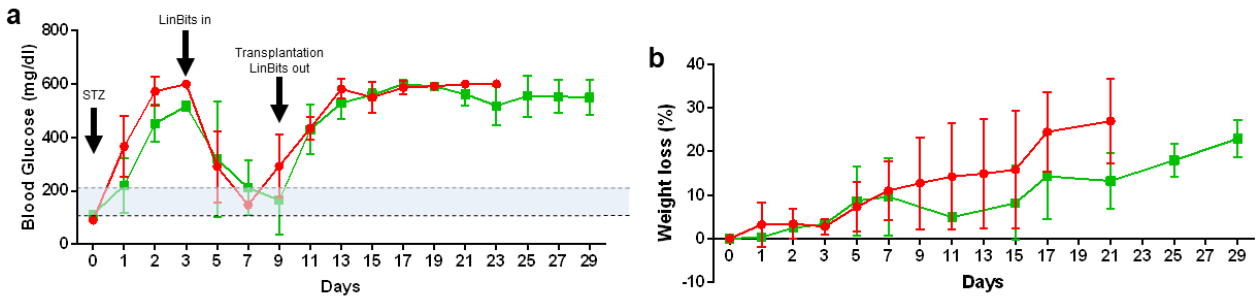

Figure 5.41. Subcutaneous transplantation of islets encapsulated in either CTRL and AlgXO. The **a)** glucose and **b)** body weights of STZed mice were tracked for a month, and there was no significant improvement in the glycemic control in any of the groups.

AlgXO's reduced FBR is partly due to the releasing of exosomes in a controlled fashion

Reducing the FBR against biomaterials is generally done through the surface modifications of the biomaterial via immune-modulators [27,87], zwitterionic compounds attachments [26]), or through the release of anti-inflammatory and/or immunomodulatory molecules (e.g. dexamethasone [31], IL-4 [32], CSF-1R inhibitor [20], and CXCL12 [28,33]). In our study, we hypothesized that XOs play the anti-inflammatory role upon release from AlgXO. We thus pursued our investigation to delineate the effect of XOs controlled release on the AlgXO's reduced inflammatory response.

We first characterized the physical and mechanical properties of AlgXO and compared them against CTRL microcapsules, as these properties remarkably influence the biological response of biomaterials. Water interactions with biomaterial surface, for example, have been recognized as a fundamental characteristic determining the immunological responses of biomaterials. Compared to hydrophilic materials, hydrophobic (and slightly hydrophilic) biomaterials adsorb more proteins. This is mainly because proteins adjacent to hydrophilic surfaces must displace more water molecules bound to biomaterial surface [23,88]. We thus sought to measure the contact angle for AlgXO and CTRL biomaterials using captive bubble contact

angle method [89]. **Figure 5.16a** shows that the contact angle for AlgXO (156.3° ± 3.8°) was higher than that of CTRL microcapsules (150.2° ± 4.9°). This suggests that AlgXO is slightly more hydrophobic; however, there was no significant correlation (n = 3, p = 0.167) between contact angles. Importance of hydrophobicity lies into the protein adsorption onto the biomaterials surface, which has been linked with the FBR.

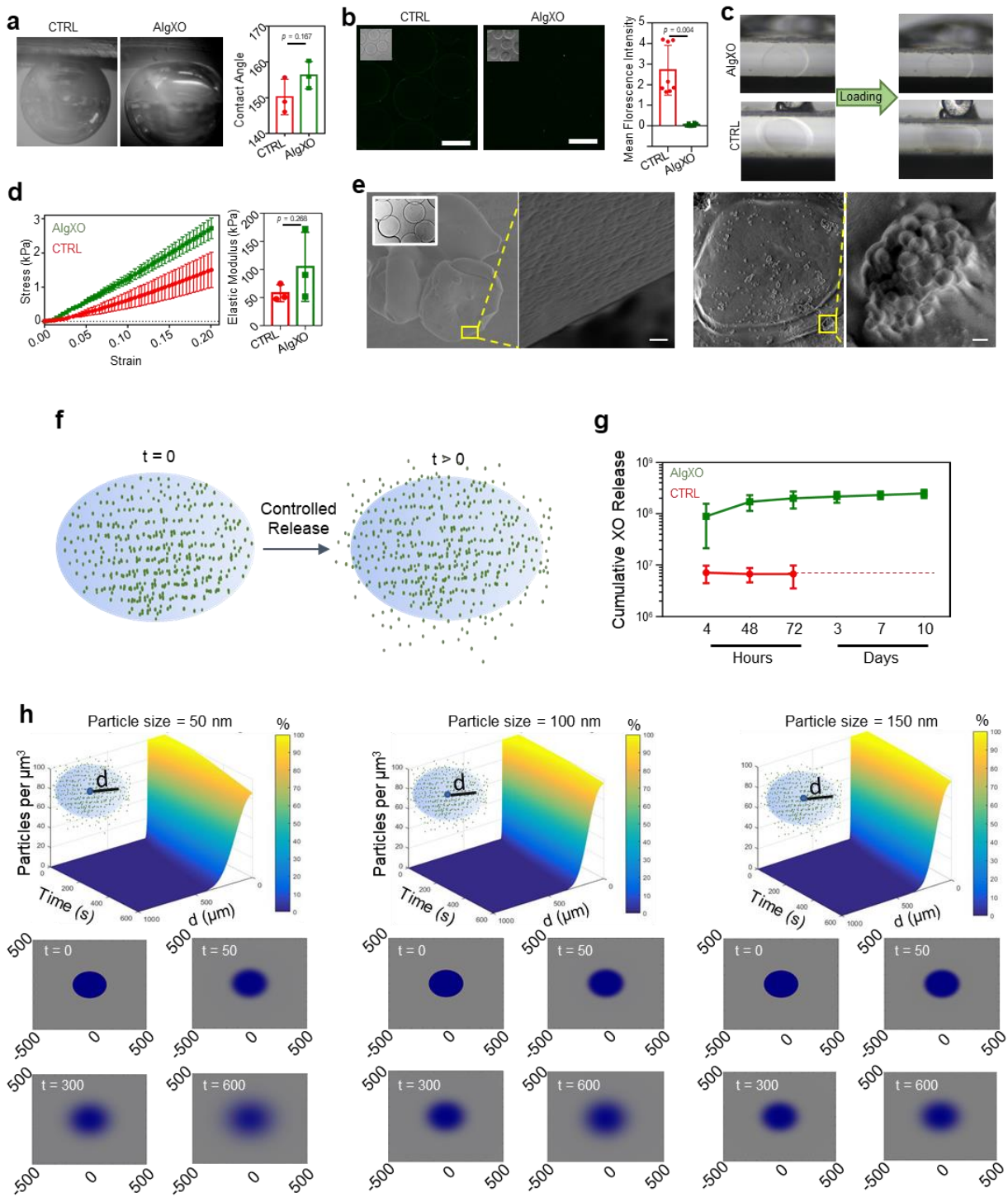

Figure 5.42. AlgXO reduces FBR partly due to releasing exosomes in a controlled fashion. a) a non-significant difference between AlgXO's and CTRL's captive bubble contact angle was observed (i.e. 156.3° ± 3.8° for AlgXO versus 150.2° ± 4.9° for CTRL). **b)** IgG protein adsorption to the surface of AlgXO and CTL microcapsules (n = 3). Microscale mechanical testing was performed for **c)** AlgXO and CTRL. **d)** Stress-Strain curve of AlgXO vs. CTRL microcapsules graphed based on the force-displacement data. Elastic modulus was not significantly different (p = 0.268) between AlgXO (104.7 ± 61.4 kPa) and CTRL (57.8 ± 14.9 kPa). **e)** to investigate the release of encapsulated exosomes, scanning electron microscopy was conducted on air-dried microcapsules, demonstrating surface pores in 50-200 nm size scale (scale = 1 μm), and encapsulation of vesicles within

AlgXO. **f)** schematic representation of our hypothesized model, where exosomes release from AlgXO microcapsules overtime. **g)** AlgXO releases exosomes in a control fashioned in vitro. Release profile reaches a threshold within a week. **h)** diffusion of nanoparticles with diameters 50, 100, and 150 nm (which are chosen due to the size ranges of exosomes). Particles number vs. time vs. distance from microcapsule center (d) are graphed in the percentage heatmap diagrams. Bottom panels show the color map of spatiotemporal diffusion rate of exosomes at t = 0, 50, 300, and 600 s upon initiation of diffusion. Expectedly, the smaller the size, the higher the diffusion rate. In addition, 600 s after the onset of diffusion, the concentration of 50 nm particles at the center of the microcapsules dropped 20%, while 100nm and 150nm, no significant decrease was obtained at the center of the microcapsules. Statistical significance is calculated through unpaired t-test with Welch's correction.

Many studies have reported that the blocking of protein adsorption of biomaterials silences the immune response [26,71,90]. These proteins may include components of the coagulation cascade (fibrinogen and tissue factors), complement cascade (C5), and other plasma-derived proteins (albumin and IgG) [91]. IgG and fibronectin adsorption led the Mac-1-mediated attachment of neutrophils and macrophages to biomaterial surfaces during the acute phase of inflammation [92]. We therefore attempted to investigate the IgG adsorption onto both AlgXO and CTRL microcapsules. IgG adhered to the surface of CTRL microcapsules more pronouncedly (2.70% ± 1.21%, n = 3, p = 0.0004) compared to AlgXO (0.05% ± 0.06%) (**Figure 5.16b)**. The less-fibrotic properties AlgXO could partly originate from the less protein adsorption onto its surface. Proteins absorption onto the biomaterials and their conformation could lead to the formation of different biomaterial-associated molecular patterns, initiating the inflammatory response [23,93-95].

Mechanical properties of biomaterials have been linked to immunological response of implants. For instance, macrophage confinement reduces their inflammatory response through reduction in actin polymerization and LPS-stimulated nuclear translocation of MRTF-A [96]. In addition, macrophages adhere to stiff surfaces more profoundly [97,98]. We thus attempted to characterize the mechanical properties of both AlgXO and CTRL microcapsules (**Figures 6.16c, d**). **Figure 5.16c** demonstrates the images of the initial and final vertical positions of the cantilevers, exerting pressure on the microcapsules. Stress-Strain curves (**Figure 5.16d**) shows

the linear behavior, where the difference between elastic modulus of AlgXO (104.7 ± 61.4 kPa) and CTRL (57.8 ± 14.9 kPa) was not significant (n = 3, p = 0.268).

We further asked other possible mechanisms that are likely to play roles in AlgXO's immunomodulatory properties. Our initial hypothesis was that the immunomodulatory effects of AlgXO is partly due to the release of XOs. MSC derived XOs have been demonstrated to possess immunosuppressive functions both *in vitro* [99,100] and in rodent models [55,101]. To better understand this possibility, we sought to find whether XOs within AlgXO release into the surrounding microenvironment of microcapsules. We first visualized and compared the CTRL and AlgXO microcapsules using Scanning electron microscopy (SEM) on air-dried microcapsules. **Figure 5.16e** demonstrates SEM micrographs of both AlgXO and CTRL microcapsules, suggesting the presence of surface pores in the 50-200 nm size scale (left panel, scale = 1 μm). SEM micrographs of AlgXO microcapsules demonstrated the encapsulation of spherical-shaped vesicles within AlgXO, and their possible release from the surface of a microcapsule (**Figure 5.16e**, right panel, scale = 1 μm). We particularly hypothesized that XOs could be released from AlgXO (**Figure 5.16f**) as they readily diffuse within the nano-meshes of extracellular matrix and communicate over long distances within the body. Recently, it has been demonstrated that due to the aquaporin-1 mediated XOs deformability, XOs could transport within and diffuse outwards of alginate matrix (as well as extracellular matrices), despite XOs being larger than the mesh size of the surrounding network [102]. We next incubated AlgXO microcapsules *in vitro* and measured the release of XOs, demonstrating the controlled release of exosomes over the course of 10 days (**Figure 5.16g**). To further understand the release profile of XOs, we modeled the release of exosomes based on the Fickian diffusion of nanoparticles ranging from 50-150 nm in diameter (i.e. the size range of XOs). **Figure 5.16h** demonstrates the simulated diffusion of XOs with 50

nm, 100 nm, and 150 nm. The top panels are time (s) *vs.* particles concentration (per μm^3) *vs.* distance from capsules center (μm). Bottom panels on **Figure 5.16h** demonstrate the heatmap representation of the XOs diffusion outwards of microcapsules. In these maps the 1 mm × 1 mm diffusion microenvironment is shown, and the blue color represents the diffusion. These simulations suggest that smaller particles (50 nm of diameter) diffuse faster than 150 nm particles. To check our simulation models beyond the scale of 50-150 nm, smaller (i.e. 10 nm) and larger (200 nm and 500 nm) particles were input into the code. It was found that in 600 s, while 10 nm possess expedited diffusion rates, 500 nm particles remain within the microcapsules and no outward diffusion was obtained (**Figure 5.17**).

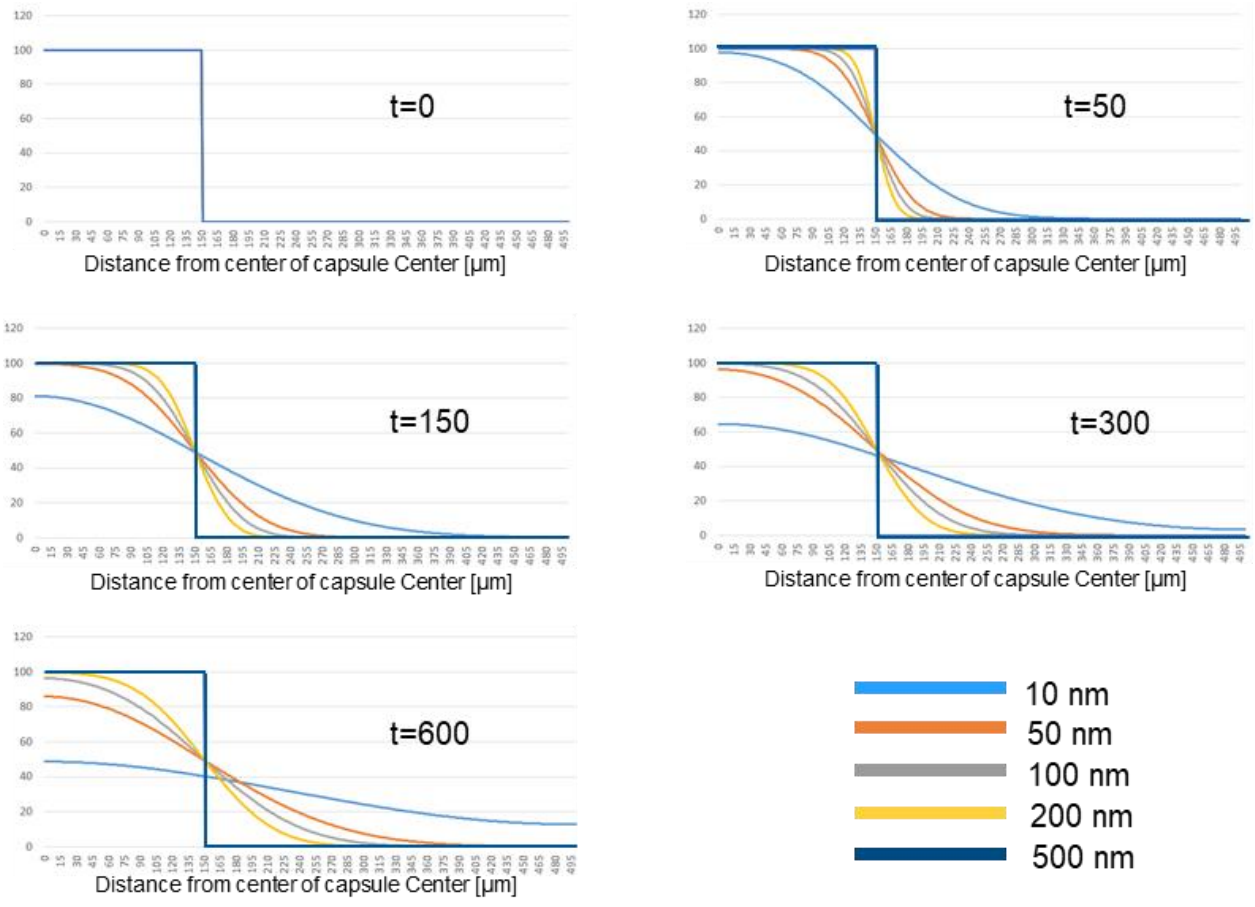

Figure 5. 43. Simulated controlled release of particles with 10, 50, 100, 200, or 500 nm of diameters. At t > 0, particles with diameter ≤ 200 nm show diffusion profiles, where smaller particles diffuse faster. Particles with diameter of 500 nm do not show diffusion out of microcapsules at least for 600 s.

XOs suppress murine macrophages and T lymphocytes

Similar to the suppressive properties of their parental cells [103,104], XOs have been demonstrated to possess immunosuppressive functions both in vitro [99,100] and in rodent models [55,101]. We recently showed that bone marrow derived MSC XOs suppress human peripheral blood mononuclear cells (PBMCs) upon activation with anti-CD3/CD28 stimulation [48]. In the splenocyte co-cultures supplemented with IL-2, bone marrow derived MSC XOs also induced CD4+CD25+FoxP3+ regulatory T cells [48]. To understand the mechanisms by which XOs exert their suppressive function, here we first studied their effects on activated murine splenocyte and then on purified CD3+ T cells isolated from splenocytes (**Figure 5.18a**). Cell Proliferation Dye eFluor670-labeled splenocytes from C57/BL6 wild-type mice were stimulated with plate bound anti-CD3 and anti-CD28 in vitro in the presence and absence of XOs. Both 20 μg/mL and 200 μg/mL XOs suppressed the splenocytes proliferation, where activated splenocytes proliferated to the number of 9603 ± 871, and addition of 20 and 200 μg/mL XOs reduced the counts to 1253 ± 1038 (n = 4, $p < 0.0001$) and 1570 ± 1010 (n = 4, $p < 0.0001$). The inhibition of splenocytes proliferation through addition of XOs has been widely reported [99].

The cellular heterogeneity within splenocytes complicates the drawing of conclusion on the XOs cellular mechanism. To delineate more detailed cellular mechanisms underlying suppressive capabilities of XOs, we focused on the XOs effect on the activation of purified T cells. We thus repeated the T cells proliferation assay in purified T cells co-cultures, which gives insight onto the interactions between XOs and T lymphocytes. Purified CD3+ T cells were activated (similar to splenocyte activation procedure), and after 4 days the CD4+ counts for CD3/CD28 activated T cells was 5217 ± 378. Addition of 20 and 200 μg/mL XOs reduced the counts to 3889 ± 2081 (n = 4, $p = 0.0031$) and 4387 ± 1397 (n = 4, p = 0.0057), respectively.

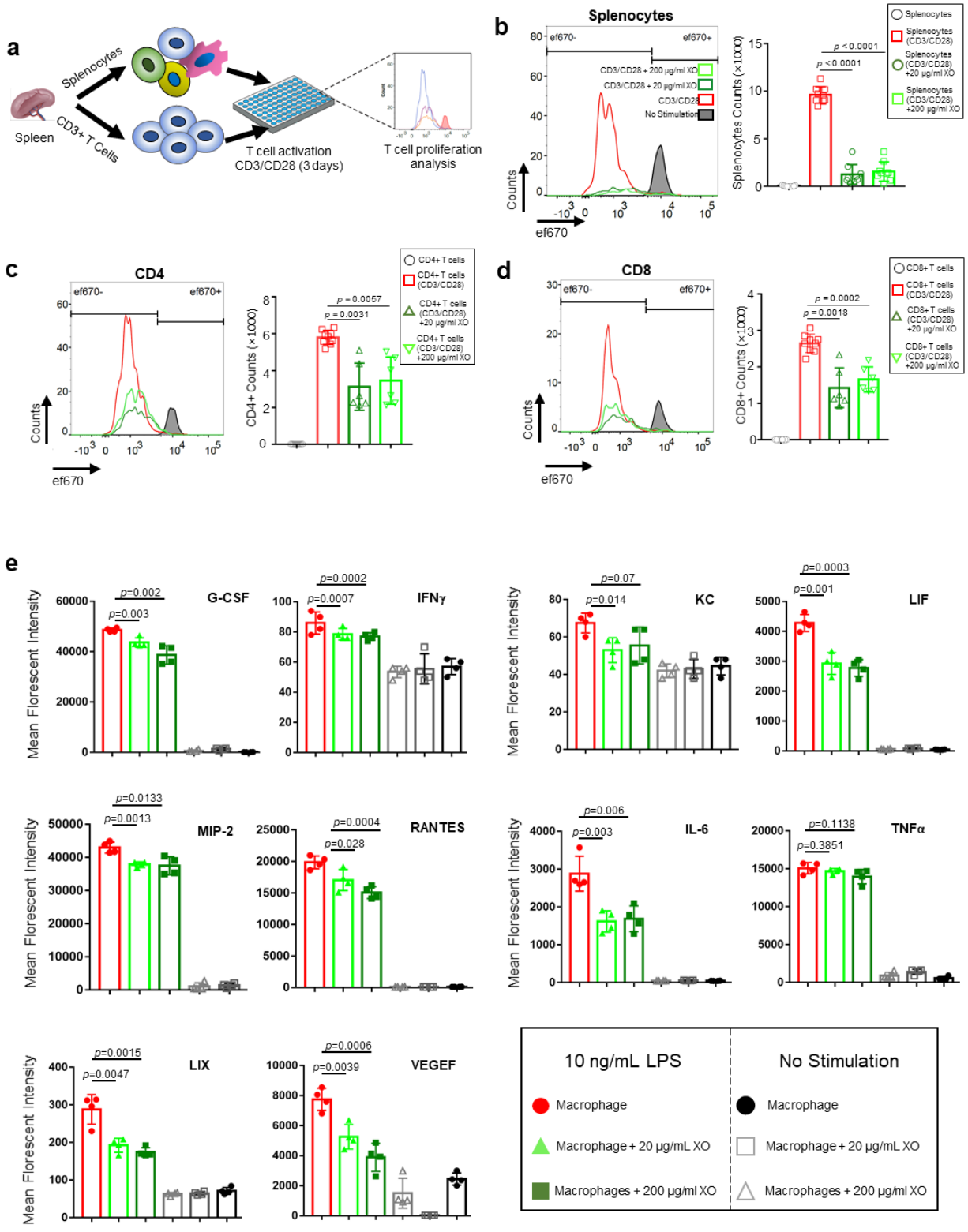

Figure 5.44. XOs suppress the proliferation of splenocytes and CD3+ T cells and reduce the production of inflammatory cytokines from LPS stimulated macrophages. a) Schematic figure showing the experimental procedure. CFSE labeled splenocytes and CD3+ T cells were co-cultured with plate bound anti-CD3 and soluble CD28 in the presence of absence of 20 and 200 µg/mL of XOs. Upon 4 days co-culture, cells were analyzed using flow cytometry. **b)** Splenocyte counts for CD3/CD28

activated cells were 9603 ± 871, and addition of 20 and 200 μg/mL XOs reduced the counts to 1253 ± 1038 (n = 4, p < 0.0001) and 1570 ± 1010 (n = 4, p < 0.0001), respectively. **c)** In the co-cultures of CD3+ cells with CD3/CD28 antibodies, CD4+ counts for CD3/CD28 activated T cells was 5217 ± 378. Addition of 20 and 200 μg/mL XOs reduced the counts to 3889 ± 2081 (n = 4, p = 0.0031) and 4387 ± 1397 (n = 4, p = 0.0057), respectively. **d)** In the co-cultures of CD3+ cells with CD3/CD28 antibodies, CD8+ counts for CD3/CD28 activated T cells was 2700 ± 252. Addition of 20 and 200 μg/mL XOs reduced the counts to 1503 ± 784 (n = 4, p = 0.0018) and 1766 ± 628 (n = 4, p = 0.0002), respectively. e) Addition of XOs to the co-cultures of murine macrophages reduce the secretion of inflammatory cytokines (G-CSF, IFNγ, IL-6, LIF, LIX, MIP-2, RANTES) in a dose dependent manner (n = 4). Statistical significance is calculated through unpaired t-test with Welch's correction.

Moreover, CD8+ counts for CD3/CD28 activated T cells was 2700 ± 252 and addition of 20 and 200 μg/mL XOs reduced the counts to 1503 ± 784 (n = 4, p = 0.0018) and 1766 ± 628 (n = 4, p = 0.0002), respectively. Interestingly, XOs were more suppressive in the splenocytes co-cultures than purified T cells. These results infer the remarkable involvement of other-than-T-cells, including antigen presenting cells (APCs), in the XOs suppressive mechanism in splenocyte co-cultures. This suggests that XOs, at least in part, target accessory cells such as APCs rather than T cells directly, which is in agreement with recent studies [52,104,105]. In a broader context, infused MSCs and their apoptotic products are suggested to be phagocytosed, leading to the generation of third-party phagocytes that ultimately mediate the observed immunomodulatory effects [103,106-108]. These observations imply that XOs first interfacing with APCs and phagocytes [52,55,109-112] and facilitate the immunosuppression. These observations are in agreement with our earlier *in vivo* results, where CD3+ T lymphocytes were absent in the lavage collected from the AlgXO microcapsules microenvironment but were present in the lavage collected from the microenvironment of CTRL microcapsules (**Figure 5.18d**).

To functionally validate whether XOs possess immunomodulatory effects on APCs, and gain insight into XOs therapeutic mechanisms, we performed co-cultures of activated murine macrophages and XOs. Recently, the anti-inflammatory potentials of XOs derived from human derived MSCs have been described in the LPS induced inflammation both *in vitro* cultures with murine macrophages and LPS injected mouse models [100]. To gain insight on possible mechanisms that XOs regulate macrophages activation, we isolated the supernatants from co-

cultures and measured the quantity of secreted cytokines. Among the panel of tested cytokines, we found that XOs significantly reduce the production of G-CSF, IFNγ, LIF, KC, MIP-2, RANTES, IL-6, LIX, and VEGEF from LPS stimulated macrophages (**Figure 5.18e**).

Table 5.1. Macrophages Cytokines Influenced by XOs

Chemokine/Cytokine	**Function**	**Ref.**
G-CSF/ CSF3	• Regulates the survival, maturation, and proliferation of neutrophil progenitors • Regulates the differentiation of granulocyte lineages • Regulates neutrophils mobilization from bone marrow to peripheral tissues • LPS-activated ERK2 functions by remodeling local chromatin, interacting with C/EBPβ and synergizing its transactivation activity to increase G-CSF expression	113,114
IFNγ	• The only known type II interferon • Upon binding to receptor, JAK1 and JAK2 are activated and phosphorylate STAT1 • Macrophages secrete upon stimulation with LPS	115,116
LIF	• LIF acts in an autocrine manner via LIF receptor to promote STAT4 activation. Activated STAT4 together with NF-kB/p65-p52 and C/EBPb enhances IL-6 transcription	117
MIP-2/ CXCL2	• Important chemokine for recruitment of neutrophils • NF-κB activation is required for MIP-2 gene expression in the LPS-signaling pathway A MIP-2 promoter could be activated by ectopical expression of NF-κB p65 or c-Jun transcription factors.	118

RANTES	• Secretes via LPS-induced NF-kB activation in monocytes through sterile α and HEAT/Armadillo motif-containing protein (SARM)toll/IL-1R domain–containing adaptor. SARM is critical for the recruitment of transcription factors and of RNA polymerase II to the Ccl5 promoter	119,120
LIX/ CXCL5	• Important chemokine in Neutrophil trafficking	121-123
KC/ CXCL1	• CXCL1 is regulated through interactions of NF-κB with other transcriptional regulatory molecules such as poly(ADP-ribose) polymerase-1 (PARP-1) and cAMP response element binding protein (CREB)-binding protein	124,125
VEGF	• Important protein for angiogenesis • VEGF production in human macrophages is NF-κB dependent and could be significantly reduced using the NF-κB inhibitor, IκBα	126

It is known that LPS activates the NFκB pathway and all three MAPK pathways (ERK, JNK/SAPK, and p38α), leading to a wide range of cellular responses, including cell differentiation, survival or apoptosis, and inflammatory responses [127]. Reduced cytokines and chemokines in macrophage culture are hallmarks of NFκB inflammatory pathway, suggesting that XOs likely possess anti-inflammatory properties through regulating this pathway (see **Table 6.1**). Inflammatory cytokines/chemokines that were not affected by XO addition include TNFα, IL-2, IL-17, and IL-1a (**Figure 5.19**). Interestingly, even the production of IL-10 was reduced by addition of XOs, demonstrating that in this specific experimental setting and timepoints, XOs have immunosuppressive roles.

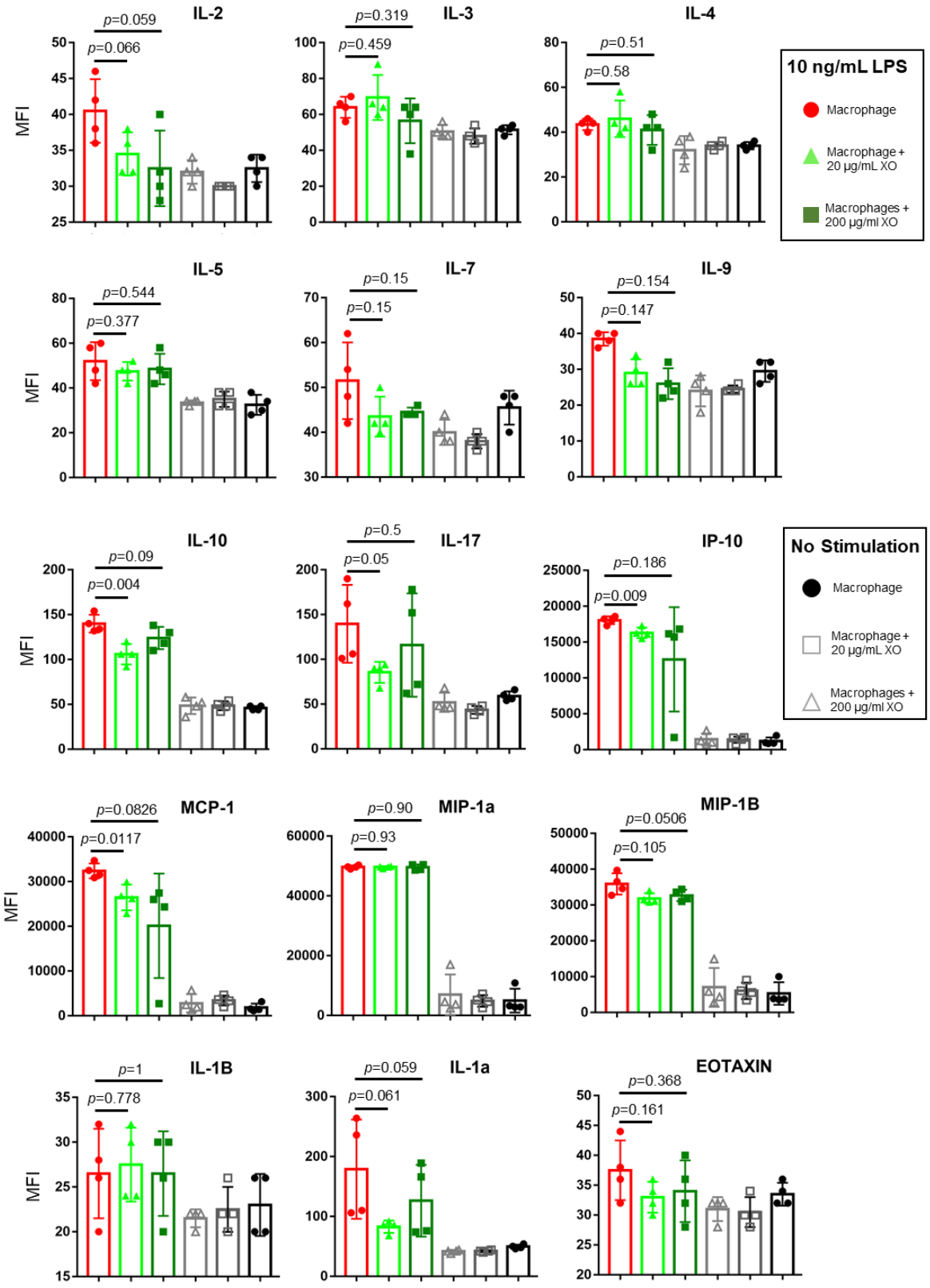

Figure 5.45. XOs effect on the production of cytokines from 10 ng/mL LPS (TLR4 agonist) stimulated macrophages. Statistical significance is calculated through unpaired t-test with Welch's correction (n = 4).

XOs suppress human T lymphocytes and regulate NfκB in human macrophages

Our *in vivo* and *in vitro* assays thus far demonstrated the xenogeneic immunosuppressive capabilities of XOs. We further asked the replicability of such immunosuppressive potency of XOs on human-derived immunocytes, i.e. an allogeneic response. Since we observed a reduction of inflammatory response and an induction of tolerance in AlgXO transplanted mice *in vivo*, and reduction of murine T-cell proliferation and macrophage activation, we attempted to understand XOs mediate immunomodulatory effects on human derived immune cells *in vitro*. We examined XOs suppressive activity on T-cell proliferation *ex vivo* using carboxyfluorescein succinimidyl ester (CFSE)-labeled human peripheral blood mononuclear cells (PBMCs). PBMCs were activated with bead-bound anti-CD3/CD28 (1:1 ratio) and further cultured with or without XOs. Both 20 μg/mL and 200 μg/mL XOs suppressed activation of PBMCs (**Figure 5.20a**). Quantitatively, addition of 20 μg/mL and 200 μg/mL XOs reduced the count of activated T cells from 24002 ± 6762 to 2342 ± 910 (n = 3; p = 0.029) and to 2102 ± 1121 (n = 3; p = 0.027), respectively (**Figure 5.20b**). These results are consistent with previous studies where the ability of MSC-derived exosomes to suppress T cell activation and proliferation was reported [48,53,60,128]. These results collectively suggest that XOs have potent suppressive effects on T cells activation, although the mechanisms behind such suppression is remained to be fully understood.

To gain a better understanding on underlying cellular pathways, we performed Luminex assay to measure some cytokine profiles in the supernatant of PBMC co-cultures (**Figure 5.20c** and **Figure 5.21**). We particularly picked cytokines that are related to pro-inflammatory T lymphocyte subsets, such as Th1 and Th17 lymphocytes that play key roles in the FBR against biomaterials [129].

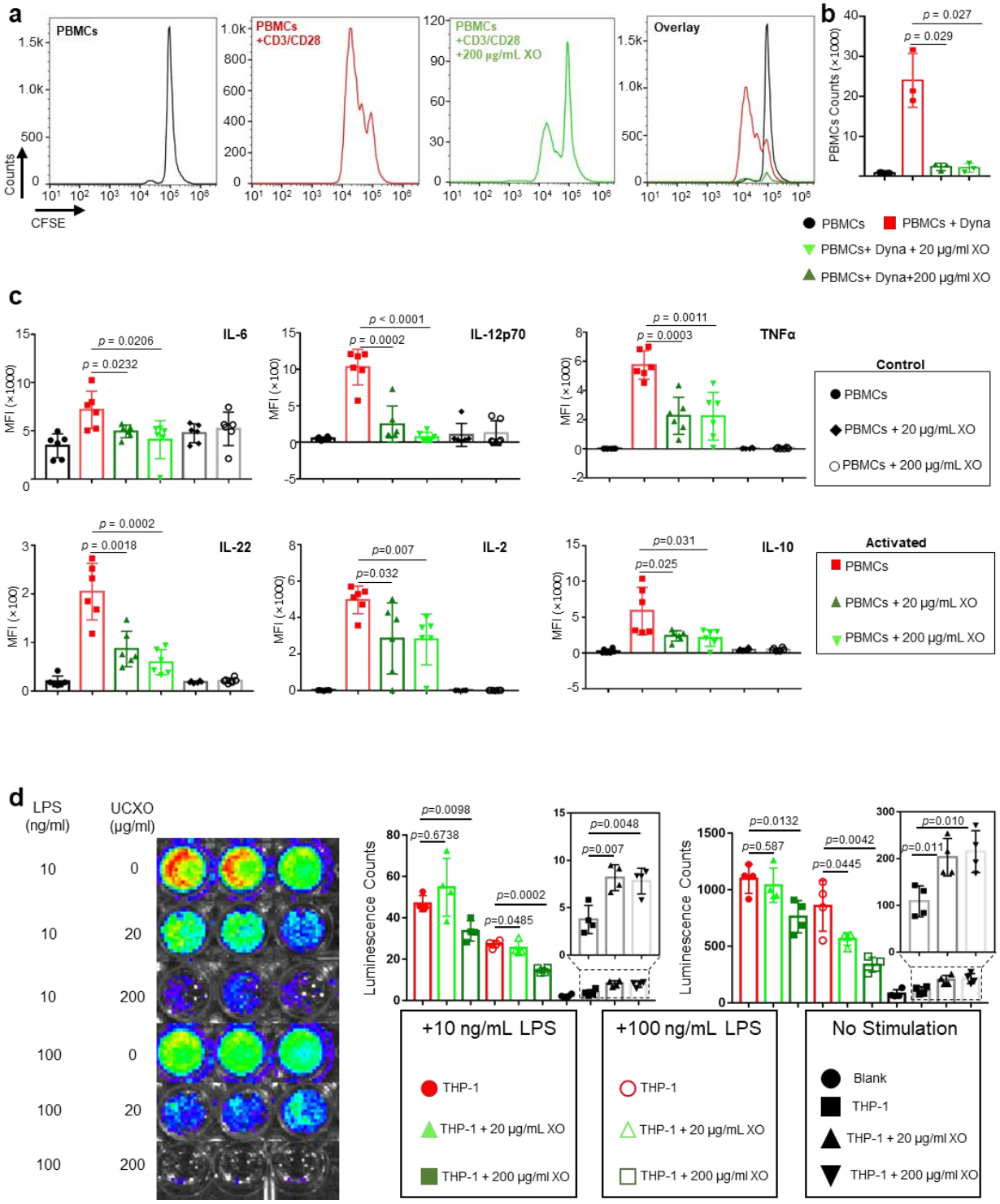

Figure 5.46. XOs suppress human peripheral blood mononuclear cells and macrophages. a) Human Peripheral Blood Mononuclear Cells (PBMCs) were activated with bead-bound CD3/CD28 antibodies in the presence and absence of XOs. **b)** Addition of 20 µg/mL and 200 µg/mL XOs reduced the count of activated PBMCs from 24002 ± 6762 to 2342 ± 910 (n = 3; p = 0.029) and to 2102 ± 1121 (n = 3; p = 0.027), respectively. To gain more insight into the XOs mechanism of action, cytokine production was evaluated in the PBMCs culture. Addition of XOs reduced the IL-6, TNFα, IL-12p70, and IL-22 production from activated PBMCs. **c)** In the co-cultures of anti-CD3/CD28 activated PBMCs, addition of Xos reduce IL-2, IL-6, IL-10, IL-12p70,

IL-22, and TNFα (n = 3). **d)** XOs suppressed the LPS mediated human macrophages activation. LPS activated NFκB pathway in THP-1 macrophages, and addition of 200 µg/mL of XOs reduces NFκB activation of both 10 ng/mL LPS (n = 4, p = 0.044) and 100 ng/mL LPS (n = 4, p = 0.004) activated THP-1 macrophages. 20 µg/mL of XOs was not enough to interfere with the NFκB activation. XOs influenced the NFκB activation of non-activated THP-1 cells. Addition of 20 µg/mL XOs upregulated the NFκB activity in THP-1 cells from 109 ± 17 to 203 ± 20 (n = 4, p = 0.0117). Furthermore, addition of 200 µg/mL XOs upregulated the NFκB activity in THP-1 cells from 109 ± 17 to 215 ± 23 (n = 4, p = 0.0105). Statistical significance is calculated through unpaired t-test with Welch's correction.

In addition, recent reports have demonstrated the suppressive effects of XOs on Th1/Th17 cells polarization both *in vitro* and *in vivo* [48,53,60]. To mechanistically probe the XOs effect in inhibiting the induction of T cell to Th1/Th17 subtypes, we measured several key representative Th1 and Th17 cytokines. In the presence of XOs, the levels of several proinflammatory Th1 and Th17 cytokines including IL-12p70 (Th1), TNFα (Th1), IL-6 (Th17), and IL-22 (Th17) were significantly reduced (**Figure 5.20c**). IFNγ (Th1) demonstrated a trend of decrease though not significant (**Figure 5.21**). Interestingly, XOs significantly reduce the production of IL-2, which is a key cytokine to stimulate the growth, proliferation, and differentiation of T lymphocytes.

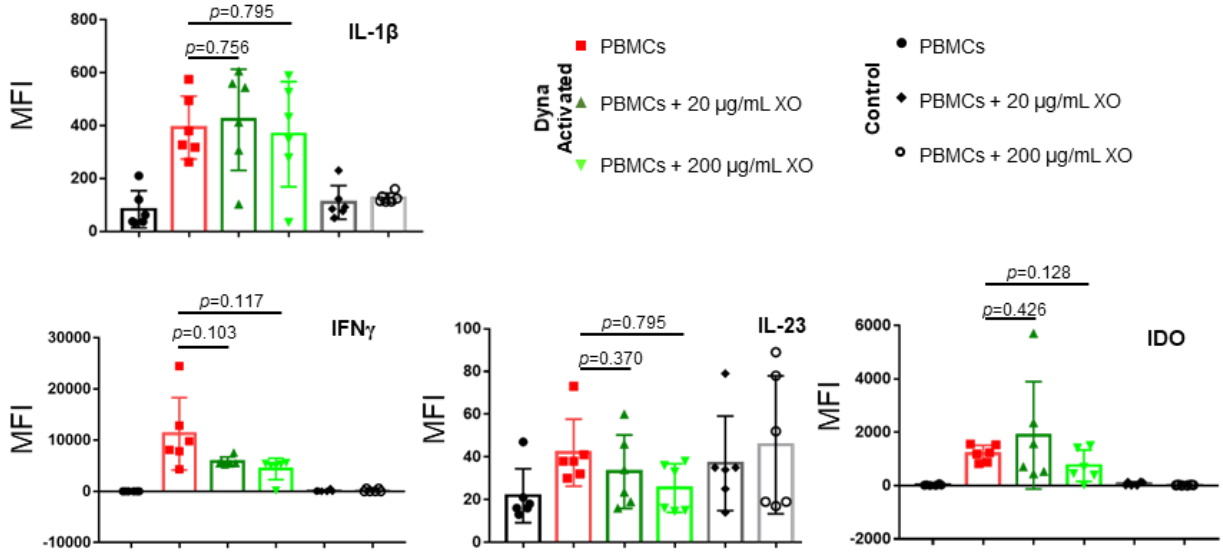

Figure 5.47. Cytokines analyses from co-cultures of human activated PBMCs. PBMCs were activated with bead-bound CD3/CD28 antibodies in the presence and absence of XOs. XOs in both 20 and 200 µg/mL concentrations slightly influenced the production of IL-1β, IL-23, IFNγ, and IDO (n = 4). Statistical significance is calculated through unpaired t-test with Welch's correction.

Cytokines are generally recognized as “signal 3”, which polarize helper T cells to Th1 (e.g. by IL-12 exposure) or Th17 (by IL-6 and IL-23) subsets. In addition, cytokines plays a fundamental role in clonal expansion and persistence of antigen-reactive T lymphocytes and their effector activity [130]. For instance, IFN-γ, IL-12, and IL-23 bind onto their receptors expressed on naïve CD4+ T cells and drive the differentiation of Th1 cell through the activation of signal transducer and activator of transcription 1 (STAT1), STAT4 and T box transcription factor (T-bet) [131,132]. Moreover, TNF–TNFR pairs control T-cell responses in two ways. First, they provide proliferative and survival signals either directly to the T cells or to the cognate APCs, regulating the frequency of effector and/or memory CD4+ or CD8+ T cells that can be differentiated from naive T cells in response to antigen stimulation. Second, they control T-cell function directly by promoting the production of cytokines such as IL-4 and IFNγ, or indirectly through stimulating the production of pro-inflammatory cytokines, such as IL-1 and IL-12, by professional or non-professional APCs [133]. Upregulated IL-6 binds onto its receptor and activates retinoid-related orphan receptor γ T (RORγt) and STAT3, driving Th17 cell differentiation and function [132,134]. Pathogenic Th17 cells are then polarized as a result of IL-23 and TGFβ3 stimulation [135].

We and others have observed that MSCs induced Treg expansion in a trans-well system only in the presence of splenocytes or peripheral blood monocytes, but not with purified CD4+ T cells [48,104,136,137]. Exosome-treated THP-1 (but not MyD88-deficient THP-1) cells polarized activated CD4+ T cells to CD4+CD25+FoxP3+ Tregs at a ratio of one exosome-treated THP-1 cell to 1,000 CD4+ T cells [54]. It is likely that XOs (as well as MSCs) play their immunosuppressive roles through interacting with myeloid lineage, and indeed, adoptive transfer of macrophages or monocytes, treated with MSC-EVs *in vitro* can protect the lung from injury [138,139]. We next sought to gain insight into the mechanisms by which XOs suppress macrophage

activation. **Figure 5.20d** shows the representative images of the SEAP activity (NFκB activation) as a result of 10 and 100 ng/mL LPS stimulation in the presence and absence of XOs. Luminescence count from IVIS imaging was quantified using equivalent regions on interest, suggesting that addition of 200 μg/mL of XOs reduces NFκB activation of both 10 ng/mL LPS (p = 0.044) and 100 ng/mL LPS (p = 0.004) activated THP-1 macrophages. Interestingly, 20 μg/mL of XOs did not efficiently reduce the NFκB activation. Same conditions were replicated, and signals were acquired using a plate reader, demonstrating a similar trend in the potency of XOs to inhibit NFκB activation (**Figure 5.20c**). Addition of 200 μg/mL XOs to the culture, reduced the luminescence counts of 10 ng/ml LPS activated THP-1 cells from 1097 ± 64 to 762 ± 71 (n = 4, p = 0.0132). Addition of 200 μg/mL XOs to the culture, reduced the luminescence counts of 100 ng/ml LPS activated THP-1 cells from 857 ± 112 to 336 ± 32 (n = 4, p = 0.0042). Surprisingly, XOs influenced the NFκB activation of non-activated THP-1 cells. Addition of 20 μg/mL XOs upregulated the NFκB activity in THP-1 cells from 109 ± 17 to 203 ± 20 (n = 4, p = 0.0117). Furthermore, addition of 200 μg/mL XOs upregulated the NFκB activity in THP-1 cells from 109 ± 17 to 215 ± 23 (n = 4, p = 0.0105). These results suggest that XOs could upregulate or downregulate the NFκB activity in macrophages, which partly recapitulates their parental MSCs, as MSCs themselves have been shown to regulate NFκB [140]. NFκB controls multiple aspects of innate and adaptive immunity, and plays a critical role in regulating the function, activation, and survival of innate immunocytes and inflammatory T cells [141]. NFκB pathway has been reported in response to PDMS [142], poly(ethylene glycol) [39], and alginate [40], and reduction in NFκB has been correlated with reduced fibrosis [42,142].

We recently showed that even ultrapure alginate activates murine macrophages to secrete pro-inflammatory cytokines, and conditioned media secreted from UC-MSCs suppress such

stimulation, partly through interfering with NfκB pathway. Such cytokine secretion is not exclusive to alginate stimulation. Even human macrophages co-cultures with endotoxin free chitosan or poly(lactic acid) have reported to secrete IL-8, MIP-1, MCP-1 and RANTES or IL-6, IL-8 and MCP-1 [143]. Two mechanisms have been described to explain the reasons for alginate-based inflammatory response. Some studies have suggested the presence of immunogens within alginate (such as lipopolysaccharide (LPS), lipoteichoic acid, and peptidoglycans) are the main inducers of inflammation [72,144]. Others reported that such contaminations were undetectable in their alginate [17,26,74], and linked the inflammatory response to the inherent properties of alginate. Alginate is a natural acidic polysaccharide extracted from marine brown seaweeds [75,76]. It is composed of different blocks of β-(1, 4)-D-mannuronate (M) and its C-5 epimer α-(1, 4)-L-guluronate (G), and Guluronate oligosaccharide derived from alginate has been reported to readily activate macrophages partly through Toll-like receptor 4 (TLR4) signaling pathway [75,76].

Conclusion

Foreign Body Response (FBR) against implanted materials creates patients discomfort and variety of health complications [23-25]. Moreover, if the goal is cell transplantation inside a biomaterial, FBR causes a non-functional graft engulfed in a scarring tissue [19]. This is one of the major challenges in clinical translation of tissue engineering and prosthesis products, sensors, and functional cell transplantation. One area that suffers from this issue is the islet transplantation to restore and maintain euglycemia in patients with T1D. This is an unmet clinical need with a significant potential health impact. We thus harnessed the anti-inflammatory properties of exosomes and fabricated an encapsulation technology that release exosomes in a controlled-fashion from alginate microcapsules (AlgXO). Rat islets encapsulated in AlgXO corrected the hyperglycemia in diabetic immunocompetent mice for > 5 months. Investigating

the plausible reasons, we found that AlgXO release its exosomal content over a week period, which then suppresses the infiltration and activation of immune cells, and macrophages in particular. While AlgXO is mainly focused on the islet transplantation, its core technology could be broadly applicable to other areas of cells transplantation and implants rejection due to immune response.

Materials and Methods

Isolation and Characterization of UC-MSCs and their XOs

Healthy pregnant women at full-term gestation (>37 weeks), maternal age 18-40 years old, and who gave birth at UCI Medical Center were chosen to be used for umbilical cord collection under IRB exemption #2016-2791. Any known complicated pregnancies were excluded from the collection. Umbilical cord derived Mesenchymal Stem Cells (UC-MSCs) were isolated according to the previously published method with some modifications. Briefly, UCs were washed with PBS under a sterile laminar flow cell culture hood and were cut longitudinally to remove blood vessels. Tissues were then cut into 2-3 mm^3 segments and incubated with 0.09% collagenase Type II (Sigma) for 45 minutes at 37 °C in a humidified incubator with 5% CO_2. After digestion, tissues were passed through a 100 μ mesh sized filters. Cells were then centrifuged at 300 ×g and 4 °C for 20 mins and resuspended in DMEM/F12 (Gibco) supplemented with 10% FBS, 1% penicillin/streptomycin and 1% L-glutamine. Cells transferred to 175 cm^2 flasks and incubated at 37°C in a humidified atmosphere with 5% CO_2. Flasks were left undisturbed for 2-3 days, after which the medium was changed to remove non-adherent cells.

UC-MSCs were further cultured in serum free media for 2 days. Next, exosome isolation was performed as previously described [48,51]. Briefly, conditioned media from cultures of MSC were centrifuged at 300 ×g for 10 minutes. Supernatant was collected and transferred to ultracentrifuge tubes (Polyallomer Quick-Seal centrifuge tubes 25×89 mm, Beckman Coulter). Samples were then centrifuged in a Beckman Coulter ultracentrifuge (Optima L-90 K or Optima XE- 90 Ultracentrifuge, Beckman Coulter) for 20 minutes at 16,500 ×g (Type Ti 45, Beckman Coulter), to remove microvesicles. Supernatant was then carefully collected and centrifuged for 2.5 h with a Type 45 Ti rotor at 4 °C at 120,000×g. Exosome pellet was resuspended in PBS and stored at -80°C.

20 μL XO was mixed with 1X RIPA (Cell signaling technologies, USA) buffer and sonicated for five minutes, three times, with vortexing in between. Protein contents were measured using a BCA protein assay kit (Thermo Scientific Pierce, Rockford, IL, USA). Then, 25 μL of BSA standard or 25 μL of sample were transferred to a 96 well plate, and 200 ml working reagent was added. The plate was incubated for 30 minutes at 37 °C and absorbance was analyzed with a SpectraMax 384 Plus spectrophotometer at 562 nm and the SoftMax Pro software (Molecular Devices, 1311 Orleans Drive, Sunnyvale, CA, USA). 20 μg of protein was then subjected to electrophoresis on a gradient precast polyacrylamide gel (Mini-PROTEAN®; Bio-Rad laboratories, Hercules, CA, USA). Samples were then transferred onto a nitrocellulose membrane which was then blocked with 5% Blotting Grade Blocker Non-Fat Dry Milk (Bio-Rad Laboratories) in Tris-buffer saline supplemented with %0.1 Polysorbate 20 (TBST) at 4°C overnight. Membrane was washed with TBST following by incubation with primary antibodies against Calnexin (clone H-70; Santa Cruz Biotechnology, Santa Cruz, CA, USA), Galectin-1/LGALS1 (D608T) Rabbit mAb (Cat# 12936), CD63 Rabbit mAb (Cat# EXOAB-CD63A-1),

GAPDH Rabbit mAb (Cat# ab181602), Hsp70 Rabbit mAb (Cat# EXOAB-Hsp70A-1), and TSG101 (clone 4A10; Abcam, Cambridge, UK) dissolved in 0.25% Blotting Grade Blocker Non-Fat Dry Milk in TBST overnight at 4 ºC. Next, membrane was washed with TBST for 10 minutes, in triplicate. Secondary antibodies ECL anti-rabbit IgG horseradish peroxidase-linked F(ab')2 fragment (donkey, anti-rabbit) (GE Healthcare, Buckinghamshire, UK) were diluted in 0.25% Blotting Grade Blocker Non-Fat Dry Milk in TBST and incubated for 1.5 hours. Membranes were analyzed with ECL Prime Western Blotting Detection (GE Healthcare) and a VersaDoc 4000 MP (Bio-Rad Laboratories).

XOs were labeled with anti-CD63-modified magnetic beads (Exosome Isolation CD63, Lot OK527, Life Technologies AS, Oslo, Norway) overnight with gentle agitation. The beads were washed with 1% exosome-depleted FBS in PBS and then incubated with human IgG (Sigma-Aldrich) for 15 minutes at 4°C. Following another washing step, the beads were incubated with PE-TGFβ, PE/Cy7-PD-L1 and APC/Cy7-MHCII or Isotype Controls (Biolegend, San Diego, USA) for 40 minutes with gentle agitation at room temperature. After another washing step, the samples were analyzed using a FACSAria (BD Bioscience) and data was processed using FlowJo Software (Tri Star, Ashland, OR, USA). Flow cytometry analysis of TGFβ, PD-L1, and MHCII expression on XOs bound to anti-CD63-coated beads demonstrated minimal expression of TGFβ-1 and MHCII, and the absence of PD-L1 (**Figure 5.1d**). We particularly sought to measure the expression of TGFβ-1 and PD-L1, as its expression on cancer cells XOs has been suggested to play a critical role in the immune evasion of tumor microenvironment [63-65].

Microcapsules Preparation

UPLVG alginate (NovaMatrix®, Sandvika, Norway) were fabricated by dissolving 2.5% w/v in 0.9% sterile saline solution and mounted on an air-driven electrostatic microcapsule generator (Nisco Engineering Inc., Oslo, Norway). The alginate solution was added dropwise into a sterile filtered (0.22 μm) gelling solution composed of sterile 20 mM barium chloride and 25 mM HEPES solution to generate circular microcapsules of ~350 microns in diameter. AlgXO

microgels were prepared by addition of $7.05 \times 10^{10} \pm 3.69 \times 10^{10}$ XOs/mL, thawed at RT for 10 to 20 mins. Microcapsules were then washed via centrifugation at 100 ×g and 4 ℃ for 5 mins.

Dissolving microcapsules and XOs collection

We first optimized microcapsule dissolution using EDTA chelator. EDTA (Sigma-Aldrich) with the concentration of 0.5 M was dissolved in DI water to make a stock solution. Dilutions were performed to test chelator activity at concentrations of 5 and 10 mM from the stock solution. 1 mL of each chelation solution was added on AlgXO or CTRL microcapsules (n = 1000 microcapsules/group) and were tested under phase contrast imaging. Images were obtained using EVOS Imaging system microscope (20/40 PH 2×; Thermo Fisher Scientific), and images were captured at 1 min intervals. To determine the dissociation, images were taken of images were analyzed using a microcapsule analysis program (Microcapsule Analysis Program.v5.0.2) in ImageJ. Images were then quantified by the number of microcapsules detected by the program as previously described [145]. Curves were made based on the following percentage: $\%\ \text{of Dissolved Microcapsules} = \frac{\text{Detected Microcapsules at t>0}}{\text{Detected Microacapsules at t=0}}$. Based on the results, microcapsules were dissolved for 10 mins in 10 mM EDTA solution (**Figure 5.3**). To quantify the XOs encapsulated within AlgXO, dissolved solution was then subjected to ultracentrifugation for 2.5 h at 4 °C and 120,000×g. Exosome pellet was resuspended in PBS and stored at -80°C until further analyses.

Rat Islet Quality Control and Viability

4 to 6 weeks old male Sprague-Dawley rats (Envigo Harlan, Houston, TX) were used as islet donors. Islet isolation was performed using standard collagenase digestion and gradient purification. Common duct was clamped on the side of mesoduodenum. Ice cold

collagenase V solution (6-7ml with concentration of 1 mg/ml in HBSS+) was injected into common bile duct (CBD) using 23G needle. Pancreas was then removed from dorsal wall of the abdominal cavity and transferred into 50ml conical tube on ice box. Pancreas in the conical tubes were kept at 37˚C water bath (with 30 rpm shaking) for 17 mins, after which 20ml cold HBSS+ was added into the conical tube and were hand shaken strongly. Islets were then isolated and purified using non-continuous density gradient as previously described. From each isolated batch, islets were tested for their quality including DTZ, viability and Glucose Stimulated Insulin Release (GSIR) assays as described below.

Upon each batch of islet isolation and prior to implantation, we ran quality control tests to identify the suitability of islets viability and function for transplantation. Islet count and purity (per rat pancreas) was 947 ± 137 IEQ as measured using DTZ staining (**Figure 5.4**). Viability of each isolation batch was more than 90% and in average it was 93% ± 2%. To quantify the viability of islets, 100 IEQ islets (either encapsulated or naked) were stained with Calcein AM (CalAM, Invitrogen, Cat# C1430) for live cells and propidium iodide (PI, Invitrogen, Cat# P3566) for dead and dying cells for 30 minutes. Stained islets were analyzed using a microplate reader (Tecan Infinite F200; Tecan). The islet viability was calculated by the equation: ($CalAM^+$ cells)/($CalAM^+$ cells + PI^+ cells) × 100.

GSIR assay was conducted to assure the islet quality prior to implantation. From each isolation batch, three technical replicates of 100 IE islets per sample were incubated at 37°C and 5% CO_2 for 1 hour in each media in the corresponding order: low glucose (2.8 mmol/L; L1), high glucose (28 mmol/L; H), high glucose plus 3-isobutyl-1-methylxanthine (28 mmol/L + 0.1 mmol/L IBMX; H+), and lastly back to low glucose (2.8 mmol/L; L2). Supernatant was collected and stored at −20°C until analysis. Insulin concentration released

during incubation was measured using a porcine insulin enzyme-linked immunosorbent assay (Mercodia, cat#10-1200-01). Absorbance was then measured using a microplate reader with 450-nm wavelength filter (Tecan Infinite F200 and Magellan V7) and presented as (μg/L). Stimulation index (SI) was calculated as the ratio of insulin concentration secreted in high glucose over the insulin concentration secreted in the first low-glucose incubation. Our islet quality control criteria were: SI units > 2, Viabilities > 90%, and purities > 90% (DTZ).

Streptozotocin Induction in Mice and Islet Transplantation

C57/BL6 mice were fasted overnight (at least 12 h) prior to Streptozotocin (STZ; Sigma CAS#: 18883-66-4) injection. STZ (180 mg/kg of mice body weight) was dissolved in 10 ml STZ buffer (0.1 M Sodium Citrate buffer pH=3.5) before injection. The buffer was vortexed and kept on ice for about 15 mins prior to i.p. administration. To assure the STZ induction, mice had to be hyperglycemic for at least a week. To minimize the surgery induced mortalities, mice blood glucose was adjusted prior to transplantation via insulin injection. All the blood glucose reads are non-fasting.

Glucose Tolerance Testing

Mice were fasted 10 to 14 h prior to Oral Glucose Tolerance Testing (OGTT) measurements. Next, a fresh glucose solution was prepared by dissolving 30% glucose in DPBS. Prior to glucose administration, mice blood glucose was measure. Mice were anesthetized with 2% isoflurane inhalation, and BW/100 ml of the glucose solution was orally injected into the stomach of the mice. Next, blood glucoses were measured through tail-vein snipping upon 10, 20, 30, 60, 90, 120, and 180 mins after glucose injection.

Fibrotic Tissue Sectioning

Fibrotic tissues (containing microcapsules) were cut and fixed in 4% PFA at 4 °C overnight. Next, tissues were washed with PBS 3× and embedded in 2% agar (CAT#: A1296, Sigma, USA). Agar molds were then embedded in plastic with wax. The entire cassette was placed in 58 °C paraffin bath for 15 minutes. Tissues were then sectioned with 7 μm thickness using an RM2255 microtome (Leica) with Superfrost slides. Prior to staining, an ethanol gradient dehydration and paraffin embedding cycle were performed.

Lavage and Fibrotic Tissue Flow Cytometry

Prior to removing the implants from the subcutaneous area, small incision was created on the distant site from the explants. 1 mL of cold DPBS was injected back and forth for 3× with pipette around the fibrotic microcapsules and suspended cells were removed and washed with DPBS. Next, cells were stained with CD3 (1:500 dilution, Biolegend Cat#: 100203), CD11b (1:200 dilution, Biolegend Cat#: 101211), I-A/I-E (1:200 dilution, Biolegend Cat#: 107628) CD19 (1:200 dilution, Biolegend Cat#: 115507) and CD206 (1:200 dilution, Biolegend, Cat#: 141711) in 2% BSA and 1% heat inactivated FBS. Similar panel was used for the cells isolated from fibrotic tissues around microcapsules with a slight difference. To isolate cells from fibrotic tissues, they were first minced into 2-5 mm pieces and then microcapsules were dissolved using 10 mM EDTA (see **supplementary Figure 3**). Clustering of flow cytometry data was completed by concatenating all 3 biological replicates into one file, and clustering with the tSNE (t-distributed stochastic neighbor embedding) plugin for 1000 iterations, operating at theta=0.5. Data are displayed as user-gated populations graphed against their respective X and Y tSNE coordinates.

Scanning Electron Microscopy

Both AlgXO or CTRL microcapsules were air-dried in an sterile chamber. prior to SEM analysis. Dried samples were placed on carbon-tapped imaging stubs. We used Philips XL-30 FEG SEM with EDS (Noran 6) system, which is a thermionic field emission SEM with a fully automatic gun configuration controlled by advanced computer technology (The magnification is up to 800,000X with 2nm resolution). The working distance was adjusted to be 10 mm at 0.5 kV voltage, and 10 pA as the beam current.

Controlled Release Studies

After fabrication, approximately 1000 AlgXO and CTRL microcapsules were plated in a 6-well plate at 37 °C in a humidified incubator with 5% CO_2. At indicated timepoints after co-incubation (**Figure 4g**), 1 mL of the culture supernatant were collected and 1 mL of sterile DPBS was replaces inside the well to keep the culture volume constant. Plates were sealed to minimize the loss of water due to evaporation. Isolated media was then measured for total protein concentration, and exosomal content using NTA.

Nanoparticle Tracking Analysis

NTA was performed using the Nanosight Nanosight NS3000system (Malvern instruments, USA). XOs (either from ultracentrifugation process or controlled release experiment) were suspended in PBS to contain approximately 107 to 1010 particles per ml, which fits within the detection limits of Nanosight NS3000. Exosomes were analyzed based on light scattering using an optical microscope aligned perpendicularly to the beam axis. A 60 s video was recorded and subsequently analyzed using NTA software.

Captive Bubble Contact Angle

We used a custom-made captive bubble, modifying the regular contact angel equipment (MCA-3, Kyowa Interface Science). Thin AlgXO and CTRL hydrogels were formed within a capillary space between two glass slides. Hydrogels on top of the glass slides were then merged into water beaker, and camera was focused on the hydrogel. Small air bubbles were then shut on the surface of hydrogel, creating the aqueous-solid-gas phase on the hydrogels surface. Images captured from the bubbles and contact angles were measured using ImageJ software with contact angle plugin, using circular and/or elliptical fits wherever appropriate.

Microcapsule Mechanical and Physical Properties

Mechanical properties of microcapsules were measured using a micro-scale tension-compression test system (MicroTester G2, CellScale, Ontario, Canada). The probe was constructed by attaching a 1 mm × 1 mm platen to a 154 μm cantilever and mounted to the instrument. Microcapsules were transferred by pipette into the test chamber, which was pre-filled with water. Single microcapsules were isolated using the platen-cantilever set-up, oriented by the attached microscope on the MicroTester to be in focus. The force as a function of time was measured for compressive strains of 0 to 50% using a 200 s loading time, a 10 s hold time, and a 20 s release time. Force Resolution was adjusted at 1 μN and spatial resolution at 1.5 μm. Measurements were recorded at 200 ms intervals. The force-displacement data was then converted into Stress-Strain, with the associated curve used to obtain a linear regression line from the Stress-Strain curve with < 0.2 Strain.

Simulation of release model for nanoparticle

To better understand the spatiotemporal profiles for the controlled release of XOs from AlgXO, we simulated such release using a MATLAB code. Simulations were run for homogenous spatially distributed XOs within AlgXO with diameter of 300 μm. Due to the 50-150 nm size distribution of XOs, we run the simulation with 50, 100, and 150 nm nanoparticle size. To further validate and characterize the release profiles other sizes (i.e. 10, 200, and 500 nm) were also tested in our simulation model. The 2.5% (weight/volume) alginate was used in our experimental studies, thus, we used the same percentage for the porosity of alginate calculations (equation 1):

Modeling assumptions

1. *Microcapsule size and porosity*

Simulations were run for uniformly sized and spatially distributed microcapsules and diameter was assumed to be 300 μm. Value of 2% (weight /volume) is evaluated as the default value for all simulations. Porosity of alginate solid is calculated by equation 1.

$$\text{porosity} = \frac{\rho 1 - \rho 2}{\rho 1 - \rho 3} \qquad (1)$$

$\rho 1$ is particle density, $\rho 2$ is bulk density, and $\rho 3$ is fluid density. For alginate solid, particle density is 1.6 g/ml, fluid density is density of water, which is 1g/ml. Bulk density will be based on the concentration of alginate, which is shown in equation 2.

$$\rho 2 = \frac{100 + C_{alg}}{100} \qquad (2)$$

2. *Surrounding media*

Assuming that capsules are implanted and surrounded by physiological fluid, surrounding viscosity was chosen to be $3.5*10^{-3}$ Pa*s.

3. *Temperature*

Assuming the capsule are implanted, temperature of microcapsule and surrounding environment should be close to body temperature, which is 37 degree.

4. *XOs concentration*

XOs are homogeneously mixed inside the microcapsules, with an initial concentration of 10 particles/μm^3.

5. *XOs size*

XOs are generally recognized to be between 30-150 nm. Thus, we set up the particle diameter as 10 nm, 50 nm, 100 nm, 200 nm, and 500 nm to see the different result as particle size changes. Particles larger than 450 nm cannot diffuse out from the capsule [18].

6. *Diffusion model*

To simplify our modeling, we just assumed that XOs diffuse out of microcapsules based on gradient density differences. We also assumed that a uniformed sphere symmetrically diffuses out in any direction. Thus, we established a 1-dimensional diffusion model for XOs.

<u>Mathematical model assumptions</u>

1. *1-D diffusion equation*

We are using heat equation to calculate the 1-dimensional diffusion of nanoparticles. Heat equation is a partial differential equation as shown in equation 3.

$$\frac{\partial c}{\partial t} = D * \frac{\partial^2 c}{\partial x^2} \qquad (3)$$

C is concentration gradient, t is time, and x is distance from center of the capsule. D is diffusion coefficient of XOs at certain position.

2. *Diffusion coefficient outside the microcapsule*

To determine diffusion coefficient outside the capsule, we use Stroke-Einstein equation (equation 4).

$$D = \frac{R}{N_A} * \frac{T}{6*\pi*\eta*r} \quad (4)$$

Where R is gas constant, NA is Avogadro constant, T is temperature in kelvin, η is viscosity of solution, and r is radius of XOs.

3. *Effective diffusion coefficient inside the capsule*

Effective diffusion coefficient inside a porous media is largely based on porosity and tortuosity of media. Generally, effective diffusion coefficient can be calculated based on equation 5.

$$D_{eff} = D * \frac{porosity}{tortuosity} \quad (5)$$

For porous media, normally we have a relationship between porosity and tortuosity, which is shown in equation 6.

$$tortuosity = porosity^{-\frac{1}{3}} \quad (6)$$

Since the microcapsule diameter is ~150 μm, the program will simulate concentration gradient from 0 to 500 μm. A 600 s run time was selected to visualize the concentration change inside the area. Diffusion of nanoparticle for 10 nm, 50 nm, 100 nm, 200 nm, and 500 nm is plotted (**Figure 5.16h**). As shown in the graph, nanoparticles with smaller diameter diffuse faster

than which with larger diameter (**Figure 5.17**). Particle with 500 nm diameter cannot diffuse out of the capsule. For particles with size of 10 nm, within 600 s, concentration of particles at center of the capsule will drop to 40% of initial concentration. For 50 nm nanoparticles, concentration at center of the capsule will drop to 80% of initial value. For 100 and 200 nm, there is no significant drop of concentration at center of the microcapsule. Concentration of nanoparticle outside the capsule also depends on particle size. For 10 nm nanoparticle, after 600 s, concentration of nanoparticle outside the capsule will larger than 15 particles/μm^3. For 50nm, 100nm, and 200nm, there is not enough nanoparticles 350 μm from center of the capsule (concentration < 1 particle/μm^3).

H&E, Masson's Trichrome and Immunofluorescence Staining

Trichrome staining was used to visualize collagen fibrosis around capsules. CTRL microcapsules were retrieved from mice after 2 weeks and fixed overnight using 4% paraformaldehyde at 4 °C, following by embedding in paraffin and sectioning. Xylene was used to deparaffinize sections prior to tissue staining. Hematoxylin and Eosin (H&E) staining was done following the standard procedure, and slides were mounted using Permount (Fisher Scientific) and 0.17 mm glass coverslips. Then, tissue samples were mounted on slides, and imaged under Nikon Ti–E fluorescent Microscope (Leica, USA).

Immunofluorescence imaging was performed to determine immune populations infiltrated around microcapsules. Microcapsules collected after 2 weeks of subcutaneous implantation were then blocked in agar and underwent paraffin embedding process then cut and mounted. Alcohol and xylene processing were performed to deparaffinized the samples then the spheres underwent heat-mediated antigen retrieval in pressure cooker with citrate buffer solution. The microcapsules were then blocked for 1 hour using a 1% bovine serum albumin (BSA)

solution. Next, tissue slides containing microcapsules were incubated for 1 hour in an immunostaining cocktail solution consisting of DAPI (500 nM), αSMA (1:500 dilution, Biolegend Cat#: MMS-466S) and CD68 (1:200 dilution, Biolegend Lot#: B229996), CD3 (1:500 dilution, Biolegend Cat#: 100203), CD11b (1:200 dilution, Biolegend Cat#: 101211), I-A/I-E (1:200 dilution, Biolegend Cat#: 107628) and CD206 (1:200 dilution, Biolegend, Cat#: 141711) in 2% BSA. To stain the microcapsules dollected from i.p. cavity, they were washed three times with a 0.1% Tween 20 dissolved in 5% BSA solution and maintained in a 50% glycerol solution. Spheres were then transferred to glass slides and imaged using an Olympus FV3000 Laser-Scanning Confocal Spectral Inverted Microscope (Olympus, USA) equipped with 5 and 10X objectives. 405 nm, 488 nm, and 640 nm solid-state lasers were used, and the laser power was adjusted to be 1%-1.5% in all channels.

Protein adsorption was also conducted via co-incubation of IgG fluorescent antibody (PE mouse $IgG^{1\kappa}$ isotype ctrl clone: MOPC-21, Biolegend, CAT#: 400111) with AlgXO or CTRL microcapsules for 24 h. Microcapsules were then transferred to glass slides and imaged using an Olympus FV3000 Laser-Scanning Confocal Spectral Inverted Microscope (Olympus, USA). The 488 nm solid-state laser was used, and the laser power was adjusted to be 1%-1.5%.

Human PBMCs Proliferation and Cytokine Assay

Peripheral blood mononuclear cells (PBMCs) were isolated from buffy coats from healthy and anonymous blood donors (UCI institute for clinical and transitional science) by density gradient centrifugation (Ficoll-Pague plus, GE Healthcare). For proliferation assay, 20 μg of XOs were incubated with 1×10^5 CFSE [5(6)-carboxyfluoresceindiacetate N-succinimidyl ester] (Molecular Probes, Eugene, OR) labeled PBMCs. To activate T-cell proliferation, Dynabeads™ Human T-Activator CD3/CD28 for T Cell Expansion and Activation was used

with 1:1 ratio of PBMCs:Dynabeads™. PBMCs proliferation was analyzed after 4 days using flow cytometry (FACSAria, BD) and data was analyzed using the FlowJo. For cytokine analysis, cells were cultured in RPMI 1640 with 10% heat inactivated FBS, 1% penicillin/streptomycin and 1% L-glutamine. Cells transferred to 96 or 48 well plates and incubated at 37°C in a humidified atmosphere with 5% CO_2. Dynabeads Human T-Activator CD3/CD28 for T cell expansion and activation was used with 1:1 ratio of PBMCs:Dynabeads. The XOs were mixed with fresh culture media (with 20 μg/mL and 200 μg/mL concentrations). DynaBeads were then added to isolated PBMCs in the presence and absence of XOs. Supernatants were collected and Luminex assay was used to analyze the secreted cytokines. 50 μl of PBMC culture supernatants were collected and either frozen at -80 °C or immediately analyzed using a human custom ProcartaPlex (11plex, ThermoFisher Scientific, Vienna, Austria) with Luminex 77. Results were then reported as Mean Fluorescence Intensity (MFI).

Splenocytes and T-cells Proliferation Assay

Spleens from C57/BL6 male mice were dissected, filtered into a single-cell suspension using 70 μm sterile filter, and red blood cells were removed using Tris-acetic-acid-chloride (TAC). Splenocytes were washed once with PBS and resuspended at 15×10^6 /mL in staining buffer (0.01% BSA in PBS). Splenocytes were stained with proliferation dye eFluor™ 670 (ThermoFisher Scientific, CAT#: 65-0840-85) using 5mM dye per 10 M cells and incubated in a 37 °C water bath for 10 min. Finally, cells were washed and resuspended at 1 M/mL in RPMI 1640 w/ HEPES+ L-glutamine (Gibco, CAT#: 22400-105) complete medium containing 10% FBS (Atlanta Biologicals, CAT#: S11150), 1X non-essential amino acids (Gibco, CAT#: 11146-050), 100U/mL penicillin-100μg/mL streptomycin (Gibco, CAT#: 15140163), 1mM sodium pyruvate (Gibco, CAT#:11360- 070), and 55 μM β-mercaptoethanol (Gibco, CAT#:21985-023),

eFluor™ 670-labeled Splenocytes were plated (50×10^3/well) in a U-bottom 96-well plate (VWR, CAT#: 10062-902) and activated with plate bound anti-Armenian hamster IgG (30μg/mL, Jackson Immuno research, CAT#:127-005-099) with CD3 (0.5 μg/mL, Tonbo, CAT#: 70-0031) and CD28 (1 μg/mL, Tonbo, CAT#: 70-0281). XOs with 20 or 200 μg/mL concentration were added to the co-cultures after cell seedings. After 4 days of culture, cells were stained with Zombie Live/Dead Dye (BioLegend, CAT#: 423105) and live cells were analyzed for proliferation.

Similar procedure was conducted for T lymphocytes, where isolated splenocytes were subjected to EasySep™ Mouse T cell Isolation Kit (StemCell Technologies, CAT#: 19851) according to the manufacturer's instructions. After 4 days of co-cultures, T cells were collected and blocked with anti-mouse CD16/32 (BioLegend, CAT#: 101302), stained with Zombie Live/Dead Dye and fluorescent-conjugated antibodies: CD4 (BioLegend, CAT#: 100512; clone RM4-5), and CD8 (BioLegend, CAT#: 100709; clone 53- 6.7). Cells were processed using the BD LSR II or BD LSRFortessa™ X-20 flow cytometer and analyzed using FlowJo software v10.0.7 (Tree Star, Inc).

Macrophage Activation Assay

RAW 264.7 cells were purchased from ATCC (CAT# TIB-71) and NFκB reporter Luc-THP-1 human cell lines were purchased from InvivoGen (CAT#: thpl-nfkb) employed for downstream experiments of this study. Passages 5-10 were cultured in RPMI 1640 supplemented with 10% of heat inactivated FBS in the presence of 1% penicillin/streptomycin and 1% L-glutamine. Cells were then stimulated with 10 or 100 ng/mL of LPS (Invitrogen, CAT#: 50-112-2025). Stimulated and non-stimulated cells were then mixed with XOs with the mentioned concentrations in the results section. Control cells, LPS stimulated cells in the presence and

absence of XOs, and non-stimulated cells in the presence and absence of XOs (100,000 cells for each condition) were co-cultured for 10-14 h at 37 °C in a humidified incubator with 5% CO_2. Next, supernatant was collected for cytokine analyses. Supernatants were centrifuges at 2500 ×g and 4 °C for 5 mins and stored at -80 °C. Samples were then shipped on dry ice to Eve Technologies (Calgary, Canada), where cytokines were analyzed using Mouse Focused 32-Plex Discovery Assay (CAT#: 17619).

IVIS Imaging

NFκB reporter Luc-THP-1 human cell lines were used which are integration of an NFκB-inducible secreted embryonic alkaline phosphatase (SEAP) reporter construct. These cells are engineered THP-1 monocyte cell line by stable integration of an NFκB-inducible Luc reporter construct. The levels of NFκB-induced secreted luciferase in the cell culture supernatant are readily assessed with Quanti-Luc (CAT#: rep-qlc2). As a result, these cells could quantitatively measure NFκB activation by determining the activity of SEAP. Cell were cultured in a phenol free media and supernatants (as described in the in vitro co-culture section of the methods) were collected. QUANT-Luc assay solution was added with a concentration of 1 mg/mL and incubated for 30 seconds. The resulted plate was then imaged in an IVIS imager (or VersaDoc 4000 MP). Exposure time was adjusted as 0.2 sec, field of view 12.5, f number 16, and binning factor of 4 were selected as optimized acquisition settings.

Animal Studies

All animal procedures were performed under approved University of California Irvine, Institutional Animal Care and Use Committee (Protocol #: AUP-17-241), in accordance with the guidelines of the National Institutes of Health.

References

1 Vegas, A. J. *et al.* Long-term glycemic control using polymer-encapsulated human stem cell–derived beta cells in immune-competent mice. *Nature Medicine* **22**, 306-311, doi:10.1038/nm.4030 (2016).

2 Mao, A. S. *et al.* Programmable microencapsulation for enhanced mesenchymal stem cell persistence and immunomodulation. *Proceedings of the National Academy of Sciences* **116**, 15392, doi:10.1073/pnas.1819415116 (2019).

3 Kojima, R. *et al.* Designer exosomes produced by implanted cells intracerebrally deliver therapeutic cargo for Parkinson's disease treatment. *Nature Communications* **9**, 1305, doi:10.1038/s41467-018-03733-8 (2018).

4 Parmar, M., Grealish, S. & Henchcliffe, C. The future of stem cell therapies for Parkinson disease. *Nature Reviews Neuroscience* **21**, 103-115, doi:10.1038/s41583-019-0257-7 (2020).

5 Wehling, M. Non-steroidal anti-inflammatory drug use in chronic pain conditions with special emphasis on the elderly and patients with relevant comorbidities: management and mitigation of risks and adverse effects. *European Journal of Clinical Pharmacology* **70**, 1159-1172, doi:10.1007/s00228-014-1734-6 (2014).

6 Srinivasan, A. & De Cruz, P. Review article: a practical approach to the clinical management of NSAID enteropathy. *Scandinavian Journal of Gastroenterology* **52**, 941-947, doi:10.1080/00365521.2017.1335769 (2017).

7 Tekin, Z. *et al.* Outcomes of Pancreatic Islet Allotransplantation Using the Edmonton Protocol at the University of Chicago. *Transplant Direct* **2**, e105-e105, doi:10.1097/TXD.0000000000000609 (2016).

8 Shapiro, A. M. J. *et al.* Islet Transplantation in Seven Patients with Type 1 Diabetes Mellitus Using a Glucocorticoid-Free Immunosuppressive Regimen. *New England Journal of Medicine* **343**, 230-238, doi:10.1056/NEJM200007273430401 (2000).

9 Shapiro, A. M. J. *et al.* International Trial of the Edmonton Protocol for Islet Transplantation. *New England Journal of Medicine* **355**, 1318-1330, doi:10.1056/NEJMoa061267 (2006).

10 Desai, T. & Shea, L. D. Advances in islet encapsulation technologies. *Nature Reviews Drug Discovery* **16**, 338, doi:10.1038/nrd.2016.232 (2016).

11 Franklin Lim & Sun, A. M. Microencapsulated Islets as Bioartificial Endocrine Pancreas. *Science* **210** (1980).

12 Tuch, B. E. *et al.* Safety and Viability of Microencapsulated Human Islets Transplanted Into Diabetic Humans. *Diabetes Care* **32**, 1887, doi:10.2337/dc09-0744 (2009).

13 Basta, G. *et al.* Long-Term Metabolic and Immunological Follow-Up of Nonimmunosuppressed Patients With Type 1 Diabetes Treated With Microencapsulated Islet Allografts. *Diabetes Care* **34**, 2406, doi:10.2337/dc11-0731 (2011).

14 Orive, G. *et al.* Engineering a Clinically Translatable Bioartificial Pancreas to Treat Type I Diabetes. *Trends in Biotechnology* (2018).

15 Evron, Y. *et al.* Long-term viability and function of transplanted islets macroencapsulated at high density are achieved by enhanced oxygen supply. *Scientific Reports* **8**, 6508, doi:10.1038/s41598-018-23862-w (2018).

16 Veiseh, O. *et al.* Size- and shape-dependent foreign body immune response to materials implanted in rodents and non-human primates. *Nature Materials* **14**, 643, doi:10.1038/nmat4290 https://www.nature.com/articles/nmat4290#supplementary-information (2015).

17 Doloff, J. C. *et al.* Colony stimulating factor-1 receptor is a central component of the foreign body response to biomaterial implants in rodents and non-human primates. *Nature Materials* **16**, 671, doi:10.1038/nmat4866 https://www.nature.com/articles/nmat4866#supplementary-information (2017).

18 Rezaa Mohammadi, M., Rodrigez, S., Cao, R., Alexander, M. & Lakey, J. R. T. Immune response to subcutaneous implants of alginate microcapsules. *Materials Today: Proceedings* **5**, 15580-15585, doi:https://doi.org/10.1016/j.matpr.2018.04.166 (2018).

19 Bochenek, M. A. *et al.* Alginate encapsulation as long-term immune protection of allogeneic pancreatic islet cells transplanted into the omental bursa of macaques. *Nature Biomedical Engineering* **2**, 810-821, doi:10.1038/s41551-018-0275-1 (2018).

20 Farah, S. *et al.* Long-term implant fibrosis prevention in rodents and non-human primates using crystallized drug formulations. *Nature Materials* **18**, 892-904, doi:10.1038/s41563-019-0377-5 (2019).

21 de Vos, P., Hamel, A. F. & Tatarkiewicz, K. Considerations for successful transplantation of encapsulated pancreatic islets. *Diabetologia* **45**, 159-173, doi:10.1007/s00125-001-0729-x (2002).

22 Vaithilingam, V. & Tuch, B. E. Islet transplantation and encapsulation: an update on recent developments. *The Review of Diabetic Studies* **8** (2011).

23 Mohammadi, M. R., Luong, J. C., Kim, G. G., Lau, H. & Lakey, J. R. T. in *Handbook of Tissue Engineering Scaffolds: Volume One* (eds Masoud Mozafari, Farshid Sefat, & Anthony Atala) 127-152 (Woodhead Publishing, 2019).

24 Swanson, E. Analysis of US Food and Drug Administration Breast Implant Postapproval Studies Finding an Increased Risk of Diseases and Cancer: Why the Conclusions Are Unreliable. *Ann Plast Surg* **82**, 253-254, doi:10.1097/SAP.0000000000001732 (2019).

25 Headon, H., Kasem, A. & Mokbel, K. Capsular Contracture after Breast Augmentation: An Update for Clinical Practice. *Arch Plast Surg* **42**, 532-543, doi:10.5999/aps.2015.42.5.532 (2015).

26 Vegas, A. J. *et al.* Combinatorial hydrogel library enables identification of materials that mitigate the foreign body response in primates. *Nature Biotechnology* **34**, 345, doi:10.1038/nbt.3462 https://www.nature.com/articles/nbt.3462#supplementary-information (2016).

27 Headen, D. M. *et al.* Local immunomodulation with Fas ligand-engineered biomaterials achieves allogeneic islet graft acceptance. *Nature Materials* **17**, 732-739, doi:10.1038/s41563-018-0099-0 (2018).

28 Alagpulinsa, D. A. *et al.* Alginate-microencapsulation of human stem cell–derived β cells with CXCL12 prolongs their survival and function in immunocompetent mice without systemic immunosuppression. *American Journal of Transplantation* **19**, 1930-1940, doi:10.1111/ajt.15308 (2019).

29 Liu, Q. *et al.* Zwitterionically modified alginates mitigate cellular overgrowth for cell encapsulation. *Nature Communications* **10**, 5262, doi:10.1038/s41467-019-13238-7 (2019).
30 Spasojevic, M. *et al.* Reduction of the Inflammatory Responses against Alginate-Poly-L-Lysine Microcapsules by Anti-Biofouling Surfaces of PEG-b-PLL Diblock Copolymers. *PLOS ONE* **9**, e109837, doi:10.1371/journal.pone.0109837 (2014).
31 Vacanti, N. M. *et al.* Localized Delivery of Dexamethasone from Electrospun Fibers Reduces the Foreign Body Response. *Biomacromolecules* **13**, 3031-3038, doi:10.1021/bm300520u (2012).
32 Hachim, D., LoPresti, S. T., Yates, C. C. & Brown, B. N. Shifts in macrophage phenotype at the biomaterial interface via IL-4 eluting coatings are associated with improved implant integration. *Biomaterials* **112**, 95-107, doi:https://doi.org/10.1016/j.biomaterials.2016.10.019 (2017).
33 Chen, T. *et al.* Alginate Encapsulant Incorporating CXCL12 Supports Long-Term Allo- and Xenoislet Transplantation Without Systemic Immune Suppression. *American Journal of Transplantation* **15**, 618-627, doi:10.1111/ajt.13049 (2015).
34 Cannarile, M. A. *et al.* Colony-stimulating factor 1 receptor (CSF1R) inhibitors in cancer therapy. *Journal of Immunotherapy of Cancer* **5** (2017).
35 Papadopoulos, K. P. *et al.* First-in-human study of AMG 820, a monoclonal anti-colony-stimulating factor 1 receptor antibody, in patients with advanced solid tumors. *Clinical Cancer Research* **23**, 5703-5710 (2017).
36 Sanchez, A. B. *et al.* CXCL12-induced neurotoxicity critically depends on NMDA receptor-gated and l-type Ca2+ channels upstream of p38 MAPK. *Journal of Neuroinflammation* **13**, 252, doi:10.1186/s12974-016-0724-2 (2016).
37 Lin, J. T. *et al.* TNFα blockade in human diseases: An overview of efficacy and safety. *Clinical Immunology* **126**, 121-136 (2008).
38 Walton, K. L., Johnson, K. E. & Harrison, C. A. Targeting TGF-β Mediated SMAD Signaling for the Prevention of Fibrosis. *Front Pharmacol* **8**, 461-461, doi:10.3389/fphar.2017.00461 (2017).
39 Amer, L. D. *et al.* Inflammation via myeloid differentiation primary response gene 88 signaling mediates the fibrotic response to implantable synthetic poly(ethylene glycol) hydrogels. *Acta Biomaterialia*, doi:https://doi.org/10.1016/j.actbio.2019.09.043 (2019).
40 Yang, D. & Jones, K. S. Effect of alginate on innate immune activation of macrophages. *Journal of Biomedical Materials Research Part A* **90A**, 411-418, doi:10.1002/jbm.a.32096 (2009).
41 Lawlor, C. *et al.* Treatment of Mycobacterium tuberculosis-Infected Macrophages with Poly(Lactic-Co-Glycolic Acid) Microparticles Drives NFκB and Autophagy Dependent Bacillary Killing. *PLOS ONE* **11**, e0149167, doi:10.1371/journal.pone.0149167 (2016).
42 Moore, L. B. & Kyriakides, T. R. in *Immune Responses to Biosurfaces.* (eds John D. Lambris, Kristina N. Ekdahl, Daniel Ricklin, & Bo Nilsson) 109-122 (Springer International Publishing).
43 Moreno, J. L., Mikhailenko, I., Tondravi, M. M. & Keegan, A. D. IL-4 promotes the formation of multinucleated giant cells from macrophage precursors by a STAT6-dependent, homotypic mechanism: contribution of E-cadherin. *Journal of leukocyte biology* **82**, 1542-1553 (2007).

44 Mukherjee, S., Darzi, S., Paul, K., Werkmeister, J. A. & Gargett, C. E. Mesenchymal stem cell-based bioengineered constructs: foreign body response, cross-talk with macrophages and impact of biomaterial design strategies for pelvic floor disorders. *Interface Focus* **9**, 20180089, doi:10.1098/rsfs.2018.0089 (2019).

45 Su, V. Y.-F., Lin, C.-S., Hung, S.-C. & Yang, K.-Y. Mesenchymal Stem Cell-Conditioned Medium Induces Neutrophil Apoptosis Associated with Inhibition of the NF-κB Pathway in Endotoxin-Induced Acute Lung Injury. *Int J Mol Sci* **20**, 2208, doi:10.3390/ijms20092208 (2019).

46 Vigo, T. *et al.* IFN-γ orchestrates mesenchymal stem cell plasticity through the signal transducer and activator of transcription 1 and 3 and mammalian target of rapamycin pathways. *Journal of Allergy and Clinical Immunology* **139**, 1667-1676, doi:https://doi.org/10.1016/j.jaci.2016.09.004 (2017).

47 Chen, C.-P. M. D. P. D., Tsai, P.-S. P. D. & Huang, C.-J. M. D. P. D. Antiinflammation Effect of Human Placental Multipotent Mesenchymal Stromal Cells Is Mediated by Prostaglandin E2via a Myeloid Differentiation Primary Response Gene 88-dependent Pathway. *Anesthesiology: The Journal of the American Society of Anesthesiologists* **117**, 568-579, doi:10.1097/ALN.0b013e31826150a9 (2012).

48 Riazifar, M. *et al.* Stem Cell-Derived Exosomes as Nanotherapeutics for Autoimmune and Neurodegenerative Disorders. *ACS Nano* **13**, 6670-6688, doi:10.1021/acsnano.9b01004 (2019).

49 Yin, J. Q., Zhu, J. & Ankrum, J. A. Manufacturing of primed mesenchymal stromal cells for therapy. *Nature Biomedical Engineering* **3**, 90-104, doi:10.1038/s41551-018-0325-8 (2019).

50 Riazifar, M., Pone, E. J., Lötvall, J. & Zhao, W. Stem Cell Extracellular Vesicles: Extended Messages of Regeneration. *Annual Review of Pharmacology and Toxicology* **57**, 125-154, doi:10.1146/annurev-pharmtox-061616-030146 (2017).

51 Mohammadi, M. R. *et al.* Isolation and characterization of microvesicles from mesenchymal stem cells. *Methods*, doi:https://doi.org/10.1016/j.ymeth.2019.10.010 (2019).

52 Zhang, B. *et al.* Mesenchymal stromal cell exosome–enhanced regulatory T-cell production through an antigen-presenting cell–mediated pathway. *Cytotherapy* **20**, 687-696, doi:https://doi.org/10.1016/j.jcyt.2018.02.372 (2018).

53 Bai, L. *et al.* Effects of Mesenchymal Stem Cell-Derived Exosomes on Experimental Autoimmune Uveitis. *Scientific Reports* **7**, 4323, doi:10.1038/s41598-017-04559-y (2017).

54 Zhang, B. *et al.* Mesenchymal Stem Cells Secrete Immunologically Active Exosomes. *Stem Cells and Development* **23**, 1233-1244, doi:10.1089/scd.2013.0479 (2013).

55 Lankford, K. L. *et al.* Intravenously delivered mesenchymal stem cell-derived exosomes target M2-type macrophages in the injured spinal cord. *PLOS ONE* **13**, e0190358, doi:10.1371/journal.pone.0190358 (2018).

56 Fan, Y. *et al.* Human Fetal Liver Mesenchymal Stem Cell-Derived Exosomes Impair Natural Killer Cell Function. *Stem Cells and Development* **28**, 44-55, doi:10.1089/scd.2018.0015 (2018).

57 Burrello, J. *et al.* Stem cell-derived extracellular vesicles and immune-modulation. *Frontiers in cell and developmental biology* **4**, 83 (2016).

58 Khare, D. *et al.* Mesenchymal Stromal Cell-Derived Exosomes Affect mRNA Expression and Function of B-Lymphocytes. *Front Immunol* **9**, 3053-3053, doi:10.3389/fimmu.2018.03053 (2018).
59 Carreras-Planella, L., Monguió-Tortajada, M., Borràs, F. E. & Franquesa, M. Immunomodulatory Effect of MSC on B Cells Is Independent of Secreted Extracellular Vesicles. *Front Immunol* **10**, 1288 (2019).
60 Shigemoto-Kuroda, T. *et al.* MSC-derived Extracellular Vesicles Attenuate Immune Responses in Two Autoimmune Murine Models: Type 1 Diabetes and Uveoretinitis. *Stem Cell Reports* **8**, 1214-1225, doi:https://doi.org/10.1016/j.stemcr.2017.04.008 (2017).
61 Mennan, C., Garcia, J., Roberts, S., Hulme, C. & Wright, K. A comprehensive characterisation of large-scale expanded human bone marrow and umbilical cord mesenchymal stem cells. *Stem Cell Research & Therapy* **10**, 99, doi:10.1186/s13287-019-1202-4 (2019).
62 LV, F.-J., TUAN, R. S., CHEUNG, K. M. C. & LEUNG, V. Y. L. Concise Review: The Surface Markers and Identity of Human Mesenchymal Stem Cells. *Stem Cells* **32**, 1408–1419 (2014).
63 Daassi, D., Mahoney, K. M. & Freeman, G. J. The importance of exosomal PDL1 in tumour immune evasion. *Nature Reviews Immunology*, doi:10.1038/s41577-019-0264-y (2020).
64 Chen, G. *et al.* Exosomal PD-L1 contributes to immunosuppression and is associated with anti-PD-1 response. *Nature* **560**, 382-386, doi:10.1038/s41586-018-0392-8 (2018).
65 Haderk, F. *et al.* Tumor-derived exosomes modulate PD-L1 expression in monocytes. *Science Immunology* **2**, eaah5509, doi:10.1126/sciimmunol.aah5509 (2017).
66 Sun, Y. *et al.* Human Mesenchymal Stem Cell Derived Exosomes Alleviate Type 2 Diabetes Mellitus by Reversing Peripheral Insulin Resistance and Relieving β-Cell Destruction. *ACS Nano* **12**, 7613-7628, doi:10.1021/acsnano.7b07643 (2018).
67 Matsumoto, S. *et al.* Clinical Porcine Islet Xenotransplantation Under Comprehensive Regulation. *Transplantation Proceedings* **46**, 1992-1995, doi:https://doi.org/10.1016/j.transproceed.2014.06.008 (2014).
68 Ekser, B., Bottino, R. & Cooper, D. K. C. Clinical Islet Xenotransplantation: A Step Forward. *EBioMedicine* **12**, 22-23, doi:https://doi.org/10.1016/j.ebiom.2016.09.023 (2016).
69 Chinnakotla, S. *et al.* Factors Predicting Outcomes After a Total Pancreatectomy and Islet Autotransplantation Lessons Learned From Over 500 Cases. *Annals of Surgery* **262**, 610–622 (2015).
70 Nie, W. *et al.* Human mesenchymal-stem-cells-derived exosomes are important in enhancing porcine islet resistance to hypoxia. *Xenotransplantation* **25**, e12405, doi:10.1111/xen.12405 (2018).
71 Yesilyurt, V. *et al.* A Facile and Versatile Method to Endow Biomaterial Devices with Zwitterionic Surface Coatings. *Advanced Healthcare Materials* **6**, 1601091, doi:10.1002/adhm.201601091 (2017).
72 Paredes-Juarez, G. A., de Haan, B. J., Faas, M. M. & de Vos, P. The role of pathogen-associated molecular patterns in inflammatory responses against alginate based microcapsules. *Journal of Controlled Release* **172**, 983-992, doi:https://doi.org/10.1016/j.jconrel.2013.09.009 (2013).

73 Paredes Juárez, G. A., Spasojevic, M., Faas, M. M. & de Vos, P. Immunological and Technical Considerations in Application of Alginate-Based Microencapsulation Systems. *Frontiers in Bioengineering and Biotechnology* **2**, 26 (2014).
74 Jhunjhunwala, S. *et al.* Neutrophil Responses to Sterile Implant Materials. *PLOS ONE* **10**, e0137550, doi:10.1371/journal.pone.0137550 (2015).
75 Bi, D. *et al.* Alginate enhances Toll-like receptor 4-mediated phagocytosis by murine RAW264.7 macrophages. *International Journal of Biological Macromolecules* **105**, 1446-1454, doi:https://doi.org/10.1016/j.ijbiomac.2017.07.129 (2017).
76 Fang, W. *et al.* Identification and activation of TLR4-mediated signalling pathways by alginate-derived guluronate oligosaccharide in RAW264.7 macrophages. *Scientific Reports* **7**, 1663, doi:10.1038/s41598-017-01868-0 (2017).
77 Stock, A. A. *et al.* Conformal Coating of Stem Cell-Derived Islets for β Cell Replacement in Type 1 Diabetes. *Stem Cell Reports*, doi:https://doi.org/10.1016/j.stemcr.2019.11.004 (2019).
78 Shi, C. & Pamer, E. G. Monocyte recruitment during infection and inflammation. *Nature Reviews Immunology* **11**, 762-774, doi:10.1038/nri3070 (2011).
79 Madan, R. *et al.* Role of Leptin-Mediated Colonic Inflammation in Defense against Clostridium difficile Colitis. *Infection and Immunity* **82**, 341, doi:10.1128/IAI.00972-13 (2014).
80 Lacey, D. C. *et al.* Defining GM-CSF– and Macrophage-CSF–Dependent Macrophage Responses by In Vitro Models. *The Journal of Immunology* **188**, 5752, doi:10.4049/jimmunol.1103426 (2012).
81 Sica, A. & Mantovani, A. Macrophage plasticity and polarization: in vivo veritas. *The Journal of Clinical Investigation* **122**, 787-795, doi:10.1172/JCI59643 (2012).
82 Yoshimura, T. The chemokine MCP-1 (CCL2) in the host interaction with cancer: a foe or ally? *Cellular & Molecular Immunology* **15**, 335-345, doi:10.1038/cmi.2017.135 (2018).
83 Kornfield, T. E. & Newman, E. A. Regulation of Blood Flow in the Retinal Trilaminar Vascular Network. *The Journal of Neuroscience* **34**, 11504, doi:10.1523/JNEUROSCI.1971-14.2014 (2014).
84 Chung, L. *et al.* Interleukin-17 and senescence regulate the foreign body response. *bioRxiv*, 583757, doi:10.1101/583757 (2019).
85 Vlahos, A. E., Cober, N. & Sefton, M. V. Modular tissue engineering for the vascularization of subcutaneously transplanted pancreatic islets. *Proceedings of the National Academy of Sciences* **114**, 9337–9342 (2017).
86 Hey, Y.-Y., Tan, J. K. H. & O'Neill, H. C. Redefining Myeloid Cell Subsets in Murine Spleen. *Front Immunol* **6**, 652 (2016).
87 Mohammadi, M. R., Corbo, C., Molinaro, R. & Lakey, J. R. T. Biohybrid Nanoparticles to Negotiate with Biological Barriers. *Small* **15**, 1902333, doi:10.1002/smll.201902333 (2019).
88 Seong, S.-Y. & Matzinger, P. Hydrophobicity: an ancient damage-associated molecular pattern that initiates innate immune responses. *Nature Reviews Immunology* **4**, 469-478, doi:10.1038/nri1372 (2004).

89 Zhang, W. & Hallström, B. Membrane characterization using the contact angle technique I. methodology of the captive bubble technique. *Desalination* **79**, 1-12, doi:https://doi.org/10.1016/0011-9164(90)80067-L (1990).
90 Zhang, L. *et al.* Zwitterionic hydrogels implanted in mice resist the foreign-body reaction. *Nature Biotechnology* **31**, 553, doi:10.1038/nbt.2580 https://www.nature.com/articles/nbt.2580#supplementary-information (2013).
91 Anderson, J. M., Rodriguez, A. & Chang, D. T. Foreign body reaction to biomaterials. *Seminars in Immunology* **20**, 86-100, doi:https://doi.org/10.1016/j.smim.2007.11.004 (2008).
92 Hu, W. J., Eaton, J. W. & Tang, L. Molecular basis of biomaterial-mediated foreign body reactions. *Blood* **98**, 1231-1238, doi:10.1182/blood.V98.4.1231 (2001).
93 Keselowsky, B. G., Collard, D. M. & García, A. J. Surface chemistry modulates fibronectin conformation and directs integrin binding and specificity to control cell adhesion. *Journal of Biomedical Materials Research Part A: An Official Journal of The Society for Biomaterials, The Japanese Society for Biomaterials, and The Australian Society for Biomaterials and the Korean Society for Biomaterials* **66**, 247-259 (2003).
94 Pelaz, B. *et al.* Surface functionalization of nanoparticles with polyethylene glycol: effects on protein adsorption and cellular uptake. *ACS nano* **9**, 6996-7008 (2015).
95 Sigal, G. B., Mrksich, M. & Whitesides, G. M. Effect of surface wettability on the adsorption of proteins and detergents. *Journal of the American Chemical Society* **120**, 3464-3473 (1998).
96 Jain, N. & Vogel, V. Spatial confinement downsizes the inflammatory response of macrophages. *Nature Materials* **17**, 1134-1144, doi:10.1038/s41563-018-0190-6 (2018).
97 Jansen, L. E. *et al.* Zwitterionic PEG-PC Hydrogels Modulate the Foreign Body Response in a Modulus-Dependent Manner. *Biomacromolecules* **19**, 2880-2888, doi:10.1021/acs.biomac.8b00444 (2018).
98 Meli, V. S. *et al.* Biophysical regulation of macrophages in health and disease. *Journal of Leukocyte Biology* **106**, 283-299, doi:10.1002/JLB.MR0318-126R (2019).
99 Cosenza, S. *et al.* Mesenchymal stem cells-derived exosomes are more immunosuppressive than microparticles in inflammatory arthritis. *Theranostics* **8**, 1399-1410, doi:10.7150/thno.21072 (2018).
100 Pacienza, N. *et al.* In Vitro Macrophage Assay Predicts the In Vivo Anti-inflammatory Potential of Exosomes from Human Mesenchymal Stromal Cells. *Molecular Therapy - Methods & Clinical Development* **13**, 67-76, doi:https://doi.org/10.1016/j.omtm.2018.12.003 (2019).
101 Zhao, J. *et al.* Mesenchymal stromal cell-derived exosomes attenuate myocardial ischaemia-reperfusion injury through miR-182-regulated macrophage polarization. *Cardiovascular Research* **15** (2019).
102 Lenzini, S., Bargi, R., Chung, G. & Shin, J.-W. Matrix mechanics and water permeation regulate extracellular vesicle transport. *Nature Nanotechnology*, doi:10.1038/s41565-020-0636-2 (2020).
103 Braza, F. *et al.* Mesenchymal Stem Cells Induce Suppressive Macrophages Through Phagocytosis in a Mouse Model of Asthma. *STEM CELLS* **34**, 1836-1845, doi:10.1002/stem.2344 (2016).
104 English, K. *et al.* Cell contact, prostaglandin E2 and transforming growth factor beta 1 play non-redundant roles in human mesenchymal stem cell induction of

CD4+CD25Highforkhead box P3+ regulatory T cells. *Clinical & Experimental Immunology* **156**, 149-160, doi:10.1111/j.1365-2249.2009.03874.x (2009).
105 Zhang, B. *et al.* Mesenchymal stem cells secrete immunologically active exosomes. *Stem Cells Dev* **23**, 1233-1244, doi:10.1089/scd.2013.0479 (2014).
106 de Witte, S. F. H. *et al.* Immunomodulation By Therapeutic Mesenchymal Stromal Cells (MSC) Is Triggered Through Phagocytosis of MSC By Monocytic Cells. *STEM CELLS* **36**, 602-615, doi:10.1002/stem.2779 (2018).
107 Galleu, A. *et al.* Apoptosis in mesenchymal stromal cells induces in vivo recipient-mediated immunomodulation. *Science Translational Medicine* **9**, eaam7828, doi:10.1126/scitranslmed.aam7828 (2017).
108 Luk, F. *et al.* Inactivated Mesenchymal Stem Cells Maintain Immunomodulatory Capacity. *Stem Cells and Development* **25**, 1342-1354, doi:10.1089/scd.2016.0068 (2016).
109 Riazifar, M., Pone, E. J., Lotvall, J. & Zhao, W. Stem Cell Extracellular Vesicles: Extended Messages of Regeneration. *Annu Rev Pharmacol Toxicol* **57**, 125-154, doi:10.1146/annurev-pharmtox-061616-030146 (2017).
110 Domenis, R. *et al.* Pro inflammatory stimuli enhance the immunosuppressive functions of adipose mesenchymal stem cells-derived exosomes. *Scientific Reports* **8**, 13325, doi:10.1038/s41598-018-31707-9 (2018).
111 Gonçalves, F. d. C. *et al.* Membrane particles generated from mesenchymal stromal cells modulate immune responses by selective targeting of pro-inflammatory monocytes. *Scientific Reports* **7**, 12100, doi:10.1038/s41598-017-12121-z (2017).
112 Song, Y. *et al.* Exosomal miR-146a Contributes to the Enhanced Therapeutic Efficacy of Interleukin-1β-Primed Mesenchymal Stem Cells Against Sepsis. *STEM CELLS* **35**, 1208-1221, doi:10.1002/stem.2564 (2017).
113 Lieschke, G. J. *et al.* Mice lacking granulocyte colony-stimulating factor have chronic neutropenia, granulocyte and macrophage progenitor cell deficiency, and impaired neutrophil mobilization. *Blood* **84**, 1737-1746 (1994).
114 Chang, S.-F. *et al.* LPS-Induced G-CSF Expression in Macrophages Is Mediated by ERK2, but Not ERK1. *PLOS ONE* **10**, e0129685, doi:10.1371/journal.pone.0129685 (2015).
115 Fultz, M. J., Barber, S. A., Dieffenbach, C. W. & Vogel, S. N. Induction of IFN-γ in macrophages by lipopolysaccharide. *International Immunology* **5**, 1383-1392, doi:10.1093/intimm/5.11.1383 (1993).
116 Platanias, L. C. Mechanisms of type-I- and type-II-interferon-mediated signalling. *Nature Reviews Immunology* **5**, 375-386, doi:10.1038/nri1604 (2005).
117 Nguyen, H. N. *et al.* Autocrine Loop Involving IL-6 Family Member LIF, LIF Receptor, and STAT4 Drives Sustained Fibroblast Production of Inflammatory Mediators. *Immunity* **46**, 220-232, doi:https://doi.org/10.1016/j.immuni.2017.01.004 (2017).
118 Kim, D.-S., Ho Han, J. & Kwon, H.-J. NF-κB and c-Jun-dependent regulation of macrophage inflammatory protein-2 gene expression in response to lipopolysaccharide in RAW 264.7 cells. *Molecular Immunology* **40**, 633-643, doi:https://doi.org/10.1016/j.molimm.2003.07.001 (2003).
119 Karlsen, A. *et al.* Anthocyanins Inhibit Nuclear Factor-κB Activation in Monocytes and Reduce Plasma Concentrations of Pro-Inflammatory Mediators in Healthy Adults. *The Journal of Nutrition* **137**, 1951-1954, doi:10.1093/jn/137.8.1951 (2007).

120 Gürtler, C. *et al.* SARM Regulates CCL5 Production in Macrophages by Promoting the Recruitment of Transcription Factors and RNA Polymerase II to the Ccl5 Promoter. *The Journal of Immunology* **192**, 4821, doi:10.4049/jimmunol.1302980 (2014).
121 Lin, M., Carlson, E., Diaconu, E. & Pearlman, E. CXCL1/KC and CXCL5/LIX are selectively produced by corneal fibroblasts and mediate neutrophil infiltration to the corneal stroma in LPS keratitis. *Journal of leukocyte biology* **81**, 786-792, doi:10.1189/jlb.0806502 (2007).
122 Wang, L.-Y., Tu, Y.-F., Lin, Y.-C. & Huang, C.-C. CXCL5 signaling is a shared pathway of neuroinflammation and blood-brain barrier injury contributing to white matter injury in the immature brain. *J Neuroinflammation* **13**, 6-6, doi:10.1186/s12974-015-0474-6 (2016).
123 Chandrasekar, B. *et al.* Chemokine-Cytokine Cross-talk THE ELR+ CXC CHEMOKINE LIX (CXCL5) AMPLIFIES A PROINFLAMMATORY CYTOKINE RESPONSE VIA A PHOSPHATIDYLINOSITOL 3-KINASE-NF-κB PATHWAY. *Journal of Biological Chemistry* **278**, 4675-4686 (2003).
124 Bhattacharyya, S., Borthakur, A., Dudeja, P. K. & Tobacman, J. K. Lipopolysaccharide-induced activation of NF-κB non-canonical pathway requires BCL10 serine 138 and NIK phosphorylations. *Exp Cell Res* **316**, 3317-3327, doi:10.1016/j.yexcr.2010.05.004 (2010).
125 Amiri, K. I. & Richmond, A. Fine tuning the transcriptional regulation of the CXCL1 chemokine. *Prog Nucleic Acid Res Mol Biol* **74**, 1-36, doi:10.1016/s0079-6603(03)01009-2 (2003).
126 Kiriakidis, S. *et al.* VEGF expression in human macrophages is NF-κB-dependent: studies using adenoviruses expressing the endogenous NF-κB inhibitor IκBα and a kinase-defective form of the IκB kinase 2. *Journal of Cell Science* **116**, 665, doi:10.1242/jcs.00286 (2003).
127 Guha, M. & Mackman, N. LPS induction of gene expression in human monocytes. *Cellular Signalling* **13**, 85-94, doi:https://doi.org/10.1016/S0898-6568(00)00149-2 (2001).
128 Fujii, S. *et al.* Graft-Versus-Host Disease Amelioration by Human Bone Marrow Mesenchymal Stromal/Stem Cell-Derived Extracellular Vesicles Is Associated with Peripheral Preservation of Naive T Cell Populations. *STEM CELLS* **36**, 434-445, doi:10.1002/stem.2759 (2018).
129 Sommerfeld, S. D. *et al.* Interleukin-36γ–producing macrophages drive IL-17–mediated fibrosis. *Science Immunology* **4**, eaax4783, doi:10.1126/sciimmunol.aax4783 (2019).
130 Balkhi, M. Y., Wittmann, G., Xiong, F. & Junghans, R. P. YY1 Upregulates Checkpoint Receptors and Downregulates Type I Cytokines in Exhausted, Chronically Stimulated Human T Cells. *iScience* **2**, 105-122, doi:https://doi.org/10.1016/j.isci.2018.03.009 (2018).
131 Luckheeram, R. V., Zhou, R., Verma, A. D. & Xia, B. CD4+T Cells: Differentiation and Functions. *Journal of Immunology Research* **2012** (2012).
132 Acharya, S. *et al.* Amelioration of Experimental autoimmune encephalomyelitis and DSS induced colitis by NTG-A-009 through the inhibition of Th1 and Th17 cells differentiation. *Scientific Reports* **8**, 7799, doi:10.1038/s41598-018-26088-y (2018).
133 Croft, M. The role of TNF superfamily members in T-cell function and diseases. *Nature Reviews Immunology* **9**, 271-285, doi:10.1038/nri2526 (2009).

134 Korn, T. *et al.* IL-6 controls Th17 immunity in vivo by inhibiting the conversion of conventional T cells into Foxp3 regulatory T cells. *Proceedings of the National Academy of Sciences* **105**, 18460 (2008).
135 Lee, Y. *et al.* Induction and molecular signature of pathogenic TH17 cells. *Nature Immunology* **13**, 991, doi:10.1038/ni.2416
https://www.nature.com/articles/ni.2416#supplementary-information (2012).
136 Tasso, R. *et al.* Development of sarcomas in mice implanted with mesenchymal stem cells seeded onto bioscaffolds. *Carcinogenesis* **30**, 150-157 (2008).
137 Tasso, R. *et al.* Mesenchymal stem cells induce functionally active T-regulatory lymphocytes in a paracrine fashion and ameliorate experimental autoimmune uveitis. *Investigative ophthalmology & visual science* **53**, 786-793 (2012).
138 Mansouri, N. *et al.* Mesenchymal stromal cell exosomes prevent and revert experimental pulmonary fibrosis through modulation of monocyte phenotypes. *JCI Insight* **4**, doi:10.1172/jci.insight.128060 (2019).
139 Morrison, T. J. *et al.* Mesenchymal Stromal Cells Modulate Macrophages in Clinically Relevant Lung Injury Models by Extracellular Vesicle Mitochondrial Transfer. *American Journal of Respiratory and Critical Care Medicine* **196**, 1275-1286, doi:10.1164/rccm.201701-0170OC (2017).
140 Capcha, J. M. C. *et al.* Wharton's jelly-derived mesenchymal stem cells attenuate sepsis-induced organ injury partially via cholinergic anti-inflammatory pathway activation. *American Journal of Physiology-Regulatory, Integrative and Comparative Physiology* **318**, R135-R147, doi:10.1152/ajpregu.00098.2018 (2019).
141 Liu, T., Zhang, L., Joo, D. & Sun, S.-C. NF-κB signaling in inflammation. *Signal Transduction and Targeted Therapy* **2**, 17023, doi:10.1038/sigtrans.2017.23 (2017).
142 Moore, L. B., Sawyer, A. J., Charokopos, A., Skokos, E. A. & Kyriakides, T. R. Loss of monocyte chemoattractant protein-1 alters macrophage polarization and reduces NFkappaB activation in the foreign body response. *Acta Biomaterialia* (2015).
143 Caires, H. R. *et al.* Macrophage interactions with polylactic acid and chitosan scaffolds lead to improved recruitment of human mesenchymal stem/stromal cells: a comprehensive study with different immune cells. *Journal of The Royal Society Interface* **13**, 20160570, doi:10.1098/rsif.2016.0570 (2016).
144 Paredes-Juarez, G. A., de Haan, B. J., Faas, M. M. & de Vos, P. A Technology Platform to Test the Efficacy of Purification of Alginate. *Materials (Basel)* **7**, 2087-2103, doi:10.3390/ma7032087 (2014).
145 Rodriguez, S. *et al.* Characterization of chelator-mediated recovery of pancreatic islets from barium-stabilized alginate microcapsules. *Xenotransplantation* **n/a**, e12554, doi:10.1111/xen.12554 (2019).

CHAPTER 6

Preferences of Type 1 Diabetic Patients on Devices for Islet Transplantation

Abstract

Transplantation of pancreatic islets within a biomaterial device is currently under investigation in clinical trials for treatment of patients with Type 1 Diabetes (T1D). Patients' preferences on the design of such implants could guide the designs of next generation implantable devices; however, unfortunately such information is not currently available. We surveyed 482 patients with T1D on their preferences on the size, shape, visibility, and transplantation site of islet containing implants. Preferred location for islet transplantation within devices was under the skin (52.7%). 48.3% preferred microscopic disks and 32.3% preferred a thin device. Moreover, 58.4% preferred the implant to be as small as possible, 25.4% did not care about visibility, and 16.2% preferred their implants not to be visible. Among female participants, 81% cared about the implant visibility, whereas this number was 64% for male respondents (χ^2 test (1, n = 468) = 16.34; *p*-value < 0.0001). 22% of those younger than 50 and 30% of those older than 50 did not care about the implant (χ^2 test (4, n = 468) = 23.69; *p*-value <0.0001). These results suggest that subcutaneous site and micron-sized devices are more favorable among the cohort of type 1 diabetic patients that participated in our survey.

Keywords: Implantable devices; Biomaterials; Islet Transplantation; Type 1 Diabetes; Patients Preferences

Introduction

With the advancement of diabetes medical technology, the use of medical devices has quickly reached the forefront of how care is provided to patients with Type 1 Diabetes (T1D). Thus far, FDA approved devices have included glucometers, continuous subcutaneous insulin infusions, and continuous glucose monitors (CGMs) leading to reductions in hypoglycemia, complications and improvements in overall glycemic control. Additionally, upon introduction [1] and a multi-center trial [2] of clinical islet transplantation, many efforts have been devoted to further optimize transplantation of islets into humans with T1D as a long-term treatment. Critical barriers have impeded long-term efficacy of islet transplantation. For instance, islets are prone to Anoikis (detachment of islets from extracellular matrix after transplantation) [3] as well as instant blood mediated inflammatory reaction (IBMIR) [4], which eventually clears the transplanted islets from a recipients' body. To counteract these effects, immunosuppressive drugs have been employed, however, the amount of immunosuppressive regimen required after islet transplantation may make patients prone to infection, mouth ulcers, diarrhea, and acne [5]. To partly address these challenges, the use of a protective shield around the islets [6] has helped the functional longevity of the transplant through protection of islets from host's immune response, while still providing the diffusion of insulin and glucose across the membrane.

At least three factors are known to play vital roles in the success of islet transplantation within an immune-isolating device [7]: islet survival and function after transplantation, regulated immune response against the implant, and functional integration of the transplant with the host. While extensive research has been devoted to modulating physical, chemical, immunological, and mechanical properties of implantable devices, there is a lack of understanding regarding patients' preferences on devices. Such information is critical because it could guide the designs

of next generation implantable devices, as T1D patients are the ultimate users of these products. These devices could generally be classified into two categories i.e. macro-devices [8-18] and microdevices [19-26]. In most cases, macro-devices are few centimeter-sized made of biomaterials with channels or chambers that could hold islets within. The fundamental aspect of these devices is protection of islets from immune attack, while allowing the diffusion of nutrients, glucose, cellular waste, and insulin. Microdevice, also known as encapsulation device, refers to encapsulating islets within a semi-permeable biomaterial, mostly with a spherical shape and micron-scale diameters. Similarly, microencapsulation has also been developed to block the immune-attack against islets [27], while allowing the diffusion of nutrients, glucose, cellular waste, and insulin. These implants are now under research and clinical investigations as a means of long term glycemic control for patients with T1D [28,29].

While these efforts and discoveries are setting the stage for successful clinical outcomes, patient's preferences on the devices have not been explored to the best of our knowledge. We therefore aimed to reach out to patients with T1D to gain a better understanding on their perspectives regarding implants through an on-line survey. Such information may influence the design of the future implantable devices to better suit the needs of patients with T1D. In a broader context, this study aids the cell transplantation and implantable biomedical devices fields to consider and implement the preferences of their endpoint users.

Results

Cohort Characteristics

We first classified patients and identified our participants based on age, sex, duration of being T1D, and current treatment they use (**Table 6.1**). Cohort that participated in our survey were from different ages.

Table 6.1. Participants in the survey

	Choices	Number
Age	16-18	56
	18-30	59
	31-50	163
	51-64	115
	65+	76
Sex	Female	297
	Male	172
Duration of being Type 1 Diabetic	< 2 years	29
	2-5 years	34
	> 5 years	405
Current Treatment	MDI	65
	Insulin pump + CGM	386
	Others	18

Majority of the participants, 163 people (34.7%) were aged between 31-50, 115 people (24.5%) between 51-64, 76 people (16.2%) were 65+, 59 people (12.6%) were between 18-30, and 56 people (11.9%) were 16-18. Among participants, 297 were female (63.3%) and more than 86.5% of the cohort were diagnosed with T1D more than 5 years. Moreover, 34 (7.3%) and 29 (6.2%) patients were diagnosed with diabetes between 2-5 and less than 2 years, respectively. More than 82.3% of patients are using constant glucose monitors (CGM) and insulin pump for managing their blood glucose levels. In addition, 77 participants are using multiple daily injection (MDI),

12 of whom are using CGM simultaneously. One of the patients were transplanted with pancreas and 3 others use MDI and flash glucose monitor.

Responses to Survey

We first sought to investigate patients' preference on the physical characteristics of the implants (**Table 6.2**). **Figure 6.1** depicts the schematic representation of the implants and their transplantation location asked in the survey. We chose these shapes and locations because they resemble devices currently under investigation in clinical trials and research laboratories [29]. These preferences were defined as implant location (under the skin, in the abdomen, and outside of the body, schematically presented in **Figures 6.1a, b, and c**, respectively), shape (multiple microscopic small disks deposited in a fluid, a thin device which is soft and the size of a credit card, and rod shaped the size of a 3" pencil, schematically presented in **Figures 6.1d, e, and f**, respectively), and visibility (very small or invisible, do not care about visibility). To evaluate these data and find associations between implants' physical characteristics with age and gender, we examined the responses by gender (**Figure 6.2a**) and age (**Figure 6.2b**). We asked patients "If you receive an implant containing insulin secreting cells, where do you prefer it to be? (Assume that size and shape are comfortable in each case)". 247 (52.7%) preferred the device to be transplanted under their skin.

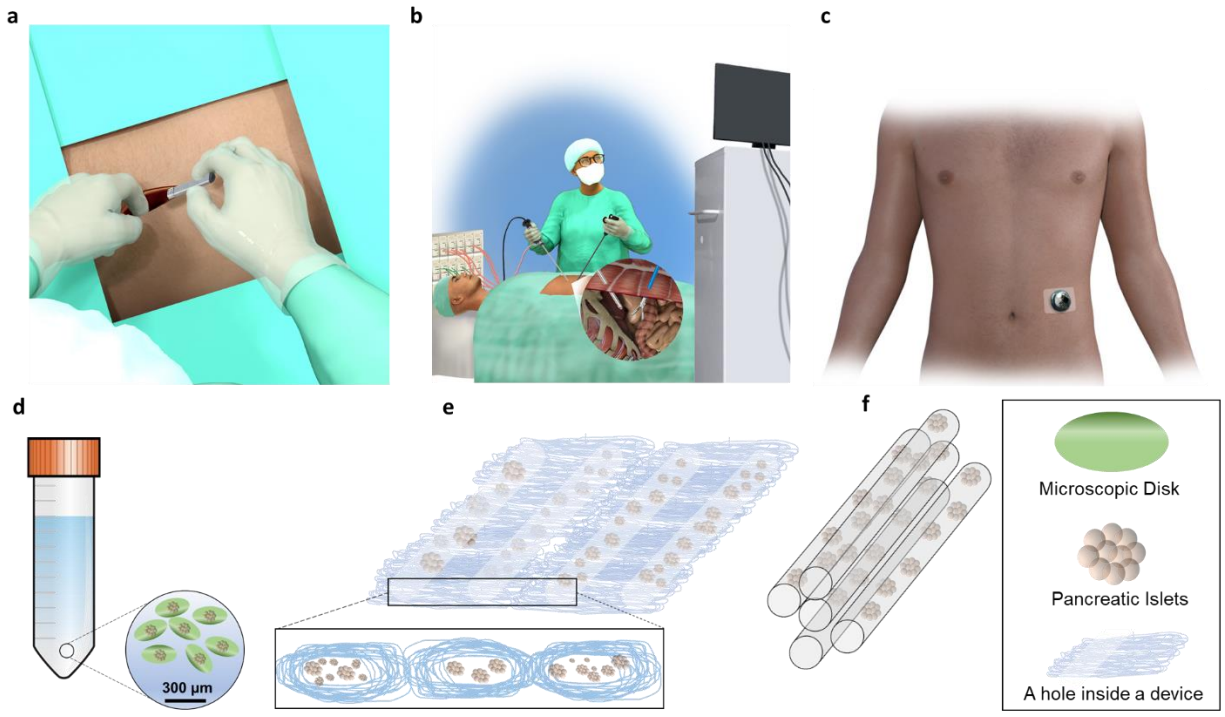

Figure 6.48. Schematic representations of the implants and possible transplantation sites. Implants could be transplanted, **a)** under the skin (subcutaneously), **b)** into the peritoneal cavity through laparoscopic surgery, **c)** or outside of the body. Implant shapes could be **d)** multiple microscopic small disks deposited in a fluid, **e)** a thin device which is soft and the size of a credit card, and **f)** rod shaped the size of a 3" pencil.

The next most popular location was intra-abdominal with 141 patients (30.1%) choosing this location. Interestingly, only 34 (7.2%) of participants responded, "outside my body". Moreover, 47 patients (10.0%) commented on the question and chose "Others" option. Some comments pointed out that depending on the longevity of the device's activity, their preferences could vary, where longer acting devices would be preferred to be transplanted into abdomen. Interestingly, 16 patients noted that as long as the device functions, they are open to any location. Considering age and gender of participants', we found no significant association between implant location and gender (χ^2 (3, n = 468) = 2.08; *p*-value = 0.6), and age group (χ^2 (12, n = 468) = 13.74; *p*-value = 0.3).

Table 6.2. Preferences of individuals with Type 1 Diabetes regarding implants characteristics

Question	Choices	Percentage
Implantation Site	Under the Skin	52.7%
	Inside abdomen	30.1%
	Outside of body	7.2%
Size and Shape of Implants	Multiple microscopic disks deposited in a fluid	48.3%
	A thin device (soft and size of the credit card)	32.3%
	Rod shaped device (Size of a 3" pencil)	9.8%
Visibility Importance	Not at all	25.4%
	Prefer it to be as small as possible	58.4%
	Not visible at all	16.2%
Immunoregulatory Implants	Implants that only regulate blood glucose	30.6%
	Implants that regulate blood glucose and immune system	69.4%
Implants with Stem Cell	Prefer an Implant Fabricated with My Own Stem Cells	83.7%
	DO NOT prefer an Implant Fabricated with My Own Stem Cells	16.3%

We then asked our participants their preferences on the device's shape. The top choice was "multiple microscopic disks deposited in a fluid" (n=226 i.e. 48.3% of participants). A thin device (soft and size of the credit card) was the second top choice with 151 (32.3%) votes. A rod shape device (size of a 3" pencil) was the least popular choice (n = 46 i.e. 9.8%). Nearly 10% (n = 45) had comments on the question and chose "Others" option, 14 of which again noted that if

functional, shape is irrelevant. The majority of the other 31 patients pointed out the visibility in their comments.

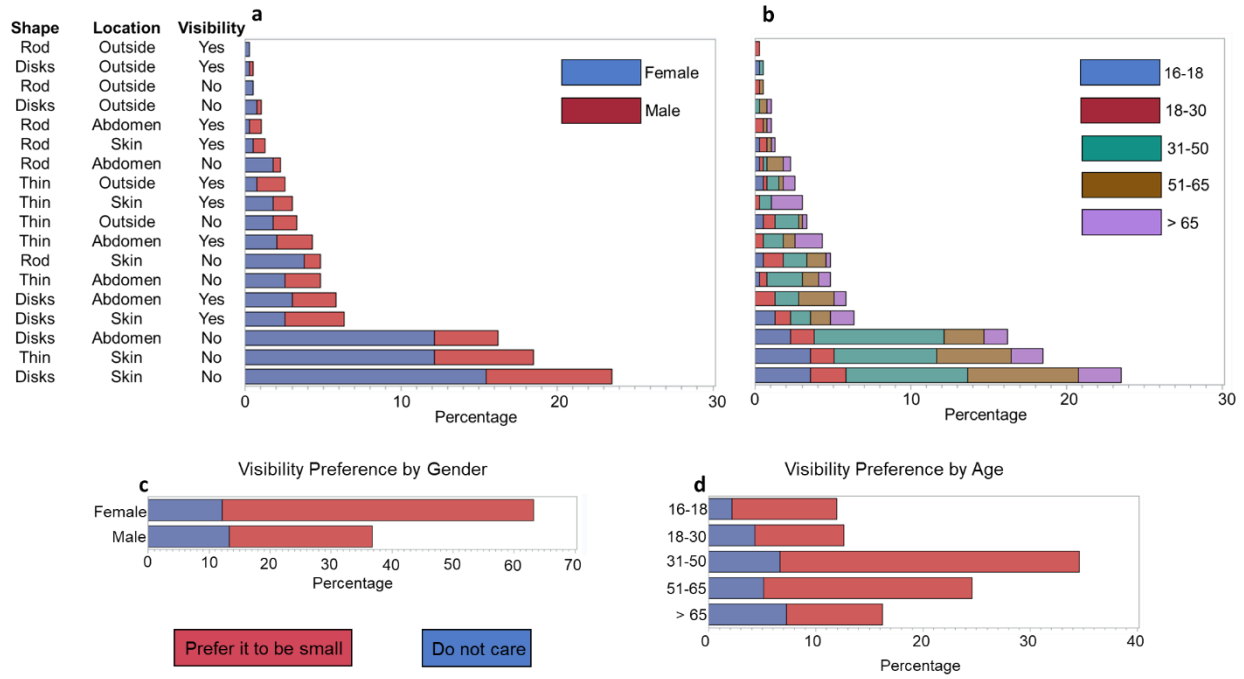

Figure 6.49. Dependence of **a)** gender and **b)** age on respondents' preference with respect to implant location (under the skin, in the abdomen, and outside of the body), shape (Multiple microscopic small disks deposited in a fluid, a thin device, soft and the size of a credit card, and rod shaped the size of a 3" pencil) and visibility (very small or invisible, do not care about visibility). Note that for the visibility, "Yes" means respondent is fine with the implant to be visible, and "No" means otherwise. There is a significant association between age and implants' shape (χ^2 (12, n = 468) = 25.59; *p*-value = 0.01). However, no significant association was found between age and implant location preference (χ^2 (12, n = 468) = 13.74; *p*-value = 0.3). Gender had no significant association with shape preference (χ^2 (3, n = 468) = 2.74; *p*-value = 0.4) and implant location (χ^2 (3, n = 468) = 2.08; *p*-value = 0.6). There was also an association of implants visibility with **c)** gender and **d)** age. Male participants were more indifferent regarding implant visibility (χ^2 (1, n = 468) = 16.34; *p*-value < 0.0001). Among male participants, 36% (62 out of 172) were indifferent about implant visibility, while this ratio was 19% (57 out of 296) for female participants. The age also was a determinant factor on the implant's visibility preference among respondents. Around 22% of those younger than 50 (61 out of 277) do not care about the implant visibility compared to 30% (58 out of 191) of those older than 50 (χ^2 (4, n = 468) = 23.69; *p*-value <0.0001).

In the next question, we asked them "how much do you care about visibility of the implant on your body"? More than 58.4% (n = 274) replied that they prefer the device to be as small as possible. 25.4% (n = 119) did not care about the visibility, while 16.2% (n=76) preferred the

device to be not visible at all. We found no significant association between shape preference and gender (χ^2 (3, n = 468) = 2.74; *p*-value = 0.4) but the association between shape preference and age group was significant (χ^2 (12, n = 468) = 25.59; *p*-value = 0.01). Among the four options (multiple microscopic small disks deposited in a fluid, thin device the size of a credit card under the skin, rod shaped device the size of 3" pencil, and other) multiple microscopic small disks deposited in a fluid is the most preferred shape among all age group (46-52%) except for the those 65 or older (38%) where they preferred thin device the size of a credit card under the skin (43%).

We also sought to further understand the possible role of gender and age on the implants' visibility (**Figures 6.2c, d**). Evaluating these results, we found a significant association (χ^2 (1, n = 468) = 16.34; *p*-value < 0.0001) between gender and participant's preference on implant visibility. Among female participants, 81% (239 out of 296) cared about the implant visibility, whereas this number was 64% (110 out of 172) for male respondents. Around 22% of those younger than 50 did not care about the implant visibility (61 out of 277), as compared to 30% (58 out of 191) for our respondents older than 50. There was a significant association between age and the participants preference on implant visibility (χ^2 (4, n = 468) = 23.69; *p*-value <0.0001).

In addition to generic details about implants, we further attempted to understand participants opinion on emerging features of implants. Among recent developments, immune-regulatory devices are showing promise in long-term glycemic control in rodents and non-human primates [19,23]. Future developments may also consider other immune-regulatory devices, where an implant could reduce and/or regulate the immune insults against β-cells, providing β-cells regeneration capability. We followed the survey question by gaining knowledge about patients'

willingness to receive immunoregulatory devices after islet transplantation. We asked "if you have Type 1 Diabetes, your immune system is dysregulated. Which option would you prefer?" There were two choices "1. An implant that only regulates my blood glucose" and "2. An implant that not only controls my glucose but also capable of regulating my immune system to a healthy state". Among responders, 143 (30.6%) chose the former, and 325 (69.4%) preferred the latter. There was no significant association between the preference on immune-regulatory implants with gender (χ^2 (1, n = 468) = 0.98; *p*-value = 0.3) or with age (χ^2 (4, n = 468) = 7.6; *p*-value = 0.14).

Lack of allogeneic cell donors is one of the main impediments for the pancreatic islet transplantation. Much effort has been devoted to develop islets from xeno-sources [30]. In addition, reprograming stem cell into insulin producing cells have been under investigation [31,32]. To understand our participants perspective on such developments we asked them "do you prefer to receive an implant fabricated with stem cells derived from your own body?". More than 83.6% (390 people) answered yes, while 16.3% (n=76) responded no, implying the acceptability of stem cell research and development among our cohort. We found no significant association between implant fabricated by one's own stem cell with gender (χ^2 (1, n = 468) = 0.28; *p*-value = 0.6) or with age (χ^2 (4, n = 468) = 2.92; *p*-value = 0.6).

Discussion

Islet transplantation has been the focus of 50 years of research to treat T1D [27,28]. The ultimate goal of islet transplantation is to routinely restore insulin independence with no (or minimal) immunosuppression in T1D patients. However, two main barriers are yet to be overcome for the successful clinical islet transplantation. The first challenge is the scarcity of the

allogeneic islet source, which heavily relies on the deceased donors. The second issue is the death of transplanted islets shortly after transplantation due to immune reactions and ischemia, which limits the intended long-term benefits of islet transplantation [7]. These two challenges have been under extensive investigations, where xenotransplantation and stem cell research are mainly under development for the former barrier. For the latter, biomedical devices with variety of sizes, shapes, and materials have been under development. While recent advances in stem cell engineering and biomaterials science have paved the way to breakdown these barriers, patients' preferences on the outcome products are largely unknown. Such information bridges the gap between science-oriented thinking paradigm in designing the biomedical devices to patient-oriented or at least patient-considered designs. This consideration could guide the designs of next generation implantable devices, as T1D patients are the ultimate users of these products. We therefore aimed to target a small population of the T1D community and get an understanding on their preferences for such devices and stem cells. We designed a short on-line survey and distributed among patients with T1D engaged in a web-based community.

In the first section of the survey, we attempted to get information on the characteristic of our participant cohort. Our participants age followed a normal distribution curve, and their duration of diabetes was weighted towards > 5 years (~ 86%). Most widely used current treatment among our cohort was CGM and insulin pump (82.3%), implying their familiarity with external devices. Interestingly, only about 7% preferred an implant outside their bodies, which may imply the patients' discomfort. The subcutaneous (under the skin) spot was the top choice for our respondents. Ease of implantation and explantation, along with less surgical complexity make subcutaneous transplantations a good choice for implantable devices. In the case of islet transplantation, however, subcutaneous implantation is challenging due to poor vascularity,

which causes islets to suffer from hypoxic conditions [33]. Therefore, strategies have been developed to vascularize and pre-vascularize the subcutaneous space for islet transplantations.

Size and shape of the implants were another aspect about which we sought to understand patients' perspective. Classically, islet transplantation devices have been classified into micro- and macro-devices. Multiple microscopic disks were preferred by ~48% of patients. This option was phrased to suggest the microencapsulation technologies to the participants. Fortunately, some recent microencapsulation technologies have shown promise for islet transplantation in rodents and non-human primates [19,23]. Participants preference on receiving microencapsulated islets matches their other preference regarding the implant's visibility, where 58.4% of patients prefer the implant to be as small as possible. The second choice of our participants was a "thin soft device in a size of a credit card", which fits to the specifications most of the current macro-devices under development.

The use of an immunoregulatory implant is an emerging concept, where the implant "engineers" the immune system of the host. A few examples are antigen-releasing scaffolds that enhance vascularization [34], biological scaffolds that inhibit tumor growth through alterations in immunocyte recruitments [35,36], and bio-responsive biomaterials for immune checkpoint blockade [37]. Immunoregulatory implants could be envisioned from two perspectives in the treatment of T1D. First, any implant including microcapsules or macro-devices need not to elicit an immune response, i.e. no immunocyte activation due to the implant itself. Second, T1D is inherently a disease of immune system dysregulation. Therefore, it is expected that immunoregulatory implants will get more attention in T1D research. Accordingly, ~70% of participants preferred implants that would address this issue.

The paucity of cell donors remains one of the main impediments for the islet transplantation into patients. Much effort has been devoted to xenotransplantation [30,38] and stem cell research [32,39]. Insulin producing cells have been generated from stem cells [31], however, the formation of functional cells that recapitulate all aspects of endogenous β-cells and/or pancreatic islets have yet to be fully achieved. Assuming that stem cell research will result in fully functional islets, we asked participants their willingness to receive stem cells. More than 83% of participants preferred to receive devices with stem cells derived from their own body, implying that autologous stem cell transplantations may be an acceptable approach among patients with T1D.

This study represents the first attempt in reflecting the perspectives of a small cohort of patients with T1D on their preferences to receive an implantable islet containing device. This work aids bridging the gap between fully science-oriented designs to patient-considered implantable devices. This study gives insight to the future developers of biomedical devices for islet transplantation, but also inspires the general biomedical devices field to seek and implement their users' perspectives.

Experimental Methods

Respondent recruitment and inclusion criteria

Inclusion criteria for this survey required respondents to be any individual diagnosed with T1D residing in the United States. Respondents were recruited from Juvenile Diabetes Research Foundation (JDRF) Orange County chapter, Savvy Diabetic, and Close Concern Communities panel of patients with T1D, who are engaged in a web-based community. Our study was

conducted in accordance with relevant guidelines stated by the Declaration of Helsinki. Based on the nature of this survey that includes the use of anonymous responses, there was no requirement for the involvement of an ethics board and informed consent from participants, and we received an IRB Exemption Approval from the University of California Irvine, Irvine CA (Exemption Category 2b Approval: 12-04-2018) for the same.

Data Handling

We set the best scientific practice by defining a minimum requirement for the validity of the responses. We eliminated responses, where respondents did not complete and surveys or completed the survey in an unpractically short time (defined as less than 1.5 minute based on the minimum amount of time required to read and answer all questions). These results were removed to produce a final validated dataset (overall, 14 participants (~3%) of surveys were excluded from subsequent analysis). No specific product or brand names were mentioned in the survey.

References

1 Shapiro, A. M. J. *et al.* Islet Transplantation in Seven Patients with Type 1 Diabetes Mellitus Using a Glucocorticoid-Free Immunosuppressive Regimen. *New England Journal of Medicine* **343**, 230-238, doi:10.1056/NEJM200007273430401 (2000).

2 Shapiro, A. M. J. *et al.* International Trial of the Edmonton Protocol for Islet Transplantation. *New England Journal of Medicine* **355**, 1318-1330, doi:10.1056/NEJMoa061267 (2006).

3 Thomas, F. T. *et al.* Anoikis, extracellular matrix, and apoptosis factors in isolated cell transplantation. *Surgery* **126**, 299-304, doi:https://doi.org/10.1016/S0039-6060(99)70169-8 (1999).

4 Bennet, W., Groth, C.-G., Larsson, R., Nilsson, B. & Korsgren, O. Isolated Human Islets Trigger an Instant Blood Mediated Inflammatory Reaction: Implications for Intraportal Islet Transplantation as a Treatment for Patients with Type 1 Diabetes. *Upsala Journal of Medical Sciences* **105**, 125-133, doi:10.1517/03009734000000059 (2000).

5 Ryan, E. A., Paty, B. W., Senior, P. A. & Shapiro, A. M. J. Risks and side effects of islet transplantation. *Current Diabetes Reports* **4**, 304-309, doi:10.1007/s11892-004-0083-8 (2004).

6 Rezaa Mohammadi, M., Rodrigez, S., Cao, R., Alexander, M. & Lakey, J. R. T. Immune response to subcutaneous implants of alginate microcapsules. *Materials Today: Proceedings* **5**, 15580-15585, doi:https://doi.org/10.1016/j.matpr.2018.04.166 (2018).
7 Kopan, C. *et al.* Approaches in Immunotherapy, Regenerative Medicine, and Bioengineering for Type 1 Diabetes. *Frontiers in Immunology* **9**, 1354 (2018).
8 So, V., Martinson, L., Green, C. & Scott, M. 3-dimensional large capacity cell encapsulation device assembly. (2013).
9 Carlsson, P.-O. *et al.* Transplantation of macroencapsulated human islets within the bioartificial pancreas βAir to patients with type 1 diabetes mellitus. *American Journal of Transplantation* **18**, 1735-1744, doi:10.1111/ajt.14642 (2018).
10 Boettler, T. *et al.* Pancreatic Tissue Transplanted in TheraCyte™ Encapsulation Devices Is Protected and Prevents Hyperglycemia in a Mouse Model of Immune-Mediated Diabetes. *Cell Transplantation* **25**, 609-614, doi:10.3727/096368915X688939 (2016).
11 Pepper, A. R. *et al.* Diabetes Is Reversed in a Murine Model by Marginal Mass Syngeneic Islet Transplantation Using a Subcutaneous Cell Pouch Device. *Transplantation* **99** (2015).
12 Aoun, R. *et al.* Preclinical validation of the mailpan®, a bioartificial pancreas to treat type 1 diabetes. *Xenotransplantation* **22** (2015).
13 Smink, A. M. *et al.* The Efficacy of a Prevascularized, Retrievable Poly(D,L,-lactide-co-ε-caprolactone) Subcutaneous Scaffold as Transplantation Site for Pancreatic Islets. *Transplantation* **101** (2017).
14 Graham, J. G. *et al.* PLG Scaffold Delivered Antigen-Specific Regulatory T Cells Induce Systemic Tolerance in Autoimmune Diabetes. *Tissue Engineering Part A* **19**, 1465-1475, doi:10.1089/ten.tea.2012.0643 (2013).
15 Berman, D. M. *et al.* Long-Term Survival of Nonhuman Primate Islets Implanted in an Omental Pouch on a Biodegradable Scaffold. *American Journal of Transplantation* **9**, 91-104, doi:10.1111/j.1600-6143.2008.02489.x (2009).
16 Najjar, M. *et al.* Fibrin gels engineered with pro-angiogenic growth factors promote engraftment of pancreatic islets in extrahepatic sites in mice. *Biotechnology and Bioengineering* **112**, 1916-1926, doi:10.1002/bit.25589 (2015).
17 Kette, F., Rojas-Canales, D., Drogemuller, C., McInnes, S. & Toby Coates, P. Modification of Polyurethane Scaffolds for Localised Immunosuppression of Subcutaneous Islet Transplantation. *Transplantation* **102** (2018).
18 An, D. *et al.* Designing a retrievable and scalable cell encapsulation device for potential treatment of type 1 diabetes. *Proceedings of the National Academy of Sciences* **115**, E263, doi:10.1073/pnas.1708806115 (2018).
19 Farah, S. *et al.* Long-term implant fibrosis prevention in rodents and non-human primates using crystallized drug formulations. *Nature Materials* **18**, 892-904, doi:10.1038/s41563-019-0377-5 (2019).
20 Vegas, A. J. *et al.* Combinatorial hydrogel library enables identification of materials that mitigate the foreign body response in primates. *Nature Biotechnology* **34**, 345, doi:10.1038/nbt.3462
https://www.nature.com/articles/nbt.3462#supplementary-information (2016).
21 Manzoli, V. *et al.* Immunoisolation of murine islet allografts in vascularized sites through conformal coating with polyethylene glycol. *Am J Transplant* **18**, 590-603, doi:10.1111/ajt.14547 (2018).

22 Weaver, J. D. *et al.* Synthetic poly(ethylene glycol)-based microfluidic islet encapsulation reduces graft volume for delivery to highly vascularized and retrievable transplant site. *American Journal of Transplantation* **19**, 1315-1327, doi:10.1111/ajt.15168 (2019).
23 Sremac, M. *et al.* Preliminary Studies of the Impact of CXCL12 on the Foreign Body Reaction to Pancreatic Islets Microencapsulated in Alginate in Nonhuman Primates. *Transplant Direct* **5**, e447-e447, doi:10.1097/TXD.0000000000000890 (2019).
24 Hwa, A. J. & Weir, G. C. Transplantation of Macroencapsulated Insulin-Producing Cells. *Current Diabetes Reports* **18**, 50, doi:10.1007/s11892-018-1028-y (2018).
25 Kozlovskaya, V. *et al.* Ultrathin polymeric coatings based on hydrogen-bonded polyphenol for protection of pancreatic islet cells. *Adv Funct Mater* **22**, 3389-3398, doi:10.1002/adfm.201200138 (2012).
26 Pedraza, E., Coronel, M. M., Fraker, C. A., Ricordi, C. & Stabler, C. L. Preventing hypoxia-induced cell death in beta cells and islets via hydrolytically activated, oxygen-generating biomaterials. *Proceedings of the National Academy of Sciences* **109**, 4245, doi:10.1073/pnas.1113560109 (2012).
27 Lim, F. & Sun, A. M. Microencapsulated islets as bioartificial endocrine pancreas. *Science* **210**, 908, doi:10.1126/science.6776628 (1980).
28 Desai, T. & Shea, L. D. Advances in islet encapsulation technologies. *Nature Reviews Drug Discovery* **16**, 338, doi:10.1038/nrd.2016.232 (2016).
29 Orive, G. *et al.* Engineering a Clinically Translatable Bioartificial Pancreas to Treat Type I Diabetes. *Trends in Biotechnology* (2018).
30 Park, C.-G., Bottino, R. & Hawthorne, W. J. Current status of islet xenotransplantation. *International Journal of Surgery* **23**, 261-266, doi:https://doi.org/10.1016/j.ijsu.2015.07.703 (2015).
31 Sneddon, J. B. *et al.* Stem Cell Therapies for Treating Diabetes: Progress and Remaining Challenges. *Cell Stem Cell* **22**, 810-823, doi:https://doi.org/10.1016/j.stem.2018.05.016 (2018).
32 Pagliuca, Felicia W. *et al.* Generation of Functional Human Pancreatic β Cells In Vitro. *Cell* **159**, 428-439, doi:https://doi.org/10.1016/j.cell.2014.09.040 (2014).
33 Vlahos, A. E., Cober, N. & Sefton, M. V. Modular tissue engineering for the vascularization of subcutaneously transplanted pancreatic islets. *Proceedings of the National Academy of Sciences* **114**, 9337, doi:10.1073/pnas.1619216114 (2017).
34 Kwee, B. J. *et al.* Treating ischemia via recruitment of antigen-specific T cells. *Science Advances* **5**, eaav6313, doi:10.1126/sciadv.aav6313 (2019).
35 Wolf, M. T. *et al.* A biologic scaffold–associated type 2 immune microenvironment inhibits tumor formation and synergizes with checkpoint immunotherapy. *Science Translational Medicine* **11**, eaat7973, doi:10.1126/scitranslmed.aat7973 (2019).
36 Kuai, R. *et al.* Subcutaneous Nanodisc Vaccination with Neoantigens for Combination Cancer Immunotherapy. *Bioconjugate Chemistry* **29**, 771-775, doi:10.1021/acs.bioconjchem.7b00761 (2018).
37 Yu, S. *et al.* Injectable Bioresponsive Gel Depot for Enhanced Immune Checkpoint Blockade. *Advanced Materials* **30**, 1801527, doi:10.1002/adma.201801527 (2018).
38 Lau, H. *et al.* Necrostatin-1 Supplementation Enhances Young Porcine Islet Maturation and In vitro Function. *Xenotransplantation*, doi:10.1111/xen.12555 (2019).

39 Christophersen, N. S., Doehn, U. & Hansson, M. Generation of Functional Beta Cells From Human Pluripotent Stem Cell-Derived Endocrine Progenitors. (2016).

Conclusions

The primary role of nanotechnology in drug delivery is to effectively deliver the drug to the desired target while maintaining its pharmacological activity. In this respect, various nanomaterials engineered to effectively be employed on the bench and beside. Apart from synthetic nanomaterials, almost all cells produce nanovesicles. Exosomes are one specific class of these vesicles that ranges between 50-150 nm and have been shown to recapitulate some of the characteristics of the cells they originate from. Our data demonstrate that exosomes derived from IFNγ activated MSCs 1) suppress PBMC cell proliferation, reduce proinflammatory cytokines in PBMCs co-cultures and enhance induction of Tregs *in vitro* and *in vivo*, 2) are distributed to the inflamed, but not healthy, spinal cords, reduce neuroinflammation and demyelination and improve functional outcomes in chronic EAE murine model. This study asserts that stem cell-derived exosomes can represent a viable approach to treat autoimmune and neurodegenerative disorders, which remains major unmet clinical needs. Interestingly, our pilot study showed inefficacy of exosomes in preventing the occurrence of autoimmune diabetes in non-obese diabetic mice.

Inspired by immunomodulatory potency of MSC secretome, we developed a biohybrid formulation that reduces the inflammatory response against alginate microcapsules. This biohybrid scaffold takes advantage of immunosuppressive capabilities of MSC secretory factors, where loading alginate microcapsules with these factors reduces immune infiltration around microcapsules and decrease the cathepsin activity of alginate *in vivo*. We found that alginate induces inflammatory response in murine macrophages in a dose dependent manner, leading to secretion of TNFα, IL-6, IL-1β, and GM-CSF. Addition of pCM to the media reduces the

macrophage activation in response to alginate ad LPS, both of which partly activate macrophages through TLR4 pathway.

The pCM-Alg platform benefits from facile preparation method, which could easily be scaled-up for high-throughput manufacturing processed. In addition, through its controlled-release nature, many drug delivery and tissue regeneration applications could be further explored using pCM-Alg. Specifically, pCM-Alg could regulate the fibrotic response against the implants, where other parenchymal cells could be formed around the microcapsules. This could encourage the tissue regeneration and wound healing around the pCM-Alg platform. Moreover, finding a molecular mechanism underlying the anti-inflammatory effects of secretome (and also extracellular vesicles secreted by stem cells) seem to be very tedious. This complexity mainly originates from the complexity and variety of molecules (including proteins, coding and non-coding RNAs, and lipids) present in the secretome and extracellular vesicles. To address this complexity, at least partly, we here propose that mechanisms underlying the effect of complex biologics could be characterized through their interactions with activated immunocytes. This interaction could be analyzed with RNAseq of immunocytes, establishing consistency and potency assays for complex biologics.

When the goal is cell transplantation inside a biomaterial, FBR causes a non-functional graft engulfed in a scarring tissue. This is one of the major challenges in clinical translation of tissue engineering and prosthesis products, sensors, and functional cell transplantation. One area that suffers from this issue is the islet transplantation to restore and maintain euglycemia in patients with T1D. This is an unmet clinical need with a significant potential health impact. We thus harnessed the anti-inflammatory properties of exosomes and fabricated an encapsulation technology that release exosomes in a controlled-fashion from alginate microcapsules (AlgXO). Rat islets encapsulated in AlgXO corrected the hyperglycemia in diabetic immunocompetent mice for > 5 months. Investigating the plausible reasons, we found that AlgXO release its exosomal content over a week period, which then suppresses the infiltration and activation of immune cells, and macrophages in particular. While AlgXO is

mainly focused on the islet transplantation, its core technology could be broadly applicable to other areas of cells transplantation and implants rejection due to immune response.